Analysis of the Ventricular Fibrillation Electrocardiogram During Cardiopulmonary Resuscitation to Predict Outcome of Out-of-Hospital Cardiac Arrest

Jason Coult

A dissertation

submitted in partial fulfillment of the

requirements for the degree of

Doctor of Philosophy

University of Washington

2019

Reading Committee:

Herbert M Sauro, Chair

Christopher Neils

Heemun Kwok

Program Authorized to Offer Degree:

Bioengineering

University of Washington

Abstract

Analysis of the Ventricular Fibrillation Electrocardiogram
During Cardiopulmonary Resuscitation to Predict Outcome
of Out-of-Hospital Cardiac Arrest

Chair of the Supervisory Committee:

Herbert M Sauro

Department of Bioengineering

Out-of-hospital ventricular fibrillation (VF) cardiac arrest results in approximately 50,000 deaths per year in the United States. Treatment includes defibrillation shock supported by cardiopulmonary resuscitation (CPR). Current defibrillator-guided resuscitation protocol follows a fixed sequence. This sequence consists of CPR interrupted at 2-minute intervals to allow rhythm classification and defibrillation when VF is detected. However, defibrillation attempts frequently fail and overall survival from VF arrest is low. Studies have demonstrated that outcomes might be improved by (1) minimizing interruptions in CPR and (2) delaying shock to allow an interim of CPR and medications when patient myocardial status is poor and likelihood of defibrillation success is low. Quantitative measures of the VF electrocardiogram (ECG) have therefore been proposed to estimate the likelihood of defibrillation success and serve as a surrogate for a patient's myocardial status. These measures have potential to improve survival by guiding the administration of shock, CPR, and medications. However, clinical application of VF waveform measures is challenged by their modest prognostic performance and the requirement to pause CPR for analysis (as interrupting CPR reduces patient survival). In these works, we therefore sought to determine whether the performance of waveform measures could be improved and whether

measures could be calculated without interrupting CPR. Using retrospective analysis of out-of-hospital cardiac arrests, we investigated the potential for VF waveform measure calculation during short incidental pauses in CPR (Chapter 2) and during continuous uninterrupted CPR (Chapter 3, Chapter 4). We also sought to determine whether a novel prognostic algorithm could improve performance during uninterrupted CPR versus existing measures (Chapter 5, Chapter 6). In these investigations, we observed that waveform measures can indeed be calculated during incidental pauses in compressions a fraction of a second in length. We confirmed that measures are compromised when applied during uninterrupted CPR, but that their performance in presence of CPR artifact can be improved by incorporating ECG rhythm history, modifying parameters to mitigate chest compression artifact, and using machine learning to combine multiple measures. Furthermore, we observed that a novel algorithm specifically designed to predict defibrillation outcomes during CPR can further-improve prognostic performance by incorporating automatic CPR detection, adaptive filtering, patient characteristics, and features of the ECG designed to reduce the effects of CPR artifact. These results suggest potential for continuous real-time monitoring of patient status during resuscitation to guide administration of therapy and improve survival from out-of-hospital VF arrest.

TABLE OF CONTENTS

LIST OF FIGURES

LIST OF TABLES

ACKNOWLEDGEMENTS

We acknowledge the Emergency Medical Services personnel of Public Health – Seattle & King County without whom this work would not be possible, and appreciate their efforts to consistently provide life-saving treatment to victims of out-of-hospital cardiac arrest.

These works were supported in part by grants provided to the University of Washington by the Medic One Foundation, the Washington State Life Sciences Discovery Fund, the Laerdal Foundation, Philips Healthcare, and the National Institute for Biomedical Imaging and Bioengineering of the National Institutes of Health (T32EB001650). The content of these works is solely the responsibility of the author(s) and does not necessarily represent the views of the funding organizations or Public Health – Seattle & King County.

Tom Rea provided valuable direction as the principal investigator for our team (the UW Center for Progress in Resuscitation), and assisted greatly with writing and study design guidance as well as securing our research funds. Peter Kudenchuk provided valuable clinical perspectives related to electrophysiology and cardiac rhythms. Heemun Kwok provided essential statistics ideas and unique insights for the implementation of ECG classification and CPR detection. Jennifer Blackwood tirelessly maintained the patient database and compiled demographic and clinical variables. Carol Farenbruch provided additional statistics advice. Christopher Neils provided insightful technical advice and instruction. Mickey Eisenberg and his ideas for improving resuscitation constantly inspire our team. Members of the Philips AED research team (including but not limited to Dawn Jorgensen, Chenguang Liu, Stacy Gehman, and Vijay Tadipatri) provided valuable input on ECG analysis and defibrillation. The enthusiasm of rotating medical students Bryce Johnson, Jessica Doan, Shiv Bhandari, Danelle Hidano, and Peter Schoene was invaluable

to the efforts of our team. My doctoral supervisory committee members (Herbert Sauro, Heemun Kwok, Christopher Neils, Robert Bruce Darling, and Daniel Ratner) offered encouragement, perspective, and essential scientific advice over the course of my studies and research.

Finally, Dr. Lawrence Sherman provided constant, compassionate guidance as my advisor and mentor until his unexpected passing in early 2019. He will be greatly missed, and his love for learning, science, books, dogs, and technology will always be an inspiration.

Chapter 1. INTRODUCTION

1.1 BACKGROUND AND SIGNIFICANCE

Sudden cardiac arrest is a loss of blood flow to the body due to inability of the heart to effectively pump blood. It is a contributing cause of death in approximately 13.5% of all deaths in the United States (contributing to approximately 370,000 deaths per year).[1] Survival from cardiac arrest is low, varying regionally from 3-22% in the out-of-hospital setting, with much of this variation due to differences in the application and availability of treatment.[1,2] The high burden of this disease and variability in survival rates suggests opportunity to improve outcomes through the continued study of the mechanisms underlying cardiac arrest and through improvements in therapy, as even modest advances in treatment could potentially save thousands of lives every year.[3]

1.1.1 *Ventricles are Essential to Blood Flow*

The human cardiovascular system enables an exchange of by-products from cellular metabolism for the products necessary for cellular metabolism. This exchange is facilitated in part by blood, which carries carbon dioxide from the organs and their surrounding tissue to the lungs for release into the environment in exchange for oxygen, and transports oxygen back to the organs for diffusion into their surrounding tissue.[4] Proper function and contraction of the heart ventricles (Figure 1.1) is essential to blood flow. Specifically, deoxygenated blood is received from the venous system into the right atrium of the heart, passed into the right ventricle, and then ejected by contraction of the right ventricle into the pulmonary system for oxygenation through gas exchange in the alveoli. Newly-oxygenated blood is accepted from the pulmonary system into the left atrium and passed into the left ventricle, where it is then ejected at high pressure by contraction

of the left ventricle into the arterial system for distribution to the organs in the body. Therefore, in the absence of proper ventricular contraction, blood (and the oxygen it distributes) ceases to flow.

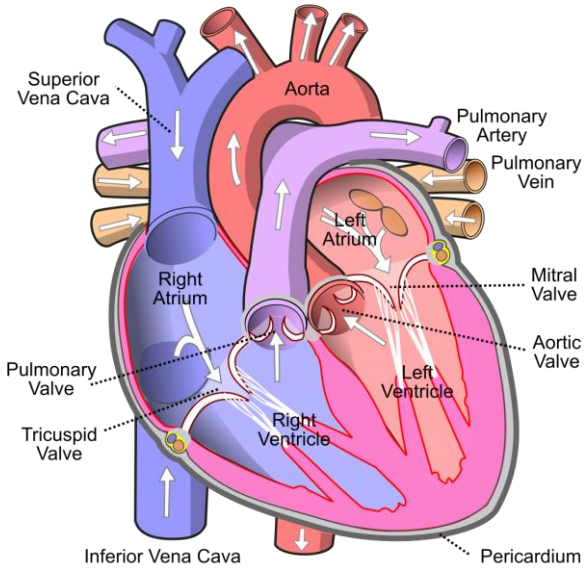

Figure 1.1 Human heart
Ventricles providing the driving force for blood flow in the body.

1.1.2 *Cardiac Myocytes are Electrically-Excitable*

Heart tissue contains electrically-coupled cardiac myocytes, which are branching elongated cells that form an interconnected electrical syncytium (Figure 1.2). The membrane potential of a cardiomyocyte describes the difference in ion concentrations inside versus outside the cell. A cardiac action potential in an individual cardiomyocyte is initiated when the membrane potential (typically resting at approximately -90mV) is increased above a voltage threshold (approximately -70mV) by ions flowing across gap junction connections at intercalated discs connecting neighboring cells. The above-threshold depolarization stimulus triggers a positive feedback sequence of inward positive ion flow.[4,5] The resulting action potential sequence is a sustained depolarization which can be transmitted to the next adjacent cell. The membrane potential of a

cardiomyocyte during an action potential changes in a distinct manner over time, corresponding to the net concentrations of ions (such as Ca^{2+}, Na^{+}, K^{+}) in the cell. Ion concentrations are controlled in a voltage- and time-dependent manner by a number of ion-specific transmembrane channels and pumps. (A basic description is provided in Figure 1.3 although a more comprehensive description is required to fully-describe these mechanisms.[5]) In a domino-like propagation of sequential action potentials from cell to cell, electrical excitation can spread through cardiac tissue. To ensure the forward propagation of action potential wavefronts, a normal action potential is only triggered when a cell is in an excitable state (Figure 1.3). An action potential is not triggered when a cell is in the absolute refractory period, and may be only triggered at a higher threshold outside the absolute refractory period but within the total refractory period. This prevents action potentials from occurring instantly after one another within the same cell, and thus ensures that action potentials propagate in a forward direction. Due to cell shape and the location of gap junctions, conduction of action potentials through cardiac tissue is anisotropic, moving primarily along the direction of the fibers.

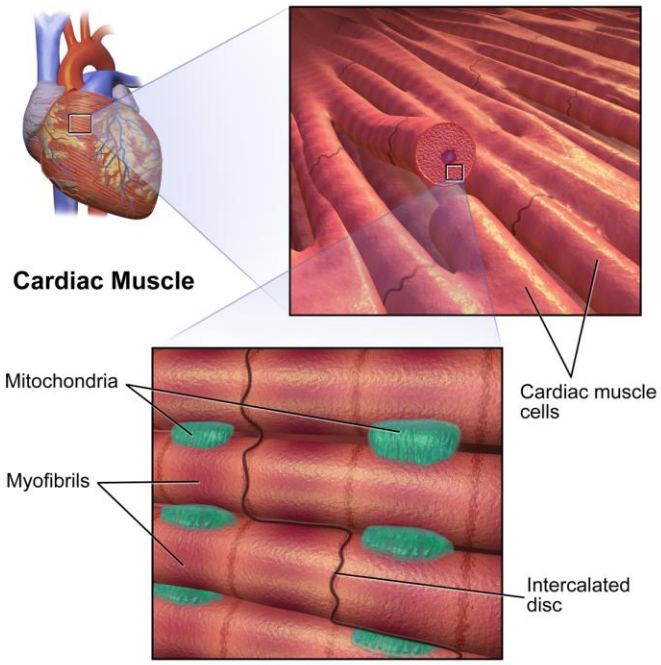

Figure 1.2 Cardiac myocytes
Cardiomyocytes are fiber-shaped and connected by intercalated discs.

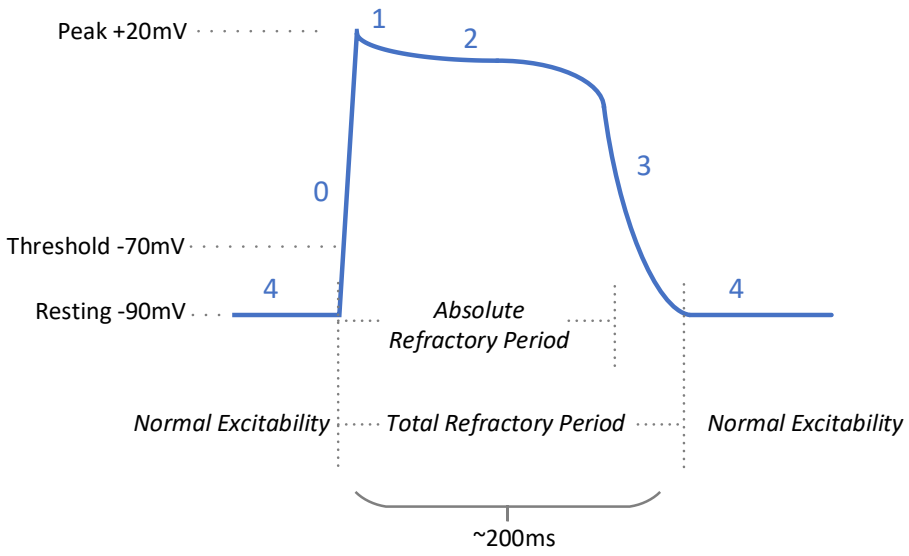

Figure 1.3 Cardiac action potential phases and membrane potential
(0) During action potential upstroke triggered by ion influx from a neighboring cell depolarization (if above the -70mV threshold), Na^+ ions quickly flow into the cell. (1) During initial repolarization, Na^+ stops flowing and K^+ flows out of the cell to begin repolarization. (2) During the action potential plateau, Ca^{2+} (and a small amount of Cl^-) flow into the cell while the outward K^+ flow is still ongoing, resulting in a temporary balance of charge flow. (3) During the final repolarization, Ca^{2+} flow stops and outward K^+ flow increases to bring the membrane voltage back to the resting potential. (4) During diastole, the resting potential is maintained by K^+ flow.

1.1.3 *Cardiac Myocytes Contract During Action Potentials*

Excitation-contraction coupling is the phenomena of physical cardiac myocyte contraction as a result of an electrical action potential. This excitation-contraction coupling results in propagation of tissue contraction in conjunction with propagation of electrical action potentials through the myocardium. Physical contraction of a cardiac myocyte relies on Ca^{2+} and adenosine triphosphate, and is described by the sliding filament theory. During phase 2 of the action potential (see Figure 1.3), a small amount of Ca^{2+} enters the cardiac myocyte. Because the surface of the myocyte is perforated with a number of transverse tubules which extend into the cell, incoming Ca^{2+} can be sensed deep inside the cell near the sarcoplasmic reticulum. This relatively small Ca^{2+} influx during an action potential activates Ca^{2+}-sensing receptors and triggers the release of large amounts

of Ca^{2+} stored within the cell's sarcoplasmic reticulum into the cytoplasm, which increases intracellular Ca^{2+} 100-fold. This process is sometimes referred to as calcium-induced-calcium-release. The presence of intracellular Ca^{2+} in the myocyte causes myofibril contraction, which involves actin-myosin binding, adenosine triphosphate hydrolysis, and ratcheting of myosin heads causing physical shortening of the myofibrils within functional units called sarcomeres (Figure 1.4). After contraction, Ca^{2+} in the cytoplasm is then pumped back into the sarcoplasmic reticulum, and the sarcomere is relaxed back to its original length. While a more complete description is recommended to fully-describe the details of this mechanism,[4,5] important concepts include the principle that cardiac myocyte contraction is signaled by a small Ca^{2+} influx during an action potential, which causes release of stored Ca^{2+} into the intracellular space to enable the contraction mechanism, and that this process also requires available adenosine triphosphate to provide the energy necessary for contraction.

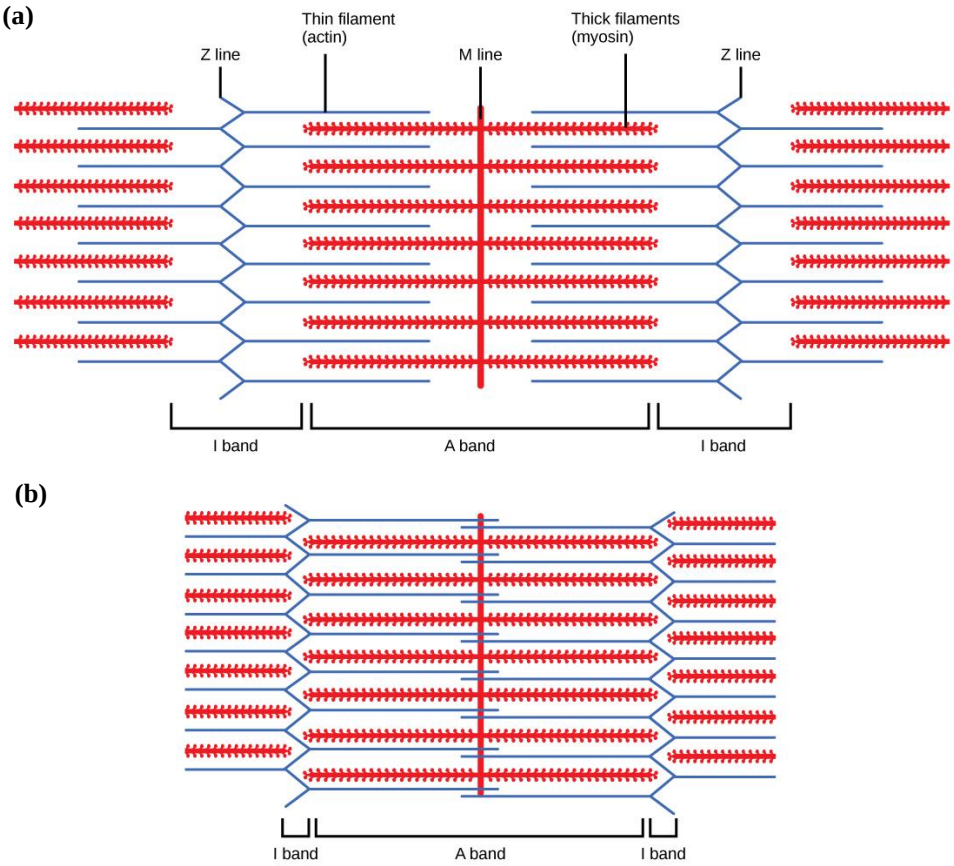

Figure 1.4 Sarcomeres are contractile units
Cardiac myocytes are composed of myofibrils. Myofibrils consist of thick myofilaments (myosin) and thin myofilaments (actin). A sarcomere is a single contractile unit within a myofibril arbitrarily defined as the region between the Z-lines. During contraction, Ca^{2+} binds to regulatory proteins on the thin actin filaments which unblock actin in a concentration-dependent manner, allowing myosin heads on the thick filaments to bind to actin and perform a ratcheting maneuver using energy from adenosine triphosphate hydrolysis. The myosin head ratcheting pulls actin filaments inward towards the M-line, changing the overall state of the sarcomere from a relaxed state (a) to a contracted state (b), thus shortening the myofibril.

1.1.4 *Cardiac Cycle Involves Coordinated Action Potential Propagation*

Effective pumping of blood from the heart during a cardiac cycle is enabled through a sequence of action potential propagations in cardiac tissue that are electrically-coordinated via the sinoatrial node, atrioventricular node, and His-Purkinje system (see Figure 1.5). Pacemaker cells, in contrast to cardiac myocytes, are especially-conductive cells that compose the network of nodal and His-

Purkinje tissues and have specialized ion channels that enable them to depolarize autonomously. The ability to autonomously depolarize allows these cells to initiate action potentials in cardiac myocytes at a regular pace. The relative intrinsic frequency of membrane voltage oscillation in these pacemaker cells is hierarchal based on their location in order to provide a top-down redundant sequence of pacing sites to ensure that the heart (especially the ventricles) continues to beat if one location is compromised: The sinoatrial node intrinsic rate is greater than the atrioventricular node rate, which in turn is greater than the His-Purkinje tissue rate. During a normal cardiac cycle, only pacemaker cells in the sinoatrial node originate initial action potential propagation. The initial action potential from the sinoatrial node spreads through the atrial cardiac myocytes (causing the atria to contract) and arrives at the atrioventricular node. The conduction velocity of the atrioventricular node is relatively slow (0.05m/s) compared to the conduction in cardiac myocytes (0.5m/s), which allows time for atrial contraction to move blood down into the ventricles prior to ventricular contraction. The atrial and ventricular chambers are electrically-isolated from one other with the exception of the atrioventricular node, ensuring that depolarization is conducted from the atria to the ventricles only through the relatively-slow atrioventricular node. Conduction continues to the His bundle and through the bundle branches to the branching network of Purkinje fibers which terminate in the ventricular myocardium. The conduction velocities of bundle branches and His-Purkinje tissue are 2m/s and 4m/s, respectively (as compared to 0.5m/s for cardiomyocytes).[4] This ensures that action potentials in the ventricular tissue are initiated by the His-Purkinje system in a simultaneous fashion rather than traveling top-down through the ventricular cardiomyocytes alone (which would likely only serve to force blood down towards the bottom of the ventricles rather than ejecting it up through the pulmonary artery and aorta). The Purkinje fibers in the ventricles receive the stimulus through the bundle branches and initiate action

potentials from their locations in the endocardium along the inner lining of the ventricular walls, allowing ventricular depolarization to begin at the ventricular endocardium and propagate through the thickness of the ventricular wall to the epicardium nearly simultaneously throughout the ventricles.[6] This allows the ventricular walls to contract inwardly at approximately the same time for maximum pumping efficacy.

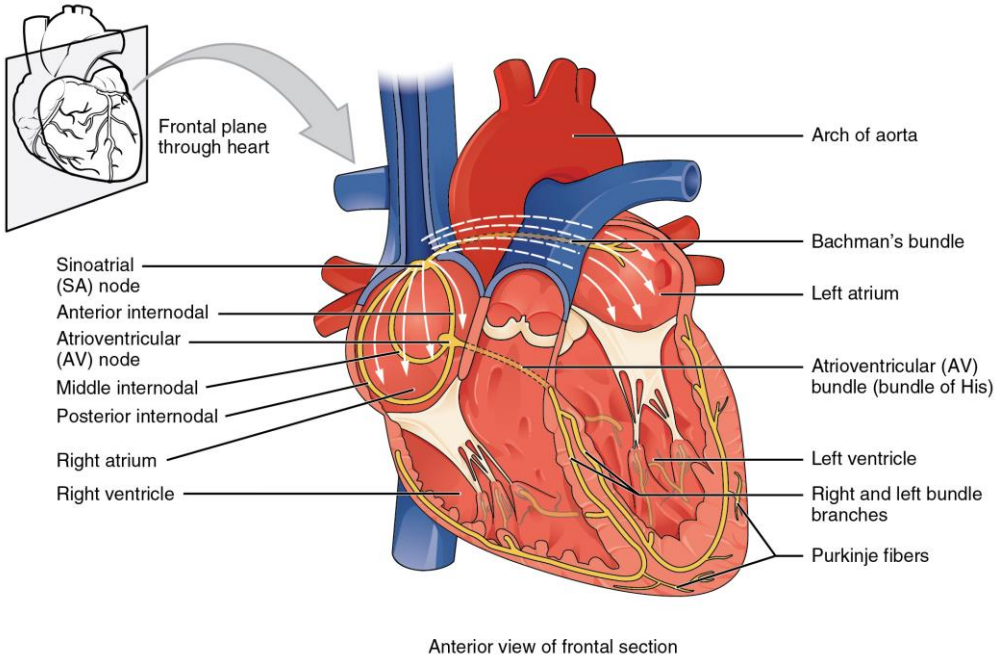

Image: "2018_Conduction_system_of_heart" by OpenStax is licensed under CC BY 3.0.

Figure 1.5 Electrical system of human heart
A normal cardiac cycle is initiated by the sinoatrial node and eventually distributed throughout the ventricles via the His-Purkinje network.

1.1.5 *Electrocardiogram*

Depolarizations in the heart are conducted into surrounding tissue and can be detected on the surface of the body.[4] The electrocardiogram (ECG) is measured by placing electrodes on the skin and monitoring the potential between them. This potential represents the net electrical vector of all depolarizations and repolarizations occurring in the myocardium from the perspective of the

electrodes. In the lead II configuration, the positive electrode is placed towards the left leg and the negative electrode towards the right arm. Thus, a propagating depolarization wave in the heart traveling down towards the apex of the ventricles will be reflected as a positive change in the ECG voltage. Depolarizations largely perpendicular to the electrode lead axis will therefore produce only small changes in the ECG. A normal cardiac cycle can be observed as a distinctive pattern in the ECG, and is typically illustrated from a lead II perspective with the Q-R-S complex from ventricular depolarization reflected as a sharp positive voltage increase (Figure 1.6).

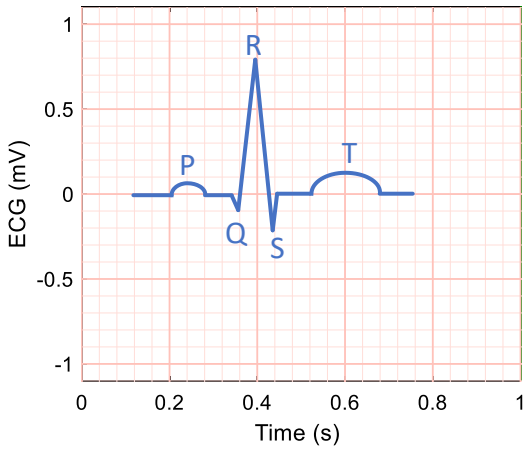

Figure 1.6 ECG for normal cardiac cycle
Stylized representation of a single normal cardiac cycle. (P) Atrial depolarization. (Q-R-S) Ventricular depolarization. (T) Ventricular repolarization.

1.1.6 *Ventricular Fibrillation is a Lethal Arrhythmia*

Ventricular fibrillation is an arrhythmia characterized by uncoordinated, low-amplitude electrical activity in the ventricular myocardium, resulting in ineffective asynchronous contraction of ventricular cardiomyocytes and a complete loss of blood flow.[4] This uncoordinated electrical activity manifests in the ECG as chaotic high frequency waves with varying levels of underlying structure and size depending on a number of factors (such as how long the VF has persisted) (Figure 1.7).[7–12] Reentry is the onset of VF (Figure 1.8) and generally is caused when a conduction

pathway is prematurely re-stimulated by a previously-occurring action potential rather than by a new one from a normal cardiac cycle.[4] Reentry may thus occur when an action potential wave encounters a heterogenous region of tissue with compromised conduction, such as a patch of scar tissue from a prior myocardial infarction or a region of tissue that is slightly depolarized from ischemia. When a propagating wave from a normal action potential encounters such a heterogenous region, the wavefront may break apart and circle back to 'chase its tail' (i.e. reentry), thus forming a wave of cyclically-depolarizing tissue.[13] Reentry results in circuits (rotors) in the ventricular myocardium which have some degree of underlying structure, but also produces random meandering wavefronts.[14] Rotors and vortexes of action potential propagations during VF are three-dimensional rotating waves, are relatively high-frequency, and can be self-perpetuating. The refractory period and conduction velocity of cardiac myocytes play an important role in the initiation and perpetuation of VF.[4] Lagged wavefront fragments propagating through a slower-conducting heterogeneity in tissue can activate adjacent tissue only if that tissue is excitable and not within the absolute refractory period (hence, medications that affect refractory period may reduce the likelihood of reentry). While reentry can occur as a result of an abnormal heterogeneity in tissue, reentry can also occur in the absence of a local tissue heterogeneity in an otherwise healthy heart due to external stimulus, such a premature local depolarization in the myocardium caused by physical impact or by an electrical shock applied during ventricular repolarization.[14,15] Whether a stimulus will initiate reentry depends on factors such as the refractory state of the tissue at the time the stimulus is applied; for instance if the ventricles are within the absolute refractory period during a transient stimulus, reentry is less likely.

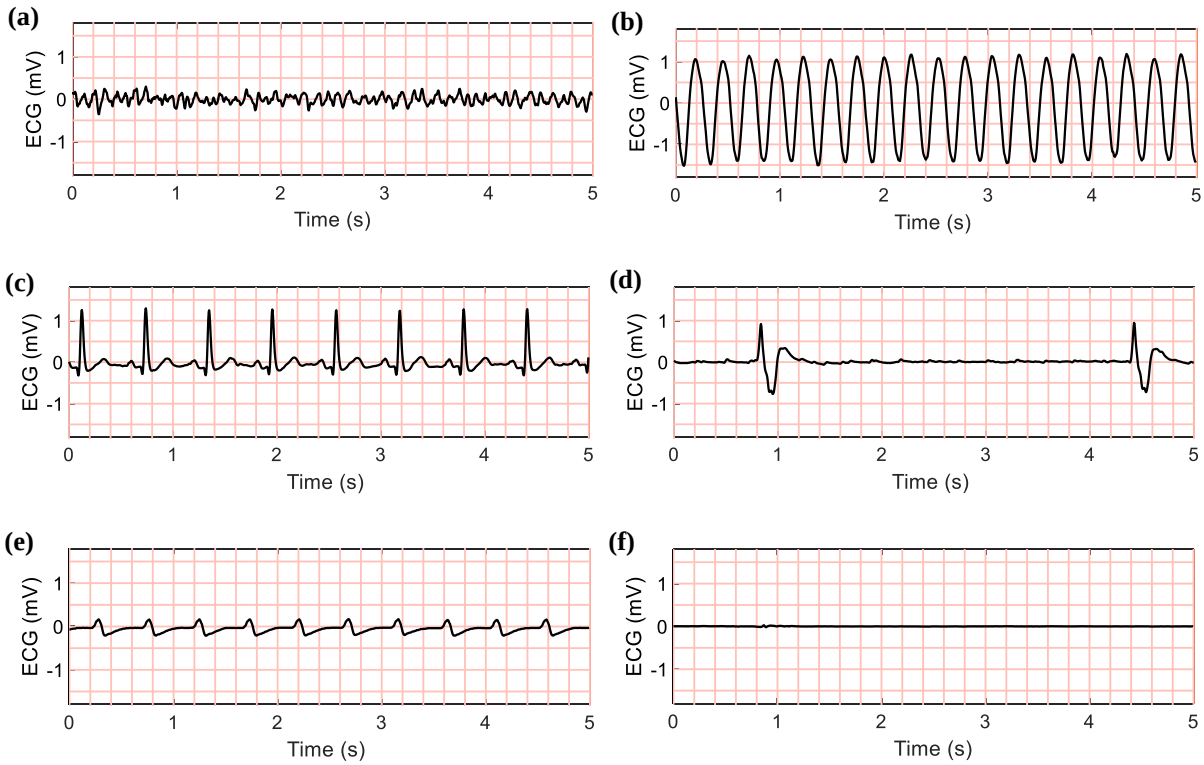

Figure 1.7 ECG rhythm examples
Select examples of ECG rhythms recorded through defibrillator paddles during treatment of cardiac arrest. (a) Ventricular fibrillation. (b) Ventricular tachycardia. (c) Normal sinus rhythm. (d) Bradycardia. (e) Pulseless electrical activity. (f) Asystole. Further description of rhythm types is available elsewhere.[16]

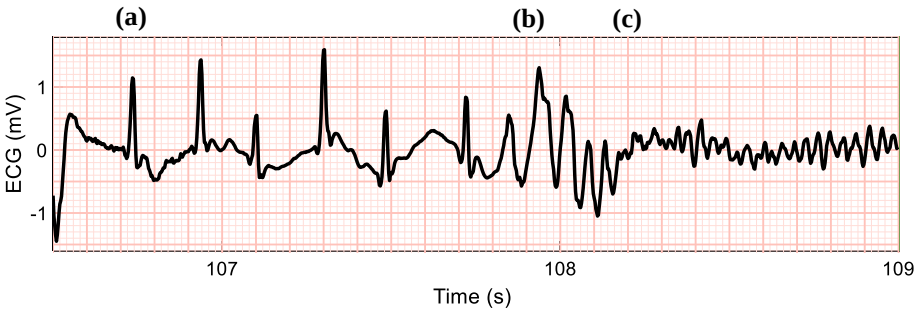

Figure 1.8 Onset of ventricular fibrillation (reentry)
Transition from (a) sinus rhythm to (b) ventricular tachycardia with a single rotor for only a few cycles during reentry to (c) sustained ventricular fibrillation as the rotor breaks apart.

VF is hypothesized to be sustained by multiple underlying mechanisms such as a large mother rotor sweeping through a large volume of ventricular myocardium or multiple smaller rotors.[17] The number of independent rotors in the human heart during VF can range from a single rotor up to a maximum of 10-20.[18] Less-structured fibrillation presents as disorganized localized contractions throughout the myocardium as a result of random wavebreaks and interactions originating from rotors or meandering waves.[13] Individual driving rotors in tissue can have varying morphologic characteristics (see Figure 1.9 for generic wave examples).[19] As VF progresses from initial reentry, rotors may continually fragment throughout the anisotropic ventricular tissue as the propagations increasingly encounter heterogeneities and boundaries at different angles while simultaneously colliding and self-terminating, causing the VF to become generally more disorganized and chaotic over time.[20,21] VF can thus be considered both a deterministic and stochastic process that exhibits a variable amount of underlying structure that is difficult to quantify, with the amount of structure generally decreasing over time as VF progresses. Ultimately, the exact mechanisms of VF are not clearly understood, and the complex behavior of VF can only be partially explained by any of the multiple theories proposed to describe it.[14]

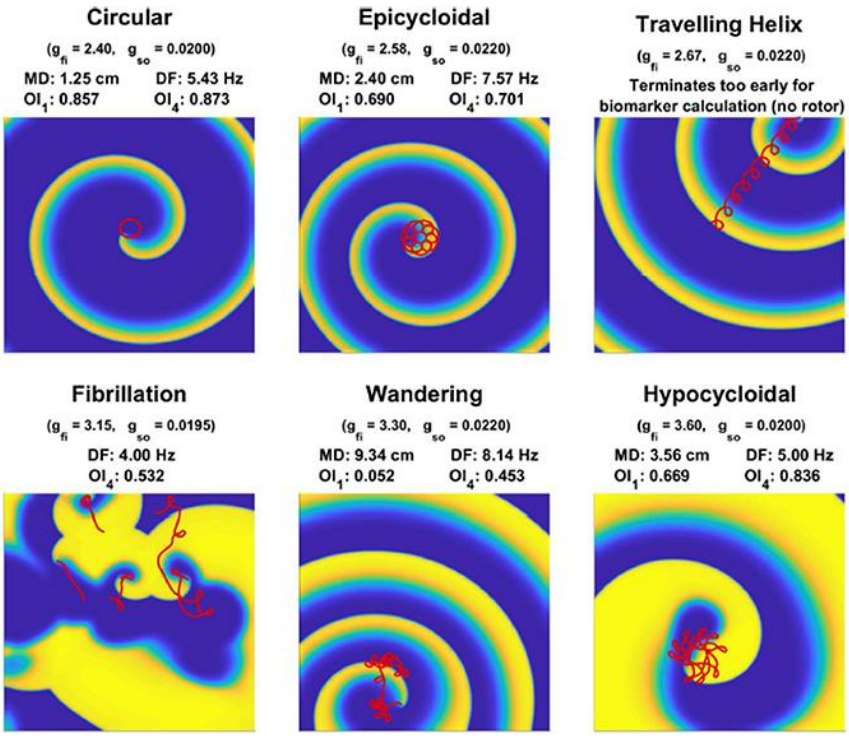

Figure 1.9 Generic wave examples
Examples of simulated propagations of action potential wavefronts. Note that this example is only representative of basic wave types, and is simulated in a homogenous medium (as opposed to anisotropic cardiac tissue).

1.1.7 *Ventricular Fibrillation Degrades Due to a State of Ischemia*

During VF, coronary blood flow to the heart muscle tissue itself is ceased, causing a state of ischemia in the tissue. The exact mechanisms by which ischemia affects the ECG are not all completely understood.[4] It is known however that ischemia results in reduced adenosine triphosphate concentrations, compromising the ability of cells to regulate the ion channels essential for normal action potentials and contraction. The initial Na^+ influx during the action potential upstroke is for instance slowed during ischemia, causing reduced conduction velocity of action potentials through cardiomyocyte tissue.[4] Intracellular Ca^{2+} concentrations also increase during ischemia, and may trigger spontaneous depolarizations (i.e. afterdepolarizations) during phase 3

or the beginning of phase 4 in cardiac myocytes.[4] Hypoxia and its effects are particularly exacerbated during the energetically-demanding arrhythmia of VF as compared to other cardiac rhythms, leading to a rapid decline of cardiomyocyte tissue contractile function during this arrhythmia. The effects of prolonged ischemia and resulting depletion of high-energy phosphates in the myocardium can have a visible effect on the VF ECG, reducing the speed, maximum amplitude, sharpness, and organization of the fibrillating waveform as ischemia persists.[22–25] Eventually, if left untreated VF progresses to a state of asystole (lack of electrical activity in the ECG) once the myocardium is severely metabolically compromised and depolarizations can no longer occur.

1.1.8 *Out-of-Hospital Ventricular Fibrillation Arrest*

Every year, approximately 360,000 persons are treated for cardiac arrest by emergency medical services (EMS) personnel in an out-of-hospital setting, while approximately 210,000 are treated for cardiac arrest that occurs in-hospital.[2] Survival from out-of-hospital cardiac arrest is poor: Of persons treated for out-of-hospital arrest, over 300,000 die annually.[26] VF causes approximately 20% of all out-of-hospital cardiac arrests in the United States, and results in approximately 50,000 EMS-treated out-of-hospital cardiac arrest deaths in the United States every year.[3] Survival rates from out-of-hospital VF arrest are approximately 18% overall, but can vary regionally from approximately 3-40%.[3,27,28] This disparity in mortality suggests that different regional treatment approaches and response times greatly affect outcomes, and that there may be opportunity to improve survival through continued optimization of current treatment and development of novel therapies.

1.1.9 *Current Therapy*

1.1.9.1 Defibrillation Shock

Defibrillation shock is the essential, definitive therapy for VF. Shock is administered by applying a current through specialized defibrillator paddle electrodes attached to the skin near the sternum and lower left side of the chest such that the current passes through the heart (Figure 1.10). Using a biphasic waveform, a defibrillation shock delivers a total of 150-360 J of energy to the patient.[15] The current delivered to the myocardium causes a bulk hyper- and de-polarization in the cells which results in termination of fibrillation wavefronts.[29] Once the myocardium is electrically-excitable again following shock, the autorhythmic pacemaker cells (e.g. the sinoatrial node) can reinitiate normal action potential propagations and restore a normal sinus rhythm if there are sufficient metabolic reserves for contraction in the myocardial tissue.

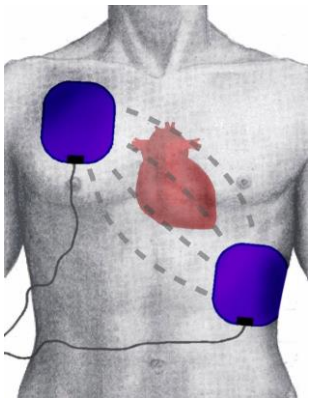

Figure 1.10 Defibrillation
Defibrillation shock by a defibrillator is administered through paddle electrodes on the chest.

1.1.9.2 Cardiopulmonary Resuscitation

Cardiopulmonary resuscitation (CPR) provides circulation during resuscitation and consists of chest compressions and artificial respirations. The perfusion that CPR provides counteracts the effects of ischemia on the brain and myocardium. Thus, CPR prolongs the time that VF can remain

active before degrading into asystole (extending the time cardiac myocytes are able to function), therefore increasing the time after VF onset that a defibrillation may be successful.[30] Current guidelines dictate a target chest compression rate of 100-120 compressions per minute during CPR.[31] Best-practice chest compressions should be allowed to fully recoil, be delivered at adequate depth (e.g. ≥5 cm), and be minimally-interrupted. Ventilations (forced artificial respirations) are initially provided between alternating periods of chest compressions and ventilations at a ratio of 30 compressions to 2 ventilations; then, once the patient is intubated, continuous compressions may be applied while ventilations are administered at a target rate of 10 ventilations/min.[31,32]

1.1.9.3 Medication

During resuscitation from out-of-hospital VF arrest, guidelines dictate administration of epinephrine every 3-5 minutes as well as amiodarone if reentry occurs after initial shock.[31] Amiodarone is an antiarrhythmic drug used to prevent recurrence of VF after repeated defibrillation attempts by inhibiting K^+ channels. Inhibition of K^+ channels slows cardiac myocyte repolarization caused by inward K^+ flow during phase 3 of the cardiac action potential (see Figure 1.3), thus prolonging the refractory period. A prolonged refractory period may reduce the likelihood of VF reentry, thus increasing likelihood of return of circulation after shock (although evidence for improvement in long-term survival using Amiodarone is not definitive).[26,33]

During resuscitation, CPR is estimated to only provide approximately one third of normal cardiac output; hence, increasing the effect of CPR is beneficial to counteracting the effects of ischemia on the brain and heart.[34] Epinephrine is a vasopressor (i.e. it constricts the blood vessels to raise blood pressure) that increases cerebral and coronary perfusion during chest compressions, thereby improving the effectiveness of CPR.[35] If administered during the first 10 minutes of CPR

during resuscitation, epinephrine has been demonstrated to improve neurologically-intact survival.[36]

1.1.9.1 Resuscitation Protocol

Treatment of cardiac arrest follows a 'chain-of-survival' theme that emphasizes the importance of early administration of therapy. The chain-of-survival emphasizes early arrest identification and emergency medical services activation, early CPR, early defibrillation, and advanced cardiovascular life support and post-resuscitation care.[37,38] Current American Heart Association guidelines for treatment of out-of-hospital cardiac arrest caused by VF are therefore centered around immediate application of a defibrillator to monitor the ECG and deliver defibrillation shock with minimal delay. These guidelines prioritize early shock and near-continuous CPR.[31] Analysis of the ECG to determine whether VF is present occurs initially once the defibrillator is attached and then occurs subsequently during scheduled pauses in CPR at fixed 2-minute intervals. CPR pause is required for ECG rhythm classification due to electrical artifact introduced into the ECG from chest compression perturbation of the defibrillator electrodes.[39] Defibrillation shocks are subsequently administered during these scheduled CPR pauses if VF is detected during rhythm classification. There are two variations of American Heart Association guidelines for treatment. First-responder emergency medical technician firefighters provide Basic Life Support,[32] which includes automatic defibrillator-guided defibrillation and a 30:2 compression-to-ventilation ratio, while paramedics trained in Advanced Cardiovascular Life Support[31] follow a similar protocol but with the option to employ manual ECG analysis, manual shock delivery, and intubation to allow continuous ventilations during chest compressions. Paramedics can also administer vasopressor and antiarrhythmic medications. A simplified protocol representation is given in Figure 1.11.

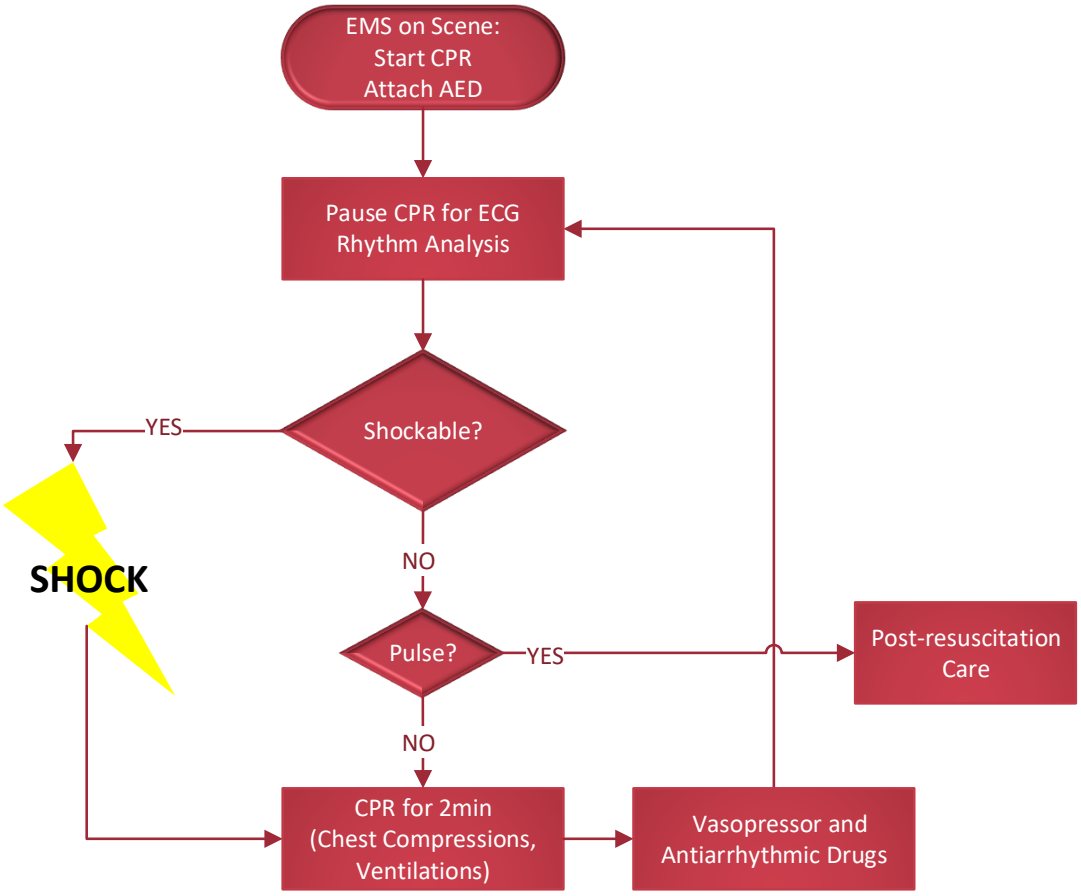

Figure 1.11 American Heart Association resuscitation protocol
Simplified representation of treatment for out-of-hospital VF arrest (AED = automated external defibrillator, CPR = cardiopulmonary resuscitation, ECG = electrocardiogram).

1.1.10 *Shortcomings of Current Therapy*

There are two major shortcomings in current treatment. The first is that delivering immediate shock (when VF is detected) is not necessarily beneficial to the patient because immediate shock may not result in a successful defibrillation depending on the metabolic state of the myocardium.[40–42] The second shortcoming is that ECG analysis (e.g. rhythm classification to detect VF) requires pause in CPR due to chest compression artifact,[34,39,43–45] but ceasing CPR even for a short pause results in a drastic, instant loss in perfusion pressure that reduces patient survival rates.[46–48]

1.1.10.1 Shortcoming 1: Fixed Timing for Shock Delivery

Delivering immediate shock once VF is detected may not result in successful outcome depending on the metabolic state of the myocardium.[22] Thus a significant fraction of shocks are unsuccessful under current protocol.[49] However, current guidelines dictate immediate defibrillation when VF is detected regardless of the underlying state of the myocardium.[31] In addition, rhythm analysis only occurs at 2-minute intervals; hence, reentry into VF after a failed defibrillation attempt may persist for two minutes without the arrhythmia being detected or receiving a shock, and treatments are only adjusted in response to the patient's condition evaluated at the 2-minute intervals. As stated previously, during ventricular fibrillation a state of ischemia persists in the myocardial tissue as coronary circulation ceases. Progressive hypoxia causes adenosine triphosphate levels in the myocardium to rapidly deplete[25] and become insufficient for cardiac muscle contraction.[4,22] As the metabolic state of cardiac tissue deteriorates over time, the likelihood of successful defibrillation decreases, since cardiac tissue with reduced contractile function may be unable to respond to shock. (For instance, in the out-of-hospital setting, survival from VF decreases approximately 7-10% per minute VF is untreated, indicating that a delay of mere minutes – or even seconds – can affect the ability to treat VF.[50])

Therefore, while immediate defibrillation is ideal in cases where the heart is likely to convert to organized rhythm after shock, defibrillation should be delayed if the metabolic state of the myocardium is severely compromised. This delay may allow partial reperfusion of cardiac tissue with chest compressions and vasopressors, thus increasing the likelihood that a sinus rhythm and circulation will result from a defibrillation attempt. Indeed, in cases where VF has persisted >4-5 minutes (and hence the myocardium is assumed to be in a metabolically compromised state), human studies have demonstrated improved outcomes when initial shock is delayed to first allow CPR to perfuse the myocardium prior to shock.[40–42] This finding resulted in 2005 guideline

recommendations to delay initial shock and allow 1-3 minutes of CPR for patients where VF was initially unwitnessed (i.e. when VF was assumed to have persisted for a prolonged period).[51–53] However, these guidelines failed to show improved outcomes, and current guidelines have thus since reverted to recommending a one-size-fits-all protocol of early defibrillation in all instances regardless of the assumed state of the myocardium.[27,31] The failure to definitively improve outcome using delayed shock when VF is assumed to be in a compromised state may have been due to difficulty in assessing time since VF onset in the out-of-hospital setting, especially for unwitnessed arrest. Furthermore, time since VF onset is only a surrogate estimate of the true state of VF myocardium; hence even if VF duration is known, VF duration alone may not accurately represent the condition of the myocardium and its potential to sustain coordinated contractions following defibrillation. Therefore, rather than relying on a surrogate of patient status (such as witnessed versus unwitnessed arrest), an alternative method to directly evaluate the physiologic state of the myocardium (ideally using the already-available ECG) may provide an improved means to prioritize shock-versus-CPR on a patient-specific basis.

1.1.10.2 Shortcoming 2: CPR Pause

CPR pause during resuscitation results in a rapid drop in perfusion pressure that is detrimental to patient outcome. Some data suggest that CPR pause reduces the chance of survival by up to approximately 18% for every additional 5-second pre-shock CPR pause when pauses are on the order of $\leq$40 seconds.[46–48] Thus ideal resuscitation treatment would involve continuous CPR. Current protocol, however, dictates pause in CPR to allow ECG rhythm analysis due to the current limitations of ECG classification algorithms.[31,54] Rhythm analysis and charging during a resuscitation guided by an automated external defibrillator (AED) typically requires a total chest

compression pause on the order of approximately 16-22 seconds prior to shock in the out-of-hospital setting, although estimates vary across studies.[47,55]

As an example of the shortcomings of required CPR pause and fixed protocol, Figure 1.12 illustrates treatment of a hypothetical VF case under current protocol. In this example the patient is in prolonged VF at the start of treatment, but following current protocol the VF is shocked prematurely (and ineffectively) during the first scheduled CPR pauses. The metabolic state of the myocardium is only improved to a point that VF is amenable to shock after several CPR cycles. The requirement to pause CPR for rhythm analysis is detrimental not only because of loss in perfusion pressure, but because the requirement to pause for analysis limits decision-making and administration of shocks to 2-minute intervals rather than in a continuous real-time manner.

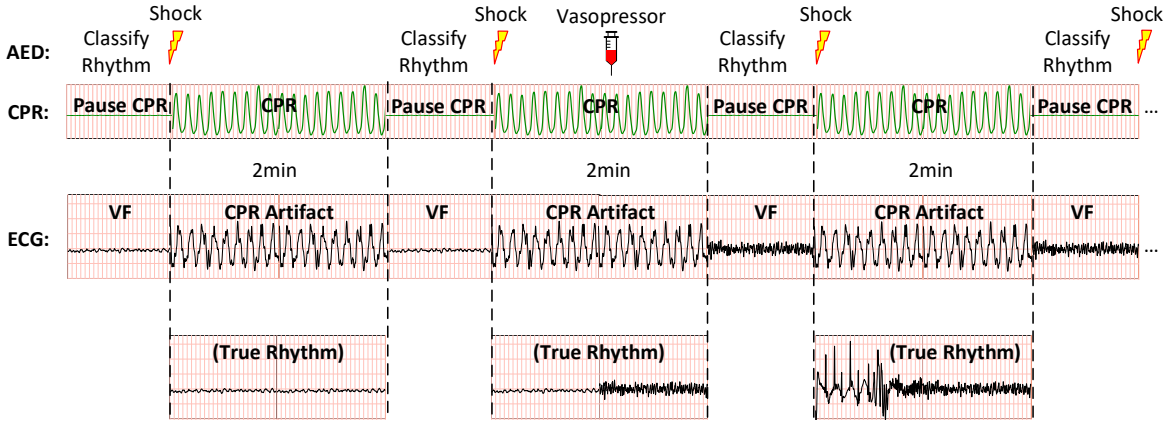

Figure 1.12 Hypothetical VF arrest treatment example with current protocol
Stylized representation of current protocol for initial treatment of a VF arrest. CPR is paused for rhythm classification, which hinders progression of VF from a hypoxic state to a robust state that is responsive to shock. The true underlying rhythm is indicated beneath the ECG for illustration. (AED = automated external defibrillator, CPR = cardiopulmonary resuscitation, ECG = electrocardiogram, VF = ventricular fibrillation).

1.1.11 *Ideal Therapy*

Treatment of VF arrest is currently constrained in part by the limitations of ECG algorithms. Ideally, continuous rhythm classification would occur without interruption in chest compressions

(Figure 1.13). Furthermore, continuous prognostic assessment of the patient's myocardial status (once VF is detected) could potentially indicate when drugs and continued CPR should be applied versus when an immediate defibrillation shock is likely to result in return of circulation (Figure 1.14). Under such a protocol, CPR would only be paused to deliver a shock. Hence there is consensus in literature that an ideal algorithm able to perform real-time rhythm analysis and real-time prognostic assessment of VF could potentially improve survival by minimizing pauses in chest compressions while prompting the rescuer to provide CPR, defibrillation, or other interventions as needed based on the real-time status of the patient.[45,56]

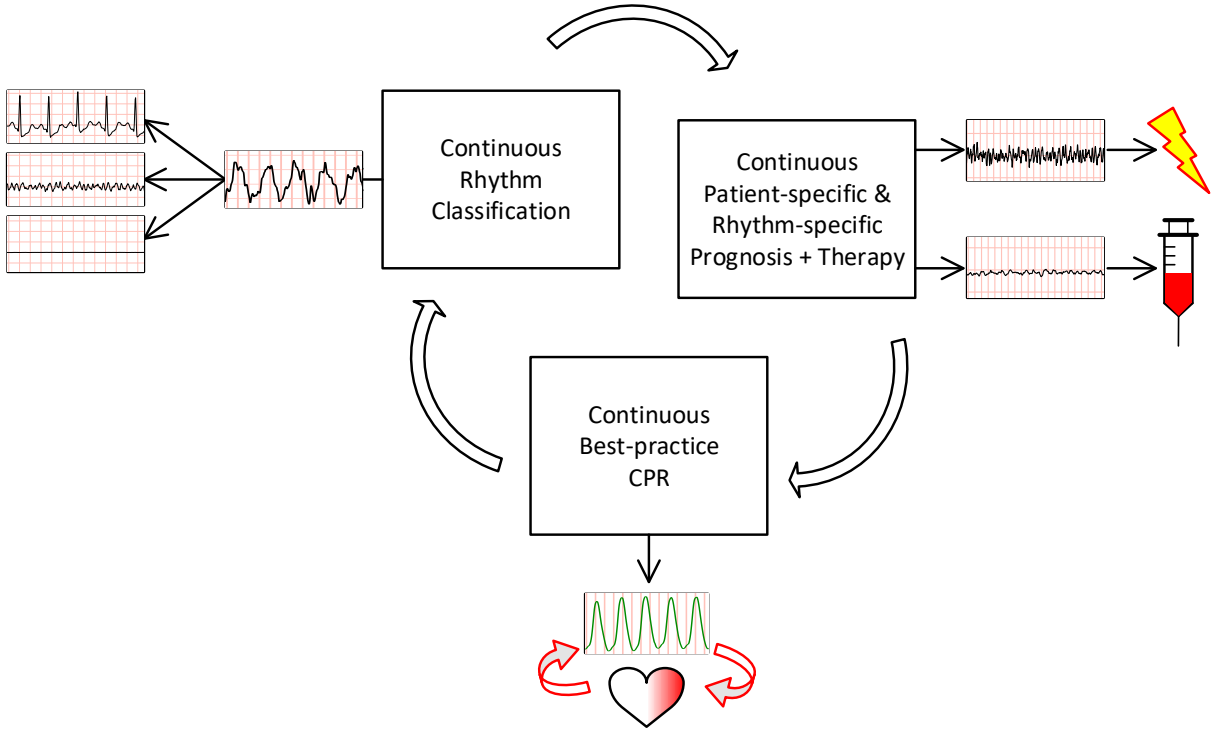

Figure 1.13 Concept of ideal treatment for VF arrest
Ideally, rhythm classification, prognostic assessment of the myocardium, and CPR would be conducted continuously. In the case of VF during cardiac arrest, prognostic assessment of patient status during VF would prompt continued CPR or medications until a shock is was predicted likely to result in a pulsatile rhythm; only then would CPR be paused to allow shock.

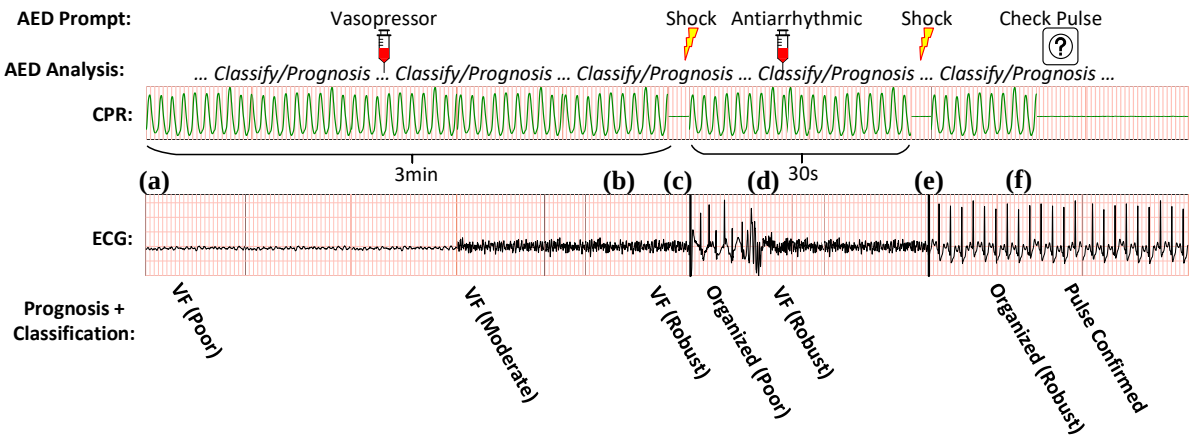

Figure 1.14 Stylized example of ideal protocol for hypothetical VF arrest
Idealized protocol incorporating rhythm classification and VF quality assessment continuously during CPR. (a) VF with poor prognosis is not shocked initially (as would be dictated by current protocol), but rather given continuous uninterrupted CPR with vasopressors until the VF is robust enough to respond to shock. (b) VF is thus restored to a robust state more quickly than it would under a protocol with periodic CPR pauses. (c) VF is shocked once deemed robust, and converts briefly into organized rhythm after shock. (d) Reentry into VF following initial shock is detected immediately during CPR, with antiarrhythmic drugs prompted. (e) Robust VF is shocked immediately which results in return of organized sinus rhythm. (f) Normal sinus rhythm is evaluated during compressions and predicted to be robust and likely pulse-generating; therefore, compression pause is prompted to check pulse and confirm return of circulation. (AED = automated external defibrillator, CPR = cardiopulmonary resuscitation, ECG = electrocardiogram, VF = ventricular fibrillation).

1.1.12 *Ventricular Fibrillation Waveform Analysis*

Quantitative ‘measures’ of the ventricular fibrillation waveform have been proposed to estimate the state of the myocardium based on the ECG. These measures of the VF ECG may offer a more direct means to evaluate patient status than relying on time since VF onset or other surrogates. Measures of VF are based on ECG frequency, amplitude, and organization, and are associated with likelihood of shock success and time since VF onset.[34,45,57] (Further background on existing waveform measures is provided in section 4.8.) Importantly, VF waveform measures have been observed to reflect the metabolic state (e.g. adenosine triphosphate concentrations) of myocardial

tissue.[22,58] Some studies have even suggested that VF waveform measures are associated with the underlying cardiac etiology during arrest (i.e., ischemic versus non-ischemic).[59–61] Waveform measures therefore offer a means to assess the robustness of VF and potentially guide shock timing, such as whether a shock should be delayed to allow additional CPR or be administered immediately.[62,63] However, overall performance of waveform measures remains modest, with area under the receiver operating characteristic curve (AUC) values typically between 0.70-0.84 for predicting patient outcomes in validation studies.[64,65] Hence when applied prospectively, waveform measure-guided therapy did not definitively result in improved survival.[66] Improvements to waveform measure performance and application strategy may therefore be required to enable clinical use.

One major shortcoming of VF waveform measures is that they currently require chest compression pause for accurate evaluation; hence, if implemented in conjunction with rhythm classification under current protocol, measures would be limited to assessing VF only at scheduled 2-minute intervals.[34,39,43–45,67] Ideally, waveform measures would continually monitor the state of the myocardium, with or without CPR, to provide instantaneous notification when shock is likely to be successful so that compressions could be ceased for defibrillation only when the rhythm is VF and the waveform measure predicts shock is likely to be successful.[45] While it has been demonstrated that CPR artifact may affect waveform measures, reduction in waveform measure performance due to CPR artifact has not been directly evaluated in humans and it is unclear to what degree waveform measures are affected by CPR.[68,69]

1.2 Scope of Current Investigation and Related Collaborative Works

1.2.1 *Scope of Current Investigation*

The current investigation explores prognostic evaluation of out-of-hospital cardiac arrest patients undergoing ventricular fibrillation. This investigation complements related collaborative studies led by other members of our group which examine rhythm classification, CPR administration, or factors related to VF arrest cause and outcome (Figure 1.15). These investigations by our group and collaborators collectively support the concept of an ideal defibrillator-guided resuscitation protocol involving continuous rhythm classification, continuous CPR, and continuous prognostic assessment of patient status to guide patient-specific therapy.

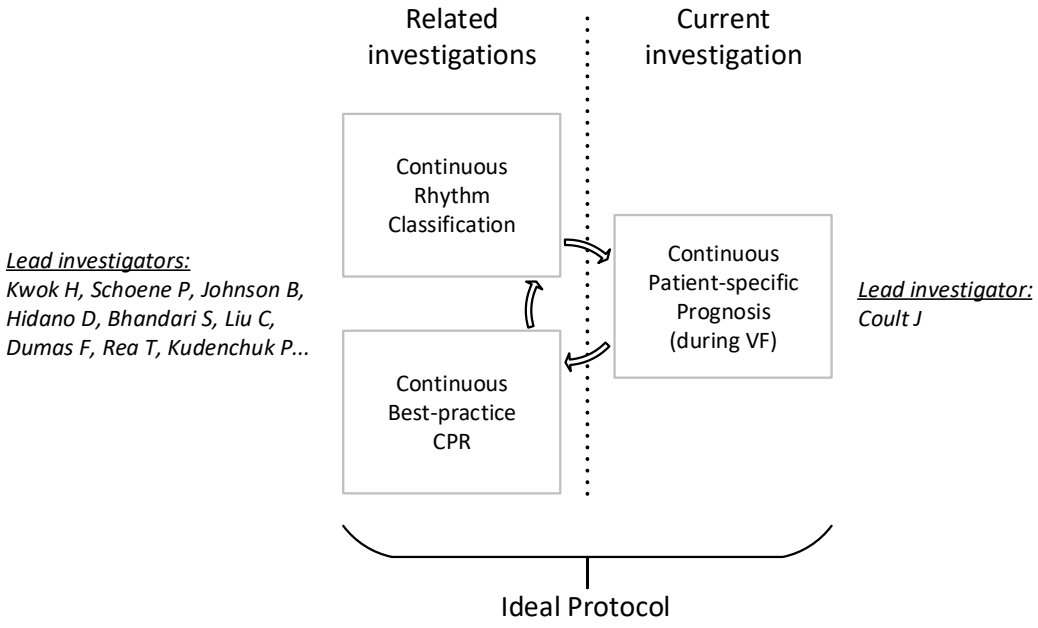

Figure 1.15 Scope of the current investigation versus related investigations by group
The current investigation examines the potential for defibrillator-guided patient prognosis (during ventricular fibrillation specifically), and complements related works conducted by our group and collaborators.

1.2.2 *Key Findings of Related Investigations by Our Group*

Here, related investigations led by members of our group or conducted in collaboration with our group are described; these related studies support the concept of continuous rhythm classification, continuous CPR, and continuous prognostic assessment. For optional expanded reading, abstracts from peer-reviewed publications of these works (with links to their respective manuscripts) are provided in Chapter 8.

1.2.2.1 Rhythm Classification During Chest Compressions

Current protocol for treatment of out-of-hospital VF arrest requires CPR pause for classification of the ECG rhythm by the AED or paramedics (to determine if the rhythm is shockable). Prior studies have evaluated the potential for rhythm classification during chest compressions using techniques such as adaptive filtering; however, such methods have generally not demonstrated sufficient accuracy for clinical application.[39,44] Works by our group have thus investigated rhythm classification during chest compressions by calculating features to describe high-frequency content in the ECG (Figure 1.16) and by leveraging the temporal sequence of analysis buffers to improve accuracy (Figure 1.17), in contrast to current algorithms which typically limit analysis to lower-frequency ECG morphology observed in an isolated analysis buffer.[70–73] A subsequent industry collaboration with our group thus resulted in a retrospective validation of a read-through-CPR classification algorithm conducted by a leading defibrillator manufacturer.[74] Given these advances, as well as a recent prospective pilot investigation by another leading defibrillator manufacturer,[75] it is likely that the standard of care for defibrillator-guided treatment of arrest will soon change to include continuous rhythm classification during CPR. Thus, the current resuscitation guideline requirement to pause chest compressions at 2-minute intervals will likely change to allow continuous-analysis-continuous-CPR (e.g. as illustrated in Figure 1.13). Therefore, any future

next-generation ECG algorithms (such as algorithms designed to assess patient myocardial status as described in the current investigation) will also be required to function during uninterrupted CPR.

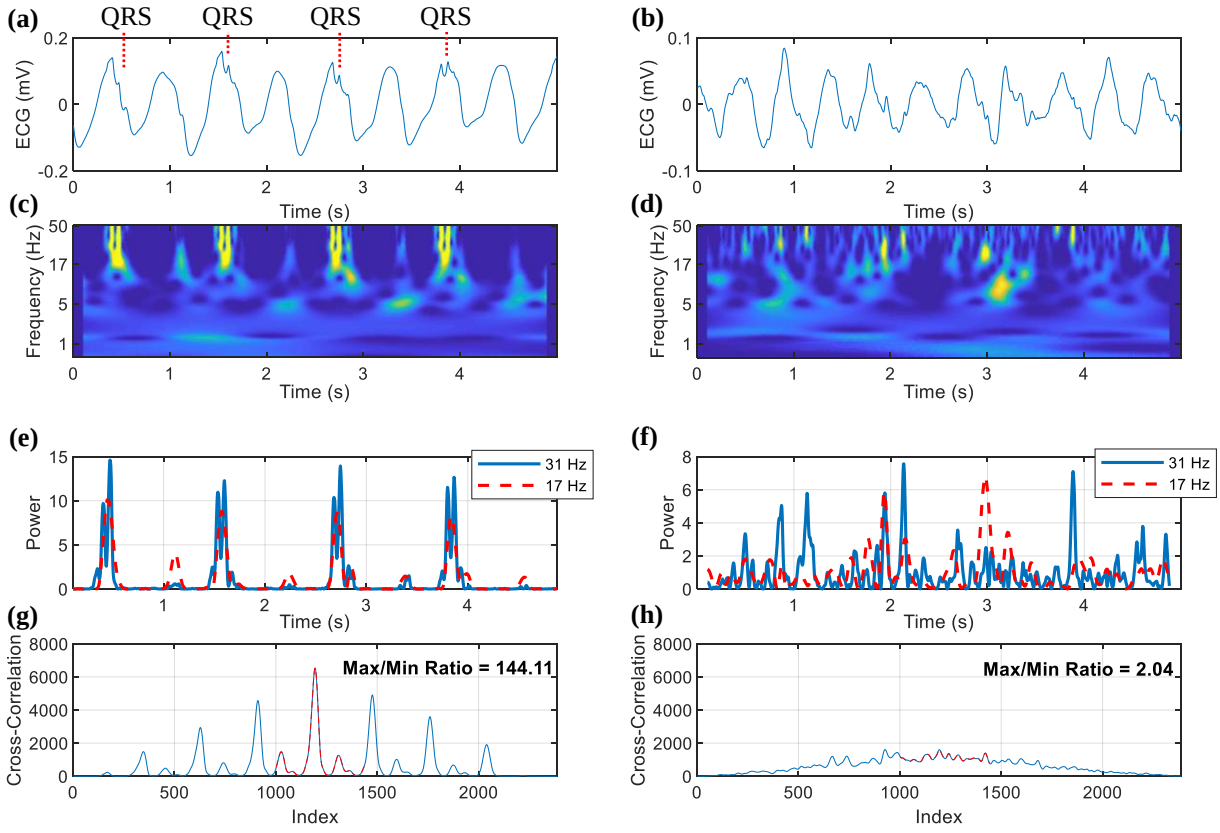

Figure 1.16 Rhythm classification example during CPR (single buffer)
Discrimination of organized rhythm versus VF during CPR following the methods described in Coult 2011.[70] (a) Sinus ECG (i.e. contains QRS complexes) during CPR. (b) VF ECG during CPR. (c) Intrafrequency-normalized wavelet transform of sinus rhythm. (d) Intrafrequency-normalized wavelet transform of VF. (e) Cross-sections of sinus rhythm normalized wavelet transform at 17 Hz and 31 Hz are similar. (f) Cross-sections of VF normalized wavelet transform at 17 Hz and 31 Hz are dissimilar. (g) Cross-correlation of the 17 Hz and 31 Hz sinus rhythm profiles has high max/min ratio in center indicating likely QRS complexes. (h) Cross-correlation of the 17 Hz and 31 Hz VF profiles has low max/min ratio in center, indicating likely VF.

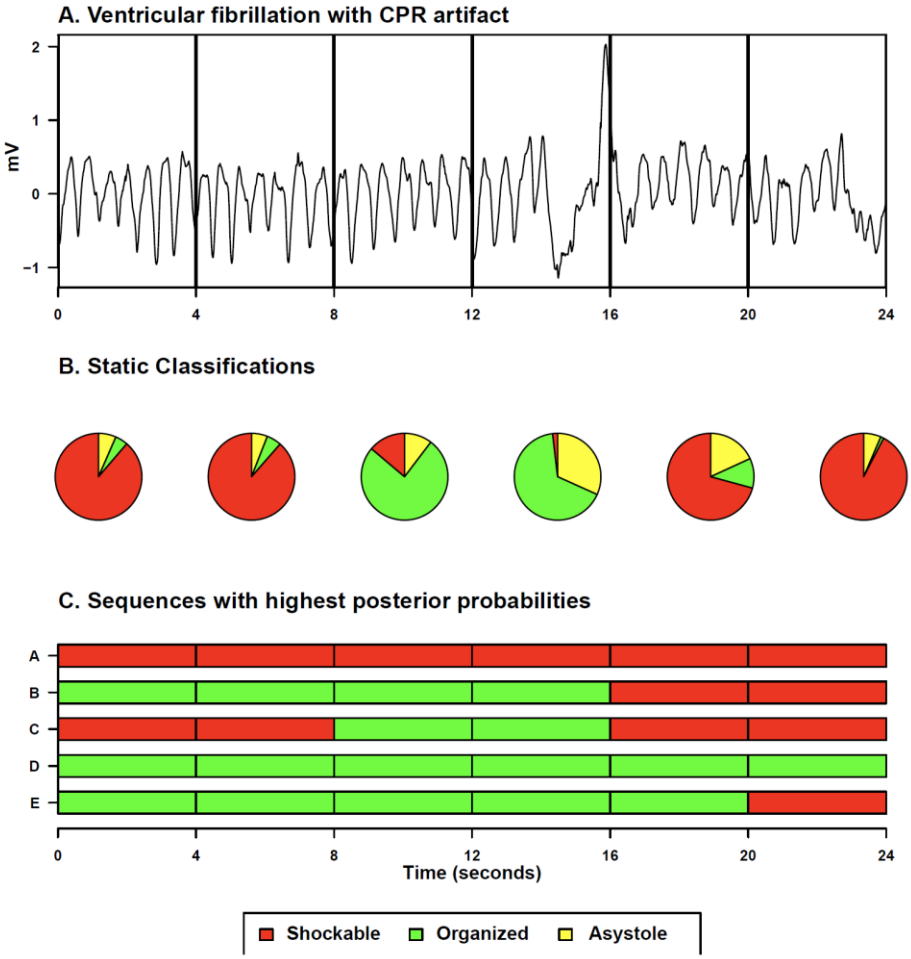

Image from: Kwok H, Coult J, Drton M, Rea T, and Sherman L. Adaptive rhythm sequencing: A method for dynamic rhythm classification during CPR. Resuscitation 2015; 91:26-31. https://doi.org/10.1016/j.resuscitation.2015.02.031

Figure 1.17 Rhythm classification example during CPR (sequence)
Rhythm classification accuracy for individual isolated ('static') analysis buffers can be improved by determining the most likely sequence of individual buffer states.

1.2.2.2 Characterizing Cardiopulmonary Resuscitation

Current guidelines dictate a duty cycle of 50% for chest compression-decompression.[27] This requirement is difficult to enforce, and the actual duty cycle implemented in practice during manual compressions is unclear. However, recently-developed portable mechanical chest compression devices have been designed to automatically provide compressions; these devices

may be able to precisely control parameters such as duty cycle, and thus determination of optimal duty cycle and other CPR parameters is increasingly relevant.[76] Our group therefore performed a retrospective evaluation of true duty cycle during high-performance manual CPR by EMS personnel, and observed that high-performance EMS CPR had a significantly lower duty cycle than that proposed by guidelines, thus highlighting the need for evidence-based duty cycle parameters for potential use in automated compression devices.[77]

1.2.2.3 VF Analysis to Identify Etiology and Chronic Conditions

Preliminary studies have suggested that characteristics of the VF waveform are affected by the originating cardiac cause of VF (e.g. ischemic versus non-ischemic arrest) in controlled models such as swine.[60,61,78–80] Our group sought to determine whether this result could be applied in an out-of-hospital setting to identify the underlying cause of an arrest and thus prioritize different interventional treatments; for instance, patients with an arrest caused by an S-T elevation myocardial infarction may benefit from priority transport to a facility with percutaneous coronary interventional capability (cardiac catheterization), while patients suffering non-ischemic arrest should be transported to the nearest facility regardless of its percutaneous interventional facilities. However, we did not observe a clinically-useful relationship between VF waveform characteristics and cardiac etiology, suggesting that VF waveform analysis may not be useful for identifying the underlying cardiac cause of an arrest.[81]

Chronic health conditions are associated with lower odds of patient survival from VF arrest.[82,83] Because measures of the VF waveform are also associated with survival, it is possible that waveform measures (as a surrogate for myocardial metabolism) mediate the effect of chronic health conditions on survival. Such a mediation effect would imply that chronic health conditions directly affect the myocardium, and that poor prognosis is subsequently directly affected by the

myocardium. However, we observed that waveform measures do not primarily mediate the relationship between chronic health conditions and survival, suggesting that poor outcomes from chronic health conditions are not due exclusively to the causal effect of such conditions on the myocardium.[84]

1.2.2.4 Relationship of Rhythm Sequence and VF Trajectory to Patient Outcomes

During resuscitation from VF arrest, the specific sequence of events observed in the ECG (such as the temporal sequence of rhythm classification or the change in rhythm quality over time) may itself be related to patient outcome. For instance, if the trajectory of patient status is progressively improved during resuscitation, then it may be beneficial to continue current treatment, but if a patient's prognosis is progressively worse during treatment, then alternative treatments might be considered. Therefore, we sought to evaluate the relationship between rhythm classification sequence and patient outcome as well as the relationship between VF quality trajectory and patient outcome. We observed that specific rhythm transition patterns are associated with prognosis for survival.[85] Additionally, when limited to analysis of VF quality alone, we observed that the time-course trajectory of VF waveform robustness is also associated of the likelihood of survival.[86] These results highlight the importance of incorporating the history and trajectory of patient rhythm and rhythm quality when estimating patient prognosis. Hence, current protocol which limits analysis to isolated buffers every two minutes (and ignores prior ECG information) might potentially be improved by applying algorithms that incorporate aspects of patient ECG history.

1.3 Specific Aims

In these works, we investigate quantitative assessment of patient myocardial status during ventricular fibrillation without requiring interruptions in CPR to explore the potential for improved

defibrillator-guided treatment of out-of-hospital VF cardiac arrest. Specifically, we evaluate the application of existing VF waveform measures during short pauses in CPR, explore whether existing VF waveform measures can be improved during CPR by incorporating ECG shock history, characterize the performance of existing measures (and combinations thereof) during CPR, and evaluate a novel method designed specifically to assess patient status during CPR.

1.3.1 *Aim 1: Evaluate potential for VF prognosis during short CPR pauses.*

1.3.1.1 Aim 1 Motivation

Ideally, waveform measures would be computed without requiring additional pause in chest compressions.[45] Studies have suggested reducing the required compression pause time for rhythm classification by analyzing the ECG during short, incidental pauses in compressions which occur throughout an arrest (e.g. during pauses for non-intubated ventilations or pulse checks).[87] We sought to apply a similar principle to VF waveform measure calculation. VF waveform measures are typically evaluated using arbitrary ECG segment lengths (ranging from 1–15 seconds) without consideration for potential effects of input length on performance.[22,88] It is unknown how shortening ECG segment length affects waveform measure performance or what minimum segment length is required to sufficiently assess patient status. If waveform measures could be calculated using ECG data collected during extremely short incidental pauses, for instance, intermittent assessments of patient status may be possible throughout an arrest without requiring additional pauses in compressions.

1.3.1.2 Aim 1 Goal and Hypothesis

In Aim 1 (presented in Chapter 2), we therefore sought to characterize the relationship between VF waveform measure performance and ECG input length. We collected VF segments prior to

shocks during treatment out-of-hospital VF arrest. Segments were limited to initial shocks delivered by a single defibrillator type to control for differences in cohort sizes between shock cycles and to control for variable filter and sampling bandwidths across device types. ECG segments were shortened incrementally from a maximum of 5 seconds to a minimum of 0.2 seconds to evaluate the potential for applying VF waveform analysis during very brief incidental pauses in compressions. We sought to determine the minimum length at which predictive performance was not significantly reduced. We hypothesized that short segments (e.g. <1 second) would still be representative of patient status and predict shock success, but that performance would be reduced compared to using 5-second segments.

1.3.2 *Aim 2: Determine whether incorporating prior shock outcome improves VF waveform measure prediction of subsequent outcomes during CPR.*

1.3.2.1 Aim 2 Motivation

Assessment of patient status using VF waveform measures has traditionally been limited to analysis of isolated ECG segments collected prior to defibrillation shock without considering any additional information prior to the current point of analysis.[34,57,65] However, there may be additional variables incidentally available to an AED during arrest (e.g. information computed from the already-available ECG signal) that could be incorporated to improve waveform measure prediction of shock outcome during CPR.

1.3.2.2 Aim 2 Goal and Hypothesis

In Aim 2 (presented in Chapter 3), we therefore sought to determine whether history of response to shock is indicative of a patient's myocardial status and whether response history can be leveraged to improve prognostic assessment during CPR. We applied a representative group of VF waveform measures calculated from both CPR-artifacted and CPR-free ECGs collected prior to

shocks in out-of-hospital VF arrest patients. We evaluated prediction of shock success with waveform measures alone versus waveform measures in combination with prior shock outcome to determine if prior shock outcome could be incorporated to improve prediction. We hypothesized that prior shock success would be significantly associated with subsequent shock outcome, and that waveform measures applied in combination with a binary variable representing prior shock success would perform significantly higher than waveform measures alone.

1.3.3 *Aim 3: Characterize existing waveform measures and determine whether combining multiple measures improves performance during CPR.*

1.3.3.1 Aim 3 Motivation

Multiple studies have benchmarked the performance of multiple waveform measures. The number of measures examined in these comparative investigations has ranged from 10-18 measures.[42,65,68,88–90] However, these benchmark studies evaluated measures calculated without CPR artifact, as researchers assume that CPR prevents accurate VF measure calculation due to the fact that it significantly confounds conventional rhythm analysis.[34,39,43–45,67] While several measures have been calculated during CPR in prior studies, the direct effect of CPR on predictive performance of waveform measures calculated from human ECGs has still not been quantified.[68,69] It is therefore unclear how the prognostic performance of individual measures in humans is affected by CPR artifact, and whether any existing measures (or combinations thereof) are suitable for use during CPR.

1.3.3.2 Aim 3 Goal and Hypothesis

In Aim 3 (presented in Chapter 4), we therefore sought to characterize a comprehensive group of existing waveform measures calculated during CPR, and to determine whether machine learning combinations of multiple measures could potentially improve performance during CPR. We

implemented a group of 24 existing waveform measures (and three machine learning combinations thereof), and modified these measures using parameters designed to maximize performance during CPR. We evaluated prediction of shock outcome with these measures using both CPR-corrupted and CPR-free VF segments collected prior to shock from out-of-hospital VF arrest patients. To further characterize potential for prognostic use in a clinical setting, we compared the ability of measures to predict a range of patient outcomes with different clinical implications (e.g. return of rhythm, return of circulation, and survival). We identified the single measure best-suited for use during uninterrupted CPR based on its performance relative to other measures. We hypothesized that waveform measures would predict patient outcomes both with and without CPR, but that prediction would be compromised during CPR. We further hypothesized that machine learning combinations of measures would exhibit superior performance versus individual measures alone.

1.3.4 *Aim 4: Develop impedance-based chest compression detection function.*

1.3.4.1 Aim 4 Motivation

A future next-generation algorithm to classify the ECG or evaluate patient status during CPR would likely be required to apply separate parameters and filtering depending on the presence of compression artifact.[91] Thus, automatic detection of chest compression state would likely be required to enable real-world application of any algorithm designed to function both with and without CPR. While detecting compressions using an accelerometer sensor is trivial, many rescuers do not use AEDs with accelerometer-based sensors due to cost and inconvenience. In contrast, the impedance between defibrillator paddle electrodes is a widely-available (albeit noisy) signal that may potentially be used to infer the presence of compressions. Prior studies have demonstrated detection of chest compression state using impedance, but these investigations were

either limited to a single defibrillator type, had relatively small validation datasets, or were limited in accuracy; hence the real-world applicability of such methods is unclear.[92–96]

1.3.4.2 Aim 4 Goal and Hypothesis

In Aim 4 (presented in Chapter 5), we therefore sought to design a function to detect the presence of chest compressions based on the widely-available transthoracic impedance signal. The function was developed on training data using a combination of time- and frequency-domain features. We hypothesized that when tested on validation data from a variety of defibrillator models, the function would demonstrate high sensitivity and specificity for detecting compressions.

1.3.5 *Aim 5: Determine whether a novel prognostic algorithm improves assessment of patient status during CPR.*

1.3.5.1 Aim 5 Motivation

As described previously, there is compelling evidence that even short pauses in CPR to allow ECG analysis during resuscitation are detrimental to patient outcomes.[46–48] Thus next-generation ECG classification algorithms designed to allow rhythm classification during uninterrupted chest compressions are currently being evaluated by several defibrillator manufacturers.[74,75] However, prognostic measures of the VF waveform to assess patient status have not been designed for use during CPR. It is unclear whether a prognostic algorithm designed specifically to predict patient outcomes during CPR would offer improved performance over current methods. Such an algorithm could potentially allow continuous assessment of patient status during CPR, providing a real-time metric by which to guide therapy and monitor the effect of treatment during resuscitation.[45]

One of the few pilot studies of waveform measures during CPR demonstrated increased similarity of waveform measure values with and without CPR by limiting the use of frequency content below 10 Hz (although actual predictive performance of measures was not compared),

suggesting that high-pass behavior of some form is necessary for improved analysis during CPR.[43] Therefore features based on spectral characteristics of the ECG may offer an advantage over traditional time-domain methods during CPR due to their ability to ignore lower CPR artifact frequencies, especially if applied after adaptive filtering to remove the majority of CPR artifact. However, a large number of features based on the Fourier spectrum have already been developed (with moderate results), and it is unlikely any improvement could be gleaned from further analysis of the Fourier spectrum over existing methods.[65] In contrast, time-frequency-based waveform measures are relatively few, and the majority of existing time-frequency methods fail to exploit time-varying features of the spectrogram.[88]

Wavelet time-frequency methods that examine temporal behavior of the VF signal reportedly may offer increased predictive value over leading Fourier-based and complexity-based methods.[42,97–99] Time-frequency observation of the ECG over sustained periods of VF has suggested that power is initially concentrated in higher frequencies but shifts to lower frequencies over time.[100] During VF, concentrations of high-energy phosphates in the myocardium are rapidly depleted, and since cardiac cells lose contractile ability and have lower conduction velocity over time, high-frequency content is progressively less as VF progresses.[4,22] The number of self-sustaining rotors in VF may also increase over time, increasing the disorganization in cardiac tissue as the number of excitation sources increase.[18] Such time-dependent changes in frequency content and organization as VF degrades from a robust to a poor condition suggest that complexity metrics calculated from time-frequency transforms of the ECG may be useful for estimating ventricular fibrillation status.[101] While the utility of these characteristics during CPR is unknown, it is possible that optimizing such features to ignore CPR artifact by limiting analysis to mid- and high-frequency content could allow improved prognostic evaluation during CPR.

During VF resuscitation, categorical variables may be incidentally available in addition to the ECG itself. For example, patient characteristics such (e.g. sex) are associated with outcome.[102] However, such variables have not been combined with quantitative features of the ECG to evaluate patient status during CPR. Additionally, it is unclear whether such variables could be realistically incorporated into a defibrillator to improve prognostic evaluation during resuscitation. If a small number of useful patient characteristics could be easily noted by rescuers and entered into a defibrillator during resuscitation, these characteristics might potentially be incorporated into a prognostic algorithm to improve ability to assess patient status.

1.3.5.2 Aim 5 Goal and Hypothesis

In Aim 5 (presented in Chapter 6) we therefore sought to develop a novel prognostic algorithm to predict patient outcomes during CPR, and to determine whether the algorithm exhibited improved performance over existing methods. The algorithm applies an adaptive filter and incorporates novel time-frequency, complexity, and amplitude features of the VF ECG designed to mitigate CPR artifact. The algorithm combines ECG features with categorical variables presumed to be available to rescuers or visible in the ECG during resuscitation. The algorithm determines presence of CPR automatically using the chest compression detection function proposed in Aim 4, and uses the presence of CPR to inform filter and parameter settings. We hypothesized that using validation data, the novel algorithm would demonstrate improved prediction of patient outcomes versus the best-performing existing method identified in Aim 3, indicating improved potential to monitor patient status in real time to guide therapy during uninterrupted CPR.

Chapter 2. SHORT VENTRICULAR FIBRILLATION ECG SEGMENTS PREDICT DEFIBRILLATION OUTCOMES DURING OUT-OF-HOSPITAL CARDIAC ARREST

Adapted from: **Coult J**, Kwok H, Sherman L, Blackwood J, Kudenchuk P, Rea T. Short ECG segments predict defibrillation outcome using quantitative waveform measures. *Resuscitation* 2016; 109:16-20. https://doi.org/10.1016/j.resuscitation.2016.09.020

2.1 ABSTRACT

Aim: Quantitative waveform measures of the ventricular fibrillation (VF) electrocardiogram (ECG) predict defibrillation outcome. Calculation requires an ECG epoch without chest compression artifact. However, pauses in CPR can adversely affect survival. Thus, the potential use of waveform measures is limited by the need to pause CPR. We sought to characterize the relationship between the length of the CPR-free epoch and the ability to predict outcome. *Methods:* We conducted a retrospective investigation using the CPR-free ECG prior to first shock among out-of-hospital VF cardiac arrest patients in a large metropolitan region (n=442). Amplitude Spectrum Area (AMSA) and Median Slope (MS) were calculated using ECG epochs ranging from 5 seconds to 0.2 seconds. The relative ability of the measures to predict return of organized rhythm (ROR) and neurologically-intact survival was evaluated at different epoch lengths by calculating the area under the receiver operating characteristic curve (AUC) using the 5-second epoch as the referent group. *Results:* Compared to the 5-second epoch, AMSA performance declined significantly only after reducing epoch length to 0.2 seconds for ROR (AUC 0.77 to 0.74, p=0.03) and with epochs of ≤ 0.6 seconds for neurologically-intact survival (AUC 0.72 to 0.70, p=0.04). MS performance declined significantly with epochs of ≤ 0.8 seconds for ROR (AUC 0.78 to 0.77, p=0.04) and with epochs ≤ 1.6 seconds for neurologically-intact survival (AUC 0.72 to 0.71, p=0.04). *Conclusion:* Waveform measures predict defibrillation outcome using very brief ECG

epochs, a quality that may enable their use in current resuscitation algorithms designed to limit CPR interruption.

2.2 INTRODUCTION

Sudden cardiac arrest due to ventricular fibrillation (VF) is a leading cause of death in the US.[3] Successful resuscitation is possible with a coordinated set of rescuer actions involving defibrillation, CPR, and advanced care. Early defibrillation is the most critical treatment. However only a portion of shocks are successful, and many defibrillation attempts do not achieve organized rhythm or return of spontaneous circulation.[49,53] Current rhythm analysis and shock timing is standardized to 2-minute intervals. This timing may not be optimal across all patients to maximize benefit from shock, given individual differences in cardiac arrest etiology and physiology. Such heterogeneity suggests opportunity to improve outcome if shock administration could be tailored and timed to individual physiologic measures.

One strategy to match patient physiology to treatment and improve shock success is use of quantitative waveform measures to guide shock delivery. Quantitative waveform measures are derived from VF electrocardiogram (ECG) characteristics, such as frequency and amplitude. These measures can be generated in real time to predict shock outcome.[53,57,86] Quantitative waveform measures require an ECG epoch that is artifact-free, necessitating interruption in chest compressions.[44,69,87] Interruptions decrease circulation, and have been associated with a reduced chance of survival.[47] Thus the potential use of waveform measures is limited by the need to pause CPR.

Studies of waveform measures have used ECG segments ranging from 1-15 seconds in length.[22,53,103,104] The minimum length of CPR-free ECG which can be used to reliably calculate a specific measure has not been established. Using very short ECG epochs to help guide resuscitation

would minimize the detrimental effects of pausing CPR but may limit predictive accuracy. We sought to characterize the relationship between the length of the CPR-free epoch and the ability of two representative waveform measures to predict clinical outcome.

2.3 METHODS

2.3.1 *Study Design and Setting*

The study cohort was a retrospective subset of patients who were treated for out-of-hospital VF cardiac arrest by a HeartStart MRx defibrillator (Philips Medical Systems, Andover, MA, USA) in King County, WA from 2007-2014. The study used cases from only one defibrillator type to control for heterogeneity in sampling rates and filter settings between defibrillator models. Cases were excluded if the ECG recording was unavailable, if a public access defibrillator was used, or if 5 seconds of CPR-free and artifact-free VF ECG was unavailable prior to the initial shock. This study was approved by the Investigational Review Boards at the University of Washington Human Subjects Division and King County Public Health.

2.3.2 *Data Elements and Collection*

King County Emergency Medical Services maintains a registry of all treated cardiac arrests with data organized according to the Utstein template. ECGs were recorded at 250 samples/second and included impedance data to assess for CPR. For each case, a 5-second CPR-free ECG clip was collected immediately preceding the first shock. Only the first shock was included to eliminate correlation from multiple samples for the same patient.

2.3.3 *Quantitative Waveform Measures*

We evaluated Amplitude Spectrum Area (AMSA)[97,98,105] and Median Slope (MS).[68,105,106] These measures represent spectral and time-domain techniques, respectively. The AMSA was computed using a Hanning window to remove edge discontinuities and a 1250-point discrete Fourier transform normalized by ECG length. Each frequency magnitude between 1-26 Hz was multiplied by its frequency and summed.[65] The MS was calculated as the median absolute value of the amplitude differences between adjacent samples in the ECG divided by the time between them. Waveform measures were calculated from ECG epochs ranging from 5.0 seconds to 0.2 seconds. Epochs were shortened by removing data evenly from both ends of the original 5-second clip.

2.3.4 *Outcomes*

We evaluated short- and long-term outcomes. For short-term outcome, return of organized rhythm (ROR) was defined as the presence of at least two QRS complexes within 5 seconds in the two minutes following a defibrillation attempt. For long-term outcome, we used survival to hospital discharge with favorable neurologic status as defined by a Cerebral Performance Category (CPC) of 1 or 2, determined by review of the medical record for the arrest hospitalization.[107,108]

2.3.5 *Data Analysis*

To assess the prognostic relationship between waveform measures and the outcome of interest, we calculated the area under the receiver operating characteristic curve (AUC) for each epoch length. The AUCs were compared using DeLong's test for correlated receiver operating characteristic curves.[109] The AUC of the 5-second epoch served as the reference. An alpha level of ≤ 0.05 (two-sided) determined statistical significance. As a secondary analysis, we calculated the odds ratios of ROR for standard deviation and unit changes of the waveform measures at each epoch length

(Appendix). MATLAB 2014a (The Mathworks, Natick, MA, USA), R 3.0.2 (R Foundation for Statistical Computing, Vienna, Austria), and SPSS Statistics 19 (IBM, Armonk, NY) were used for signal and statistical analysis.

2.4 RESULTS

2.4.1 *Study Cohort*

From 2007-2014, 750 out-of-hospital cardiac arrest cases presented with VF and were treated with an MRX defibrillator. Of these, 135 were excluded due to missing part or all of the defibrillator recording. An additional 173 had recordings available but were excluded because they did not contain a 5-second CPR-free epoch prior to the initial shock, leaving a final 442 cases available for analysis (Table 2.1). Of this final study group, shock resulted in ROR in 289 (65.4%) patients, and 194 (43.9%) patients survived to hospital discharge with favorable neurological outcome (CPC 1-2).

Table 2.1. Patient characteristics
Results are presented for all eligible patients, excluded patients, and the final study group.

Patient Characteristics	Eligible (n=750)	Excluded (n=308)	Included (n=442)
Female, n(%)	180 (24)	79 (25.6)	101 (22.9)
Age, median (IQR)	63 (52, 74)	67 (53, 77)	62 (52, 73)
Cardiac etiology, n(%)	654 (87.2)	247 (80.2)	407 (92.1)
Location, n(%)			
Home	471 (62.8)	201 (65.3)	270 (61.1)
Public	220 (29.3)	78 (25.3)	142 (32.1)
Nursing Home	59 (7.9)	29 (9.4)	30 (6.8)
Arrest before EMS arrival, n(%)	658 (87.7)	246 (79.9)	412 (93.2)
Witnessed, n(%)	544 (72.5)	206 (66.9)	338 (76.5)
Bystander CPR, n(%)	478 (63.7)	178 (57.8)	300 (67.9)
Response time (minutes), median (IQR)	5 (4, 6)	5 (3, 6)	5 (4, 6)
Total shocks, median (IQR)	3 (1, 5)	2 (1, 5)	3 (1, 6)
ROSC, n(%)	485 (64.7)	177 (57.5)	308 (69.7)
Died in Field	201 (26.8)	104 (33.8)	97 (21.9)
Admit to hospital	486 (64.8)	174 (56.5)	312 (70.6)
Survive to hospital discharge, n(%)	319 (42.5)	104 (33.8)	215 (48.6)
Survival with CPC 1 or 2	290 (38.7)	96 (31.2)	194 (43.9)

2.4.2 *Waveform Measures versus Epoch Length*

For AMSA, the reference AUC using 5-second epochs was 0.77 for predicting ROR and 0.72 for favorable CPC (Figure 2.1, Table 2.2). For epoch lengths decreasing from 5.0 to 0.8 seconds, AMSA performance did not differ significantly from the reference for either outcome. The prognostic ability of AMSA declined significantly at epoch lengths of 0.2 seconds for predicting ROR (AUC = 0.74, $p = 0.03$) and at lengths ≤ 0.6 seconds for predicting neurologically-intact survival (AUC = 0.70, $p = 0.04$).

Using 5-second epochs with MS, the reference AUC was 0.78 for predicting ROR and 0.72 for predicting neurologically-intact survival (Figure 2.1, Table 2.3). For ROR, MS performance declined significantly with epoch lengths of 0.8 seconds (AUC = 0.77, $p = 0.04$). Prediction of survival declined significantly and consistently with epochs ≤ 1.6 seconds (AUC = 0.71, $p = 0.04$).

Table 2.2. AUC values for AMSA
AUC values for prediction of ROR and survival are presented stratified by epoch length. P-values are presented for differences between the referent 5-second epoch.

	Return of Rhythm		Survival	
Length	**AUC [95% CI]**	**p-value**	**AUC [95% CI]**	**p-value**
5.0 s	0.77 [0.73-0.82]	referent	0.72 [0.67-0.77]	referent
4.0 s	0.77 [0.72-0.82]	0.170	0.72 [0.67-0.77]	0.685
3.0 s	0.77 [0.72-0.82]	0.310	0.72 [0.67-0.77]	0.833
2.0 s	0.77 [0.72-0.82]	0.674	0.72 [0.67-0.77]	0.997
1.8 s	0.77 [0.72-0.82]	0.663	0.72 [0.67-0.77]	0.835
1.6 s	0.77 [0.72-0.82]	0.595	0.72 [0.67-0.77]	0.702
1.4 s	0.77 [0.72-0.82]	0.616	0.72 [0.67-0.77]	0.576
1.2 s	0.77 [0.72-0.82]	0.621	0.71 [0.67-0.76]	0.378
1.0 s	0.77 [0.72-0.82]	0.629	0.71 [0.66-0.76]	0.211
0.8 s	0.77 [0.72-0.82]	0.608	0.71 [0.66-0.75]	0.104
0.6 s	0.76 [0.72-0.81]	0.405	0.70 [0.65-0.75]	0.044*
0.4 s	0.76 [0.71-0.81]	0.183	0.69 [0.64-0.74]	0.011*
0.2 s	0.74 [0.69-0.79]	0.033*	0.68 [0.63-0.73]	0.006*

*p<0.05

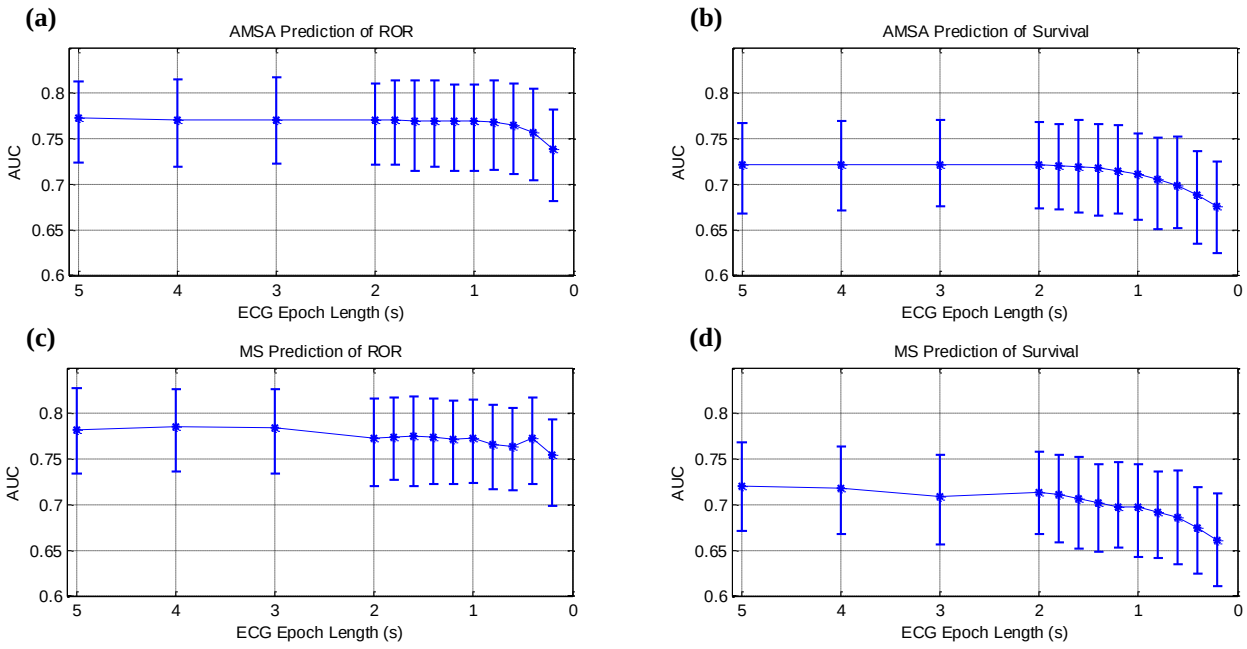

Figure 2.1. AUCs with 95% CIs for prediction of outcome versus ECG epoch length
Results are shown for (a) AMSA prediction of ROR, (b) AMSA prediction of survival with favorable CPC score, (c) MS prediction of ROR, and (d) MS prediction of survival with favorable CPC score.

Table 2.3. AUC values for MS
AUC values are presented for prediction of ROR and survival, stratified by epoch length. P-values are presented for differences between the referent 5-second epoch.

	Return of Rhythm		Survival	
Length	**AUC [95% CI]**	**p-value**	**AUC [95% CI]**	**p-value**
5.0 s	0.78 [0.74-0.83]	referent	0.72 [0.67-0.77]	referent
4.0 s	0.79 [0.74-0.83]	0.164	0.72 [0.67-0.77]	0.804
3.0 s	0.78 [0.74-0.83]	0.795	0.71 [0.66-0.76]	0.011*
2.0 s	0.77 [0.73-0.82]	0.053	0.71 [0.67-0.76]	0.334
1.8 s	0.78 [0.73-0.82]	0.228	0.71 [0.66-0.76]	0.160
1.6 s	0.77 [0.73-0.82]	0.201	0.71 [0.66-0.75]	0.039*
1.4 s	0.78 [0.73-0.82]	0.270	0.70 [0.65-0.75]	0.016*
1.2 s	0.77 [0.72-0.82]	0.103	0.70 [0.65-0.75]	0.005*
1.0 s	0.77 [0.73-0.82]	0.183	0.70 [0.65-0.75]	0.018*
0.8 s	0.77 [0.72-0.81]	0.043*	0.69 [0.64-0.74]	0.005*
0.6 s	0.76 [0.72-0.81]	0.043*	0.69 [0.64-0.74]	0.003*
0.4 s	0.77 [0.73-0.82]	0.352	0.67 [0.62-0.73]	<0.001*
0.2 s	0.75 [0.71-0.80]	0.044*	0.66 [0.61-0.71]	<0.001*

*p<0.05

2.5 DISCUSSION

In this cohort of human VF cardiac arrest, AMSA and MS predicted short-term rhythm outcome (ROR) and long-term outcome (neurologically-intact survival). Both measures predicted ROR better than survival. Referent AUCs ranged from 0.72-0.78, which is generally consistent with previous work predicting shock success with various outcome definitions.[64] The ECG epoch length at which prognostic performance declined varied depending on the particular waveform measure and outcome used. Prognostic ability of AMSA for ROR and survival was significantly reduced with epochs of 0.2 and 0.6 seconds, respectively. For MS, prognostic performance declined with epochs of 0.8 seconds for ROR and 1.6 seconds for survival. The reduced ability to predict survival compared to ROR may be due to additional confounding influences on long-term outcome other than the VF waveform. Additionally, while AMSA allowed for shorter epochs than MS before exhibiting a significant decline in AUC, the absolute prediction as reflected by AUC was fairly similar between the two measures, for instance at 1 second.

These results are consistent with our physiological understanding of VF. The median frequency of VF is approximately 3-6 cycles per second.[110] Epochs on the order of 1 second would generally include multiple VF cycles from which to derive waveform measures. This VF characteristic may enable some measures to retain their predictive qualities even with very short ECG epochs.

The finding that very short ECG epochs can retain predictive characteristics has clinical implications. Waveform measures possess potentially useful qualities: they are prognostic, can be calculated in real time, and can be modified by treatment. However, they have not yet been successfully integrated into resuscitation care.[66] Recent studies highlight the potential to detect VF during short pauses in CPR and even during ongoing CPR.[39,72,87] Additionally, while some progress has been made to calculate AMSA during CPR using filtering techniques, it is generally necessary to interrupt CPR for waveform measure calculation.[44,69,87,111] The use of short epochs to calculate waveform measures, as demonstrated in this study, combined with methods to instantaneously detect pauses in CPR,[73] may allow application of waveform measures during existing gaps in CPR without increasing pause time. Additionally, models that predict shock success by combining waveform measures with other variables could improve prognostic performance to a clinically relevant level.[106,112] Collectively these advances provide motive to optimize waveform measures for use with very brief CPR-free ECG epochs.

2.6 LIMITATIONS

The study was limited in part because it tested only two waveform measures. Other measures may perform differently. The predictive performance of the two waveform measures declined at different time points, indicating a need to consider the particular waveform measure when determining the balance of prognostic yield and epoch length. Moreover, we observed that the

magnitude of AMSA changed with different epoch lengths, suggesting that the magnitude of AMSA (as opposed to MS) is likely not directly comparable across mixed-length epochs (see Appendix A in section 2.8). The ability of waveform measures to predict shock success is influenced by the outcome definition; the current study used a specific rhythm and clinical outcome. The study investigated a single model of defibrillator. The investigation excluded cases where the defibrillator information would not support confirmation of CPR-free epoch prior to the first shock. These exclusions and restrictions may limit the generalizability of the findings.

2.7 CONCLUSIONS

In this study of out-of-hospital VF arrest, AMSA and MS comparably predicted rhythm and clinical outcome using CPR epochs as short as 0.8 seconds for AMSA and 1.8 seconds for MS compared to a full 5-second CPR-free epoch. These findings suggest that waveform measures retain predictive characteristics without requiring protracted interruptions in CPR, and thus they could be more readily incorporated into current resuscitation algorithms designed to limit CPR interruption.

2.8 APPENDIX A: WAVEFORM MEASURE VALUES VERSUS LENGTH

2.8.1 *Introduction*

As a secondary analysis, we sought to evaluate whether waveform measures calculated from mixed-length epochs could be compared. Ability to utilize waveform measures calculated from arbitrary ECG epoch lengths could further enable waveform measure calculation using VF segments collected from incidental pauses in chest compressions of any length. Additionally, we

sought to confirm the primary results for minimum epoch length required for equivalent waveform measure performance versus the 5-s referent using odds ratios instead of AUC.

2.8.2 *Methods*

Mean absolute waveform measure values were evaluated for all epoch lengths. Waveform measure means were compared using a paired two-sided T-test to determine if magnitudes remain similar across epoch length. To confirm primary study results using odds ratios, odds ratios for absolute and standardized natural log waveform measures were computed for prediction of ROR for all epoch lengths and compared to AUC performance.

2.8.3 *Results*

Mean (SD) AMSA for 5-second and 0.2-second epochs was 6.54 (3.51) mV-Hz and 35.61 (24.23) mV-Hz ($p < 0.001$ for difference) (Figure 2.2, Table 2.4). Mean (SD) MS for 5-second and 0.2-second epochs was 4.08 mV/s (2.39) and 4.18 mV/s (2.83) ($p = 0.18$ for difference) (Figure 2.3, Table 2.5).

The odds ratios [95% CI] for increases in one standard deviation natural log AMSA were 3.2 [2.4, 4.1] and 2.5 [2.0, 3.2] for 5-second and 0.2-second epochs, respectively. Odds ratios [95% CI] for unit increases in absolute AMSA were 1.44 [1.31, 1.58] and 1.04 [1.03, 1.06] for 5-second and 0.2-second epochs, respectively (Table 2.4).

The odds ratios [95% CI] for standard deviation increases in natural log MS were 3.3 [2.6, 4.4] and 2.8 [2.1, 3.5] for 5-second and 0.2-second epochs, respectively. Odds ratios [95% CI] for unit increases in absolute MS were 1.8 [1.5, 2.0] and 1.5 [1.3, 1.7] for 5-second and 0.2-second epochs, respectively (Table 2.5).

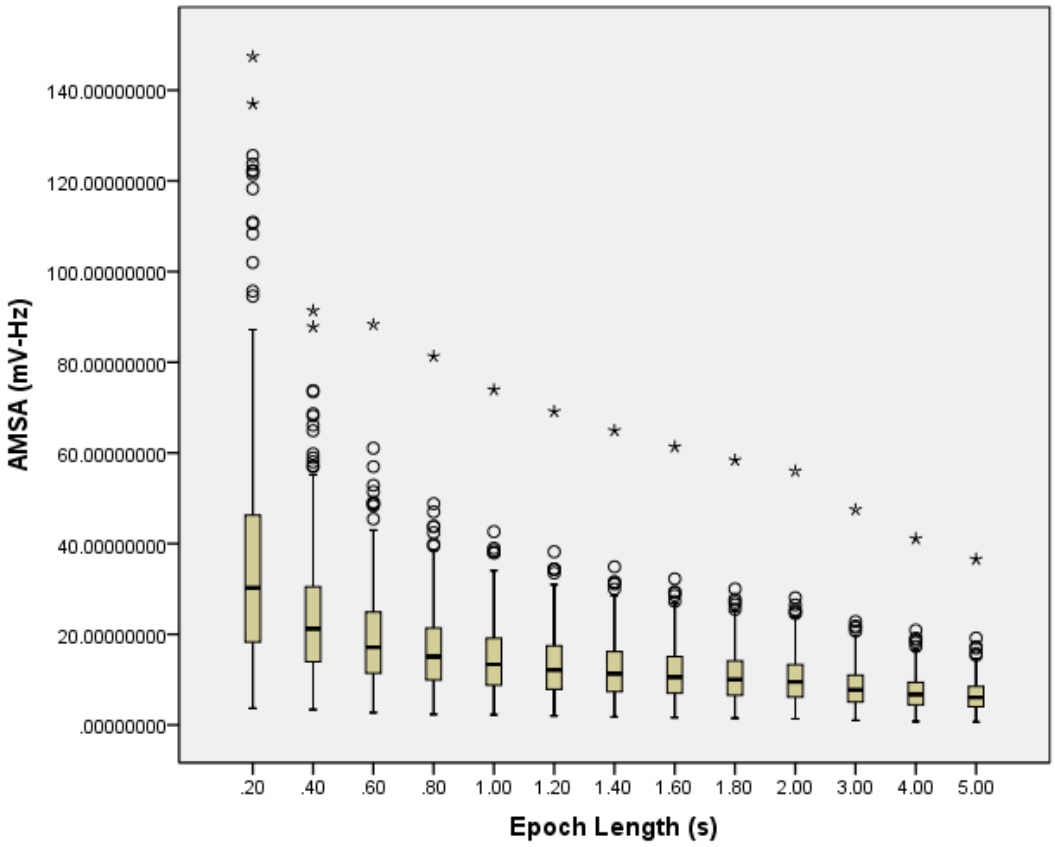

Figure 2.2. AMSA mean versus epoch length
AMSA values decrease as epoch length increases (n=442 cases). Mean AMSA values are significantly different between the 5-second and 0.2-second epoch lengths ($p<0.001$). Skew in the distribution of AMSA values was corrected prior to subsequent analysis using natural log transformation.

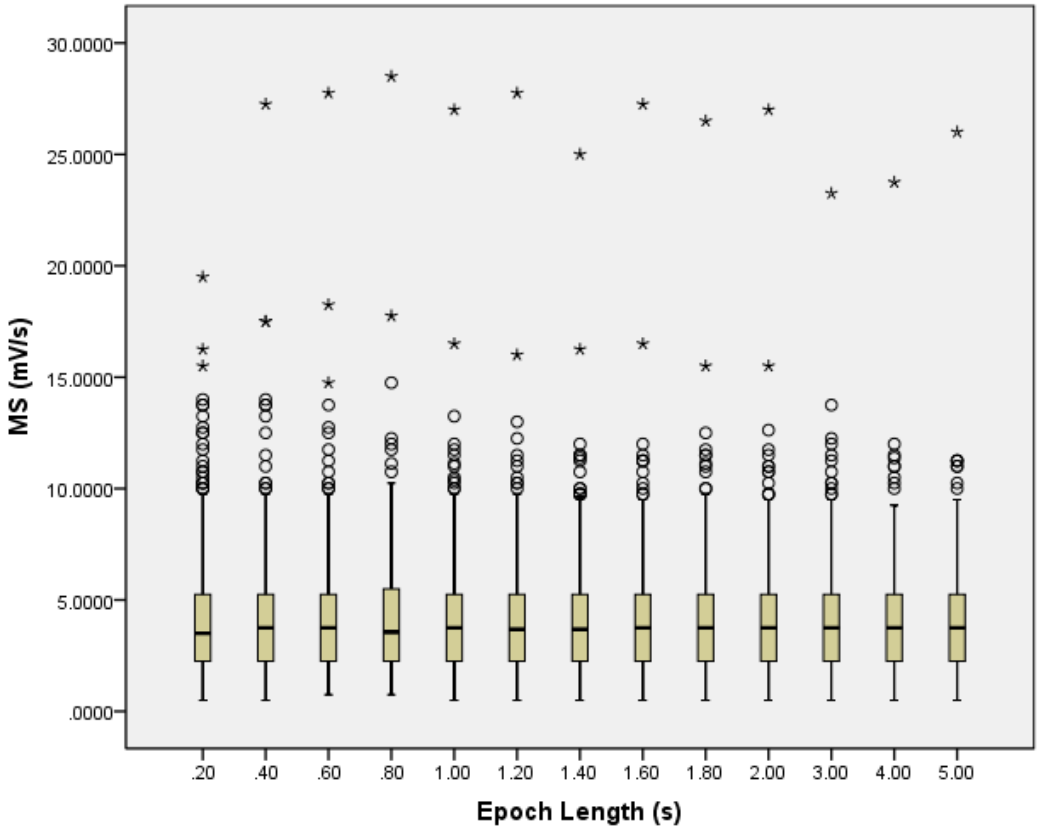

Figure 2.3. MS mean versus epoch length
MS maintains a similar scale across epoch lengths (n=442 cases). Mean MS values were not statistically different even between the 5-second and 0.2-second epochs (p=0.18). Skew in the distribution of MS values was corrected prior to subsequent analysis using natural log transformation.

Table 2.4. Mean AMSA values and odds ratios versus epoch length
Results are presented for AMSA values overall (n=442), for cases that achieved ROR (n=289), and for cases that did not achieve ROR (n=153), along with odds for increase in unit and standard deviation (SD) AMSA. Natural log transformations were performed on AMSA values prior to standardization. All values are presented as value [95% confidence interval].

Epoch Length (s)	All Cases: Mean AMSA (mv-Hz)	ROR Cases: Mean AMSA (mV-Hz)	No-ROR Cases: Mean AMSA (mV-Hz)	Odds for Unit Increase in AMSA	Odds for SD Increase in AMSA
5	6.5 [6.2, 6.9]	7.5 [7.1, 7.9]	4.7 [4.3, 5.1]	1.44 [1.31, 1.58]	3.2 [2.4, 4.1]
4	7.3 [6.9, 7.7]	8.4 [7.9, 8.8]	5.3 [4.8, 5.7]	1.38 [1.27, 1.50]	3.1 [2.4, 4.1]
3	8.4 [8.0, 8.6]	9.7 [9.2, 10.2]	6.0 [5.5, 6.6]	1.32 [1.23, 1.42]	3.1 [2.4, 4.0]
2	10.3 [9.8, 10.8]	11.9 [11.2, 12.5]	7.4 [6.7, 8.1]	1.25 [1.18, 1.33]	3.1 [2.4, 4.0]
1.8	10.9 [10.3, 11.4]	12.5 [11.8, 13.2]	7.8 [7.0, 8.5]	1.24 [1.17, 1.31]	3.1 [2.4, 4.0]
1.6	11.5 [11.0, 12.1]	13.3 [12.6, 14.0]	8.3 [7.5, 9.0]	1.22 [1.16, 1.29]	3.1 [2.4, 4.0]
1.4	12.4 [11.7, 13.0]	14.2 [13.5, 15.0]	8.8 [8.0, 9.6]	1.20 [1.15, 1.26]	3.1 [2.4, 4.0]
1.2	13.4 [12.7, 14.1]	15.4 [14.6, 16.3]	9.5 [8.6, 10.4]	1.18 [1.13, 1.24]	3.0 [2.4, 3.9]
1.0	14.7 [15.7, 17.4]	16.9 [16.0, 17.9]	10.5 [9.5, 11.5]	1.16 [1.12, 1.21]	3.0 [2.3, 3.9]
0.8	16.5 [15.7, 17.4]	19.1 [18.0, 20.1]	11.8 [10.6, 13.0]	1.14 [1.10, 1.18]	3.0 [2.3, 3.8]
0.6	19.3 [18.3, 20.3]	22.2 [20.9, 23.4]	13.8 [12.3, 15.2]	1.11 [1.08, 1.14]	2.9 [2.2, 3.7]
0.4	24.0 [22.7, 25.3]	27.6 [26.0, 29.2]	17.1 [15.2, 19.1]	1.08 [1.06, 1.10]	2.8 [2.1, 3.5]
0.2	35.6 [33.3, 37.9]	41.2 [38.4, 44.0]	25.0 [21.7, 28.2]	1.04 [1.03, 1.06]	2.5 [2.0, 3.2]

Table 2.5. Mean MS values and odds ratios versus epoch length
Results are presented for MS overall (n=442), for cases that achieved ROR (n=289), and for cases that did not achieve ROR (n=153), along with absolute and standardized odds ratios. Natural log transformations were performed on MS values prior to standardization. All values are presented as value [95% confidence interval].

Epoch Length (s)	All Cases: Mean MS (mV/s)	ROR Cases: Mean MS (mV/s)	No-ROR Cases: Mean MS (mV/s)	Odds for Unit Increase in MS	Odds for SD Increase in MS
5	4.1 [3.9, 4.3]	4.7 [4.5, 5.0]	2.8 [2.5, 3.1]	1.8 [1.5, 2.0]	3.3 [2.6, 4.4]
4	4.1 [3.9, 4.3]	4.7 [4.5, 5.0]	2.8 [2.5, 3.1]	1.8 [1.5, 2.0]	3.3 [2.6, 4.4]
3	4.1 [3.9, 4.3]	4.8 [4.5, 5.1]	2.8 [2.5, 3.1]	1.7 [1.5, 2.0]	3.3 [2.5, 4.3]
2	4.1 [3.8, 4.3]	4.7 [4.4, 5.0]	2.8 [2.5, 3.1]	1.7 [1.5, 2.0]	3.2 [2.4, 4.1]
1.8	4.1 [3.8, 4.3]	4.8 [4.5, 5.1]	2.8 [2.5, 3.1]	1.7 [1.5, 2.0]	3.2 [2.5, 4.2]
1.6	4.1 [3.9, 4.3]	4.8 [4.5, 5.1]	2.8 [2.5, 3.1]	1.7 [1.5, 2.0]	3.2 [2.4, 4.1]
1.4	4.1 [3.9, 4.4]	4.8 [4.5, 5.1]	2.8 [2.5, 3.1]	1.7 [1.5, 2.0]	3.1 [2.4, 4.1]
1.2	4.1 [3.9, 4.4]	4.8 [4.5, 5.1]	2.8 [2.6, 3.1]	1.7 [1.5, 1.9]	3.1 [2.4, 4.0]
1.0	4.1 [3.9, 4.4]	4.8 [4.5, 5.1]	2.8 [2.5, 3.1]	1.7 [1.5, 1.9]	3.1 [2.4, 4.0]
0.8	4.2 [3.9, 4.4]	4.8 [4.5, 5.2]	2.9 [2.6, 3.2]	1.6 [1.4, 1.9]	3.0 [2.3, 3.9]
0.6	4.2 [3.9, 4.4]	4.9 [4.5, 5.2]	2.8 [2.5, 3.1]	1.7 [1.5, 1.9]	3.0 [2.3, 3.9]
0.4	4.2 [3.9, 4.4]	4.9 [4.6, 5.3]	2.8 [2.5, 3.1]	1.7 [1.5, 1.9]	3.1 [2.4, 4.0]
0.2	4.2 [3.9, 4.4]	4.9 [4.6, 5.2]	2.8 [2.5, 3.2]	1.5 [1.3, 1.7]	2.8 [2.1, 3.5]

2.8.4 *Discussion*

AMSA values changed scale when epoch length was shortened, indicating that the current AMSA implementation is not comparable across mixed-length epochs. This is likely due to the increasing effect of larger sidelobes and decreased frequency resolution as input length is shortened. Since AMSA is the sum of the spectral magnitude at each frequency multiplied by its frequency value, changes in the amount of sidelobe ripple and central peak width as a result of decreased frequency resolution (especially in higher frequencies) would likely increase the final AMSA. Additionally, in this instance the Fourier transform magnitudes were normalized by the ECG input length, which results in increased AMSA as input length decreases. (AMSA was still observed to change scale even without normalizing the Fourier transform, however.) Other normalization techniques (such as scaling by the number of points in the discrete Fourier transform or by the area under the spectrum) could have differing effects on AMSA across varying ECG input lengths, and perhaps allow AMSA to be compared more equitably across different epoch lengths. In contrast, MS remained on a similar scale across epoch lengths, and appears usable across mixed-length ECG epochs. This follows intuition, as MS is the median of the slope between pairs of points in the ECG and should maintain a similar scale regardless of epoch length, assuming the signal is stationary.

2.8.5 *Conclusion*

Odds ratios for AMSA and MS prediction of ROR followed a similar trend to AUC. Standardized odds ratios of log AMSA and MS had similar trends for both measures, with the most abrupt reductions in performance occurring at epoch lengths below 1 second. MS (but not AMSA) also may be useful for analysis with mixed-length epochs, which could allow integration of repeated waveform measure readings during incidental CPR pauses, even if pause times are varied.

Chapter 3. INCORPORATION OF PRIOR SHOCK OUTCOME IMPROVES VENTRICULAR FIBRILLATION WAVEFORM MEASURE PERFORMANCE DURING CHEST COMPRESSIONS

Adapted from: **Coult J,** Kwok H, Sherman L, Blackwood J, Kudenchuk P, Rea T. Ventricular fibrillation waveform measures combined with prior shock outcome predict defibrillation success during cardiopulmonary resuscitation. *Journal of Electrocardiology* 2018; 51:99-106. https://doi.org/10.1016/j.jelectrocard.2017.07.016

3.1 ABSTRACT

Aim: Amplitude Spectrum Area (AMSA) and Median Slope (MS) are ventricular fibrillation (VF) waveform measures that predict defibrillation shock success. Cardiopulmonary resuscitation (CPR) obscures electrocardiograms and must be paused for analysis. Studies suggest waveform measures better predict subsequent shock success when combined with prior shock success. We determined whether this relationship applies during CPR. *Methods:* AMSA and MS were calculated from 5-second pre-shock segments with and without CPR, and compared to logistic models combining each measure with prior return of organized rhythm (ROR). *Results:* VF segments from 692 patients were analyzed during CPR before 1372 shocks and without CPR before 1283 shocks. Combining waveform measures with *Prior ROR* increased areas under receiver operating characteristic curves for AMSA/MS with CPR (0.66/0.68 to 0.73/0.74, $p<0.001$) and without CPR (0.71/0.72 to 0.76/0.76, $p<0.001$). *Conclusions: Prior ROR* improves prediction of shock success during CPR, and may enable waveform measure calculation without chest compression pauses.

3.2 INTRODUCTION

Sudden cardiac arrest caused by ventricular fibrillation (VF) is a major cause of death in the US.[3] Defibrillation and cardiopulmonary resuscitation (CPR) are the definitive treatments for VF. However some shocks may fail to terminate VF, fail to result in an organized rhythm, or fail to produce return of spontaneous circulation.[49,63] Moreover, shocks require cessation of CPR for rhythm analysis and shock delivery, a circumstance adversely associated with the likelihood of resuscitation.[46–48] Ideally, shocks could be timed to achieve optimal likelihood of resuscitation while limiting interruption in CPR.

Quantitative measures of the VF electrocardiogram (ECG) are dynamic over the course of resuscitation[86] and predict shock success,[57] and thus have the potential to serve as real-time prognostic markers to guide therapy and shock timing. For instance, if a shock is likely to be unsuccessful due to prolonged VF, temporarily delaying shock and continuing CPR may improve outcome.[40,41] However, chest compressions obscure the ECG, requiring a pause in CPR for accurate waveform measure calculation.[34,43–45,69] A next-step strategy to predict shock outcome combines VF waveform measures with other features of the ECG to improve performance during CPR.

Research has suggested that prior rhythm and perfusion state are associated with subsequent likelihood of return of spontaneous circulation following shock,[106] and that this information in combination with waveform measures may improve prediction of shock success.[112] However, this relationship has not been tested during CPR, challenging real-world implementation of such a strategy. If a combination algorithm could more accurately predict shock success during CPR, then shock delivery might be timed based on a real-time prognostic likelihood calculated during continuous CPR.[34,45]

We sought to assess the predictive characteristics of two representative waveform measures, and to evaluate whether combining waveform measures with prior shock outcome improves prediction of shock success both with and without CPR.

3.3 METHODS

3.3.1 *Study Design, Population, and Setting*

The study was a retrospective cohort investigation of adult out-of-hospital cardiac arrest patients presenting with an initial rhythm of VF in King County, WA, from 2005-2014. Because the study in part evaluated the role of the ECG response to the prior shock, the primary study cohort was restricted to patients who required at least two shocks. Cases were excluded if the defibrillator model did not record chest impedance, a public access defibrillator was used to deliver a shock prior to Emergency Medical Services (EMS) arrival, defibrillator data was missing or corrupted, or a 5-s VF ECG segment was not available before any of the first three subsequent shocks following initial shock. The study was approved by the Investigational Review Board at the University of Washington Human Subjects Division.

The EMS system in King County is composed of two tiers. The first tier consists of firefighter emergency medical technicians equipped with automated external defibrillators. The second tier consists of paramedics trained in advanced cardiac life support, ECG rhythm identification, and manual defibrillation. Resuscitation by EMS agencies in King County follows American Heart Association guidelines.[31]

3.3.2 *Data Collection and Definitions*

Cardiac arrest cases were collected using the Utstein template.[113] ECGs from MRx defibrillators (Philips Healthcare, Bothell, WA) were recorded at a sample rate of 250 Hz, and ECGs from Lifepak 12 and Lifepak 15 defibrillators (Physio-Control, Redmond, WA) were recorded at 125 Hz and resampled to 250 Hz. For each patient, one 5-s VF ECG segment was collected with CPR and one segment was collected without CPR prior to the first three subsequent shocks following initial shock, when available. Presence of chest compressions was determined through manual review of the chest impedance signal (Figure 3.1). Presence of VF during CPR was verified during adjacent pauses in CPR and adjudicated by physician review if necessary.

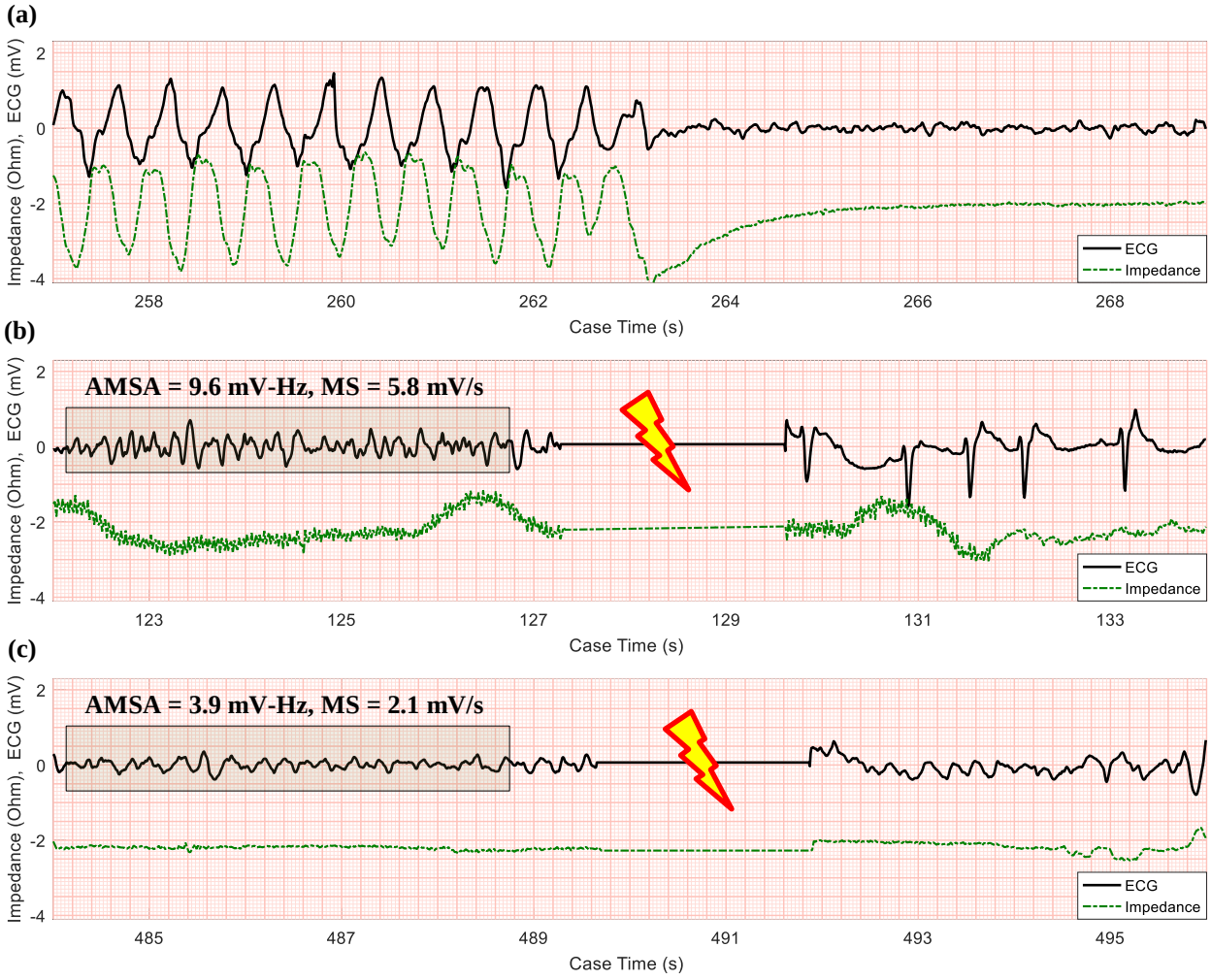

Figure 3.1. Ventricular fibrillation examples
(a) VF is obscured during CPR and visible once compressions cease; (b) VF with good prognosis, as indicated by high AMSA and MS, results in return of rhythm following shock; (c) VF with poor prognosis, as indicated by low AMSA and MS, results in a failed shock (c). Shocks are indicated by the lighting graphic. Impedance is shifted vertically for illustration.

3.3.3 *ECG Processing and Quantitative Waveform Measure Calculation*

We computed the Amplitude Spectrum Area (AMSA)[97,98] and Median Slope (MS)[68,106] as representative frequency-domain and time-domain quantitative waveform measures. Prior to waveform measure calculation, ECG segments were filtered with a 4th-order Butterworth filter

from 4-30 Hz to reduce chest compression artifact and high-frequency noise (Figure 3.2).

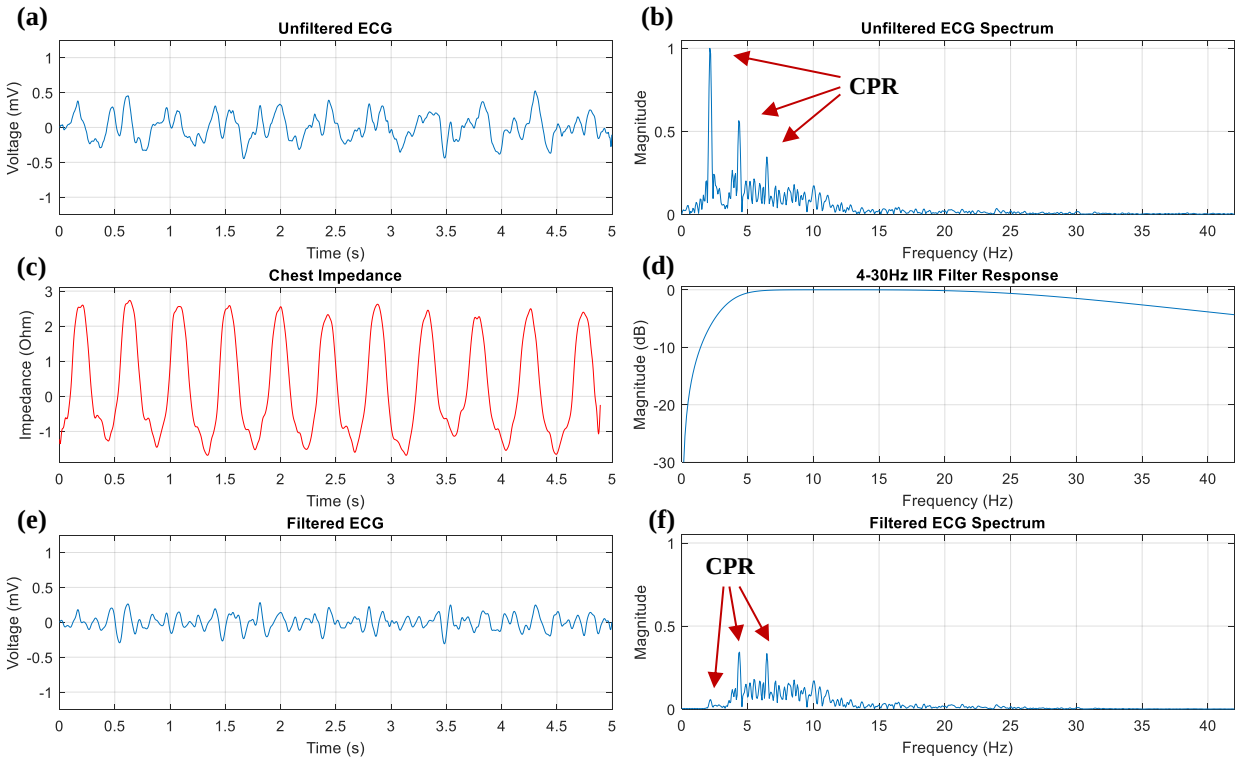

Figure 3.2. Bandpass filtering only partially removes CPR artifact
(a) Unfiltered VF ECG segment during collected during CPR, with compression artifact, (b) Normalized magnitude spectrum of unfiltered VF segment showing CPR artifact at approximately 2.3 Hz, with harmonics at approximately 4.6 Hz and 6.9 Hz, (c) Chest impedance signal (shifted for visibility) confirms presence of CPR, (d) 4th-order 4-30 Hz Butterworth bandpass filter magnitude response, (e) Filtered ECG segment with reduced CPR artifact at fundamental frequency of compressions, (f) Spectrum of ECG showing removal of fundamental CPR frequency and a marginal reduction in the first CPR harmonic. The magnitude response suggests that a higher filter frequency cutoff would remove more CPR artifact but would also remove VF content.

After filtering, AMSA was calculated from 1-26 Hz[65] as:

$$AMSA = \sum_{m=1Hz\cdot(N/f_s)}^{26Hz\cdot(N/f_s)} (X_m f_m) \qquad (3.1)$$

where $X_0,...,X_m,...,X_{N/2}$ are the one-sided Discrete Fourier Transform magnitudes calculated from ECG voltages $x_0,...,x_n,...,x_{N-1}$ sampled at rate f_s, and the frequency values f_m are defined

in terms of the frequency index m and input length N, such that $f_m = m \cdot f_s / N$. Likewise, MS was calculated as:

$$MS = (\text{median} \left| x_{n+1} - x_n \right| f_s) \tag{3.2}$$

for $n = 0, ..., N-2$.

3.3.4 *Shock Success*

Shock success was defined as return of organized rhythm (ROR) with at least two QRS complexes in a 5-s interval within two minutes following shock (Figure 3.1).[114] Each shock was also annotated with a dichotomous variable, *Prior ROR*, indicating whether the prior shock was successful. To provide an estimate of inter-rater reliability, a second reviewer annotated ROR for a random subset of 20% of patients in the study group. Shocks with indeterminate ROR or *Prior ROR* were excluded.

3.3.5 *Data and Statistical Analysis*

We characterized cases according to inclusion in the primary study cohort using descriptive statistics. Patients in the study group were randomly divided into 30% training and 70% test groups. ECG segments were sorted based on training and test patient group and presence of CPR. Using the training segments, we developed logistic models to predict ROR: the first model type used a waveform measure alone (AMSA or MS) and the second used a waveform measure combined with *Prior ROR*. For instance, for AMSA, the probabilities of successful shock were calculated as:

$$P(ROR \left| AMSA) = \frac{1}{1 + \exp\left[-\left(\beta_0 + \beta_1 \cdot AMSA \right) \right]} \right. \tag{3.3}$$

and

$$P(ROR \mid AMSA, Prior\ ROR) = \frac{1}{1+\exp\left[-\left(\beta_0 + \beta_1 \cdot AMSA + \beta_2 \cdot Prior\ ROR\right)\right]} \quad (3.4)$$

where P is the probability of ROR following shock, $AMSA$ is the natural log amplitude spectrum area calculated from a 5-s VF sample, $Prior\ ROR$ is a binary variable representing whether prior shock was successful, and the β parameters are logistic regression coefficients trained either with or without CPR.

Area under the receiver operating characteristic curve (AUC) was used to assess model performance for prediction of shock success. AUC values for receiver operating characteristic curves were compared using Delong's method.[109,115] Waveform measure medians were compared using a two-sided Wilcoxon rank-sum test. The Pearson phi coefficient was used to evaluate association of shock outcomes between adjacent shocks. Cohen's kappa was used to estimate inter-rater reliability. As a supplementary analysis to examine whether training dataset size or patient allocation to training or test groups affected results, AUCs were also re-estimated using 10-fold cross-validation across all data.[116–118] MATLAB 2016b (The Mathworks, Natick, MA, USA) and R 3.0.2 (R Foundation for Statistical Computing, Vienna, Austria) were used for statistical and signal analysis.

3.4 RESULTS

3.4.1 *Study Group*

During the study period, there were 1434 primary VF patients who received more than one shock and were eligible for inclusion in the study (Figure 3.3). Of eligible patients, 742 (52%) were excluded, most commonly due to absence of defibrillator data or treatment with a device that did

not record chest impedance. After exclusions, there were 692 (48%) patients included in the final study group.

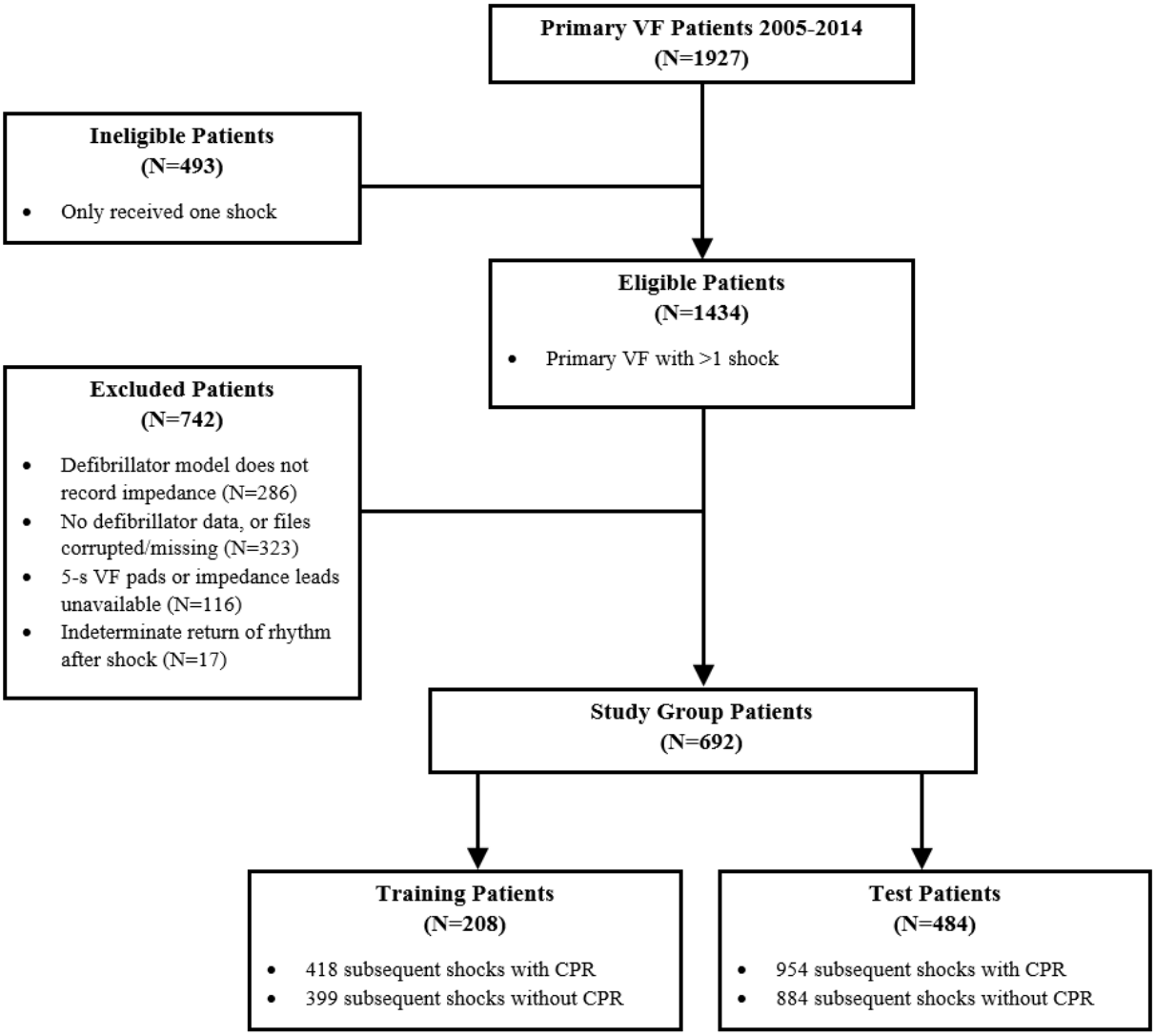

Figure 3.3. Study group
The number of patients removed based on ineligibility and exclusion criteria are presented, as well as the final number of shocks sampled from the training and test subsets of the study group.

Demographic characteristics of included and excluded patients were similar (Table 3.1). Of the 692 patients included in the study group, 208 (30%) were randomly assigned to the training group and 484 (70%) to the test group. VF segments were collected during CPR prior to 1372

subsequent shocks and without CPR prior to 1283 shocks. Of all VF segments collected, there were 418/399 segments with/without CPR from patients in the training group, and 954/884 segments with/without CPR from patients in the test group.

Table 3.1. Patient characteristics by inclusion-exclusion
Presented are all primary VF 2005-2014, all primary VF patients with >1 shock, excluded patients, and the final study group.

Characteristic	All VF 2005-2014 (N=1927)	All VF, >1 Shock (N=1434)	Excluded (N=742)	Study Group (N=692)
Female, n(%)	454 (23.6)	333 (23.2)	168 (22.6)	165 (23.8)
Age, median (IQR)	62 (52, 73)	62 (52, 73)	63 (52, 73)	61 (52, 73)
Cardiac etiology, n(%)	1742 (90.4)	1314 (91.6)	672 (90.6)	642 (92.8)
Location, n(%)				
Home	1208 (62.7)	908 (63.3)	455 (61.3)	453 (65.5)
Public	627 (32.5)	467 (32.6)	248 (33.4)	219 (31.6)
Nursing Home	92 (4.8)	59 (4.1)	39 (5.3)	20 (2.9)
Arrest before EMS arrival, n(%)	1713 (88.9)	1300 (90.7)	645 (86.9)	655 (94.7)
Witnessed, n(%)	1482 (76.9)	1110 (77.4)	576 (77.6)	534 (77.2)
Bystander CPR, n(%)	1249 (64.8)	939 (65.5)	477 (64.3)	462 (66.8)
Response time (mins), median (IQR)	5 (4, 6.6)	5 (4, 6.9)	5 (4, 7)	5 (4, 6.2)
Total shocks, median (IQR)	3 (1, 6)	4 (3, 7)	4 (3, 6)	5 (3, 7)
ROSC, n(%)	1281 (66.5)	891 (62.1)	456 (61.5)	435 (62.9)
Died in Field	498 (25.8)	405 (28.2)	210 (28.3)	195 (28.2)
Admit to hospital	1254 (65.1)	876 (61.1)	439 (59.2)	437 (63.2)
Survive to hospital discharge, n(%)	818 (42.4)	550 (38.4)	276 (37.2)	274 (39.6)

3.4.2 *Return of Organized Rhythm*

ROR occurred after 801 (58%) of segments with CPR and 750 (58%) of segments without CPR. When stratified by shock number, the first, second, and third subsequent shocks all had similar rates of ROR. There was significant association between ROR from adjacent shocks (φ=0.36, $p<0.001$). Inter-rater reliability of ROR annotation between two reviewers, estimated from a random subset of 292 shocks from 138 patients, was high (κ [95% CI] = 0.85 [0.78-0.91]).

3.4.3 *Waveform Measures and Prognostic Performance*

Median AMSA was 6.27 [IQR 4.03, 8.51] mV-Hz during CPR and 5.02 [IQR 3.06, 6.99] mV-Hz without CPR ($p<0.001$ for difference). Median MS was 3.51 [IQR 2.17, 4.86] mV/s during CPR and 2.80 [IQR 1.56, 4.05] mV/s without CPR ($p<0.001$ for difference). Median AMSA and MS were significantly higher before successful shocks compared to unsuccessful shocks both with and without CPR (Table 3.2).

Table 3.2. Waveform measures for successful versus unsuccessful shocks
Median values are presented with and without CPR for all AMSA and MS samples that resulting in ROR after shock versus those resulting in no ROR after shock.

	With CPR		**Without CPR**	
	ROR (n=801)	**No ROR** (n=571)	**ROR** (n=750)	**No ROR** (n=533)
AMSA Median [IQR] (mV-Hz)	7.15 [4.95, 9.35]*	5.21 [3.26, 7.16]	6.00 [4.02, 7.97]*	3.74 [2.21, 5.27]
MS Median [IQR] (mV/s)	4.11 [2.74, 5.48]*	2.82 [1.74, 3.90]	3.47 [2.22, 4.73]*	2.02 [1.10, 2.94]

*ROR median significantly higher than No ROR median ($p<0.001$, two-sided Wilcoxon rank-sum test)

In all logistic models, waveform measures and *Prior ROR* were associated with a successful shock (Table 3.3). Predictive performance was significantly improved when *Prior ROR* was added to either waveform measure, regardless of whether CPR was ongoing (Table 3.4). For example, during CPR, AUC for AMSA alone was 0.66 [95% CI 0.63-0.70], while AUC for AMSA with *Prior ROR* was 0.73 [95% CI 0.70-0.76].

Table 3.3. Odds ratios for logistic model coefficients
Odds ratios are presented with 95% CIs for waveform measures alone and for waveform measures in combination with *Prior ROR*. Results are shown with and without CPR. Logistic models were fit on the N=208 training patients (418 shocks with CPR and 399 shocks without CPR).

		With CPR		Without CPR	
Model Type	**Variable**	**Odds [95% CI]**	**Standardized Odds [95% CI]**	**Odds [95% CI]**	**Standardized Odds [95% CI]**
Measure Alone	AMSA (mV-Hz)	1.22 [1.14-1.31]	1.98 [1.58-2.48]	1.31 [1.21-1.42]	2.21 [1.75-2.78]
Combination	AMSA (mV-Hz)	1.16 [1.08-1.24]	1.68 [1.33-2.12]	1.21 [1.11-1.32]	1.75 [1.37-2.24]
	Prior ROR	3.58 [2.31-5.55]	N/A	3.48 [2.17-5.56]	N/A
Measure Alone	MS (mV/s)	1.43 [1.28-1.61]	2.19 [1.70-2.81]	1.57 [1.37-1.79]	2.47 [1.89-3.22]
Combination	MS (mV/s)	1.32 [1.17-1.48]	1.82 [1.41-2.35]	1.38 [1.20-1.59]	1.91 [1.45-2.53]
	Prior ROR	3.44 [2.21-5.35]	N/A	3.33 [2.07-5.34]	N/A

Table 3.4. AUC for prediction of shock success
AUC values are presented for prediction of shock success on N=484 patients in test group (954 shocks with CPR, 884 shocks without CPR). AUC is significantly increased due to inclusion of *Prior ROR* versus waveform measures alone.

Logistic Model	**With CPR: AUC [95% CI]**	**Without CPR: AUC [95% CI]**
AMSA only	0.66 [0.63-0.70]	0.71 [0.67-0.74]
AMSA + Prior ROR	0.73 [0.70-0.76]	0.76 [0.72-0.79]
(Change)	0.07 [0.04-0.10]*	0.04 [0.02-0.07]*
MS only	0.68 [0.64-0.71]	0.71 [0.68-0.75]
MS + Prior ROR	0.74 [0.71-0.77]	0.76 [0.72-0.79]
(Change)	0.06 [0.04-0.09]*	0.05 [0.03-0.07]*

*p<0.001 for change (DeLong's method)

The increase in AUC due to *Prior ROR* varied across individual shocks and CPR state (Figure 3.4, Figure 3.5). For instance, during CPR, inclusion of *Prior ROR* increased the AMSA AUC by 0.04 for shock 2, 0.07 for shock 3, and 0.15 for shock 4 over that of AMSA alone (Appendix B: Effect of CPR and Bandpass Filtering). Results using 10-fold cross-validation were similar (Appendix A: Cross-Validation).

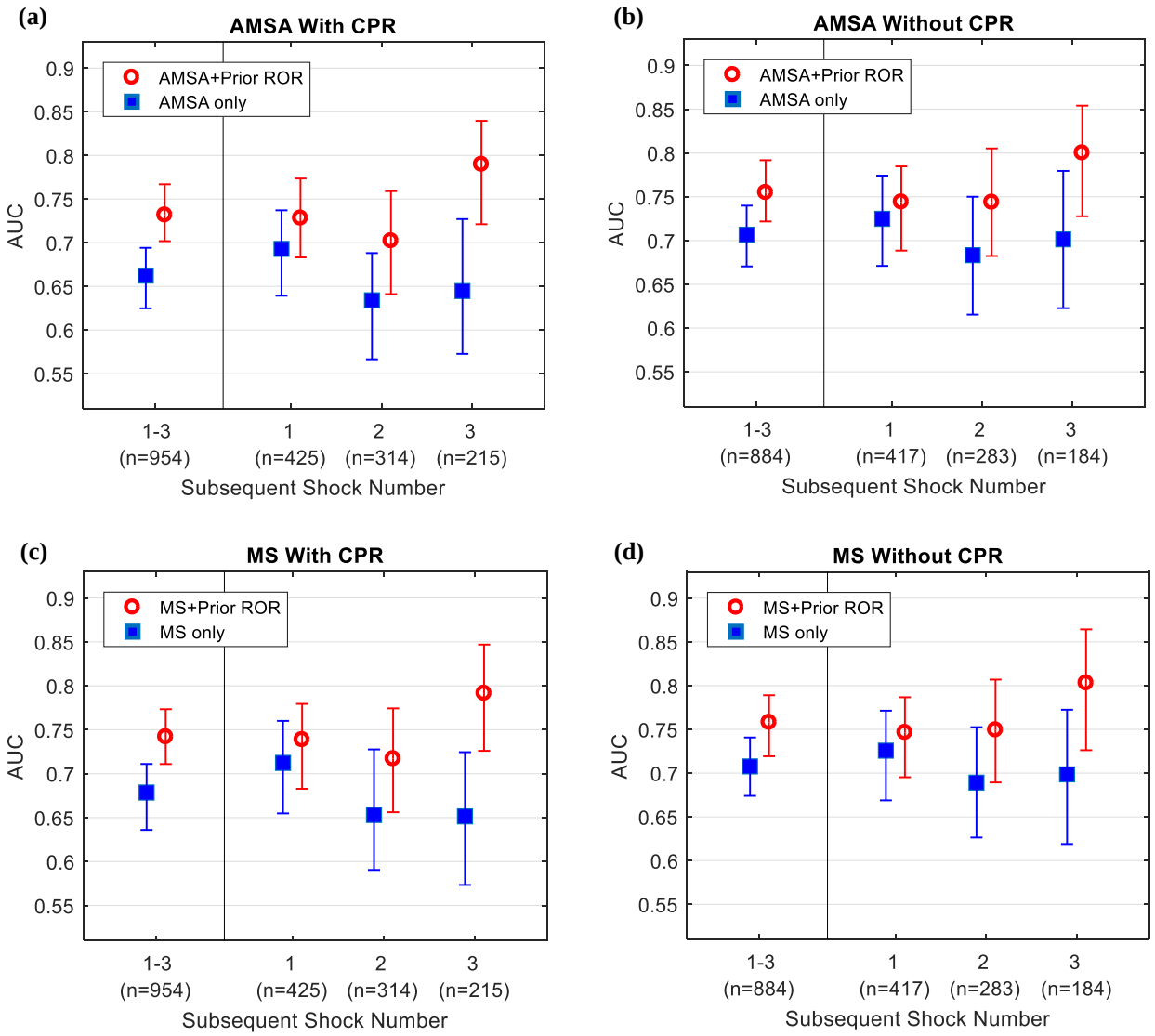

Figure 3.4. AUC values for predicting shock success
AUCs with 95% CIs are shown for all subsequent shocks using (a) AMSA with CPR, (b) AMSA without CPR, (c) MS with CPR, and (d) MS without CPR. AUC values are presented for all subsequent shocks combined and also by individual shock number. Combined AUCs are significantly higher for waveform measures in combination with *Prior ROR* versus waveform measures alone.

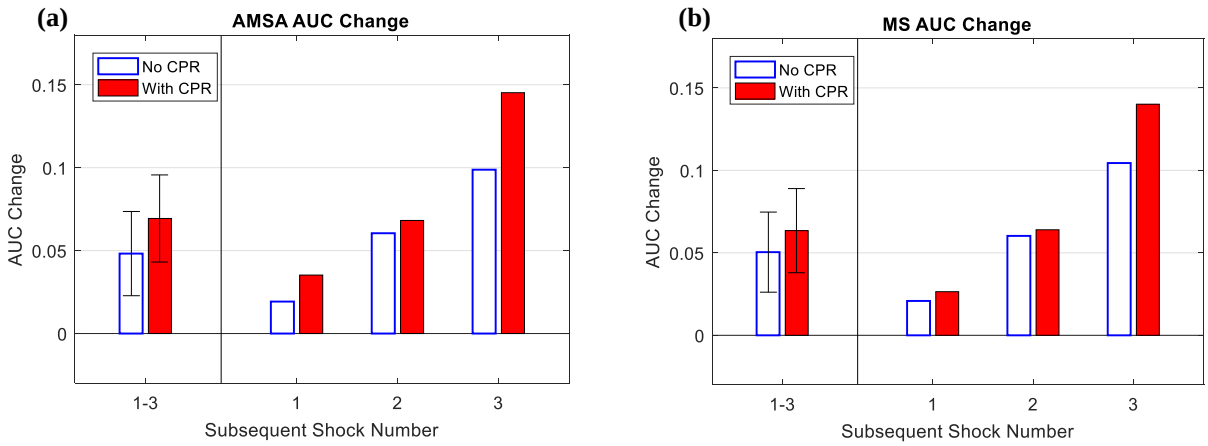

Figure 3.5. AUC increase for waveform measures combined with *Prior ROR*
AUC change for *Prior ROR* combined with waveform measures compared to measures alone (n=884 shocks without CPR, n=984 shocks with CPR). Change is indicated by shock cycle with and without CPR, for (a) AMSA and (b) MS. Absolute increase is greater as shock sequence progresses. Error bars on combined shocks represent 95% CI for change.

3.5 DISCUSSION

In this investigation of out-of-hospital arrest, we confirmed that two representative VF waveform measures, AMSA and MS, predict shock outcome as determined by return of rhythm in the ECG. We observed that the measures retain some prognostic capability during CPR but AUC is reduced compared to CPR-free analysis. Moreover, in novel investigation, we demonstrated that inclusion of previous shock outcome improves waveform measures during CPR and offsets the reduction in waveform measure performance caused by CPR artifact. Combining information from waveform measures and the resuscitation history thus offers a step forward towards achieving near-continuous CPR while guiding treatment and its timing.

Ideally cardiac arrest treatment would be tailored to match individual pathophysiology in order to achieve the greatest likelihood of resuscitation.[119] Shocks that are less likely to result in ROR could be temporarily postponed to allow additional perfusion with CPR (or other interim treatments) that might enhance subsequent shock success.[40,41,57] Conversely, shocks more certain

to result in ROR could be administered immediately. Such an approach would not necessarily delay receipt of an immediate shock, since rhythm analysis (to determine whether the rhythm is shockable or non-shockable) and prognostic assessment could both be performed concurrently. However, current protocol uses a uniform approach that delivers shocks using fixed timing based on information available at predetermined 2-minute intervals.[45] Outcomes might be improved if care could be guided by real-time physiologic measures throughout the course of resuscitation, especially if these measures incorporated accumulating information about patient-specific response to therapy. The approach is largely untested in human resuscitation, but such "patient-specific" resuscitation is supported by the results of experimental research.[120,121]

Multiple prior studies have highlighted the ability of waveform measures to predict shock outcome, i.e. return of rhythm or survival.[57] However these studies require CPR-free ECG epochs in order to calculate quantitative waveform measures. Such interruptions undermine the goals of continuous circulatory support during resuscitation.[31] Given this understanding, we previously evaluated the prognostic ability of waveform measures using ever-shorter CPR-free segments, and found that measures retain comparable prediction even as the CPR-free segment length approaches <1 second.[114] Nonetheless, even these brief interruptions are logistically challenging to coordinate, and would not support continuous VF waveform assessment during CPR.

Hence, we evaluated the prognostic characteristics of two well-characterized waveform measures – AMSA and MS – *during* uninterrupted CPR. As part of the investigation, we applied a bandpass filter to improve the usability of the ECG waveform (Appendix B: Effect of CPR and Bandpass Filtering). The fundamental frequency of chest compressions is approximately 2 Hz, while VF frequencies are primarily between 3-8 Hz.[122] However, harmonics and higher-frequency CPR artifact lie within the spectral range of the VF signal, such that removal via filtering cannot

be easily accomplished without degrading the VF signal itself.[45] Waveform measures therefore cannot be calculated optimally during CPR even after filtering the ECG.[43,44,69,123] Since AMSA is computed from the product of each frequency and its magnitude, and MS computes the pointwise derivative, both measures increasingly emphasize higher-frequency content. Consequently, AMSA and MS may still be relatively better-suited to evaluate VF during chest compressions as they inherently ignore some CPR artifact. In our investigation, AMSA and MS did indeed predict ROR after shock during CPR, though the AUC was notably less compared to CPR-free analysis.

We sought to evaluate whether additional information might be combined with quantitative waveform measures to increase prognostic accuracy during CPR. Research has suggested that prior rhythm is associated with subsequent likelihood of return of spontaneous circulation following shock, and that this information may improve prediction when combined with waveform measures calculated during CPR-free epochs.[106,112] However little is known about whether ROR from prior shock would improve prediction when combined with waveform measures calculated during CPR. We observed that *Prior ROR* was associated with the response to a subsequent shock. Moreover, *Prior ROR* in combination with waveform measures significantly increased AUC for prognosis regardless of whether CPR artifact was present. Additionally, the increase in AUC by incorporating *Prior ROR* was greater as shock sequence progressed, suggesting that patient response to shock may be increasingly related to previous shock response over the course of resuscitation.

In this study we demonstrated that when prior shock outcome is known, it can be leveraged to improve waveform measure prognostic ability during CPR. Clinical benefit of a prognostic algorithm able to assess VF viability during CPR would be contingent on ability to also classify ECG rhythms (i.e. detect VF) during CPR. Unfortunately, current protocol for rhythm analysis

still requires a pause in chest compressions for rhythm classification.[45] Recent experimental work, however, demonstrates the possibility of real-time rhythm classification during CPR by incorporating ECG history over time.[72] This finding further highlights the value of integrating information accumulated over the course of resuscitation to improve accuracy during CPR. By including historical information from the ECG, patient-specific treatment guided by a real-time prognostic algorithm concurrent with real-time rhythm classification may be possible without interruption of chest compressions. Further efforts to develop such a prognostic algorithm would involve improving individual waveform measures as well as refining methods to integrate continuous readings (rather than using a limited number of isolated segments) to increase prognostic accuracy.

In summary, the AUC that resulted from the combination of waveform measures with prior shock success during CPR was improved over the AUC of waveform measures alone. Waveform measures during CPR combined with *Prior ROR* also exceeded the predictive capability of CPR-free waveform measures alone. These results support – at least in concept – that historical ECG information in addition to analysis of isolated segments can overcome some of the prognostic challenges introduced by CPR artifact, and in turn may enable guided resuscitation with continuous CPR.

3.6 LIMITATIONS

We used waveform measures as well as ROR from prior shock to develop a prognostic model that could predict subsequent ROR. This method incorporates previous shock success and thus would not apply to prediction of initial shock outcome. Overall predictive performance was modest, thus limiting potential clinical application of the specific measures used. The study group restriction to subsequent shocks may also have affected results due to exclusion of patients resuscitated with a

single shock; for instance, waveform measure AUC values in this study were less compared to a previous investigation of initial shocks.[114]

We used ROR as a shock-specific electrical outcome. ROR had excellent inter-reviewer reliability in the current study, but since ROR includes non-perfusing organized rhythms, its utility as a surrogate clinical outcome may be limited. Other definitions of shock success such as return of spontaneous circulation could also serve as a shock-specific outcome and may produce different results. For instance, we did observe that *Prior ROR* improved waveform measure prediction of survival, but the AUC increase was not statistically significant.

Each shock was treated as an independent sample for training and test, though multiple clips from the same patient were included in the study. This approach may produce correlation among ECG segments, although only a maximum of three subsequent shocks were collected from a single patient.

The study included ECG segments from multiple defibrillator models with different filtering bandwidths. This heterogeneity underscores the generalizability of the findings across different hardware platforms, but due to waveform measure relationship to high frequency content, may cause variation in waveform measure magnitude between devices and may reduce combined AUC. The study was retrospective and so did not actually incorporate ROR status or waveform measures in real time, and results therefore may not be indicative of prospective investigation.

3.7 CONCLUSION

AMSA and MS retained shock-specific prognostic value when generated during CPR, and their predictive ability was improved by incorporating outcome from the prior shock. Future efforts may continue to refine and evaluate how historical ECG information predicts outcome and may potentially guide patient-specific care.

3.8 Appendix A: Cross-Validation to Confirm Results

3.8.1 *Introduction*

Due to finite dataset size, the single random 30% training and 70% test split used in the primary study could produce variable results depending on which patients were randomly assigned to the training or test groups, and what percentage of the data was included in each set. For instance, a patient containing ECG segments with relatively extreme CPR artifact could affect training or test results. Or, if the training set were too small, classification models might not sufficiently train and thus underestimate the benefit of including prior return of rhythm (*Prior ROR*) in combination with waveform measures. Hence, we sought to confirm the AUC values reported in the primary study using k-fold cross-validation.[116–118]

3.8.2 *Methods*

As an alternative to randomly splitting the patients into training and test datasets with a single division, k-fold cross validation was used across *all* ECG segments to compare the performance of the logistic models with waveform measures in combination with *Prior ROR* versus waveform measure alone. K-fold cross-validation is typically used to provide an accurate estimate of classification model performance when dataset size is modest.[101] K-fold cross-validation allows use of as large a training set as possible to allow optimal model training, while also ensuring each sample is used once in the validation results and no difficult samples are excluded from the test set.

To perform cross-validation, all ECG segments from the first three subsequent shocks were separated into k=10 exclusive, random folds of equal size for both the CPR and non-CPR datasets. To ensure homogeneity and even numbers in each fold, rather than divide patients into training

and test folds, individual VF segments were divided regardless of which patient they were collected from. For each of the k=10 iterations, a logistic regression model using AMSA with *Prior ROR* was trained on nine of the ten folds (Figure 3.6). AUCs for the logistic AMSA with *Prior ROR* model and for AMSA alone were computed on the remaining validation fold. This process was repeated for each of the ten folds, resulting in ten validation AUC values for AMSA with *Prior ROR* and AMSA alone. Point estimates and standard deviations for AMSA and AMSA with *Prior ROR* mean validation AUC values, for both without-CPR and with-CPR clips, were then compared. The procedure was then repeated for MS instead of AMSA.

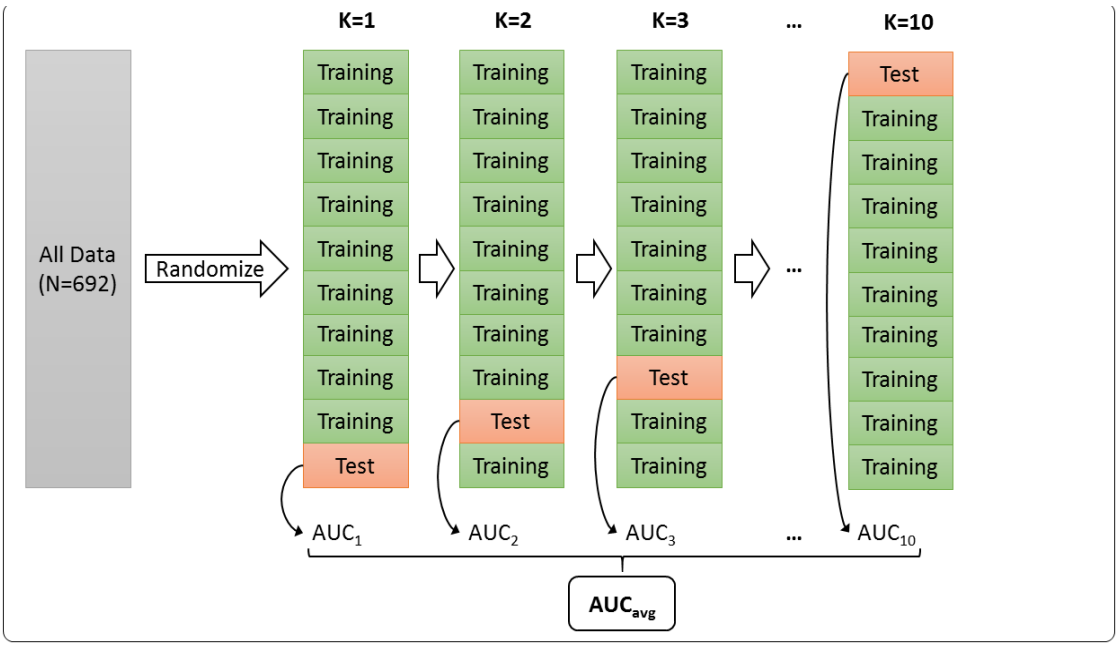

Figure 3.6 Cross-validation estimation of AUC mean
Data from all 692 study group patients (1372 clips with CPR or 1283 clips without CPR) were randomized into k=10 folds, with each holdout fold used once as a test fold.

3.8.3 *Results*

For the first three subsequent shocks with CPR (n=1372), mean cross-validation AUC was higher for AMSA and MS in combination with *Prior ROR*. For all subsequent shocks, combining *Prior*

ROR with AMSA improved mean AUC for prediction of shock success by 0.06 during CPR and by 0.04 without CPR (Table 3.5). Similarly, combining *Prior ROR* with MS improved mean MS AUC by 0.06 during CPR and by 0.05 without CPR.

Table 3.5. Mean cross-validation AUC
Mean cross-validation AUC values for prediction of shock success with and without CPR. Results are presented for the first three subsequent shocks combined and also by individual shock.

	With CPR (n=1372)				**Without CPR (n=1283)**			
Subsequent Shock #	1-3	1	2	3	1-3	1	2	3
AMSA	0.67	0.70	0.64	0.66	0.71	0.72	0.68	0.74
AMSA + *Prior ROR*	0.73	0.74	0.71	0.80	0.75	0.74	0.73	0.83
MS	0.68	0.71	0.65	0.68	0.71	0.72	0.69	0.72
MS + *Prior ROR*	0.74	0.74	0.72	0.81	0.76	0.74	0.74	0.84

3.8.4 *Discussion and Conclusion*

Inclusion of the prior shock's return of organized rhythm status improved the ability of AMSA and MS to predict shock success both during and without CPR. Mean cross-validation AUC for AMSA improved by approximately 0.06 for clips during CPR and 0.04 for clips without CPR, which is consistent with the primary study results. Similarly, mean MS AUC increased by 0.06 during CPR and 0.05 without CPR, also similar to the primary study results.

Mean k-fold cross-validation may provide a more stable estimate of model performance on limited datasets by ensuring that each and every sample, including any potentially difficult outliers, is used exactly once for validation. In this process, no difficult samples are left out of the validation. Model overfitting is reduced due to larger training set size for each fold. These results confirm that dataset size did not likely confound the primary study results, and that randomization of training and test clips did not affect the difficulty or generalizability of the test set.

In summary, K-fold cross-validation results generally confirm the primary study results. However, to confirm true generalizability, a separate validation dataset should be evaluated.

3.9 Appendix B: Effect of CPR and Bandpass Filtering

3.9.1 *Introduction*

Figure 3.2 illustrates the effect of the 4-30 Hz Butterworth filter employed in the primary study used to filter the ventricular fibrillation (VF) electrocardiogram (ECG) segments. Appendix B compares the effect of filtering on segments collected with and without chest compressions. Amplitude Spectrum Area (AMSA) and Median Slope (MS) waveform measures, calculated both with and without cardiopulmonary resuscitation (CPR) artifact, are compared before and after the filter is applied. The objective of this section is to assess the benefit of the filter on waveform measure calculation with and without CPR, and to also examine the reduction in AMSA and MS performance caused by CPR artifact.

3.9.2 *Methods*

In the primary study, VF ECG segments were collected with and without CPR prior to the first three subsequent shocks from out-of-hospital primary VF patients from 2005-2014 in King County WA. Initial shocks were ineligible for the primary study because the study involved prior shock response. However, to examine the effect of the ECG bandpass filter on AMSA and MS alone in this Appendix, the eligibility criteria for VF segments is expanded to include VF collected prior to *initial* shocks in addition to subsequent shocks. Therefore, ECG segments that were collected prior to *both* the initial shock and the first three subsequent shocks when available, with and without CPR chest compression artifact, are included. This allows for an increased number of VF samples and a more accurate assessment of filter effect on waveform measures.

After subtracting the mean from each the ECG segments, a 4^{th}-order 4-30 Hz Butterworth filter was used to filter all ECGs to mitigate the effect of chest compressions. The filter was

implemented with a forward-backward implementation, which corrects phase distortion and squares the filter magnitude response. An example with CPR is shown in Figure 3.2.

AMSA and MS were calculated using all available VF segments collected from primary VF patients within the study period, including segments prior to initial shock. Area under the receiver operating characteristic curve (AUC) for prediction of shock success was computed both with and without CPR for filtered and unfiltered AMSA and MS. DeLong's nonparametric method for paired receiver operating characteristic curves was used to compare filtered versus unfiltered AUCs, and Robin's extension of DeLong's method for unpaired curves were used to compare AUCs with and without CPR.

3.9.3 *Results*

Expanding eligibility to include patients with a single initial shock added an additional 376 patients to the experimental group in this Appendix, resulting in a total of 1068 patients with usable VF segments prior to shock. Demographics for the expanded study group had slightly improved outcome compared to the original study group but were otherwise similar (Table 3.6).

Table 3.6. Appendix B patient characteristics
Demographics of Appendix B group (includes patients with just an initial shock) versus all VF and original study group. (CPR = Cardiopulmonary Resuscitation; EMS = Emergency Medical Services; IQR = Interquartile Range; ROSC = Return of Spontaneous Circulation)

	All Primary VF Cases 2005-2014 (N=1927)	**Appendix B Cases (Including Initial Shocks) (N=1068)**
Female, n(%)	454(23.6)	257(24.1)
Age, median (IQR)	62(52, 73)	62(52, 73)
Cardiac etiology, n(%)	1742(90.4)	968(90.6)
Location, n(%)		
Home	1208(62.7)	676(63.3)
Public	627(32.5)	343(32.1)
Nursing Home	92(4.8)	47(4.6)
Arrest before EMS arrival, n(%)	1713(88.9)	1005(94.1)
Witnessed, n(%)	1482(76.9)	788(73.8)
Bystander CPR, n(%)	1249(64.8)	735(68.8)
EMS Response time (minutes), median (IQR)	5(4, 6.6)	5(4, 6.2)
Total shocks, median (IQR)	3(1, 6)	3(2, 6)
ROSC, n(%)	1281(66.5)	708(66.3)
Died in Field	498(25.8)	277(25.9)
Admit to hospital	1254(65.1)	705(66.0)
Survive to hospital discharge, n(%)	818(42.4)	456(42.7)

For the 1068 patients in the Appendix B study group, 1884 VF segments were collected during CPR and 2256 VF segments were collected without CPR prior to either the initial shock or first three subsequent shocks. During CPR, filtering the ECG improved AMSA AUC from 0.654 to 0.666 ($p<0.001$), and improved MS AUC from 0.0657 to 0.0685 ($p<0.001$) (Figure S6). Without CPR, filtering insignificantly reduced AMSA AUC from 0.723 to 0.722 ($p=0.378$) and insignificantly reduced MS AUC from 0.0733 to 0.728 ($p=0.063$). AUC values for AMSA and MS prediction of shock success were significantly lower during CPR than without CPR, both for

unfiltered data (AMSA p<0.001, MS p<0.001) and filtered data (AMSA p=0.001, MS p=0.011) (Figure S6).

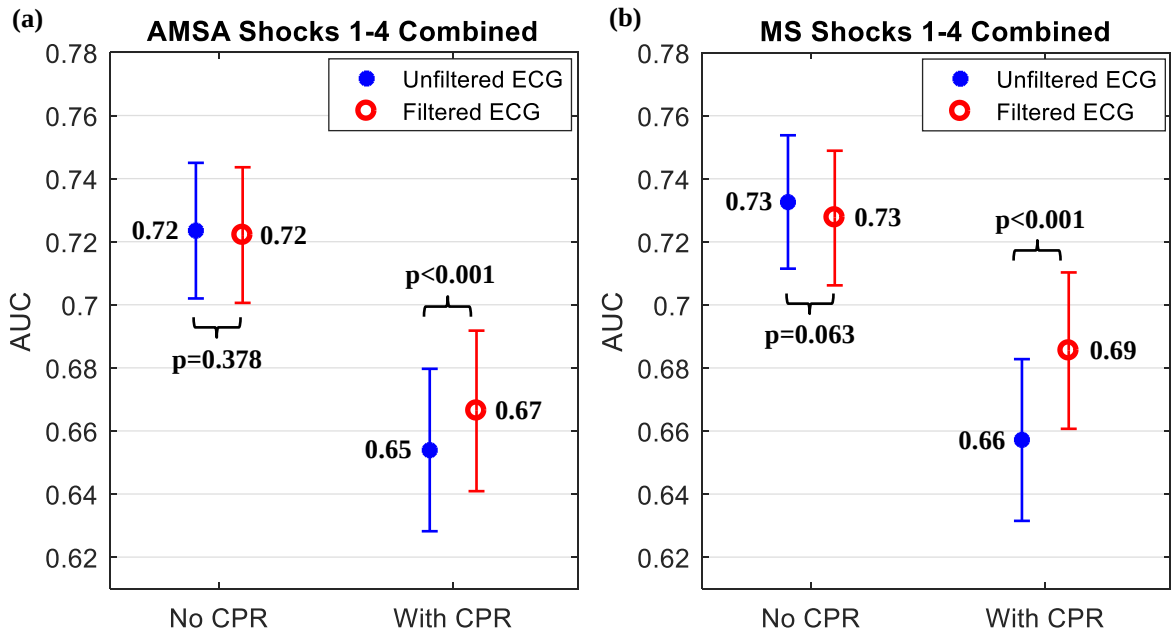

Figure 3.7. AUC for filtered and unfiltered data with and without CPR
(a) AMSA and (b) MS AUCs with 95% CIs using filtered and unfiltered data for the first four shocks combined from 1068 patients with CPR (n=1884 shocks) and without CPR (n=2256 shocks). CPR artifact significantly reduced waveform measure AUC values, and filtering significantly improved AUC values during CPR. Note that while the bootstrap-estimated 95% confidence intervals for individual AUCs have a large overlap, the paired-sample assumption in DeLong's method allows for increased discriminatory power between two receiver operating characteristic curves calculated from the same datasets (in this case, the filtered versus unfiltered comparisons), and shows a small but significant difference between them.

3.9.4 *Discussion*

AMSA and MS both inherently act as high-pass filters. AMSA, as calculated in this investigation, ignores all frequencies below 1 Hz, and multiplies each frequency magnitude between 1-26 Hz with its frequency value before summing all magnitudes to produce the AMSA. Therefore, the frequency response prior to summing is a high-pass ramp. For instance, frequency content at 20 Hz has twice the contribution towards the final AMSA than frequency content at 10 Hz. Similarly,

MS is the median absolute value of the slope, or pointwise difference, in the signal. The pointwise difference (derivative) operation affects the frequency content of the signal by also acting as a high-pass ramp, since the Fourier Transform of the derivative of a signal is related to the magnitude response multiplied by the frequency values. Ultimately this causes high frequency content to increase the MS more strongly than low frequency content.

Therefore, compared to other waveform measures, such as the median amplitude or centroid frequency, AMSA and MS may inherently benefit less from bandpass filtering the ECG, since their computation already emphasizes high-frequency content by design. Other waveform measures (such as a measure calculated from the integral of the time-domain signal) would likely be much more negatively affected by chest compression artifact, and would thus benefit more from ECG bandpass filtering. Even so, our results show that filtering increases AUC slightly, but significantly, for AMSA and MS during CPR by removing much of the fundamental CPR frequency and some of the first harmonics of CPR. Filtering also reduces waveform measure AUC slightly (albeit insignificantly) without CPR by removing some of the original VF signal, due to the filter high-pass cutoff being set to 4 Hz and slightly overlapping VF spectral content. Because of overlap between VF frequencies and CPR harmonics, choosing higher or lower cutoffs could be viewed as a trade-off between improving performance with or without compression artifact. Thus, ideally in future study, different filters would be used on CPR-artifacted signals than those used on CPR-free signals.

3.9.5 *Conclusions*

Conventional bandpass filtering improved waveform measure AUC during continuous CPR, and did not significantly reduce AUC without chest compressions. In spite of filtering, AMSA and MS AUCs are significantly lower during CPR than without CPR.

Chapter 4. CHARACTERIZING VENTRICULAR FIBRILLATION WAVEFORM MEASURES DURING CHEST COMPRESSIONS

Adapted from: **Coult J**, Blackwood J, Sherman L, Rea TD, Kudenchuk PJ, Kwok H. Ventricular fibrillation waveform analysis during chest compressions to predict survival from cardiac arrest. *Circulation: Arrhythmia and Electrophysiology* 2019; 12(1):1-10. https://doi.org/10.1161/CIRCEP.118.006924

4.1 ABSTRACT

Background: Quantitative measures of the ventricular fibrillation (VF) electrocardiogram (ECG) waveform can assess myocardial physiology and predict cardiac arrest outcomes, making these measures a candidate to help guide resuscitation. Chest compressions are typically paused for waveform measure calculation, as compressions cause ECG artifact. However, such pauses contradict resuscitation guideline recommendations to minimize CPR interruptions. We evaluated a comprehensive group of VF measures with and without ongoing compressions to determine their performance under both conditions for predicting functional survival, the study's primary outcome. *Methods:* Five-second VF ECG segments were collected with and without chest compressions prior to 2755 defibrillation shocks from 1151 out-of-hospital cardiac arrest patients. Twenty-four individual measures and three combination measures were implemented. Measures were optimized to predict functional survival (Cerebral Performance Category score ≤ 2) using 460 training cases, and their performance evaluated using 691 independent test cases. *Results:* Measures predicted functional survival on test data with an area under the receiver operating characteristic curve (AUC) ranging from 0.56-0.75 (median=0.73) without chest compressions and from 0.53-0.75 (median=0.69) with compressions ($p<0.001$ for difference). Of all measures evaluated, the support vector machine model ranked highest both without chest compressions

(AUC=0.75, 95% CI 0.73-0.78) and with compressions (AUC=0.75, 95% CI 0.72-0.78) (p=0.75 for difference). *Conclusions:* VF waveform measures predict functional survival when calculated during chest compressions, but prognostic performance is generally reduced compared to compression-free analysis. However, support vector machine models exhibited similar performance with and without compressions while also achieving the highest AUC. Such machine learning models may therefore offer means to guide resuscitation during uninterrupted CPR.

4.2 INTRODUCTION

Out-of-hospital sudden cardiac arrest is a leading cause of death. In persons with a witnessed collapse, ventricular fibrillation (VF) is a common dysrhythmia.[3] Treatment of VF arrest consists of a series of time-sensitive therapies. Termed the links in the chain of survival, these therapies include early arrest recognition, early cardiopulmonary resuscitation (CPR), early defibrillation shock, expert advanced therapies (i.e. medication and airway management), and post-resuscitation care including coronary interventions and targeted temperature management.[31] Although the "links" metaphor provides a straightforward conceptual framework, the details of how to integrate various therapies is challenging because the physiology of VF is heterogeneous; hence, a singular sequence, timing, choice, or dose of therapies may not achieve optimal outcomes across all patients.[85,124]

One potential approach to match specific treatments to specific patients is to use quantitative measures of the VF waveform to evaluate individual physiology in real time. Waveform measures are mathematical functions that quantify characteristics of the VF electrocardiogram (ECG) signal such as frequency, amplitude, organization, or combinations thereof. These measures can reflect myocardial physiology (e.g. adenosine triphosphate concentrations in cardiac tissue) and, in turn, predict a patient's likelihood of a good clinical

outcome.[22,57] Moreover, measures can be affected by treatment and change over the course of resuscitation, with the characteristics of their change also predicting outcome.[86] Thus, waveform measures have the potential to inform prognosis throughout an arrest and to better align treatment with a patient's immediate status. For instance, if a patient's VF waveform indicates a low likelihood of meaningful survival, then rescuers may consider alternative strategies that could improve survival. Such strategies might involve providing an interim period of high-quality CPR and/or medications rather than immediate shock until such a time that the waveform measure signifies the likelihood of a better outcome from defibrillation.[40,125]

A major challenge to the routine use of waveform measures to help guide care is that these measures are conventionally calculated during pauses in CPR, since chest compressions cause electrical artifact in the ECG.[39,44,126] Such interruptions generally contradict best-practice guidelines which call for minimally-interrupted CPR to support resuscitation.[31] An improved strategy would use a waveform measure that achieves consistent prognostic performance throughout an arrest even during ongoing chest compressions.[43,45] However, a pilot investigation of two waveform measures during chest compressions has confirmed a significant reduction in prognostic performance compared to compression-free analysis, a finding that challenges integration of real-time waveform measures into best-practice uninterrupted CPR.[127] Whether this finding is generalizable to other individual waveform measures, or combinations of measures, is unknown.

In the current investigation, we evaluate a comprehensive set of waveform measures with and without chest compressions to determine if comparable prognostic performance can be achieved during ongoing compressions, and, in turn, if waveform measures have potential to serve as a dynamic guide to resuscitation during high-performance CPR.

4.3 METHODS

The data that support the findings of this study, with the exception of patient ECG data, are available from the corresponding author upon reasonable request.

4.3.1 *Study Design, Population, and Setting*

The study was a retrospective cohort investigation of patients who suffered out-of-hospital VF cardiac arrests in greater King County, WA, from 2005 to 2015. The emergency medical services (EMS) system in King County is a two-tiered system. The first tier consists of firefighter emergency medical technicians equipped with automated external defibrillators. The second-tier is paramedics who perform manual rhythm interpretation and advanced cardiac life support.

Patients were eligible if they presented to EMS with an initial arrest rhythm of VF and received at least one shock from an MRx, Forerunner 3 (Philips Healthcare, Bothell, WA), Lifepak 12, or Lifepak 15 (Physio-Control, Redmond, WA) defibrillator, as these defibrillator models are the predominant models used in the EMS jurisdiction and record transthoracic chest impedance in conjunction with the ECG. Patients were *a priori* ineligible if they received public access or police defibrillation prior to EMS arrival. Eligible patients were excluded if the defibrillator recording did not include at least one five-second VF ECG segment with a concurrent impedance signal prior to a shock. Patients were also excluded if they had a paced rhythm, as pacer artifact may interfere with VF waveform analysis. This study and corresponding waiver of consent were approved by the Institutional Review Board at the University of Washington Human Subjects Division and Research Review Committee of Public Health in compliance with applicable regulations.

4.3.2 *Data Collection and Processing*

Cardiac arrest information was organized according to the Utstein template based on review of the emergency dispatch audio recording, the EMS report, the hospital record, and the electronic defibrillator recording.[128] Defibrillator recordings included real-time audio, ECG, transthoracic impedance, and in some cases accelerometer information. MRx ECGs were analyzed at their original sample rate of 250 Hz, while Forerunner 3 and Lifepak ECG data, which were recorded at 200 Hz and 125 Hz respectively, were resampled to 250 Hz. All ECGs were filtered from 1-30 Hz to remove high-frequency noise and low-frequency drift.

Prior to each of the first four shocks, one five-second VF segment without chest compressions and an adjacent segment during chest compressions were collected, when available (Figure 4.1). When such paired segments were not available, a segment without chest compressions was included even if there was not also a segment with compressions prior to the same shock, and vice versa. The rhythm during chest compressions was confirmed by review of the ECG within proximal chest compression pauses (e.g. for ventilation). The presence of chest compressions was determined by review of the transthoracic impedance signal.

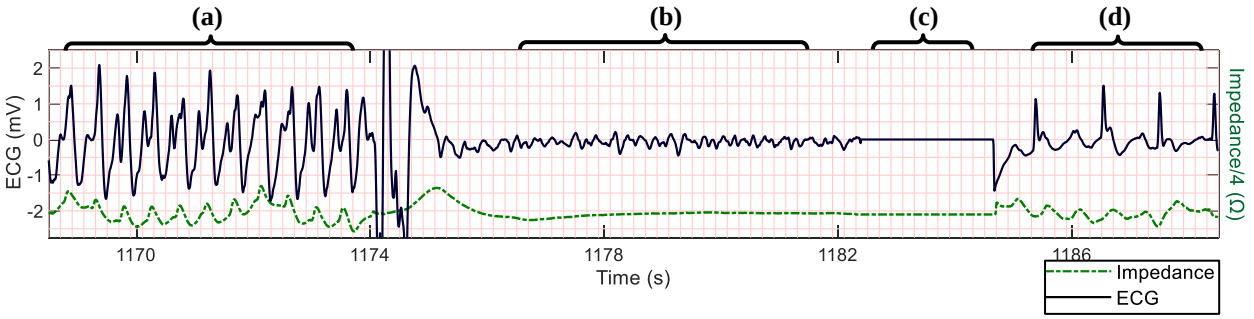

Figure 4.1 VF segment collection example
(a) Five-second VF segment during chest compressions. (b) Five-second VF segment without chest compressions. (c) Defibrillation shock. (d) Return of rhythm following defibrillation. Impedance is shifted vertically for illustration.

4.3.3 *Clinical Outcomes*

The primary outcome was functional survival, defined as survival to hospital discharge with a Cerebral Performance Category score of 1 or 2.[107,108] Intermediate outcomes were return of circulation, defined as a pulse with measurable blood pressure at end of EMS care, and return of rhythm after shock, defined as at least two QRS complexes within any five-second period during the first two minutes following a defibrillation attempt.[127] Two reviewers independently determined return of rhythm in a subset of 575 shocks from 202 patients. In this assessment of interrater reliability, Cohen's Kappa was 0.85 with 93% agreement. Prior investigations have evaluated interrater reliability for the Cerebral Performance Category and return of spontaneous circulation.[107,129,130]

4.3.4 *Waveform Measures*

We evaluated a total of 27 waveform measures which were grouped into four categories.[45,88] Individual time-domain measures quantify ECG characteristics such as amplitude and slope. Individual frequency measures include those calculated from Fourier or time-frequency transforms. Individual complexity measures represent descriptors of signal organization,

complexity, or self-similarity. Combination measures are statistical models that incorporate multiple inputs to produce a single predictive output. In this investigation, each combination model used all individual waveform measures as inputs. Waveform measure implementations are described further in Appendix A: Waveform Measures.

Patients were divided randomly into independent training (40%) and test (60%) sets, as some waveform measures have variable parameters that must be selected using training data. Using the training dataset, we chose parameters for individual waveform measures that provided optimal predictive performance as indicated by the area under the receiver operating characteristic curve (AUC). Separate parameters were selected for use with compressions and without compressions (Figure 4.2). After selecting parameters for individual measures, combination measures were trained on the training dataset. Parameter selections and training are described in Appendix B: Training Results and Parameter Selection.

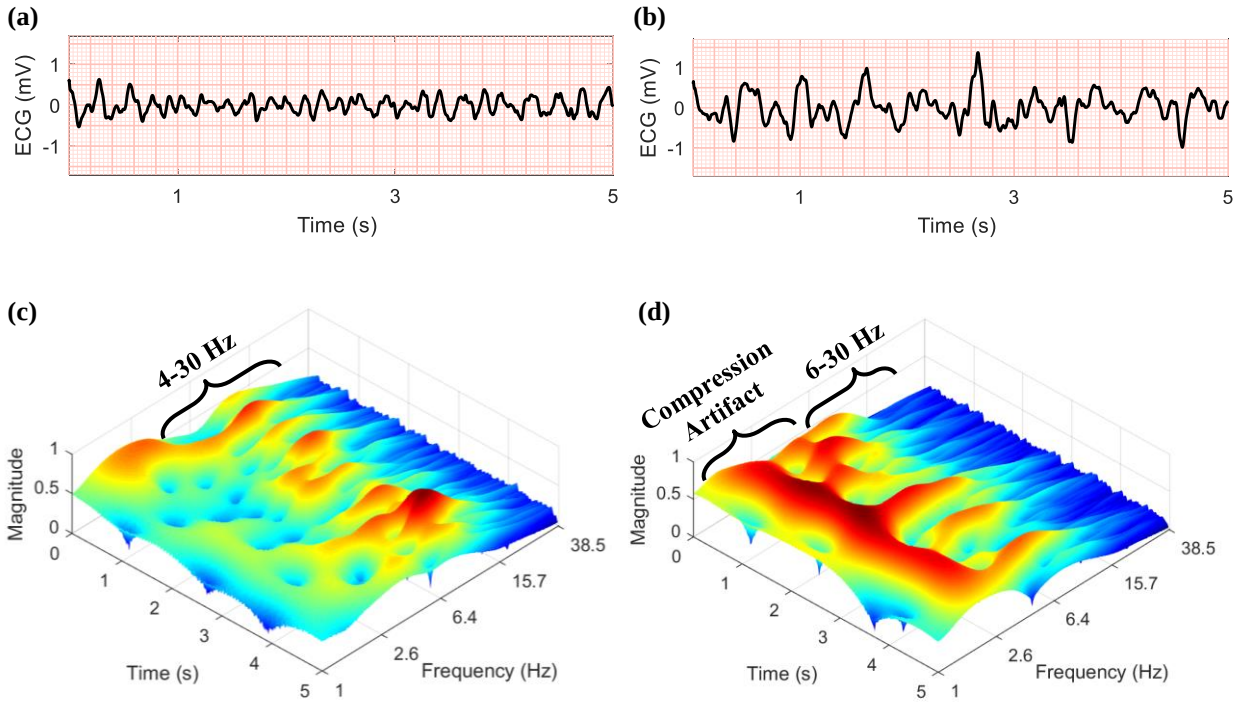

Figure 4.2 Waveform measure during chest compressions example
(a) Five-second VF segment without chest compressions. (b) Five-second VF segment with chest compressions. (c) Wavelet transform of VF without compressions is analyzed from 4–30 Hz to compute the wavelet energy measure. (d) For computing the wavelet energy measure, the wavelet transform of VF with compressions is analyzed from 6–30 Hz to capture higher-frequency VF content while ignoring the frequencies below 6 Hz that consist primarily of chest compression artifact (i.e. the fundamental at approximately 2 Hz, and in some cases the first two harmonics of compressions at approximately 4 Hz and 6 Hz). Upper-mid frequencies (e.g. from approximately 6–15 Hz) may also contain a mixture of both transient compression artifacts and VF content.

4.3.5 *Statistical Analysis*

We evaluated how well each waveform measure predicted outcomes in the test set with and without chest compressions using the AUC. AUC confidence intervals were calculated using stratified bootstrapping. In order to assess how chest compressions affect waveform measures' predictive performance overall, we compared the median of the AUC values without chest compressions to the median of the AUC values with chest compressions using the Wilcoxon signed-rank test.

In order to investigate one strategy for how a waveform measure might serve as a guide to resuscitation, we first identified the measure with the highest AUC during chest compressions.[109,115] The AUCs of the highest performing measure were also compared with and without chest compressions using DeLong's method to evaluate relative performance during CPR.[109,115] We then compared rates of functional survival according to quintiles of the highest performing waveform measure to explore how the measure might be used to stratify prognosis in a clinical setting.

Data analysis was performed using MATLAB R2017a (The Mathworks, Natick, MA, USA) and R (R Foundation for Statistical Computing, Vienna, Austria).

4.4 RESULTS

4.4.1 *Study Group*

From 2005-2015, there were 1594 patients who suffered a cardiac arrest with an initial observed rhythm of VF and were eligible for the study (Figure 4.3). Of eligible patients, 1151 (72%) had adequate data and were included in the analysis. Utstein characteristics for included and excluded patients are presented in Table 4.1. Overall, 471 (41%) patients had functional survival, 817 (71%) patients had return of circulation at end of EMS care, and 1752 (64%) of the 2755 shocks in the study group were followed by return of rhythm.

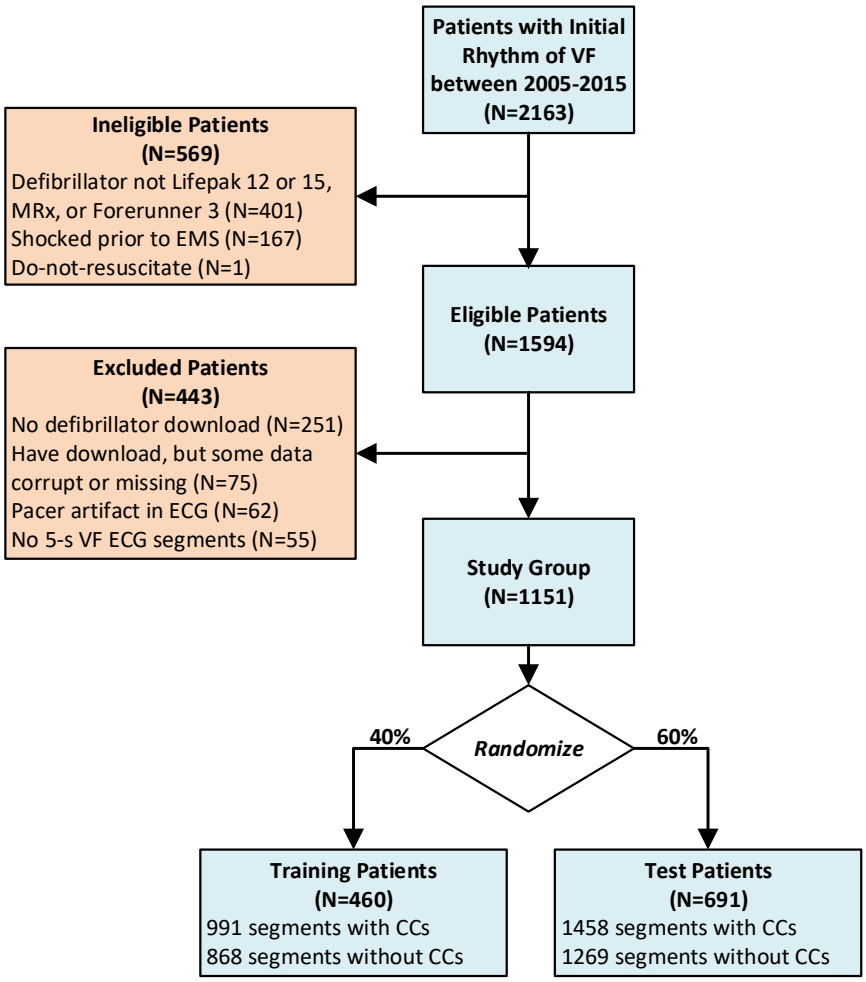

Figure 4.3 Study group and exclusions
Exclusions and division of patients into random training and test groups are illustrated. One VF segment without CCs and one VF segment with CCs was collected before each of the first four shocks from each patient in the study group, when available. (CCs = chest compressions, ECG = electrocardiogram, EMS = emergency medical services, VF = ventricular fibrillation.)

Table 4.1 Patient characteristics
Characteristics of all patients presenting to first responders with VF during the study period are presented versus excluded patients and study group patients. (CPR = cardiopulmonary resuscitation, EMS = emergency medical services, VF = ventricular fibrillation.)

Patient Characteristic	Initial Rhythm of VF from 2005-2015 (N=2163)	Ineligible or Excluded (n=1012)	Study Group (n=1151)
Female, n(%)	493(22.8)	228(22.5)	265(23.0)
Age, median (IQR)	62(52, 73)	64(53, 74)	61(52, 72)
Cardiac etiology, n(%)	1985(91.8)	905(89.4)	1080(93.8)
Location, n(%)	-	-	-
Home	1258(58.1)	551(54.4)	707(61.4)
Public	808(37.4)	409(40.4)	399(34.7)
Nursing Home	97(4.5)	52(5.1)	45(3.9)
Arrest before EMS arrival, n(%)	1949(90.1)	856(84.6)	1093(95.0)
Witnessed, n(%)	1685(77.9)	801(79.2)	885(76.9)
Bystander CPR, n(%)	1498(69.2)	665(65.7)	833(72.4)
EMS Response (minutes), median (IQR)	5(3, 6)	4(2, 6)	5(4, 6)
Total shocks, median (IQR)	3(1, 6)	3(1, 6)	3(2, 6)
Return of spontaneous circulation at end of EMS care, n(%)	1499(69.3)	682(67.4)	817(71.0)
Admit to hospital, n(%)	1468(67.9)	658(65.0)	810(70.4)
Survive to hospital discharge, n(%)	970(44.8)	446(44.1)	524(45.5)
Survival with Cerebral Performance Category 1 or 2, n(%)	877(40.6)	406(40.1)	471(40.9)

4.4.2 *Survival*

There were 691 patients in the test set, and 283 (41%) survived with intact functional status. We collected 1458 VF segments without chest compressions and 1269 segments with compressions prior to 1639 shocks from the test patients. Without chest compressions, AUCs for prediction of functional survival ranged from 0.56 to 0.75 for the 27 measures, with a median of 0.73. During chest compressions, AUCs for prediction of functional survival ranged from 0.53 to 0.75, with a median of 0.69 ($p<0.001$ for difference in medians) (Figure 4.4, Table 4.2).

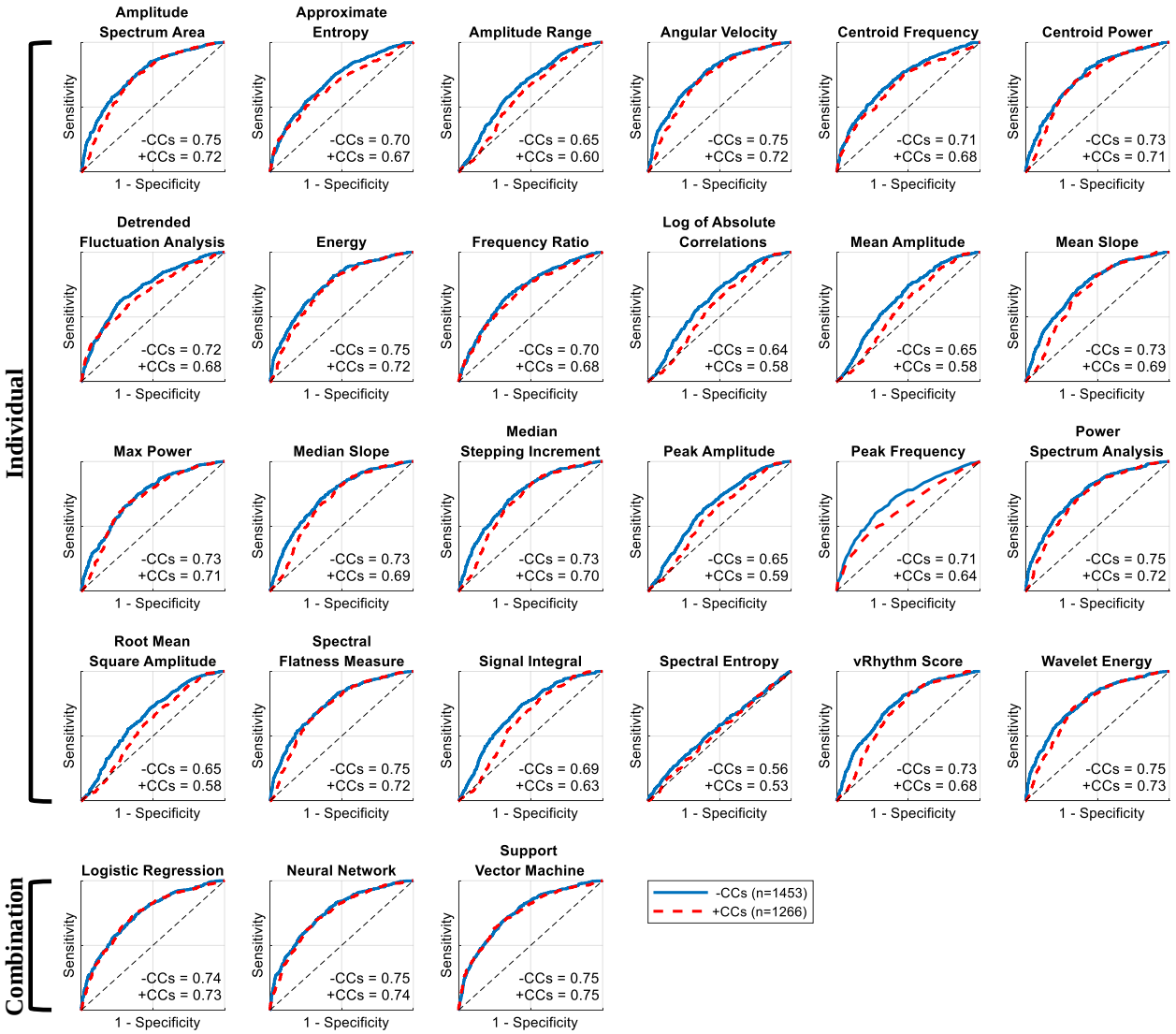

Figure 4.4 Receiver operating characteristic curves for predicting survival

Receiver operating characteristic curves are shown with area under receiver operating characteristic curve values for predicting functional survival using 24 individual measures and 3 combination measures. Results are shown for the 1453 ventricular fibrillation ECG segments without chest compressions (-CCs) and the 1266 ventricular fibrillation ECG segments with chest compressions (+CCs) collected from the 691 patients in the test group.

Table 4.2 Test AUC values for prediction of outcomes

AUC values for waveform measures on test data are presented as AUC [95% CI] sorted by AUC for predicting survival with CCs.

Waveform Measure	Survival, +CCs	Survival, -CCs	Circulation, +CCs	Circulation, -CCs	Organized Rhythm, +CCs	Organized Rhythm, -CCs
Support Vector Machine[101]	0.75 [0.72-0.78]*	0.75 [0.73-0.78]*	0.72 [0.69-0.75]*	0.72 [0.70-0.75]*	0.70 [0.67-0.73]*	0.75 [0.72-0.77]*
Neural Network[68]	0.74 [0.71-0.77]	0.75 [0.73-0.78]	0.71 [0.68-0.74]†	0.72 [0.69-0.75]	0.69 [0.66-0.72]	0.74 [0.72-0.77]
Logistic Regression[131]	0.73 [0.70-0.76]	0.74 [0.71-0.77]†	0.71 [0.68-0.74]	0.71 [0.69-0.74]	0.69 [0.66-0.72]	0.73 [0.70-0.76]†
Wavelet Energy[88,132]	0.73 [0.70-0.76]†	0.75 [0.73-0.78]	0.71 [0.68-0.74]	0.73 [0.70-0.76]	0.68 [0.65-0.71]†	0.74 [0.71-0.76]†
Amplitude Spectrum Area[97]	0.72 [0.69-0.75]†	0.75 [0.73-0.78]	0.71 [0.67-0.74]†	0.72 [0.70-0.75]	0.67 [0.64-0.70]‡	0.73 [0.71-0.76]†
Power Spectrum Analysis[68]	0.72 [0.69-0.75]†	0.75 [0.73-0.78]	0.71 [0.68-0.74]	0.73 [0.70-0.75]	0.67 [0.64-0.70]‡	0.74 [0.71-0.76]
Spectral Flatness Measure[116]	0.72 [0.69-0.75]†	0.75 [0.72-0.77]	0.70 [0.66-0.73]‡	0.71 [0.69-0.74]†	0.67 [0.63-0.70]‡	0.72 [0.70-0.75]‡
Energy[116]	0.72 [0.69-0.75]†	0.75 [0.72-0.77]	0.71 [0.68-0.74]	0.73 [0.70-0.76]	0.64 [0.61-0.67]‡	0.74 [0.71-0.76]†
Angular Velocity[133]	0.72 [0.69-0.75]†	0.75 [0.72-0.77]†	0.71 [0.68-0.74]†	0.73 [0.70-0.76]†	0.68 [0.65-0.71]†	0.74 [0.72-0.77]
Centroid Power[68]	0.71 [0.68-0.74]‡	0.73 [0.71-0.76]‡	0.70 [0.67-0.73]†	0.71 [0.69-0.74]†	0.64 [0.61-0.67]‡	0.72 [0.69-0.74]‡
Max Power[68]	0.71 [0.68-0.74]‡	0.73 [0.70-0.76]‡	0.69 [0.66-0.73]‡	0.71 [0.69-0.74]	0.64 [0.61-0.67]‡	0.72 [0.69-0.75]‡
Median Stepping Increment[134]	0.70 [0.67-0.72]‡	0.73 [0.71-0.76]‡	0.68 [0.65-0.72]‡	0.72 [0.70-0.75]	0.66 [0.63-0.69]‡	0.74 [0.72-0.77]
Median Slope[68]	0.69 [0.67-0.72]‡	0.73 [0.71-0.76]‡	0.68 [0.65-0.72]‡	0.72 [0.69-0.75]	0.66 [0.63-0.69]‡	0.74 [0.72-0.77]
Mean Slope[135]	0.69 [0.66-0.72]‡	0.73 [0.70-0.76]‡	0.68 [0.65-0.71]‡	0.72 [0.69-0.75]	0.65 [0.62-0.69]‡	0.74 [0.72-0.77]
Frequency Ratio[100]	0.68 [0.65-0.71]‡	0.70 [0.67-0.73]‡	0.66 [0.63-0.69]‡	0.67 [0.65-0.70]‡	0.66 [0.63-0.69]†	0.67 [0.64-0.70]‡
Centroid Frequency[136]	0.68 [0.65-0.71]‡	0.71 [0.69-0.74]‡	0.66 [0.63-0.69]‡	0.69 [0.66-0.71]†	0.63 [0.60-0.67]‡	0.68 [0.65-0.70]‡
Detrended Fluctuation Analysis[104]	0.68 [0.65-0.71]‡	0.72 [0.69-0.74]‡	0.67 [0.64-0.70]‡	0.70 [0.67-0.72]†	0.65 [0.62-0.69]†	0.67 [0.65-0.70]‡
vRhythm[137]	0.68 [0.66-0.71]‡	0.73 [0.70-0.75]‡	0.68 [0.64-0.71]‡	0.72 [0.69-0.75]	0.65 [0.62-0.68]‡	0.74 [0.72-0.77]
Approximate Entropy[90,138]	0.67 [0.63-0.70]‡	0.70 [0.68-0.73]‡	0.66 [0.63-0.69]‡	0.65 [0.62-0.68]‡	0.64 [0.61-0.67]‡	0.62 [0.59-0.65]‡
Peak Frequency[116]	0.64 [0.61-0.67]‡	0.71 [0.68-0.74]‡	0.64 [0.61-0.67]‡	0.67 [0.64-0.70]‡	0.61 [0.58-0.64]‡	0.67 [0.64-0.70]‡
Signal Integral[111,139]	0.63 [0.60-0.66]‡	0.69 [0.67-0.72]‡	0.62 [0.59-0.66]‡	0.70 [0.67-0.73]‡	0.60 [0.56-0.63]‡	0.73 [0.70-0.76]†
Amplitude Range[140]	0.60 [0.57-0.63]‡	0.65 [0.63-0.68]‡	0.61 [0.57-0.64]‡	0.67 [0.64-0.70]‡	0.59 [0.56-0.63]‡	0.71 [0.68-0.73]‡
Peak Amplitude[140]	0.59 [0.56-0.63]‡	0.65 [0.62-0.68]‡	0.60 [0.56-0.63]‡	0.66 [0.63-0.69]‡	0.59 [0.55-0.62]‡	0.70 [0.67-0.73]‡
Mean Amplitude[140]	0.58 [0.55-0.61]‡	0.65 [0.62-0.68]‡	0.58 [0.55-0.62]‡	0.67 [0.64-0.70]‡	0.57 [0.53-0.60]‡	0.71 [0.68-0.74]‡
Log of Absolute Correlations[141]	0.58 [0.55-0.61]‡	0.64 [0.62-0.67]‡	0.58 [0.55-0.62]‡	0.66 [0.63-0.69]‡	0.57 [0.53-0.60]‡	0.71 [0.68-0.73]‡
Root Mean Square Amplitude[140]	0.58 [0.55-0.62]‡	0.65 [0.62-0.68]‡	0.58 [0.55-0.62]‡	0.66 [0.63-0.70]‡	0.57 [0.53-0.60]‡	0.71 [0.68-0.74]‡
Spectral Entropy[142]	0.53 [0.50-0.56]‡	0.56 [0.53-0.59]‡	0.53 [0.50-0.57]‡	0.59 [0.56-0.62]‡	0.54 [0.50-0.57]‡	0.56 [0.53-0.59]‡

(AUC = area under the receiver operating characteristic curve, +CCs = during chest compressions, -CCs = without chest compressions, CI = confidence interval.) *Referents for each column are support vector machine AUC values. †Significant difference versus column referent by DeLong method ($p<0.05$). ‡Significant difference versus column referent by DeLong method with Bonferroni correction ($p<0.0019$)

4.4.3 *Intermediate Outcomes*

Of the 691 patients in the test set, 491 (72%) had return of circulation at end of EMS care. Median AUC for waveform measure prediction of return of circulation was 0.71 (range 0.59-0.73) without chest compressions and 0.68 (range 0.53-0.72) during compressions ($p<0.001$ for difference in medians) (Table 4.2, Appendix C: Expanded Primary Results).

Of the 1639 individual shocks included from patients in the test set, a return of rhythm occurred after 1039 (63%). Median AUC for waveform measure prediction of return of rhythm was 0.72 (range 0.56-0.75) without compressions and 0.65 (range 0.54-0.70) during compressions ($p<0.001$ for difference in medians) (Table 4.2, Appendix C: Expanded Primary Results).

4.4.4 *Highest-performing Waveform Measure*

For prediction of the primary outcome of functional survival, the measure with the highest AUC was the support vector machine combination measure (Table 4.2). AUC values were similar without chest compressions (AUC=0.75, 95% CI 0.73-0.78) versus with chest compressions (AUC=0.75, 95% CI 0.72-0.78) ($p=0.75$ for difference). Without chest compressions, survival ranged from 12% in the lowest quintile to 71% in the highest quintile. With chest compressions, survival ranged from 13% in the lowest quintile to 69% in the highest quintile (Figure 4.5).

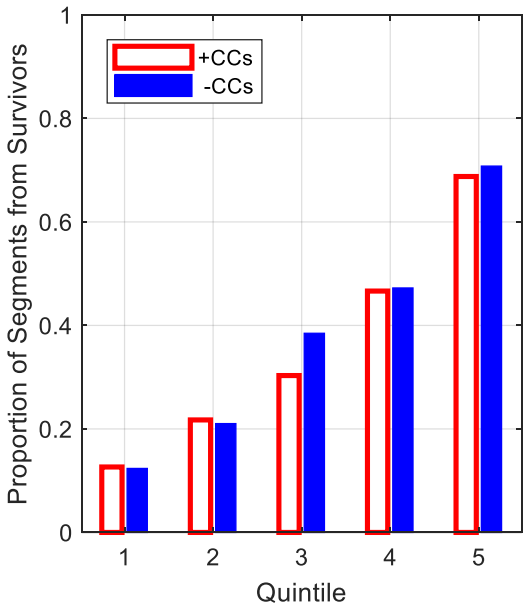

Figure 4.5 Survival stratified by support vector machine quintile
The proportions of ventricular fibrillation segments from patients with functional survival are shown stratified by their corresponding support vector machine quintiles. Results are shown using all ventricular fibrillation segments without chest compressions (-CCs) and with chest compressions (+CCs) collected from patients in the test group.

4.5 DISCUSSION

In this cohort investigation of 1151 patients with out-of-hospital VF cardiac arrest, we found that 24 individual and 3 combination waveform measures predicted functional survival, return of circulation, and return of rhythm. Measures typically performed better without chest compressions than during compressions. Importantly, the support vector machine, a machine learning model which combined information from the 24 individual measures, demonstrated the highest performance in predicting functional survival regardless of chest compressions, achieving comparable performance with and without compressions. These results highlight the potential to apply a prognostic VF waveform measure without interrupting CPR.

VF waveform measures have traditionally been evaluated using ECGs without chest compression artifact.[57,65,88,143] We observed a range of prognostic performance with all measures predicting outcome under these circumstances; for instance, median AUC=0.73 (range 0.56-0.75) for predicting functional survival. Previously, the AUC of most waveform measures during active chest compressions was unknown, although reduced prediction was expected since chest compressions produce artifact that obscure the ECG across a wide range of frequencies.[123,126] Indeed, we found that even after optimization for use during chest compressions, the predictive performance of individual waveform measures declined during CPR. Thus, the use of these individual measures to guide resuscitation would likely require repeated interruptions in chest compressions to accurately gauge the heart's physiological status, undermining the clinical benefits of CPR.

In addition to individual measures, prior studies have also investigated combination measures, with the rationale that machine learning models (e.g. neural networks or support vector machines) could optimally combine information from individual measures that quantify different aspects of the VF waveform. Although prior studies of combination measures did not demonstrate a clear advantage over individual measures, those investigations were limited to ECGs collected during CPR interruptions and used fewer individual waveform measures than the current investigation.[68,89,144] Indeed, in our investigation we did not observe significantly-improved performance with combination measures compared to the best-performing individual measures calculated from segments *without* chest compressions. However, we found that a combination model – the support vector machine – improved prediction of survival *during* chest compressions to the point of achieving performance similar to the highest performance without chest compressions. We hypothesize that this result is due to two reasons. The first is that our dataset

was large enough to leverage the advantages of support vector machines and to sufficiently optimize model parameters. Given enough training data and proper regularization to prevent overfitting, support vector machines can model high-dimensional interactions between inputs while still generalizing well to unknown data. The second is that without chest compressions, individual measures already achieve near the maximum prognostic performance possible from a two-lead ECG and leave little margin for improvement, and thus any increase using a machine learning model (such as a support vector machine) is slight. In contrast, chest compression artifact degrades the performance of individual measures to well below the theoretical maximum. A support vector machine is able to compensate for these reductions in each individual measure during compressions by using complementary information from all measures, matching the maximum performance without compressions.

The support vector machine model, which ranked highest for prediction during chest compressions across all outcomes, can potentially classify patients during ongoing CPR for whom we can predict markedly disparate survival. For example, for VF segments in the lowest quintile of the support vector machine measure calculated during chest compressions, approximately one out of ten patients survive with intact neurologic function, with the remainder of the segments representing patients with an intact survival more than three times greater (13% in the lowest quintile versus 42% in the remaining collective quintiles). This lowest prognosis group may be appropriate for an alternative resuscitation strategy, such as distinct prioritization of CPR and medications or early transport for hospital-based, interventional treatments. Conversely, for patients in higher prognosis groups, the current practice of early defibrillation should continue to be prioritized. Although the optimal strategy for clinical integration is uncertain and requires further investigation, the current results provide a proof-of-concept that VF waveform measures

could be applied in a dynamic fashion while simultaneously supporting minimally-interrupted CPR.

The investigation has a number of limitations. The study involved a large metropolitan EMS system that achieves a relatively a high survival rate, which could limit generalizability. Some cases were excluded, but Utstein characteristics were generally similar according to study status. Waveform measures had somewhat lower predictive performance with regards to predicting shorter-term intermediate outcomes versus predicting functional survival. While counterintuitive, this result is supported by prior investigation demonstrating reduced prediction using increasingly shorter-term outcomes.[145] This result could also be due in part to the challenge of defining and classifying intermediate outcomes such as return of circulation or return of rhythm.[130] For instance, this study used a return of circulation definition that evaluates circulation at the end of EMS care and not after each shock, and a return of rhythm definition that does not include QRS morphologic characteristics or account for presence of pulse. Multiple shock cycles which may have correlated outcomes were included from some patients. However, we limited data collection to a maximum of four shocks per patient, and results were similar after accounting for intra-cluster correlation (Appendix D: Intra-cluster Correlation).[146] Not every shock cycle had an available pair of VF segments with and without chest compressions. However, a majority (80%) of test segments were paired, and test results were similar when limited to adjacent pairs (Appendix E: Subgroup Analyses). Finally, the study was retrospective and did not actually evaluate measures in real time or apply them in clinical care. Additional effort is required to determine if and how measures might actually be implemented into clinical practice to improve outcome.

These limitations should be considered in the context of the study's strengths: The investigation addressed an important clinical question involving the interface between technology

and clinical care. Specifically, the study used a large, well-characterized cohort with clinical outcomes to evaluate a comprehensive set of waveform measures with a rigorous two-step training and test set methodology.

4.6 CONCLUSION

Waveform measures predict patient outcomes when calculated from VF segments collected either with or without chest compressions, although performance is generally reduced during compressions. A support vector machine combination of individual waveform measures improved prediction of functional survival during chest compressions over individual measures alone, achieving performance similar to what was observed without compressions. These observations may be useful for future development of waveform measures as we strive to better match individual physiology with specific therapy while achieving best-practice minimally-interrupted CPR.

4.7 ACKNOWLEDGEMENTS

Functions to compute the Detrended Fluctuation Analysis and Approximate Entropy were obtained from the www.physionet.org resource. The function for calculation of p-values for paired receiver operating characteristic curves by DeLong's method was provided by John W Pickering (University of Otago, Christchurch, New Zealand). The proprietary vRhythm function, as well as technical advice on defibrillator data formats, was provided by Stacy Gehman and Chenguang Liu (Philips Healthcare, Bothell, WA, USA). Manuscript organization advice was provided by Nile Wilson (University of Washington, Seattle, WA, USA).

4.8 APPENDIX A: WAVEFORM MEASURES

We implemented 24 waveform measures and 3 machine learning combination models described in prior peer-reviewed studies and grouped them into four categories (Table 4.3).[45,62,88] Time-domain measures directly describe features of the time-series ECG such as amplitude and slope. Frequency measures describe Fourier or time-frequency transforms. Complexity measures quantify signal entropy, self-similarity, or scaling properties. Combination measures are statistical models that combine individual measures to produce a single output.

Table 4.3 Waveform measures by type
Waveform measures are presented by category with references for use in VF analysis

Method	Type	Reference
Logistic Regression[131]	Combination	Kuelz et al., 1994
Neural Network[68]	Combination	Neurauter et al., 2007
Support Vector Machine[101]	Combination	Shandilya et al., 2012
Angular Velocity[133]	Complexity	Sherman et al., 2004
Approximate Entropy[138]	Complexity	Goldberger et al., 2000
Detrended Fluctuation Analysis[104]	Complexity	Lin et al., 2010
Log of the Absolute Correlations[141]	Complexity	Sherman et al., 2008
Median Stepping Increment[134]	Complexity	Gong et al., 2015
Spectral Entropy[142]	Complexity	Lever et al., 2007
Amplitude Spectrum Area[97]	Frequency	Povoas et al., 2000
Centroid Frequency[136]	Frequency	Brown et al., 1996
Centroid Power[68]	Frequency	Neurauter et al., 2007
Energy[116]	Frequency	Eftestol et al., 2000
Frequency Ratio[100]	Frequency	Sherman et al., 2006
Max Power[68]	Frequency	Neurauter et al., 2007
Peak Frequency[116]	Frequency	Eftestol et al., 2000
Power Spectrum Analysis[68]	Frequency	Neurauter et al., 2007
Spectral Flatness Measure[116]	Frequency	Eftestol et al., 2000
Wavelet Energy[88,132]	Frequency	Addison et al., 2000
Amplitude Range[140]	Time-domain	Weaver et al., 1985
Mean Amplitude[140]	Time-domain	Weaver et al., 1985
Mean Slope[135]	Time-domain	Takata et al., 2001
Median Slope[68]	Time-domain	Neurauter et al., 2007
Peak Amplitude[140]	Time-domain	Weaver et al., 1985
Root Mean Square Amplitude[140]	Time-domain	Weaver et al., 1985
Signal Integral[111,139]	Time-domain	Jekova et al., 2004
vRhythm[137]	Time-domain	Russell et al., 2006

Of twenty-four individual measures, the majority had variable parameters that were varied to maximize training AUC. Combination models were then trained using these optimized individual measures as inputs. AUC values for individual and combination measures were then generated by applying all optimized measures to test data (Figure 4.6).

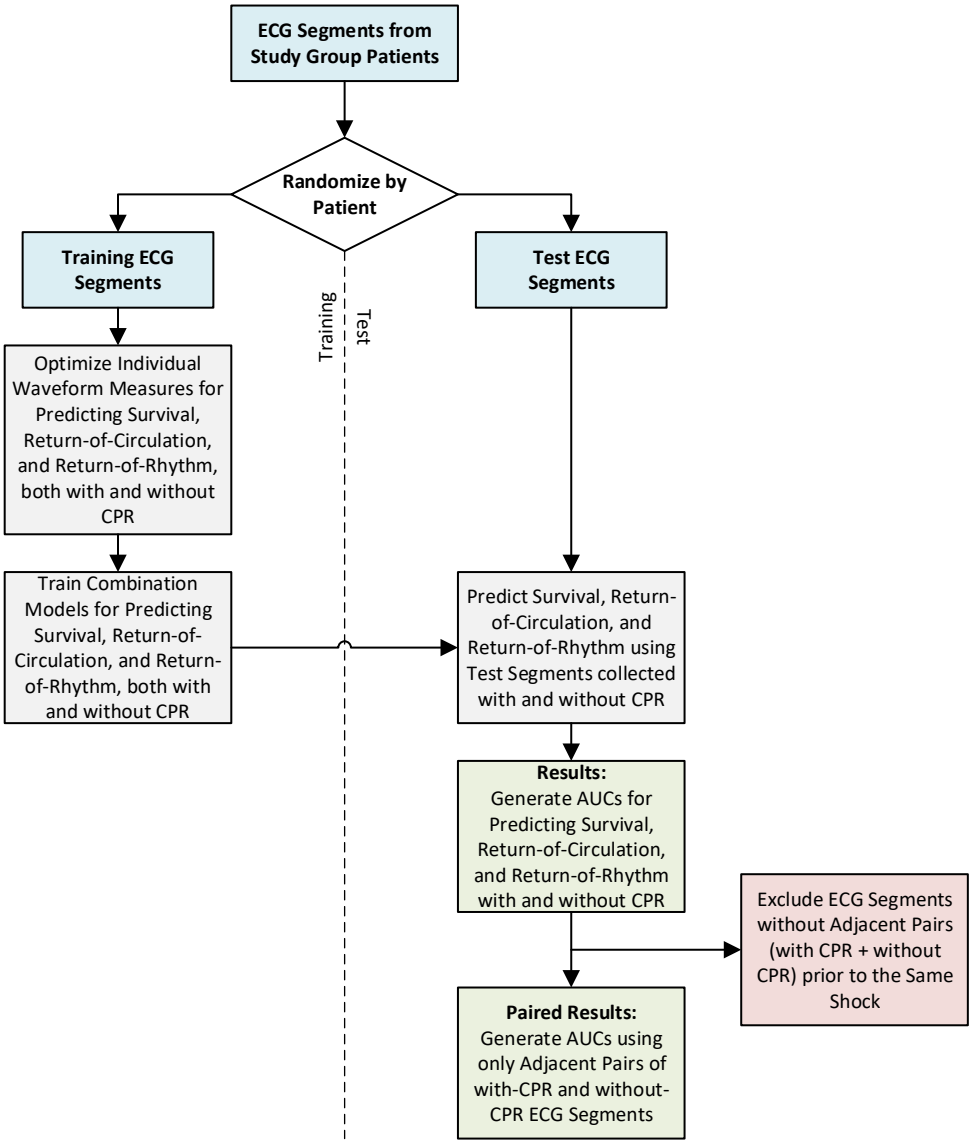

Figure 4.6 Training and test flow diagram
Individual measures were optimized to predict outcomes using training data. Combination measures were trained using all optimized individual measures.

4.8.1 *Time-Domain Waveform Measures*

Ventricular fibrillation is characterized by uncoordinated, chaotic cardiomyocyte contractions leading to loss of perfusion and a state of ischemia in the myocardium. Ischemia lowers the concentration of adenosine triphosphate in the tissue, reducing contractile effectiveness.[4] As electrical activity in cardiac tissue becomes increasingly uncoordinated during VF, and electrical rotors of depolarizing tissue break apart and become fragemented,[13,18] the amplitude of the VF ECG may be reduced as fewer cells contribute to any given depolarization wave. Hence, over time the amount of change in net electrical potential across the heart in any direction may be lower. The amplitude of the VF signal may therefore be used to estimate time since defibrillation onset, and by association, likelihood of defibrillation success.

4.8.1.1 Measures of Waveform Amplitude

VF waveform amplitude characteristics were associated with patient outcome in observations in Seattle, WA over 30 years ago by Weaver et al. that higher VF amplitude is associated with time since onset of arrest and likelihood of patient survival.[140] To represent such time-domain measures of amplitude, we calculated Mean Amplitude[98,140], Amplitude Range[65,89,134,139,140], Peak Amplitude[140,147], and Root-Mean-Square (RMS) Amplitude[53,62,89,140,144] by

$$\text{Mean Amplitude} = \frac{1}{N}\sum_{n=0}^{N-1}\left|x_n\right|, \tag{4.1}$$

$$\text{Amplitude Range} = \max(x_n) - \min(x_n), \tag{4.2}$$

$$\text{Peak Amplitude} = \max\left|x_n\right|, \tag{4.3}$$

and

$$\text{RMS Amplitude} = \sqrt{\frac{1}{N-1}\sum_{n=0}^{N-1}(x_n - \bar{x})^2}, \tag{4.4}$$

where $x_0,...,x_n,...,x_{N-1}$ are N zero-mean ECG voltage samples collected during 5 seconds of VF.

Jekova et al. introduced the integration of the time-domain ECG voltages, or Signal Integral, to estimate the energy in the VF signal.[139] Wu et al. further demonstrated improved predictive performance for Signal Integral using additional filtering to emphasize mid- and high-frequency content prior to integration.[89,111] We calculated the Signal Integral following the methods of Wu et al. as

$$\text{Signal Integral} = \sum_{n=0}^{N-1} \left| x_{n,BPF} \right|, \tag{4.5}$$

where $x_{0,BPF},...,x_{n,BPF},...,x_{N-1,BPF}$ are the ECG voltages filtered with a 32-point finite impulse response bandpass filter, with predefined band limits from Wu et al. of 5-25 Hz.[111]

4.8.1.2 Measures of Waveform Slope

Neurauter et al. demonstrated that measures of waveform slope may predict defibrillation success more accurately than basic measures of signal amplitude such as those described by Weaver et al. above.[68] Measures of slope approximate the coarseness of the waveform,[103] and also can inherently have a high-pass effect on the frequency content of the signal by the derivative property of the Fourier transform; thus they may provide a more robust assessment of the VF waveform than amplitude measures due to their ability to deemphasize lower-frequency artifact in the ECG such as motion and ventilations. We calculated Median Slope[22,43,65,68,89,90,106,114,144] and Mean Slope[65,68,89,135] as:

$$\text{Median Slope} = (\text{median} \left| x' \, f_s \right|) \tag{4.6}$$

and

$$\text{Mean Slope} = \frac{1}{N-1}\left|x' f_s\right|, \tag{4.7}$$

where f_s is the sampling rate in Hz and x' is a vector of length $N-1$ containing the pointwise differences of the samples in x_n.

VRhythm is a proprietary algorithm developed by Philips Healthcare designed to predict return of spontaneous circulation after shock.[58,66,137] We computed VRhythm using a compiled function provided by Philips, and although its specific formulation is unknown, it has been described as being similar to the Median Slope.[65]

4.8.2 *Frequency Waveform Measures*

A number of measures have been developed to quantify features of the VF frequency spectrum and predict patient outcome. After fibrillation onset, the amount of high frequency content in the VF waveform may decrease as ischemia persists in the myocardium; this decrease is associated with a reduced likelihood of successful defibrillation.[110,148] Hence, to predict outcome, frequency-based measures typically measure the relative amount of high-frequency content in VF.

4.8.2.1 Fourier Transform-based Measures of Waveform Frequency

The Amplitude Spectrum Area was designed by Povoas and Bisera to increasingly emphasize higher-frequency content in the Fourier spectrum of the ECG and predict defibrillation shock success.[97,98] As the most well-characterized waveform measure in literature, Amplitude Spectrum Area has been validated to predict outcomes ranging from immediate shock success to long-term clinical outcome, including in large human studies.[42,64,149,65,88,89,105,111,114,127,144] Changes in Amplitude Spectrum Area from shock to shock have been shown to predict long-term outcome,[86,112] Amplitude Spectrum Area has been used to distinguish VF from other cardiac

rhythms,[62,150] and it is also associated with the concentration of adenosine triphosphate in the myocardium.[22] We calculated Amplitude Spectrum Area as

$$\text{Amplitude Spectrum Area} = \sum_{m=f_{lo}(N/f_s)}^{f_{hi}(N/f_s)} (X_m f_m), \tag{4.8}$$

where f_{lo} and f_{hi} are low and high and frequency limits (in Hz), $X_0,...,X_m,...,X_{N/2}$ are the one-sided Discrete Fourier Transform (DFT) magnitudes[151] computed from the zero-mean Hanning-windowed ECG voltage samples $x_0,...,x_n,...,x_{N-1}$, f_s is the sampling rate, and $f_0,...,f_m,...,f_{N/2}$ are frequency values in Hz corresponding to each X_m magnitude. The frequency values f_m are related to the frequency index m and input length N by $f_m = f_s m / N.$ Similarly, using a frequency-weighted sum (as in Amplitude Spectrum Area) but with a power spectrum instead of a magnitude spectrum, we calculated the Power Spectrum Analysis[65,68,89] measure as

$$\text{Power Spectrum Analysis} = \sum_{m=f_{lo}(N/f_s)}^{f_{hi}(N/f_s)} (P_m f_m), \tag{4.9}$$

where $P_0,...,P_m,...,P_{N/2}$ are the values of the one-sided[151] power spectrum.

Other characteristics of the VF spectrum have been used to predict outcome, such as features of the VF spectrum center. Brown et al. employed the Centroid Frequency[42,57,136,152] (also known as median frequency), which is the frequency corresponding to the center of mass of the power spectrum, while Neurauter et al. implemented the Centroid Power[65,68,136]. We calculated the Centroid Frequency and Centroid Power from frequencies f_{lo} to f_{hi} as

$$\text{Centroid Frequency} = \frac{\sum_{m=f_{lo}(N/f_s)}^{f_{hi}(N/f_s)} (P_m f_m)}{\sum_{m=f_{lo}(N/f_s)}^{f_{hi}(N/f_s)} (P_m)} \tag{4.10}$$

and

$$\text{Centroid Power} = \frac{\sum_{m=f_{lo}(N/f_s)}^{f_{hi}(N/f_s)} (P_m)^2}{\sum_{m=f_{lo}(N/f_s)}^{f_{hi}(N/f_s)} (P_m)}. \tag{4.11}$$

Eftestol et al. computed the spectral Energy as the area within a specific band of the power spectrum.[65,116,134,139] We calculated the Energy from f_{lo} to f_{hi} as

$$\text{Energy} = \sum_{m=f_{lo}(N/f_s)}^{f_{hi}(N/f_s)} (P_m). \tag{4.12}$$

As opposed to calculating the energy in a single band as with the Energy measure, Jekova et al. calculated the ratio of energy in a wide band in the spectrum to that of a narrow band within the wider band.[139] Sherman et al. further modified this concept to use two exclusive bands in the spectrum, defining the Frequency Ratio as the ratio of energy between the upper and lower range of the Fourier magnitude spectrum.[59,100,141] We calculated Frequency Ratio as the ratio of energy in a low band calculated between 1 Hz and a midpoint frequency f_{mid}, divided by the energy in a higher band calculated between the midpoint frequency f_{mid} and the maximum frequency limit (30 Hz) as

$$\text{Frequency Ratio} = \frac{\sum_{m=1+f_{mid}(N/f_s)}^{30Hz(N/f_s)} (X_m)}{\sum_{m=1Hz(N/f_s)}^{f_{mid}(N/f_s)} (X_m)}. \tag{4.13}$$

The extreme values of the power spectrum are represented by the Max Power[68,134], defined as the maximum value of the power spectrum, and the Peak Frequency[65,88,89,116] the frequency at which the maximum power occurs. Using the power spectrum evaluated in a range between low and high frequency limits f_{lo} to f_{hi}, or $P_{f_{lo}-f_{hi}}$, we calculated Max Power as

$$\text{Max Power} = \max(P_{f_{lo}-f_{hi}}) \tag{4.14}$$

and Peak Frequency as

$$\text{Peak Frequency} = \arg\max_f (P_{f_{lo}-f_{hi}}). \tag{4.15}$$

Eftestol et al. used the Spectral Flatness Measure to quantify the flatness of the power spectrum by computing the ratio of the geometric and arithmetic spectral means.[65,89,116,153] We calculated the Spectral Flatness Measure between frequencies f_{lo} and f_{hi} as

$$\text{Spectral Flatness Measure} = \frac{\exp\left(\frac{1}{Nf_s}\sum_{m=f_{lo}(N/f_s)}^{f_{hi}(N/f_s)}\ln(P_m)\right)}{\exp\left(\frac{1}{Nf_s}\sum_{m=f_{lo}(N/f_s)}^{f_{hi}(N/f_s)}(P_m)\right)}. \tag{4.16}$$

4.8.2.2 Wavelet-based Measures of Frequency

Time-frequency measures of frequency include those based on the Wavelet or Short-Time Fourier transforms. Of the various ways to represent the time-frequency behavior of a given signal, wavelet transforms based on a Morlet wavelet are most commonly used to describe the VF waveform.[42,89,132] The general form of the continuous Morlet wavelet function $\psi(t)$ has three factors: a constant, a complex sinusoid, and a Gaussian envelope, represented in continuous time by $\psi(t) = \pi^{-1/4}\exp(\mathrm{i}2\pi f_0 t)\exp(-t^2/2)$, where t is time and f_0 is the base frequency of the

oscillations in the wavelet which is commonly defined with a value of $f_0 = \sqrt{1/(2\ln 2)}$.[154] The Morlet wavelet can be scaled and dilated to other center frequencies by varying a scaling factor a and a translation factor b in the argument of the function; i.e., $\psi\left((t-b)/a\right)$. The spectrum of a single Morlet wavelet can be considered as having characteristics similar to a bandpass filter with an adjustable passband. As an example, two Morlet wavelets and their impulse responses are shown in Figure 4.7.

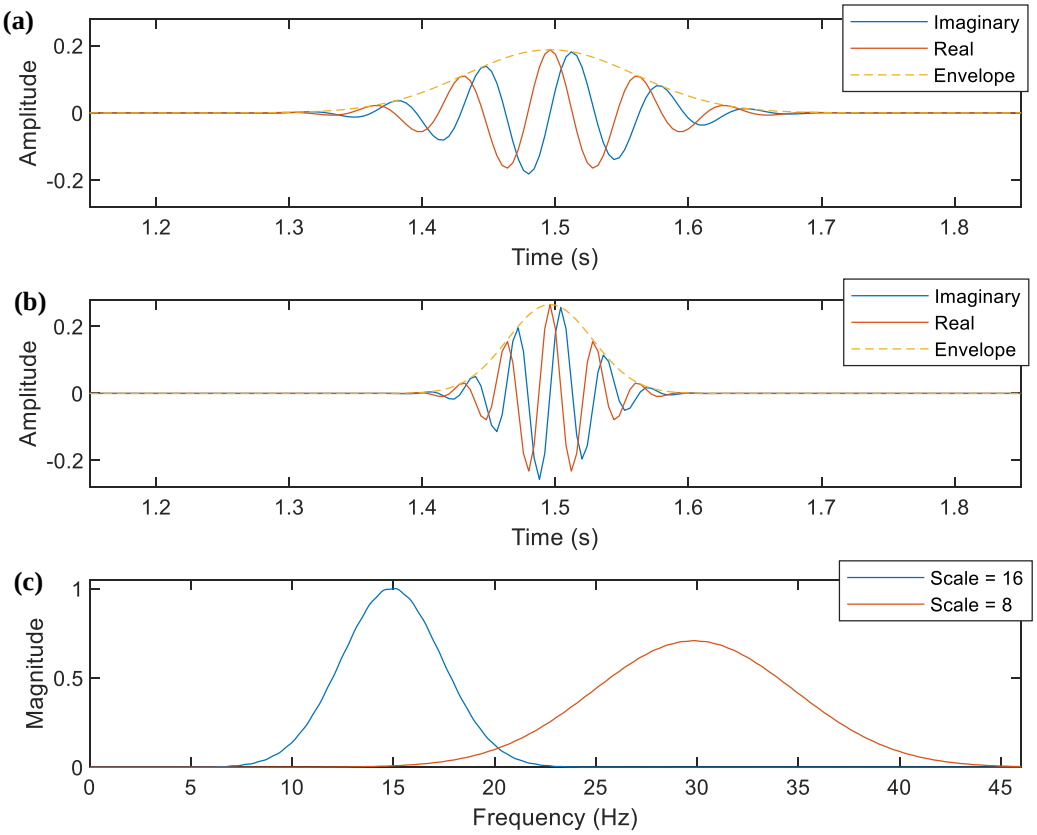

Figure 4.7 Morlet wavelet examples
(a) Real component, imaginary component, and envelope of complex Morlet wavelet with scale a = 8 (corresponding to a center frequency of approximately 30 Hz). (b) Morlet wavelet with scale a = 16 (corresponding to a center frequency of approximately 15 Hz). (c) Spectra of individual wavelets have bandpass characteristics.

For the purposes of ECG analysis, a single wavelet convolved with an input ECG can be used to target features of similar morphology or frequency to the wavelet (e.g. QRS complexes). Multiple

wavelets with a range of center frequencies can be convolved with an input signal to produce a time-frequency representation of the input ECG.

Endoh et al. described three variations of the Wavelet Energy as the integral of the power in the Morlet wavelet transform between fixed "low" (1-3 Hz), "medium" (3-10 Hz), or "high" (10-32 Hz) frequencies.[88] As it was unclear which frequency ranges are optimal, we instead chose to implement the Wavelet Energy using variable wavelet center frequency limits f_{lo} and f_{hi}, as

$$\text{Wavelet Energy} = \sum_{i=1}^{N} \sum_{j=f_{lo}}^{f_{hi}} \left| W_{i,j} \right|^2 , \tag{4.17}$$

where $W_{i,j}$ are the wavelet transform coefficients calculated from the convolution of an input ECG of length N with complex Morlet wavelets scaled to center frequencies j (Figure 4.8).[154]

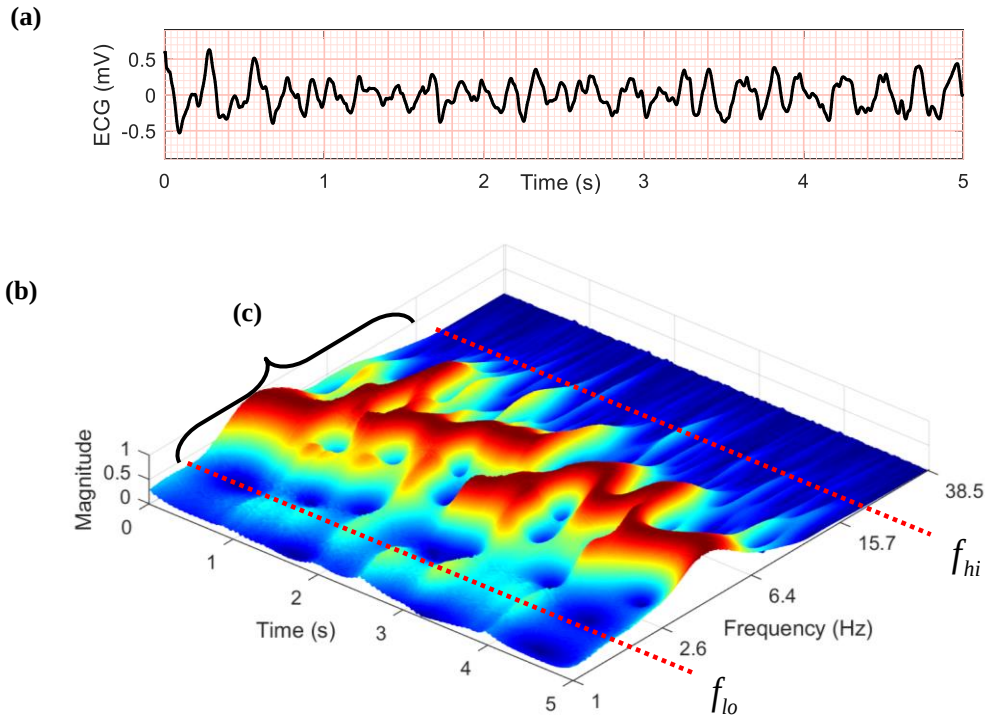

Figure 4.8 Wavelet Energy example
(a) VF ECG. (b) Normalized wavelet transform calculated from VF ECG. (c) Wavelet Energy measure is evaluated between wavelet center frequency limits f_{lo} and f_{hi}.

4.8.2.3 Parameter Selection for Frequency Measures

For each frequency-based measure above, we selected frequency limit parameters f_{lo}, f_{hi}, and/or f_{mid} (as appropriate) using training data. In the majority of prior studies, measures based on the Fourier spectrum have typically been calculated using ranges such as 1-26 Hz or 4-26 Hz.[65] However, Neurauter et al. have suggested improving predictive performance during cardiopulmonary resuscitation (CPR) by restricting waveform analysis to higher frequencies to mitigate the effect of CPR chest compressions (CCs), although exact optimal frequency ranges remain unclear.[43,45] Thus, for each frequency measure, we incremented both the low and high frequency limits f_{lo} and f_{hi} in 1 Hz steps from 1-30 Hz (inclusive) to maximize area under the

receiver operating characteristic curve on training data. Frequency ranges were selected based on data with and without CCs separately. The widest absolute frequency range resulting in an AUC within a tolerance of 0.0025 of the maximum AUC value was automatically selected to improve generalizability of measures and prevent overfitting to local AUC maxima. Maximum frequency was limited to 30 Hz due to ECG bandpass filters also being set at 1-30 Hz, and to homogenize the data bandwidth by removing high frequency content from FR3 defibrillators (which have a bandwidth above 40 Hz) and MRx defibrillators (which have a bandwidth potentially as high as 40 Hz) as compared to Lifepak devices (which have a bandwidth up to 30 Hz). Frequency limit selections were performed separately for prediction of neurologically-intact survival, prediction of return of circulation, and for prediction of return of rhythm.

4.8.3 *Measures of Waveform Complexity*

Measures of the complexity, entropy, or roughness of the VF waveform have been used to estimate time since VF onset and predict shock success. As VF progresses from an early to later state, the number of depolarizing rotors may increase, with rotor wavefronts fragmenting into smaller waves due to the anisotropic properties of ventricular tissue and breaking of depolarization waves against ventricular boundaries[20,21] (although it is unclear whether a single dominant rotor or multiple continuous smaller rotors drive fibrillation over time).[13] Regardless, over time the organization of the VF ECG waveform decreases, and may be estimated using multiple approaches.

4.8.3.1 Detrended Fluctuation Analysis

Detrended Fluctuation Analysis was first described for cardiac analysis by Peng et al., and measures the root mean square fluctuation within subdivisions of time-series data as a function of the subdivision size.[155] The log-log slope of fluctuation versus subdivision size indicates the type

of correlation within the signal. Long-term correlations have slope greater than 0.5, slopes of 0.5 indicate a random walk, and slope less than 0.5 indicates rougher, shorter-term correlation. Lin et al. first demonstrated that Detrended Fluctuation Analysis estimates VF robustness and predicts defibrillation success.[88,104] Detrended Fluctuation Analysis calculation is described by first converting the input signal $x_1,...,x_n,...,x_N$ into an integrated time series $y_1,...,y_k,...,y_N$ where $y_k = \sum_{n=1}^{k}(x_n - \bar{x})$ (Figure 4.9).[155] The integrated time series is then divided into windows of size w, and the linear trends within each window for a given window size are denoted as $Y_{w,1},...,Y_{w,k},...,Y_{w,N}$. The root mean square fluctuation $F(w)$ (as a function of window size w) about the linear trend $Y_{w,k}$ within each window is then calculated by

$$F(w) = \sqrt{\frac{1}{N}\sum_{k=1}^{N}(y_k - Y_{w,k})^2}\ . \qquad (4.18)$$

The slope of the log fluctuation versus log window size (i.e., $\log(F(w))$ versus $\log(w)$) is then calculated within a range of interest and used to estimate VF organization and predict patient outcome. We calculated DFA using the cardiac signal analysis package provided by Physio Net (www.physionet.org), and computed the slope of a linear trendline fit to the data in the $\log(F(w))$ versus $\log(w)$ plot (Figure 4.9, Figure 4.10).[138] Trendline length was selected from an initial coarse optimization such as that shown in Figure 4.10, and then trendline start location was selected using a finer optimization with a fixed length parameter. The slope of the final trendline was then used as the Detrended Fluctuation Analysis waveform measure output.

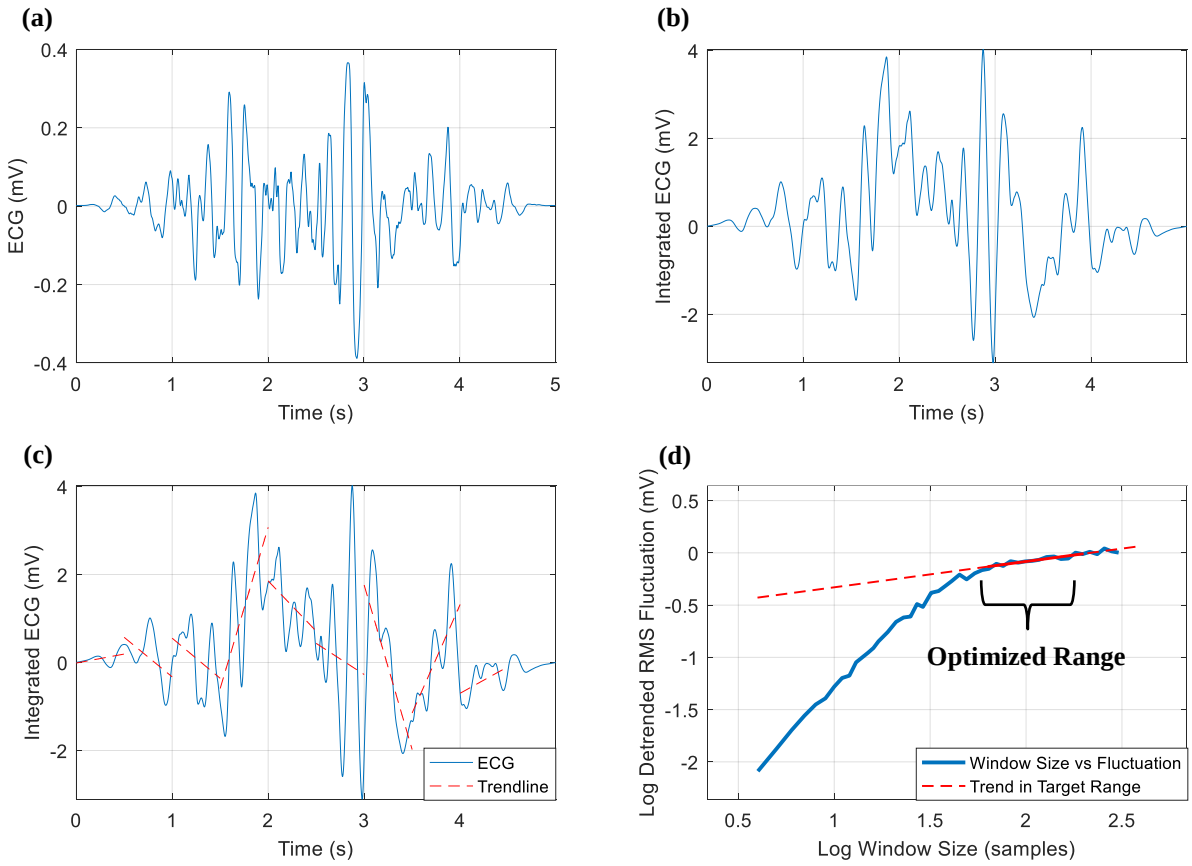

Figure 4.9 Detrended Fluctuation Analysis calculation

(a) Windowed, filtered VF ECG signal. (b) Integrated time-series signal y_k following methods of Peng et al. (c) Fluctuation of integrated signal y_k about subdivision trendline using $Y_{w,k}$ 0.5-s windows. (d) Example of slope range selection for log fluctuation $F(w)$ versus log subdivision window size w.

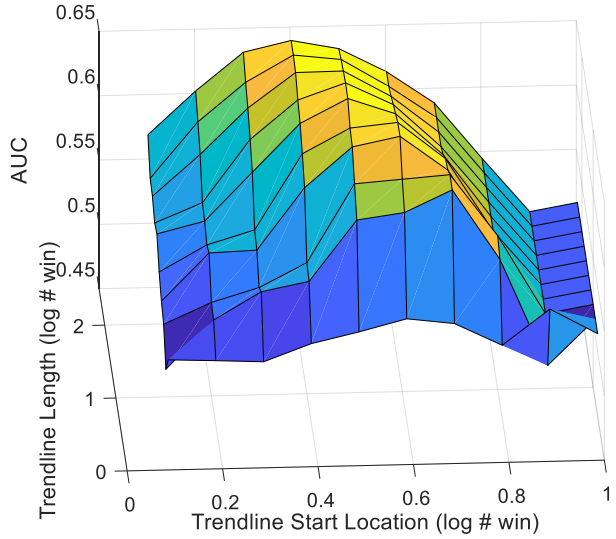

Figure 4.10 Detrended Fluctuation Analysis optimization example
Representative example for optimizing trendline length and start location based on the relationship between $\log(F(w))$ and $\log(w)$.

4.8.3.2 Median Stepping Increment

Gong et al. proposed the Median Stepping Increment of the Poincare plot to quantify the self-similarity of the VF waveform, as self-similarity describes an aspect of signal organization and may be related to likelihood of defibrillation success.[90,134] Poincare recurrence plots illustrate the relationship between a time-series signal and its lagged samples; they exhibit a uniform area when the input signal is random and aggregate about an axis when self-similar behavior occurs. We calculated Median Stepping Increment, which is defined by Gong et al. with a lag of one sample, as

$$\text{Median Stepping Increment} = \text{median}\left(f_s \sqrt{(x_{n+1} - x_n) + (x_{n+2} - x_{n+1})} \right) \qquad (4.19)$$

using ECG samples $x_0, ..., x_n, ..., x_{N-3}$ (Figure 4.11).

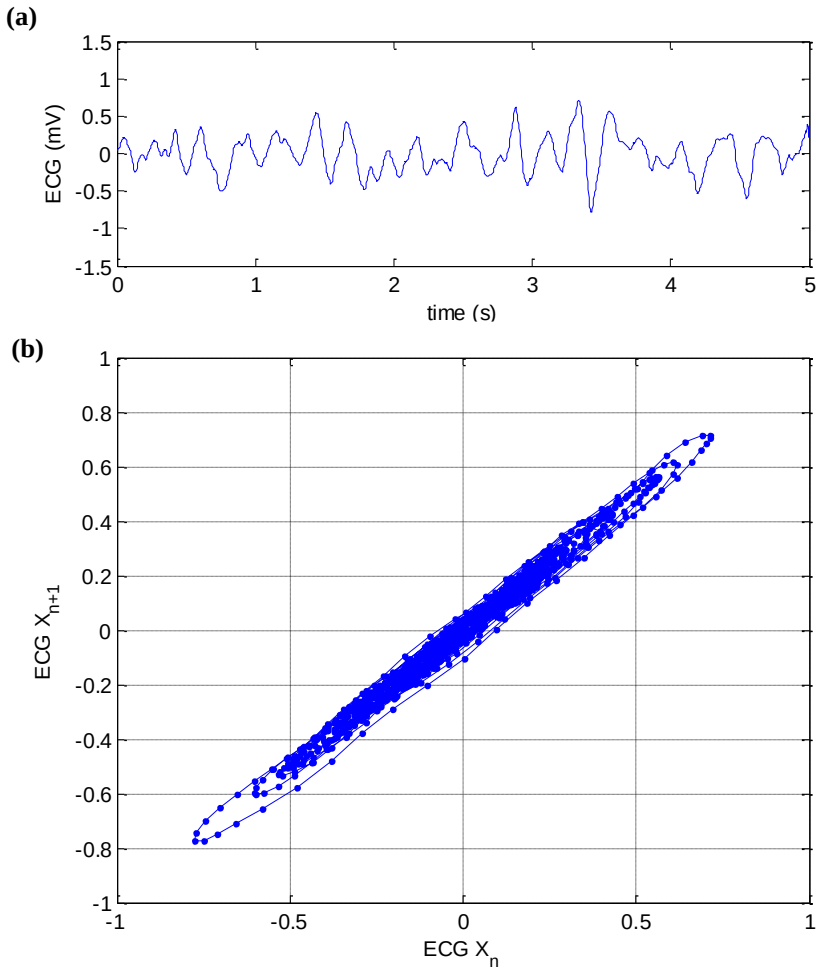

Figure 4.11 Median Stepping Increment example
(a) VF ECG. (b) Poincare plot from VF ECG with lag = 1 used to compute the Euclidean distances between points. The median of these distances is the Median Stepping Increment.

4.8.3.1 Angular Velocity

Sherman et al. developed the Angular Velocity to describe the 3-dimensional speed of rotation of the VF ECG versus two different lagged versions of itself.[59,133] We calculated Angular Velocity as the mean angle between consecutive samples by

$$\text{Angular Velocity} = \frac{1}{N}\sum_{n=0}^{N-2k-2}\left|\cos^{-1}\left(\frac{A_n \cdot A_{n+1}}{|A||A_{n+1}|}\right)\right| \tag{4.20}$$

where k is the lag amount (in samples) and $A_n = (x_n, x_{n+k}, x_{n+2k})$ are ECG samples $x_0, ..., x_n, ..., x_{N-1}$ versus their lag in three dimensions (Figure 4.12).

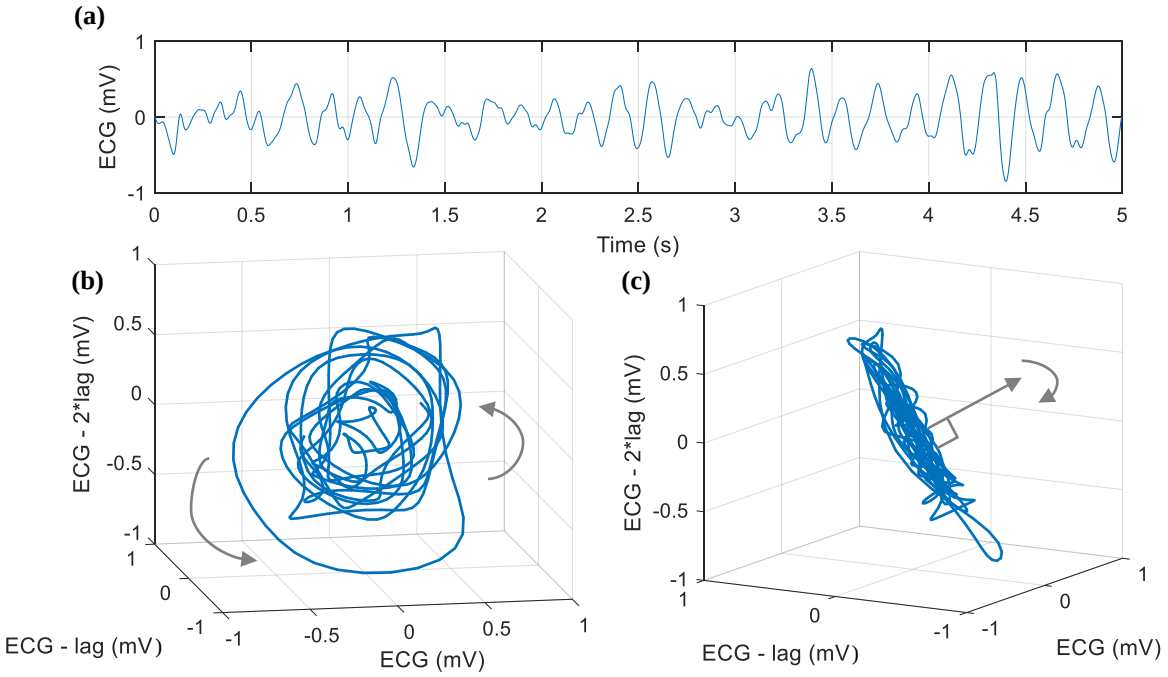

Figure 4.12 Angular Velocity example
(a) VF ECG. (b) Example of ECG versus its lag using lag k = 5. (c) Side view of [b] to illustrate disk-like shape of rotation about normal.

4.8.3.2 Log of the Absolute Correlations

Sherman et al. also demonstrated that the logarithm of the sum of the autocorrelations of a VF signal versus all possible lags of itself is associated with return of spontaneous circulation following shock.[90,141] This 'scaling' behavior can be quantified as the Log of Absolute Correlations and calculated as[141]

$$\text{Log of Absolute Correlations} = \log_{10}\left(\sum_{k=1}^{K}\left[\frac{\sum_{n=0}^{N-k-1} x_n x_{n+k}}{N-k}\right]\right) \tag{4.21}$$

where the lag k is varied from $1 \le k < N-k$ (Figure 4.13). Similar scaling behavior had also been described using the Scaling Exponent (not evaluated in the current investigation).[156,157]

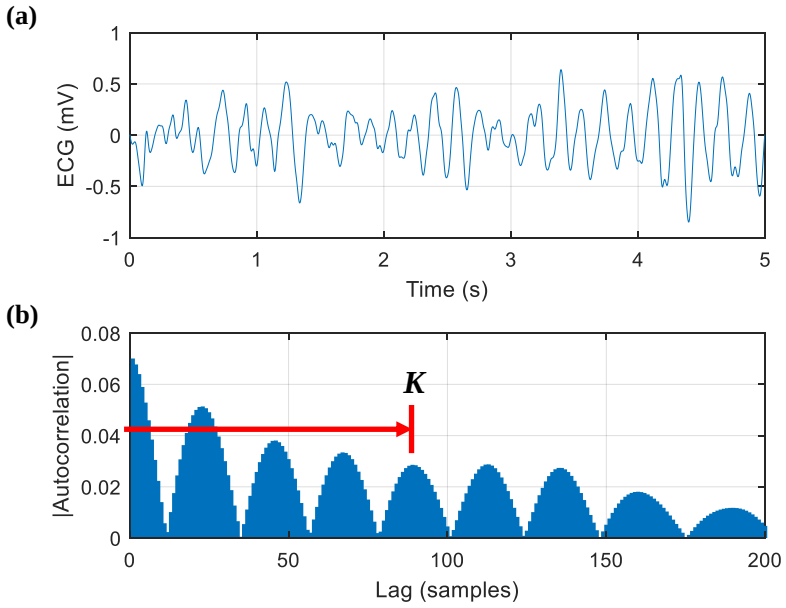

Figure 4.13 Log of Absolute Correlations example
(a) VF ECG. (b) Sum of magnitude of autocorrelations is calculated between a beginning lag of 1 sample up to the variable maximum lag value.

4.8.3.3 Approximate Entropy

We examined two measures describing aspects of the VF waveform entropy. Approximate Entropy was first described by Pincus et al. to estimate the complexity of a signal based on similarities of subdivisions across various subdivision lengths.[158] In subsequent study, Approximate Entropy has been shown to predict defibrillation success.[88,90,143] Approximate Entropy is described as follows[90]: Given an ECG input $x_1,...,x_n,...,x_N$, represent a series of vectors v of length L as $v_n = x_n, x_{n+1},..., x_{n+L-1}$. Next, define a series of Chebychev distances d between vectors by $d_{ij}^{L} = \max_{k=1,...,L-1}(|v_{i+k} - v_{j+k}|)$.[90] Then, for each vector v, count the number C of vectors with a

distance d that is less than a tolerance parameter R, by $C_n^L = (N-L+1)^{-1}\sum_{j=1}^{N-L+1}\Theta(R-d_{i,j}^L)$, where Θ is the Heaviside function. R is calculated by $R = r(SD/2)$ where SD is the standard deviation of the input x and r is a variable parameter.[88] Then, the probability Φ that two vectors within the tolerance distance are the same is calculated by $\Phi^L = (N-L+1)^{-1}\sum_{n=1}^{N-L+1}\ln C_n^L(R)$. Approximate Entropy can therefore be represented as

$$\text{Approximate Entropy}(L,R,N) = \Phi^L(R) - \Phi^{L+1}(R). \quad (4.22)$$

We calculated Approximate Entropy using a package for cardiac signal analysis provided by Physio Net (www.physionet.org)[138], with variables values for L (in samples) and r (scaling factor for standard deviation) selected based on training data.

4.8.3.4 Spectral Entropy

Various forms of the Shannon entropy, $-\sum x\log_2 x$, have been applied to the time-series or frequency-domain ECG.[90,101,142] The Shannon entropy equation is typically applied to the probability distribution of the values in a signal (e.g. to a vector of histogram bin heights representing the distribution of ECG sample values). However, in this case we applied the Shannon equation to the normalized Fourier spectrum of the ECG (treating the normalized spectrum itself, a representation of relative frequency content, as a probability distribution) rather than applying the equation to a probability distribution of the spectrum magnitude values. Specifically, we calculated the Spectral Entropy of the normalized power spectrum between frequencies f_{lo} and f_{hi} as

$$\text{Spectral Entropy} = -\sum_{m=f_{lo}(N/f_s)}^{f_{hi}(N/f_s)}\left(\frac{P_m}{\sum P}\log_2\left(\frac{P_m}{\sum P}\right)\right) \quad (4.23)$$

where $P_0,...,P_m,...,P_{N/2}$ represent the one-sided power spectrum values normalized to an area of 1. The frequency indices m are calculated in terms of the frequency of interest f_m, Discrete Fourier Transform length N, and sample rate f_s, by $m = f_m(N / f_s)$.

4.8.4 *Combination Waveform Measures*

We defined combination measures as any statistical or machine learning model that combines multiple individual VF waveform measures to produce a likelihood of positive outcome. The rationale for using such models is that if different individual waveform features have partially-orthogonal information describing the VF signal, it is possible that a combination of measures may yield higher predictive performance than individual measures. However, prior studies using VF without CC artifact have suggested that prediction of shock success is not significantly improved using combination models of multiple measures versus individual measures.[45,68,89] Still, only a limited number of measures have been tested in combination models, and studies of combination models have so far only included data without chest compression artifact.[68,89,101,116,144] Prior to the current study, it was unknown if combination methods would be beneficial for measures calculated during CCs administered during CPR. Additionally, even if waveform measures alone are not improved in a combination model, determining which combination models perform best may be useful for future study, as information from additional variables such as carbon dioxide levels or prior shock outcome may improve prognosis when used in combination with VF waveform measures.[101,112,127] Hence it is likely a VF prognostic algorithm used in a clinical setting would use a combination approach that integrates multiple ECG waveform measures with additional metrics.

4.8.4.1 Logistic Regression

Binary logistic regression has been used in VF waveform analysis to combine features predictive of shock success, including dichotomous variables (e.g. previous shock outcome) and continuous variables (e.g. quantitative waveform measures).[28,112,127] Logistic regression has also been used to estimate odds ratios for individual waveform measures and to examine the effect of covariates (such as age or sex) on models to predict patient outcome.[86,102]

The general form of a logistic model is of the form

$$P_{(y=1)} = \frac{\exp(\beta^T x + \beta_0)}{1 + \exp(\beta^T x + \beta_0)} \tag{4.24}$$

where probability of positive class P is computed as a function of observations x and model parameters β.[159] The odds of P are definition $\frac{P}{1-P}$. Thus alternatively the logistic model function can be expressed in terms of the logit (log-odds)[160] function $\text{logit}(P) = \ln\left(\frac{P}{1-P}\right)$ as

$$\text{logit}(P) = \beta^T x + \beta_0. \tag{4.25}$$

The optimal logistic model parameters β are estimated by maximum likelihood estimation. This process solves for β values that maximize a likelihood function. This likelihood function L is of the form $L(\beta_0, \beta) = \prod_i P(x_i)^{y_i}(1 - P(x_i))^{1-y_i}$ and represents the overall probability of input samples x_i and their known classes $y_i \in \{0,1\}$ given a set of parameters (β_0, β).[161,162] The parameters (β_0, β) can be estimated by treating L as a function of the parameters, taking the logarithm (to simplify, since L is a product of multiple functions), and solving for the extreme points of the function.[163] This convex optimization problem is typically solved through numerical methods (e.g. Newton-Raphson).[159] Estimated odds and 95% confidence intervals of a particular variable x may

be calculated once the model is trained (i.e. β is solved) by $odds +/- 95\%\text{CI} = \exp(\beta +/- 1.96SE)$ (assuming a significance level of $\alpha = 0.05$), where SE is the standard error of a the estimated β coefficient corresponding to a particular input feature x.

We implemented Logistic Regression as a combination of individual waveform measures using the MATLAB `glmfit` function. Our model was of the linear form (with no product interaction terms) and can be represented by

$$P = \frac{1}{1+\exp\left[-\left(\beta_0 + \beta_1 \cdot x_1 + ... + \beta_n \cdot x_n + ... + \beta_L \cdot x_L\right)\right]} \tag{4.26}$$

where in this application, P is the probability of shock success, x_n is an input vector of L log-transformed individual waveform measures, the parameter β_0 is a constant, and the parameter β_n is a vector of regression coefficients developed on training data.

4.8.4.2 Neural Network

Feedforward Neural Networks have been used to combine VF features to predict shock success without CPR CCs, but in prior studies have not exhibited improved predictive performance over individual measures.[68,89,112] To describe a basic network, we first describe a single node by

$$y = \tanh\left(-\sum w_{in} x_{in} - b\right) \tag{4.27}$$

where y is the output from the current node ranging between [-1,1], x_{in} is a vector of inputs to the current node from all nodes in the previous layer, w_{in} is a vector of weights that are multiplied by inputs to the current node, and b is a bias offset for the current node (Figure 4.14).[164]

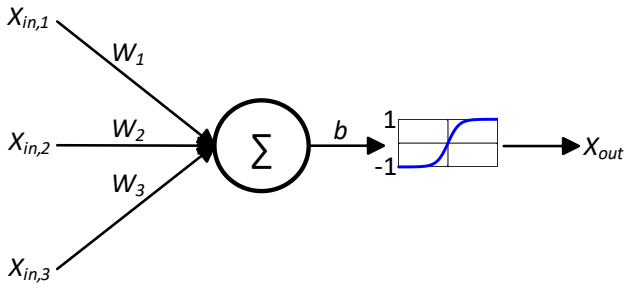

Figure 4.14 Neural network node
Representation of a single neural network node with hyperbolic tangent activation function

We implemented feedforward Neural Networks with all 24 individual waveform measures as input features, hidden layers with hyperbolic tangent activation functions, and an output node with a sigmoid activation function. Networks were fully-connected, with each node accepting all weighted inputs from the previous layer (Figure 4.15).

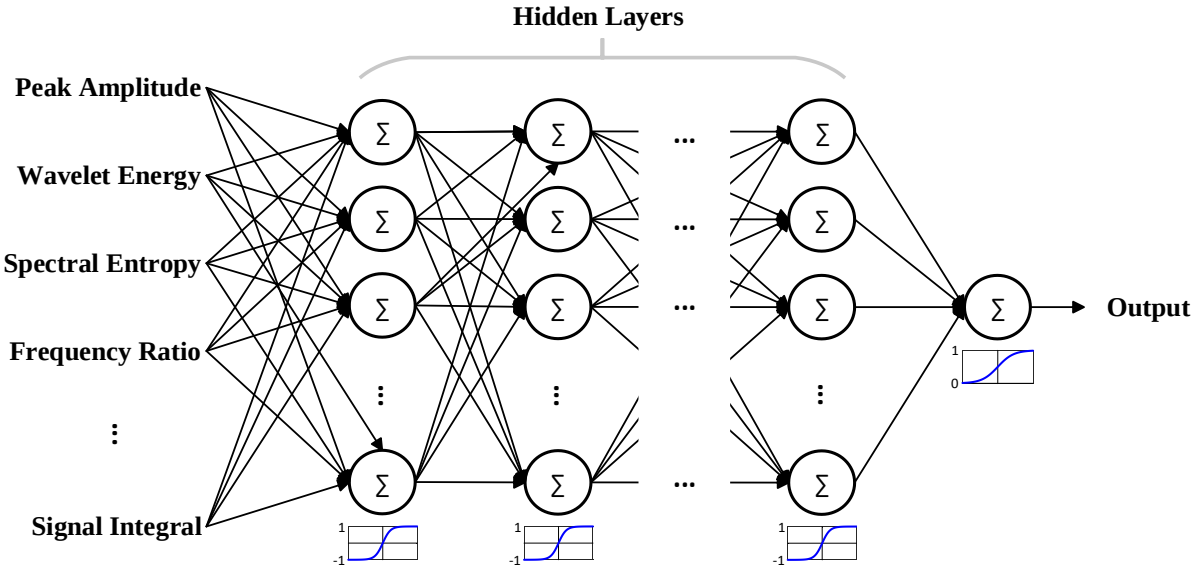

Figure 4.15 Neural Network overview
Simplified network architecture illustration. All waveform measures were used as input features.

If the current layer is the first layer in the network, x_{in} input values for each node are the weighted input features (in this case, log-transformed waveform measure values) that are fed into the network, whereas if the current layer is in the middle of the network, x_{in} values are the outputs of the previous layer. The last layer consists of an output node represented by

$$P = \left[1 + \exp\left(-\sum\ w_{in} x_{in} - b\ \right)\right]^{-1} \tag{4.28}$$

where P is the final network output representing likelihood of shock success between [0,1], x_{in} is an input vector of outputs from the previous layer, w_{in} is a vector of weights applied to the incoming values from the prior layer, and b is a bias offset for the output layer node.

4.8.4.3 Neural Network Training and Parameter Selection

Once a network with a given structure is initialized, input weights and bias offsets w and b must be selected for each node using training data. For each training epoch, input weight and bias offset parameters for all nodes in a layer are updated backwards layer-wise through the network through a backpropagation process. Weights and biases are incremented in the direction of the steepest gradient of the network error function until the network error function is optimized. We used the MATLAB neural network training function `train` for network training, with equal weights assigned to positive and negative predictions, and input features (i.e. waveform measure values) automatically scaled to a range of [-1, 1] using `mapminmax`. We trained networks using two different backpropagation training methods and then selected the training method for the final model based on training results. The first training method was the default scaled conjugate gradient method `trainscg`. The second training method was the Bayesian regularization `trainbr` procedure used by Neurauter[68] and He[89] for waveform measure analysis.

For the scaled conjugate gradient backpropagation training method, cross-entropy was used as the performance function and can be calculated as

$$\text{cross-entropy error} = \frac{1}{N}\sum_{n=1}^{N} -t_n \log(P_n) - (1-t_n)\log(1-P_n) \qquad (4.29)$$

for N pairs of binary training target classes and continuous predicted output probabilities (t_n, P_n). The scaled conjugate gradient training procedure uses 'early stopping' criteria to cease training and select final weight and bias values. Early stopping requires dividing the study's overall training dataset into two randomized subsets: cross-validation training data (training_{tr}) and cross-validation validation data (training_{val}). We used a random division of 70% training_{tr} and 30% training_{val} VF segments from the study training data. During the repeated training epochs where all weights and biases are updated in the direction of the negative gradient of the training data cross-entropy error, training_{tr} and training_{val} error values decrease in concert until the network reaches an optimal configuration; at this point training_{val} error begins to increase rather than decrease (a 'validation failure') with continued subsequent training epochs. We allowed a maximum of four consecutive validation failures before training was ceased (as opposed to the default maximum value of six) in order to improve generalizability. The network weights and biases from the training epoch prior to the four consecutive validation failures were then used in the final model for a given network structure. The training_{val} cross-entropy error of the final model after validation stopping was saved after each model was trained. The entire training sequence was repeated 100 times for each network structure, and the mean training_{val} cross-entropy error of all final models compared to select the optimal structure.

We implemented Bayesian regularization as an alternative training method. For Bayesian regularization backpropagation training, a combination of the network's mean-squared error and

weight values are used in the error function. In general, regularization refers to penalizing network overfitting by incorporating network weight and bias values into the error function, as smaller weights and biases tend to result in networks that less-overfit to training data. The error function in this case can be represented by a mean-squared error term and a regularization term as

$$\text{regularized error} = (1-\alpha)\left(\frac{1}{N}\sum_{i=1}^{N}(t_i - P_i)\right) + (\alpha)\left(\sum_{j=1}^{n} w_j^2\right) \qquad (4.30)$$

where α is a ratio parameter that controls the amount of regularization, N is the number of training data points with predicted values P and true target classes t, and n is the number of w weight values. Bayesian regularization automatically determines the regularization ratio parameter α that defines the proportional contribution of network mean-squared error and network parameter values. The Bayesian regularization method, by default, uses all training data to train the network, and ceases training when convergence criteria are met after a large number of training epochs. Training is ceased until the network parameters (weight, bias, and regularization values) reach convergence as defined by default limits in the `trainbr` method. However, when we implemented the default training method, the default criteria resulted in models that were overfit based on training AUC. Therefore, we added an additional validation failure-based early stopping condition similar to that used with the scaled conjugate gradient method, using a 70% cross-validation training (training_{tr}) and 30% cross-validation validation (training_{val}) division of the training data samples. Training was ceased either when convergence criteria were met on the 70% training_{tr} subset or when 18 consecutive validation failures were observed in the 30% training_{val} validation subset. The mean-squared error of the final model on training_{val} data was saved after each model was trained. The entire training sequence was repeated 100 times for each network

structure, and the average mean-squared training$_{val}$ error of all final models compared to select the optimal structure.

We varied hyperparameter values (i.e., numbers of nodes and layers) to determine the optimal network structure. There are no universal criteria for determining the appropriate number of layers and nodes for a feedforward neural network, although some general guidelines have been proposed. For example, for networks with a single hidden layer and n input features, an upper limit of $2n+1$ nodes in the hidden layer has been suggested (49 nodes in this case).[165] For networks with two hidden layers, others have derived a theoretical upper limit for the max number of nodes required to adequately describe any relationship between N input samples and m outputs as $2\sqrt{(m+2)N}$, or 109 maximum nodes in our case.[166] With regards to use for VF analysis, a prior study of neural networks to combine VF waveform measures used feedforward networks with 1-3 hidden layers of 1-8 nodes each,[68] while a subsequent VF waveform study used a similarly-sized 2-layer network.[89] In general, as few layers and nodes as possible should be used to prevent overparameterization and overfitting. Since many of the input features used in this study were highly correlated (e.g. mean slope and median slope), we selected a maximum total number of nodes of 72, approximately halfway between the two proposed theoretical maxima.[165,166] Specifically, we varied the number of hidden layers from 1-3, and the number of nodes in each layer from 1-24. Since each training sequence began with a different set of random initial weights, and each training sequence used a re-randomized division of 70% training$_{tr}$ and 30% training$_{val}$ subsets of the study's training dataset, individual training runs each converged to different final weight and bias values. Therefore, for each of the two training methods explored in this study (scaled conjugate gradient and Bayesian regularization), we trained each network structure 100 times with random initial weights and random training$_{tr}$ and training$_{val}$ divisions of the overall

training data, and selected the structure with the lowest training$_{val}$ validation error averaged over 100 training runs. In the case of scaled conjugate gradient training, the network structure with the lowest mean training$_{val}$ cross-entropy was selected. In the case of Bayesian regularization training, the network with the lowest mean training$_{val}$ mean-squared error was selected. After selecting the optimal network structure for each of the two training methods, we compared AUC values and Pearson regression correlation coefficients for predicted versus target values on training data using the final network structures using all training data, and selected the single training method that resulted in models with the highest AUC and highest correlation coefficients.

4.8.4.4 Support Vector Machine

Support Vector Machines have been employed in multiple VF waveform studies to combine features predictive of shock success, and are thought to potentially add robustness to otherwise noise-prone waveform measures since they can operate on high-dimensional combinations of input features and can generalize well.[89,101,144] Support vectors are subsets of data points in the training set that define the boundary of a hyperplane that maximally-separates (i.e., separates with the largest possible margin) two classes of data. The Support Vector Machine classification of a new observation x_{input} can be represented by

$$f(x) = \text{sign}\left(\sum_{t=1}^{T} y_t \alpha_t K(x_{input}, x_t) + w_0 \right), \tag{4.31}$$

where K is the kernel function to evaluate similarity of training points with unknown input x_{input}, x_t is a vector of T N-dimensional training points, α_t are Lagrange multiplier parameters, $y_t \in \{-1,1\}$ are class assignments, and w_0 is a constant.[164] The radial kernel function K was selected for this study as it allows nonlinear decision boundaries and can map data into higher-

dimensional feature space to enable class separation in the higher-dimensional space. This radial kernel function quantifies the similarity (weighted Euclidean distance) between an unknown N-dimensional input sample x_{input} and the gaussian 'landmarks' generated by each N-dimensional training sample x_t by

$$K(a,b) = \exp(-\gamma \sum_{j=1}^{N} \left(a_j - b_j\right)^2), \tag{4.32}$$

where γ is a kernel tuning parameter, N is the number of features per data sample, and j is the feature index for a given $N-$dimensional sample.[164] The kernel size constant γ is related to curve width (specifically, the variance value σ^2) in a traditional gaussian equation by $\gamma = 1/2\sigma^2$.[167] Similar to parameter selection for neural networks described previously, selection of optimal parameter values is performed by minimizing an objective function that contains both a term describing the parameter weights w and a term representing the amount of misclassification ξ_t of training points.[167,168] The objective function is minimized subject to constraints using Lagrangian optimization. Specifically, the following function is minimized to determine weight parameters w and w_0 and Lagrange multipliers α_t:

$$\text{minimize}\left[\frac{1}{2}\|w\|^2 + C\left(\sum_{t=1}^{T}\xi_t\right)\right], \tag{4.33}$$

subject to the constraint

$$y_t\left(w^T x_t + w_0\right) \geq 1 - \xi_t, \tag{4.34}$$

given parameter weights w, tuning parameter C, and the soft error $\sum \xi_t$ representing the total of slack variables ξ_t which quantify the absolute distance from the separating hyperplane for each training point (where $\xi_t = 0$ for correctly-classified points, $0 < \xi_t < 1$ for points close to the

separating hyperplane that violate the margin but are correctly classified, and $\xi_t > 1$ for misclassified points on the wrong side of the margin).[167,169,170] The majority of α_t will be zero; the remaining points x_t corresponding to nonzero α_t are the support vectors for the model.[171] In practice therefore only the training points corresponding to nonzero α_t (i.e. the support vectors) are stored as they define the decision boundaries of the model. Thus, the basic intuitive interpretation of a support vector classifier with gaussian kernels is that unknown inputs x_{input} (each containing N input features) are compared to boundaries defining known landmarks generated from training points x_t and assigned a predicted class based on their weighted similarity to the boundaries of the known landmarks.

4.8.4.5 Support Vector Machine training and parameter selection

During training, support vector machines can be regularized by adjusting the box constraint and kernel hyperparameters (i.e. slack variable constant C and kernel constant γ). Box constraint C denotes the penalty for datapoints that violate the margin between classes; a high box constraint 'hardens' the margin between classes which results in tighter, more jagged boundaries around training points in order to separate the data and reduce the number of misclassified training points. A smaller box constraint softens the margin by allowing more margin violations, which may result in improved generalizability and smoother, wider margins (at the risk of underfitting the data). Kernel size can be adjusted to control the radii of the gaussian 'landmarks' generated by the training data; hence larger kernels may result in smoother classification boundaries and better generalizability.[171]

We trained Support Vector Machine models with radial gaussian kernels and all 24 individual log-transformed, standardized waveform measures as inputs using MATLAB's

`svmtrain` function. To allow generation of receiver operating characteristic curves (which require continuous probabilities), model outputs were mapped to pseudo-probabilities via a sigmoid transformation using `fitSVMPosterior`. Hyperparameters (kernel size and box constraint) were optimized to predict outcomes with and without CCs separately, based on 5-fold mean cross-validation error on training data. Cross-validation error for each of the 5 folds was calculated as the mean weighted fraction of misclassified observations for the holdout fold after training on the 4 training folds.

We observed that hyperparameters that minimized cross-validation error produced models that were overfit and had high training AUC values (as compared to logistic regression training AUC). To compensate for this tendency to overfit and for the fact that the current dataset has a particularly high rate of misclassifications (i.e. AUC values on the order of 0.65-0.75), we underfit box constraint and kernel size hyperparameters by automatically decreasing box constraint and increasing kernel size until cross-validation error was raised to within predefined tolerances of the absolute minimum cross-validation error (Figure 4.16). We selected these tolerances empirically by varying the tolerance values until the model's training AUC values were reduced to a value similar to the Logistic Regression training AUC. The hyperparameter selection procedure was as follows: 1) Find the box constraint and kernel sizes corresponding to the minimum 5-fold classification loss on training data, 2) in the case of predicting return of circulation (which had a stronger tendency to overfit), decrease the box constraint until classification loss is increased to a maximum of 0.01 above the minimum observed loss at the given kernel size, and 3) increase kernel size until classification loss is raised to a maximum of 0.03 above the minimum loss at the current box constraint. The intuitive effect of this procedure was to automatically select kernel size and box constraint values that were slightly underfit compared to those selected based on the minimum

cross-validation error while still ensuring that hyperparameter selections were along the ‘floor’ of the hyperparameter optimization surface.

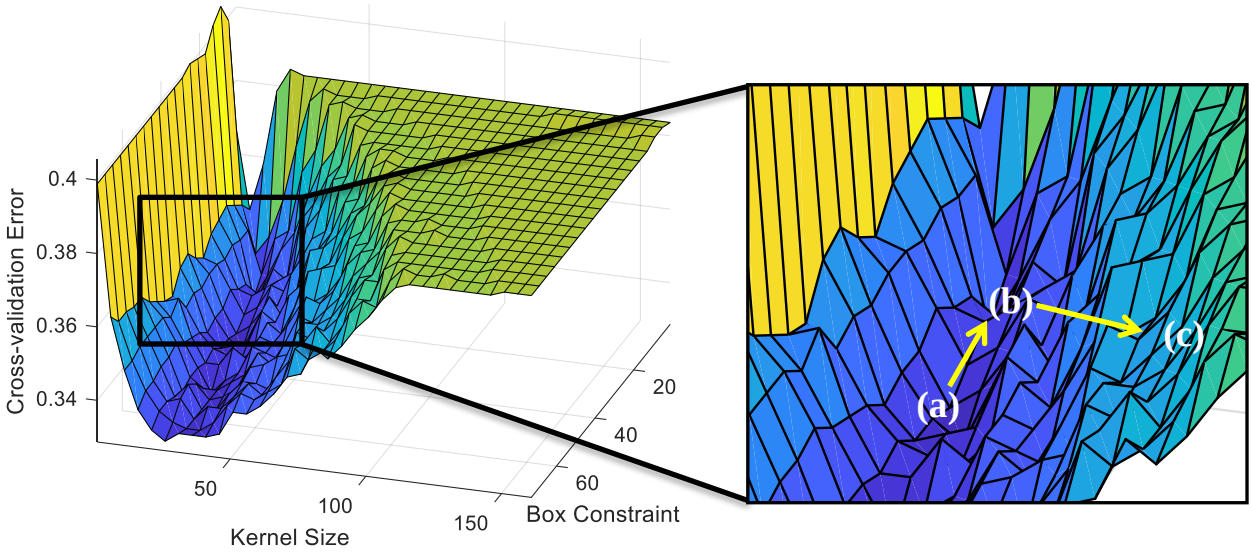

Figure 4.16 Representative Support Vector Machine hyperparameter optimization
Gaussian kernel size and box constraint parameter values were underfit by maximizing kernel size and minimizing box constraint within empirically-selected tolerances of the minimum 5-fold cross validation training error. Optimizations were performed with and without chest compressions. In this example of predicting return of circulation (for illustration only, not to scale), the hyperparameter combination with absolute minimum cross-validation error (a) is automatically adjusted to (b), decreasing box constraint while maintaining a cross-validation error within a tolerance of +/- 0.01 from the absolute minimum error. The current location is then adjusted to (c), which maximizes kernel size while maintaining a cross-validation error within a tolerance of +/- 0.03 of the minimum cross-validation error at the current box constraint.

4.9 Appendix B: Training Results and Parameter Selection

Of the twenty-seven total measures, seventeen measures (fourteen individual measures and two combination models) in this study had variable parameters that were selected based on training data (Table 4.3). Parameter selection methods for each measure are described in the previous section.

4.9.1 *Parameter Optimizations on Training Data*

For measures with adjustable parameters, different parameters were selected to 1) maximize AUC for predicting functional survival, return of circulation, and return of rhythm without CCs, and to 2) maximize AUC for predicting functional survival, return of circulation, and return of rhythm during CCs. Hence, for each measure with adjustable parameters, six parameter selection optimizations were performed. As described previously, in the case of frequency-domain measures, parameter combinations resulting in the widest absolute frequency range within a tolerance of +/- 0.0025 of the maximum AUC were automatically selected. Selections were based on AUC using 991 training VF segments collected during CCs and 868 segments collected without CCs collected prior to 1116 unique shock cycles from 460 training patients.

4.9.1.1 Frequency-domain Measures

Optimal low, mid, or high frequency limit selections, f_{lo}, f_{mid}, f_{hi}, for frequency-domain waveform measures are illustrated (as applicable) in Figure 4.17 through Figure 4.27 below.

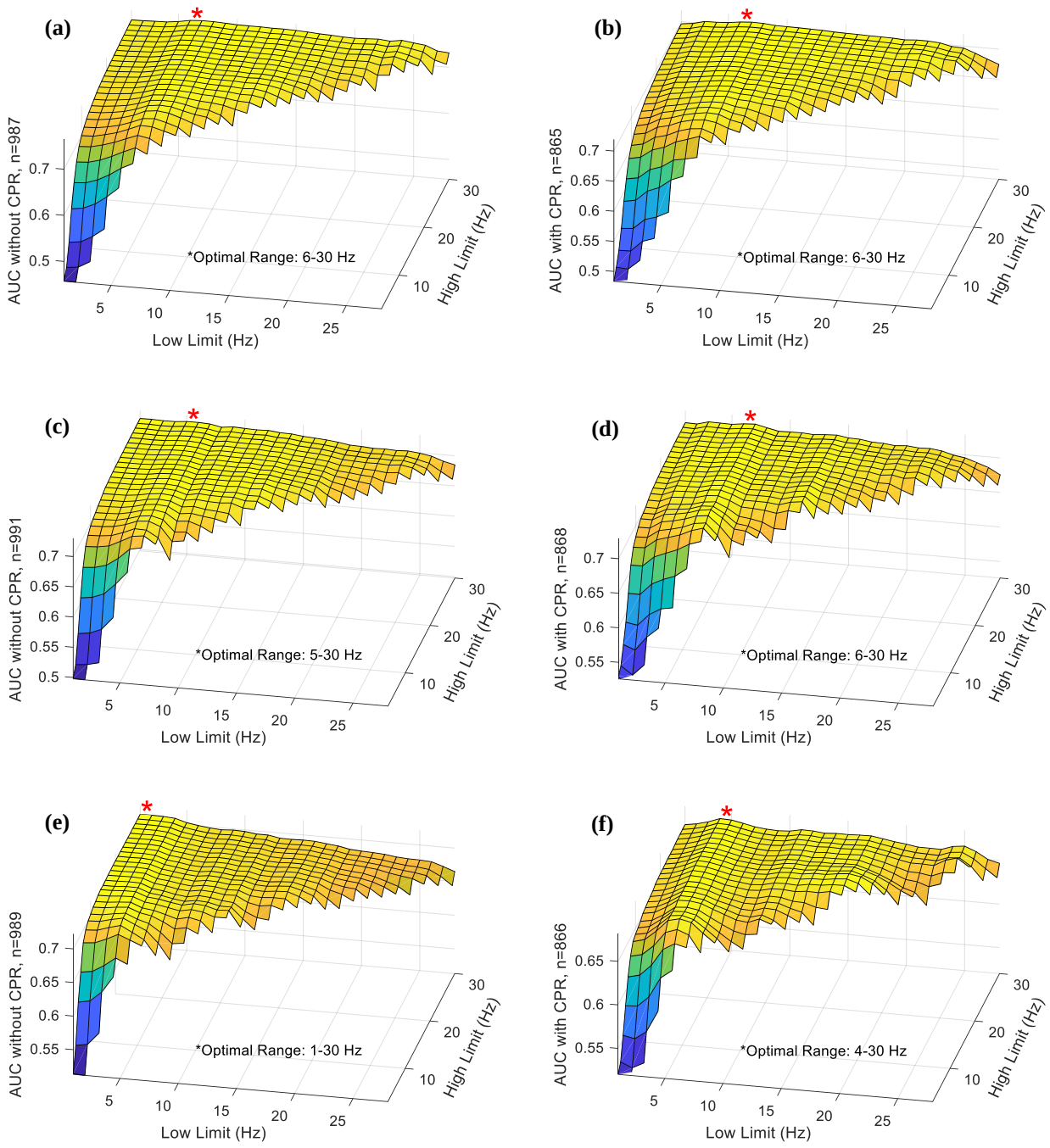

Figure 4.17 Amplitude Spectrum Area frequency range selection

Optimal frequency limits f_{lo} and f_{hi} are shown for (a) predicting survival without CCs, (b) predicting survival with CCs, (c) predicting return of circulation without CCs, (d) predicting return of circulation with CCs, (e) predicting return of rhythm without CCs, (f) predicting return of rhythm with CCs.

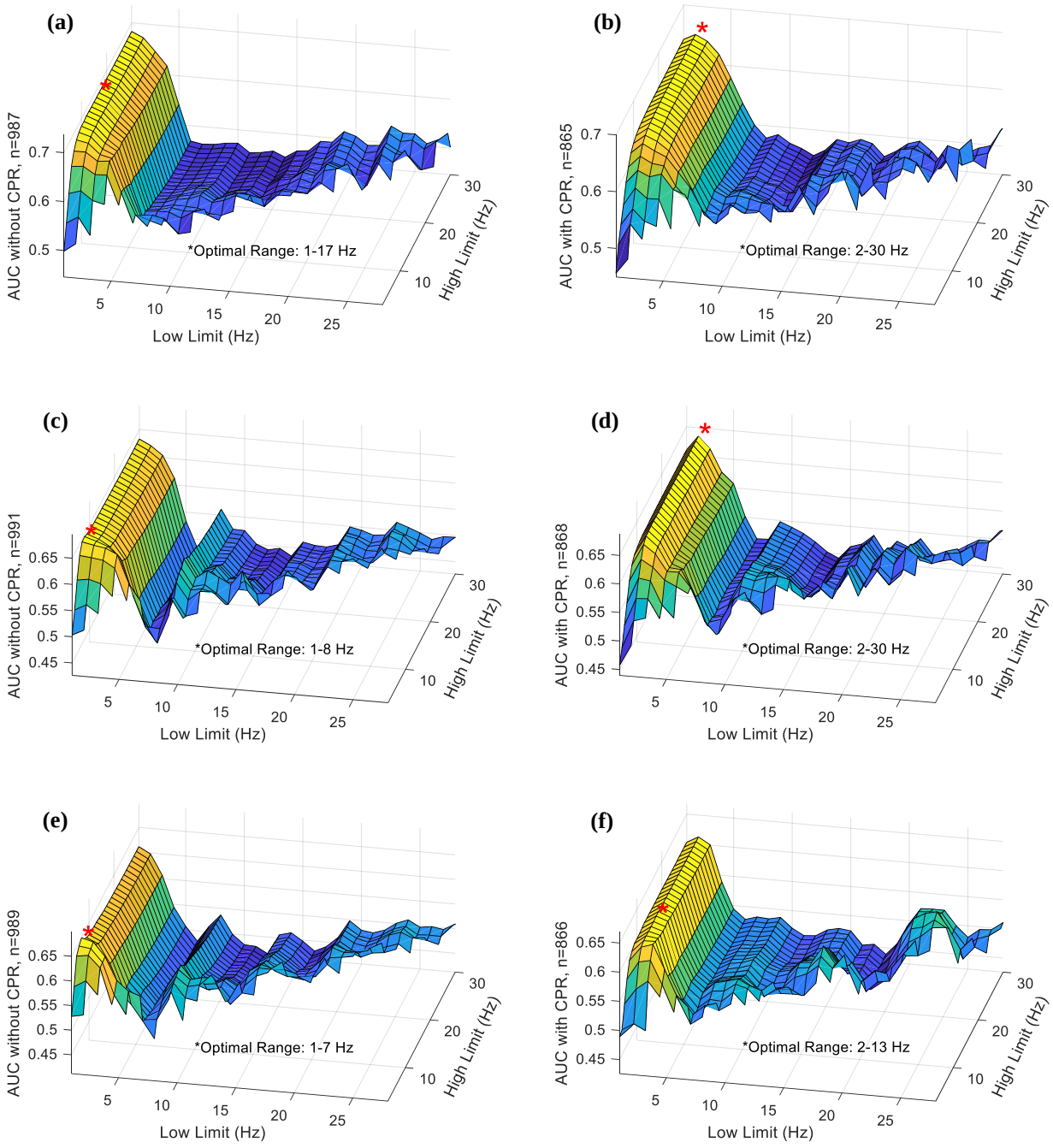

Figure 4.18 Centroid Frequency frequency range selection

Optimal frequency limits f_{lo} and f_{hi} are shown for (a) predicting survival without CCs, (b) predicting survival with CCs, (c) predicting return of circulation without CCs, (d) predicting return of circulation with CCs, (e) predicting return of rhythm without CCs, (f) predicting return of rhythm with CCs.

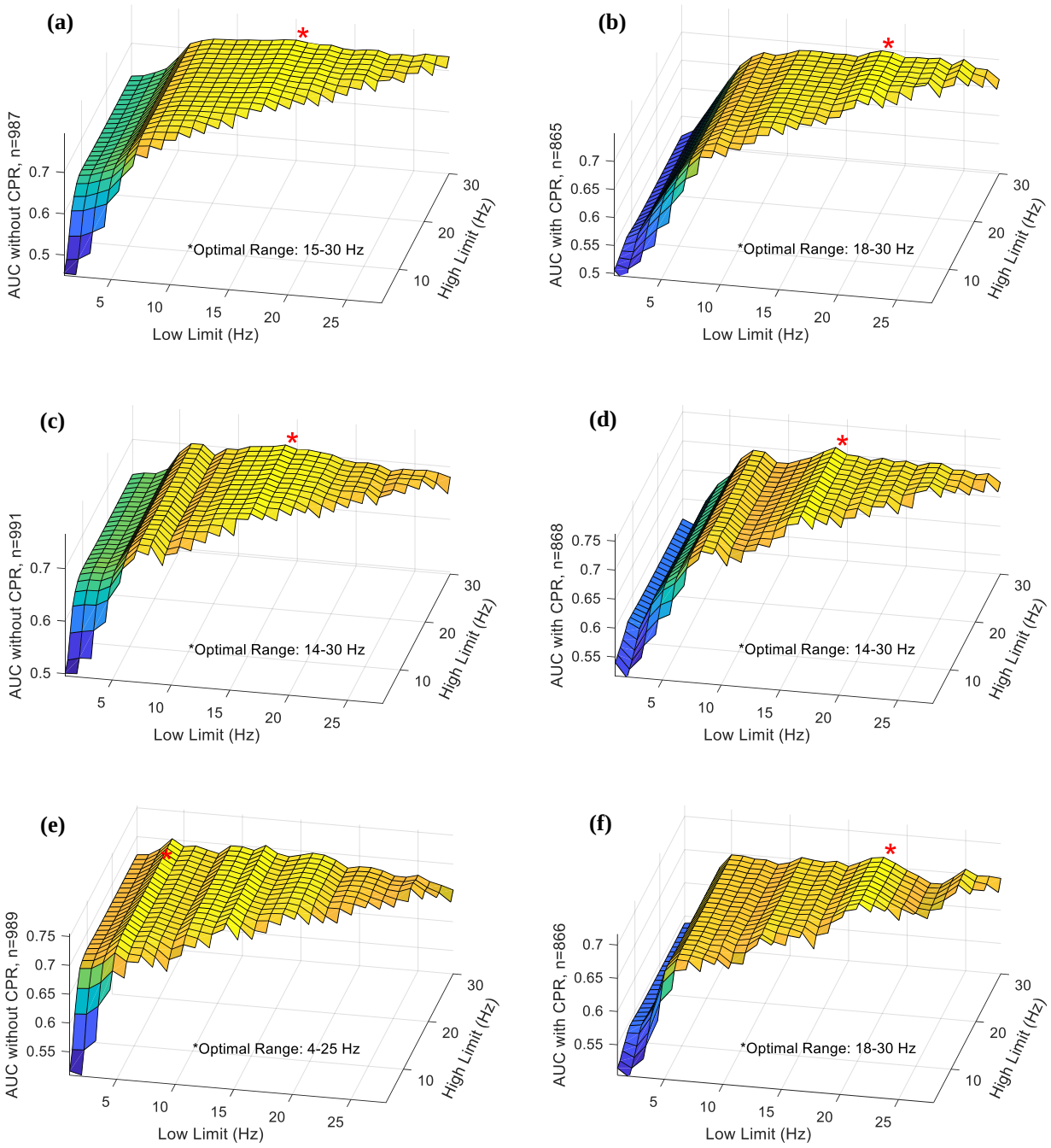

Figure 4.19 Centroid Power frequency range selection

Optimal frequency limits f_{lo} and f_{hi} are shown for (a) predicting survival without CCs, (b) predicting survival with CCs, (c) predicting return of circulation without CCs, (d) predicting return of circulation with CCs, (e) predicting return of rhythm without CCs, (f) predicting return of rhythm with CCs.

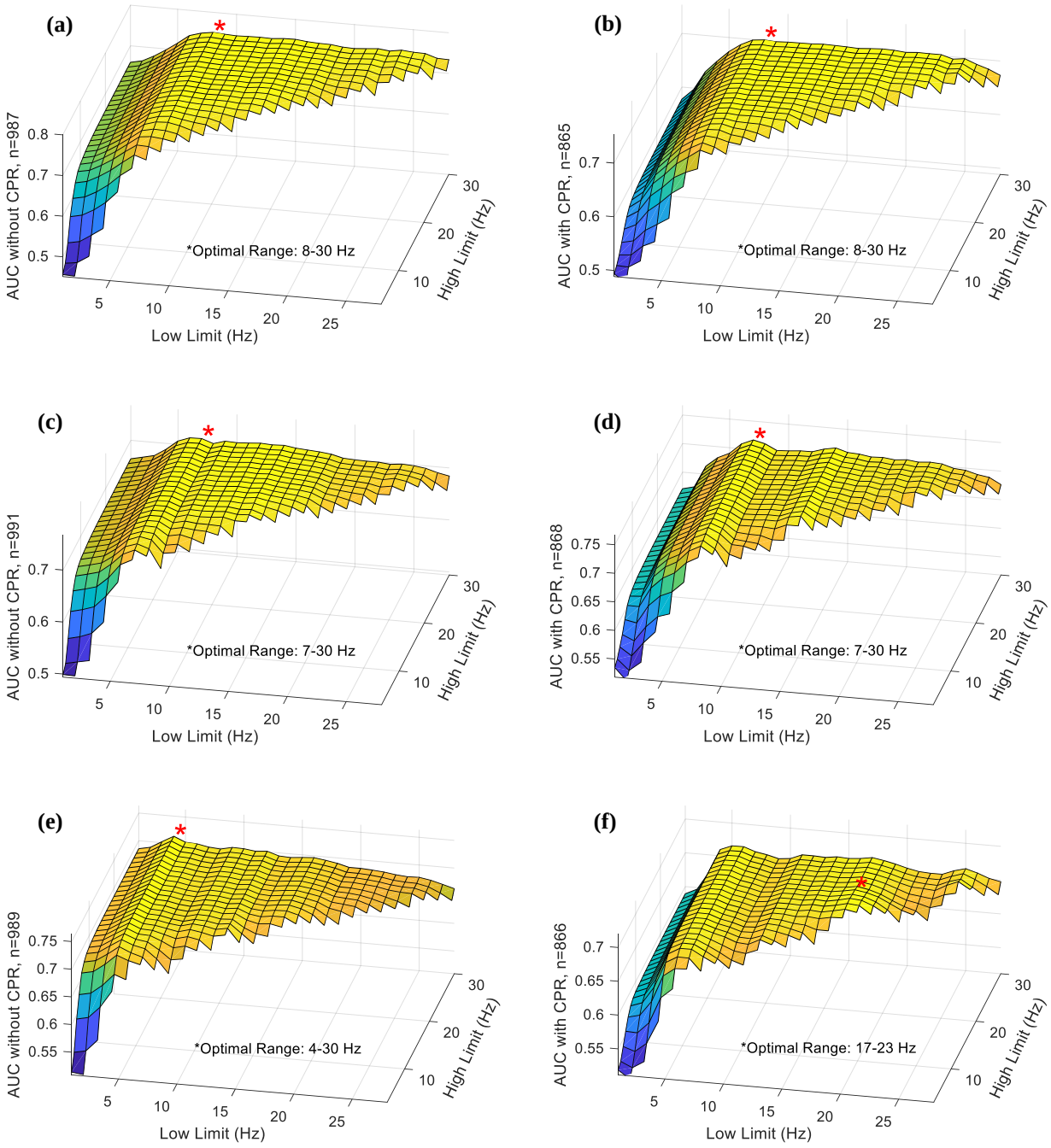

Figure 4.20 Energy frequency range selection

Optimal frequency limits f_{lo} and f_{hi} are shown for (a) predicting survival without CCs, (b) predicting survival with CCs, (c) predicting return of circulation without CCs, (d) predicting return of circulation with CCs, (e) predicting return of rhythm without CCs, (f) predicting return of rhythm with CCs.

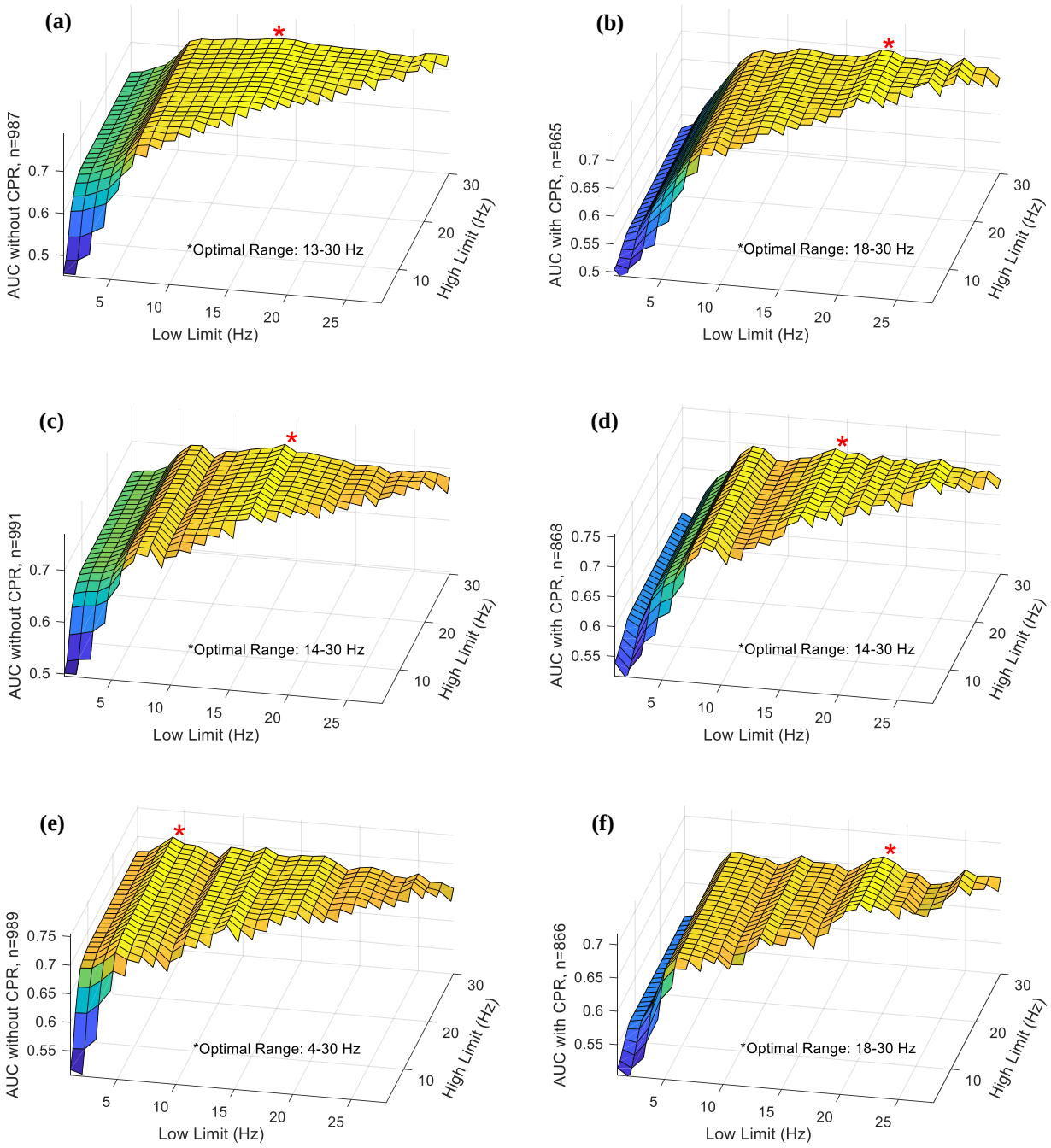

Figure 4.21 Max Power frequency range selection

Optimal frequency limits f_{lo} and f_{hi} are shown for (a) predicting survival without CCs, (b) predicting survival with CCs, (c) predicting return of circulation without CCs, (d) predicting return of circulation with CCs, (e) predicting return of rhythm without CCs, (f) predicting return of rhythm with CCs.

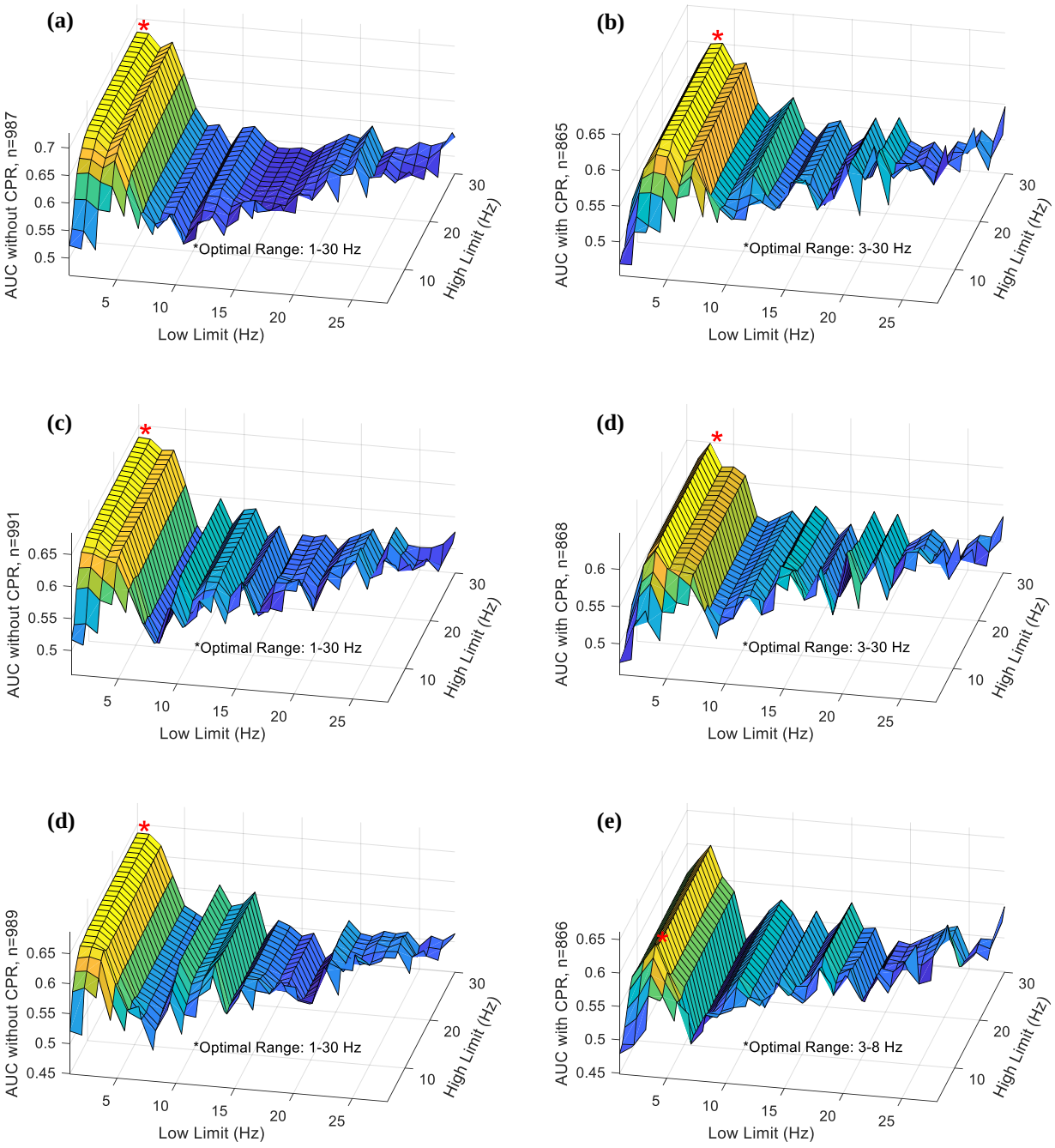

Figure 4.22 Peak Frequency frequency range selection

Optimal frequency limits f_{lo} and f_{hi} are shown for (a) predicting survival without CCs, (b) predicting survival with CCs, (c) predicting return of circulation without CCs, (d) predicting return of circulation with CCs, (e) predicting return of rhythm without CCs, (f) predicting return of rhythm with CCs.

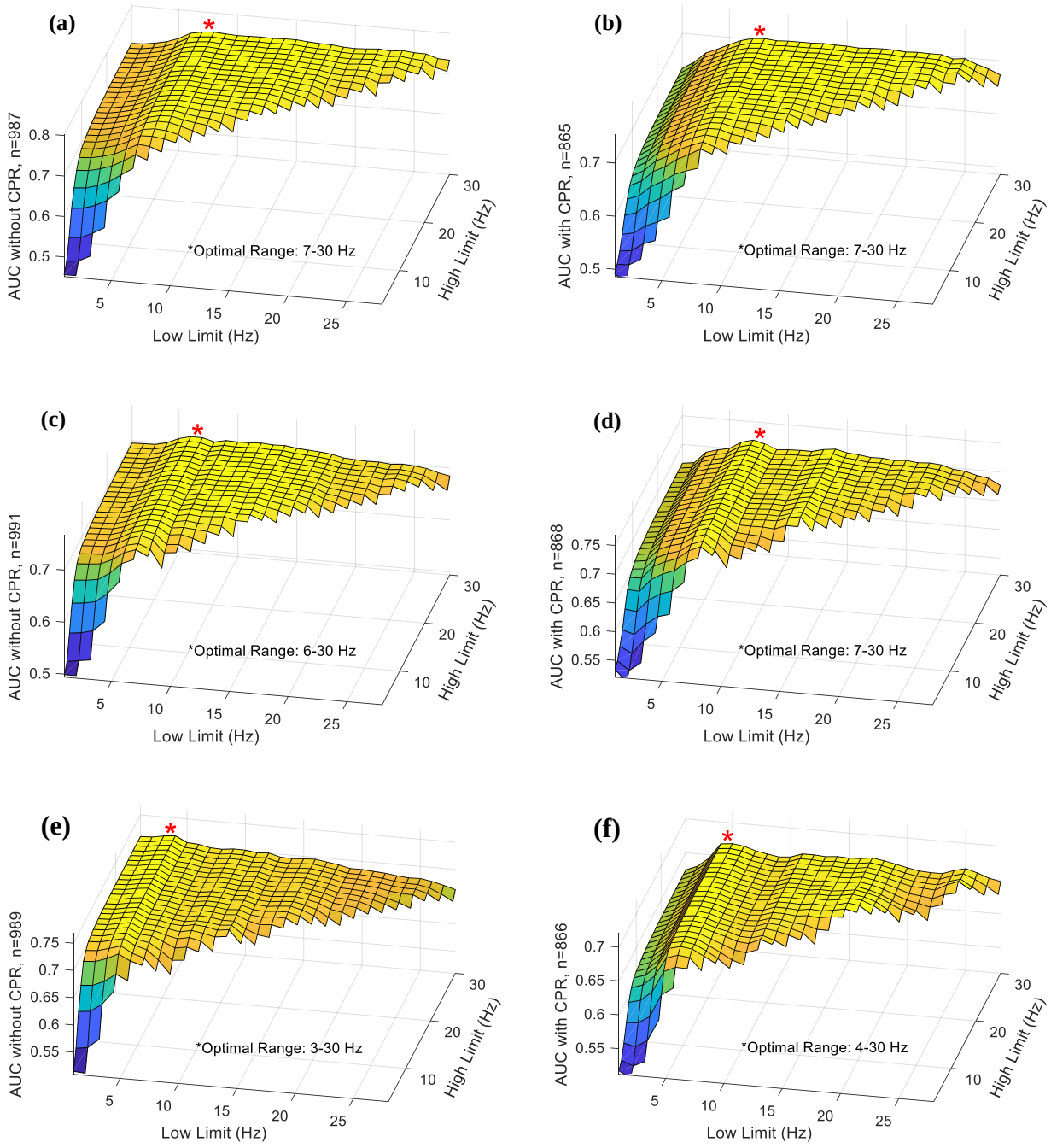

Figure 4.23 Power Spectrum Analysis frequency range selection

Optimal frequency limits f_{lo} and f_{hi} are shown for (a) predicting survival without CCs, (b) predicting survival with CCs, (c) predicting return of circulation without CCs, (d) predicting return of circulation with CCs, (e) predicting return of rhythm without CCs, (f) predicting return of rhythm with CCs.

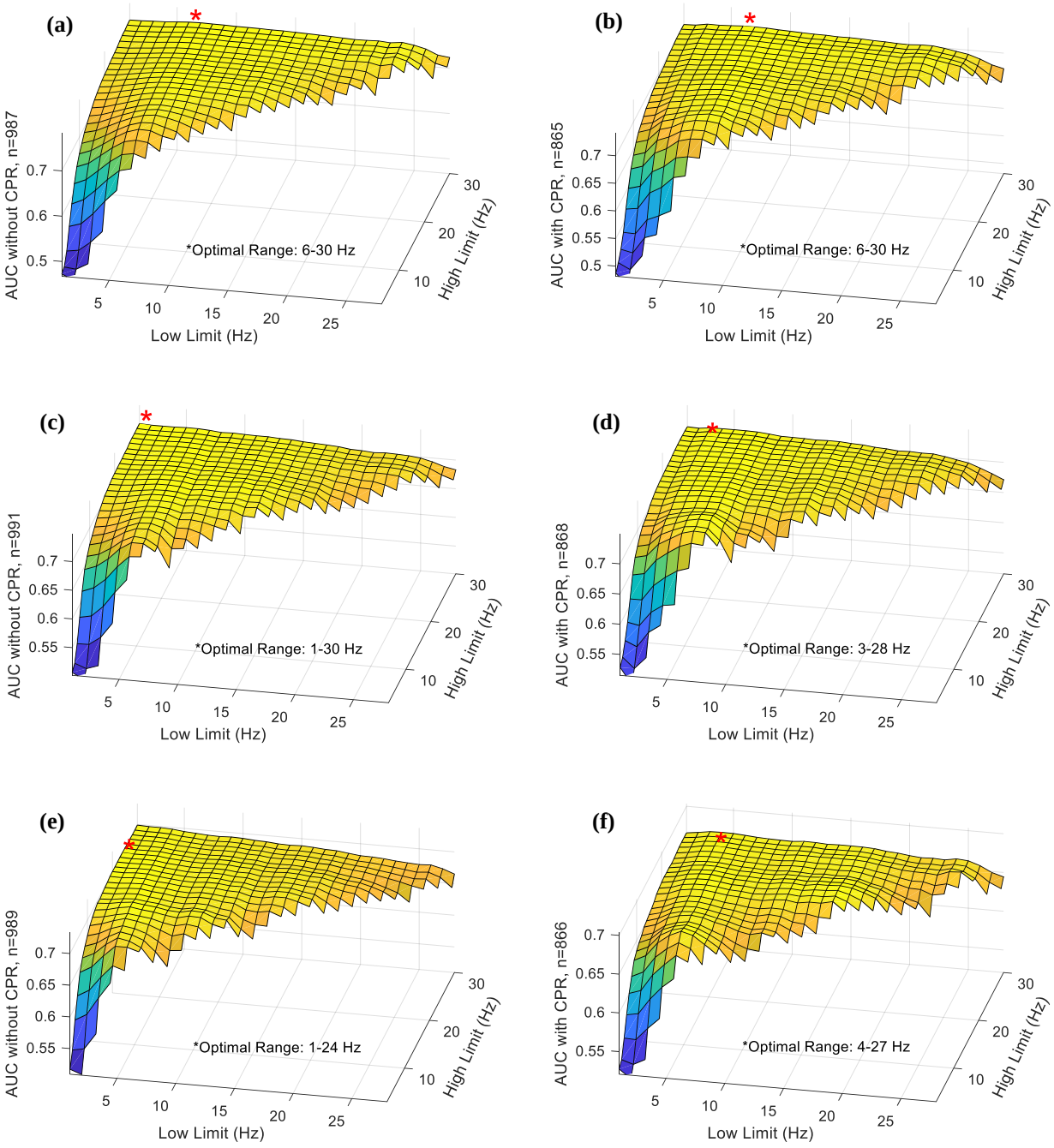

Figure 4.24 Spectral Flatness Measure frequency range selection

Optimal frequency limits f_{lo} and f_{hi} are shown for (a) predicting survival without CCs, (b) predicting survival with CCs, (c) predicting return of circulation without CCs, (d) predicting return of circulation with CCs, (e) predicting return of rhythm without CCs, (f) predicting return of rhythm with CCs.

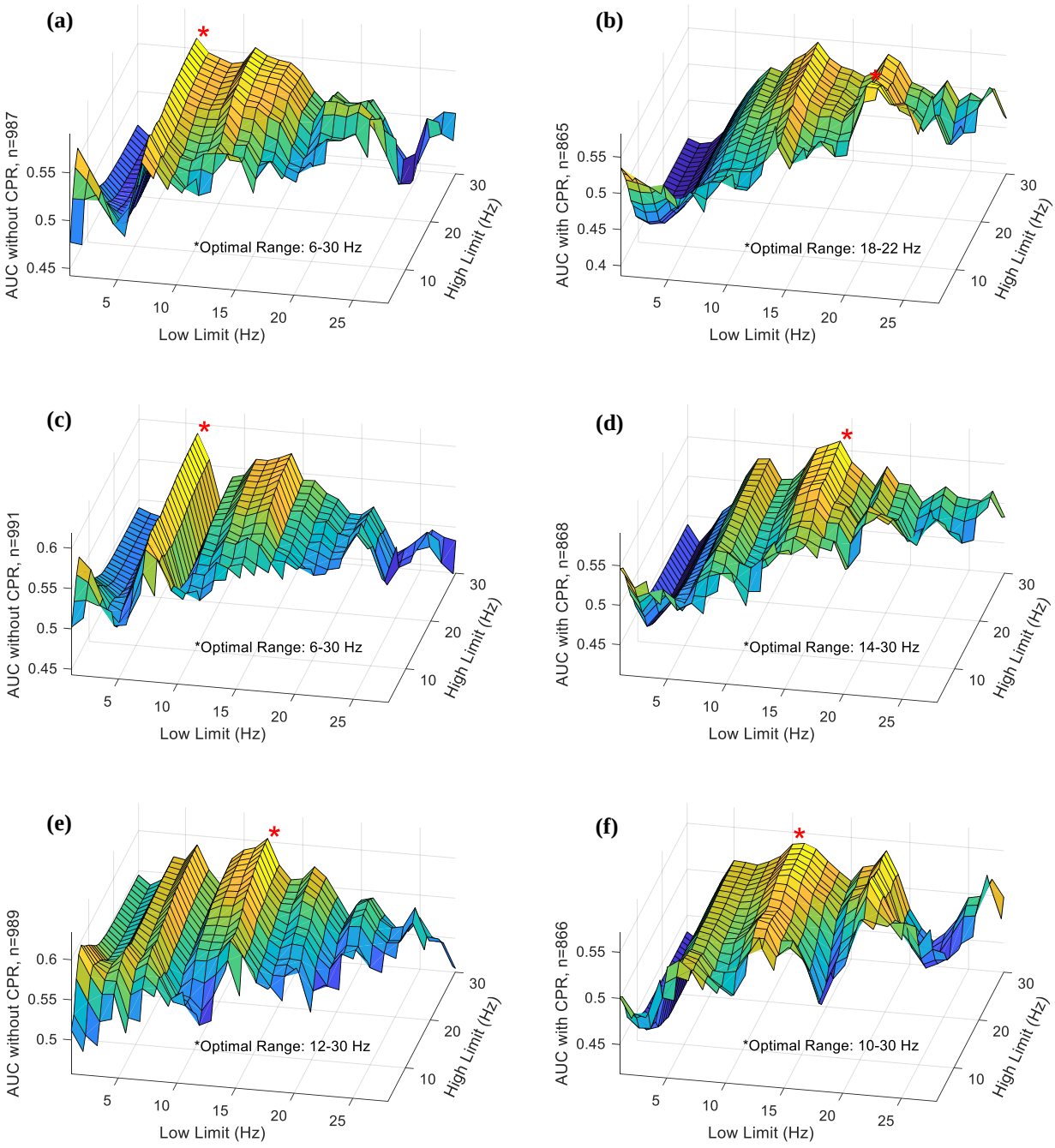

Figure 4.25 Spectral Entropy frequency range selection

Optimal frequency limits f_{lo} and f_{hi} are shown for (a) predicting survival without CCs, (b) predicting survival with CCs, (c) predicting return of circulation without CCs, (d) predicting return of circulation with CCs, (e) predicting return of rhythm without CCs, (f) predicting return of rhythm with CCs.

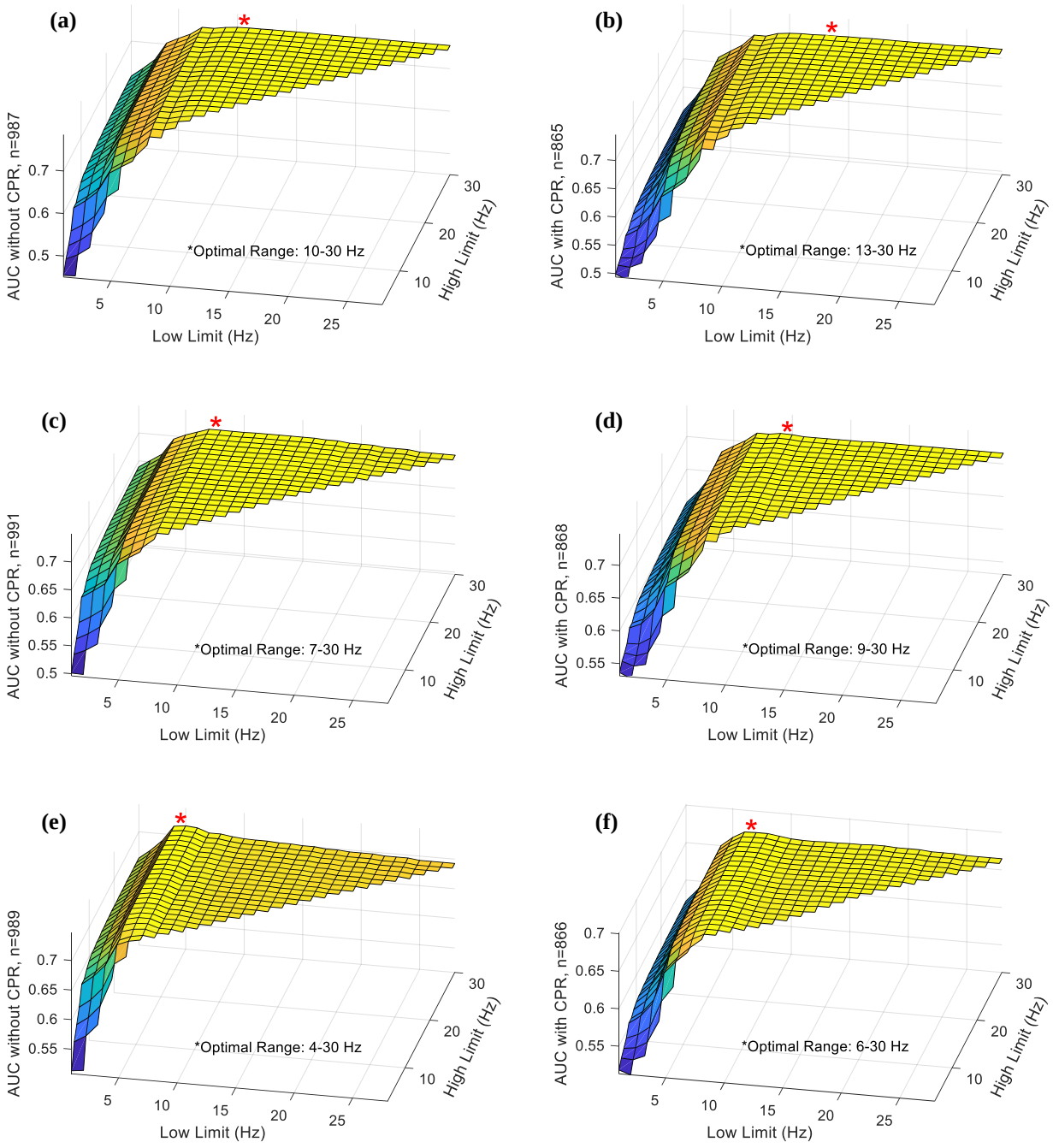

Figure 4.26 Wavelet Energy frequency range selection

Optimal frequency limits f_{lo} and f_{hi} are shown for (a) predicting survival without CCs, (b) predicting survival with CCs, (c) predicting return of circulation without CCs, (d) predicting return of circulation with CCs, (e) predicting return of rhythm without CCs, (f) predicting return of rhythm with CCs.

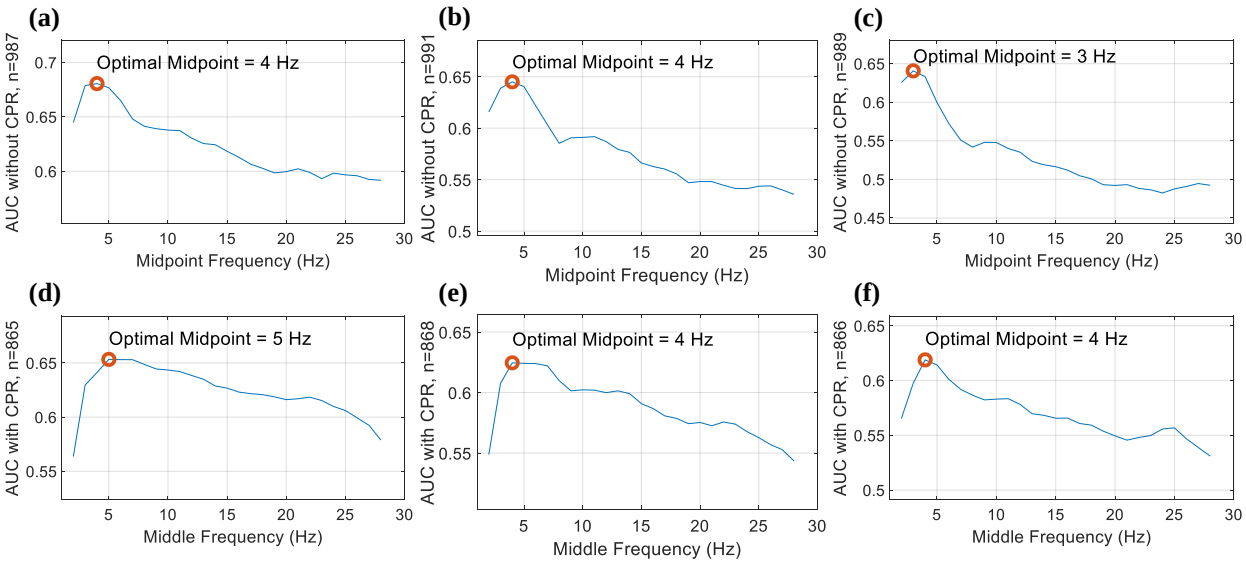

Figure 4.27 Frequency Ratio midpoint frequency selection
Middle frequency f_{mid} optimization for predicting survival (a) without and (d) with CCs, return of circulation (b) without and (e) with CCs, and return of rhythm (c) without and (f) with CCs.

4.9.1.2 Complexity Measures

Parameter selections for measures of waveform complexity are illustrated in Figure 4.28–Figure 4.31.

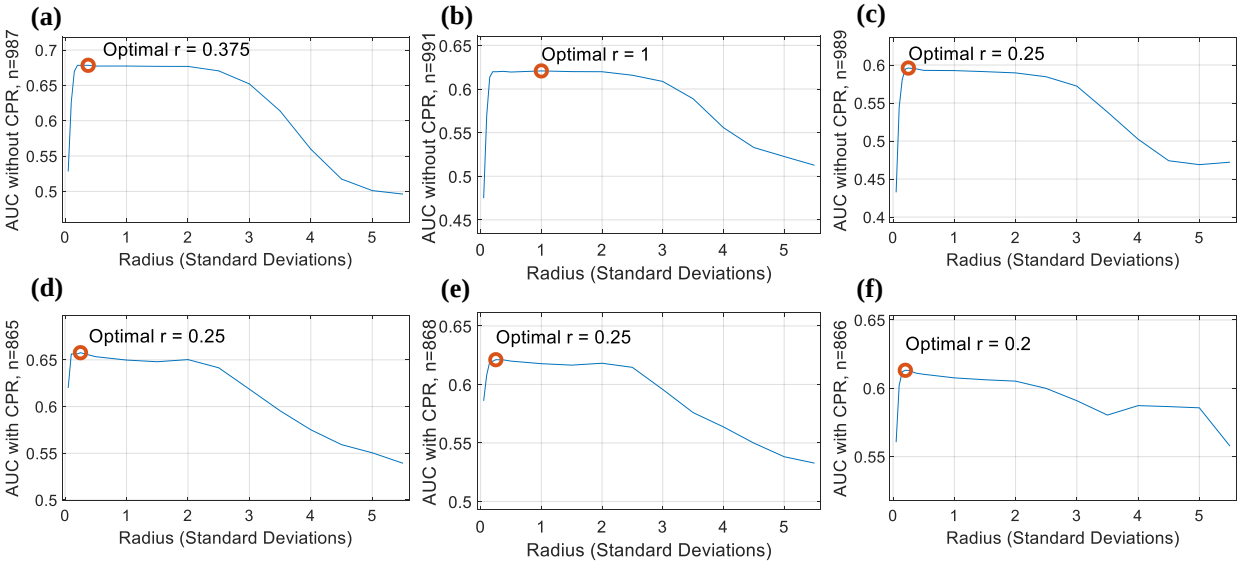

Figure 4.28 Approximate Entropy radius scale selection
Radius *r* optimizations with *L*=1, for predicting survival (a) without and (d) with CCs, return of circulation (b) without and (e) with CCs, and (c) return of rhythm without and (f) with CCs.

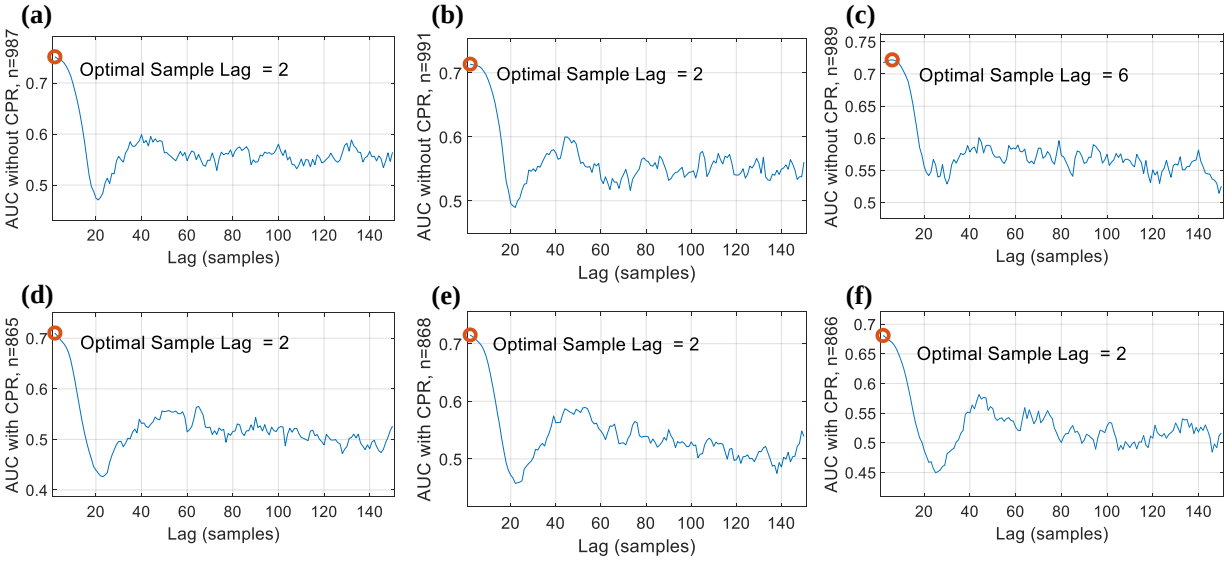

Figure 4.29 Angular Velocity lag selection
Lag optimizations are shown for predicting survival (a) without and (d) with CCs, return of circulation (b) without and (e) with CCs, and return of rhythm (c) without and (f) with CCs.

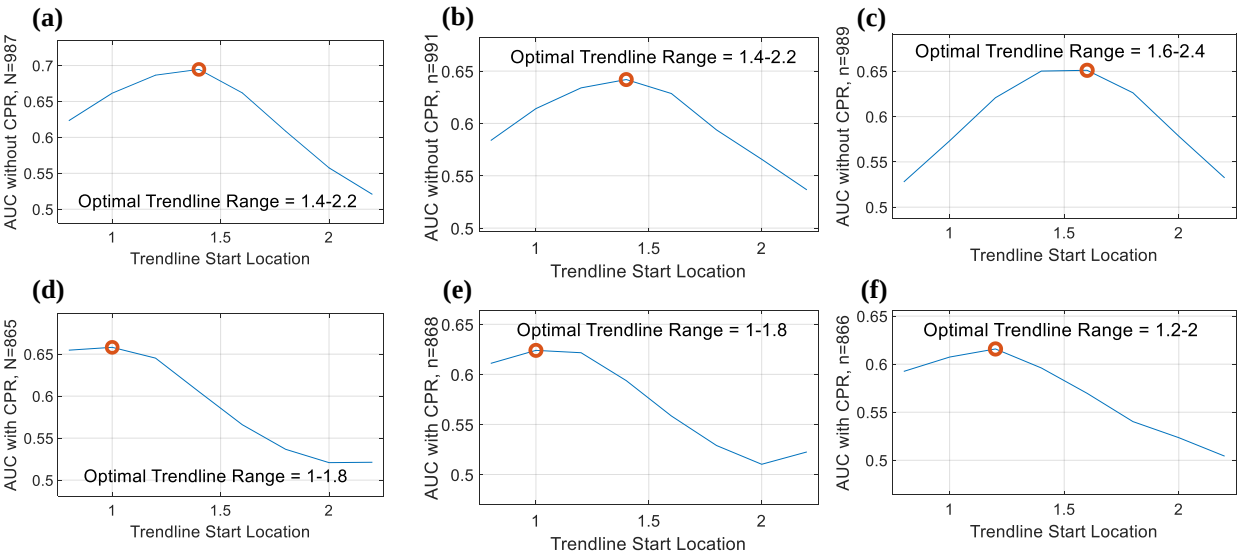

Figure 4.30 Detrended Fluctuation Analysis trendline range selection
Trendline range optimization given trend length = 0.8 are shown for predicting survival (a) without and (d) with CCs, return of circulation (b) without and (e) with CCs, and return of rhythm (c) without and (f) with CCs.

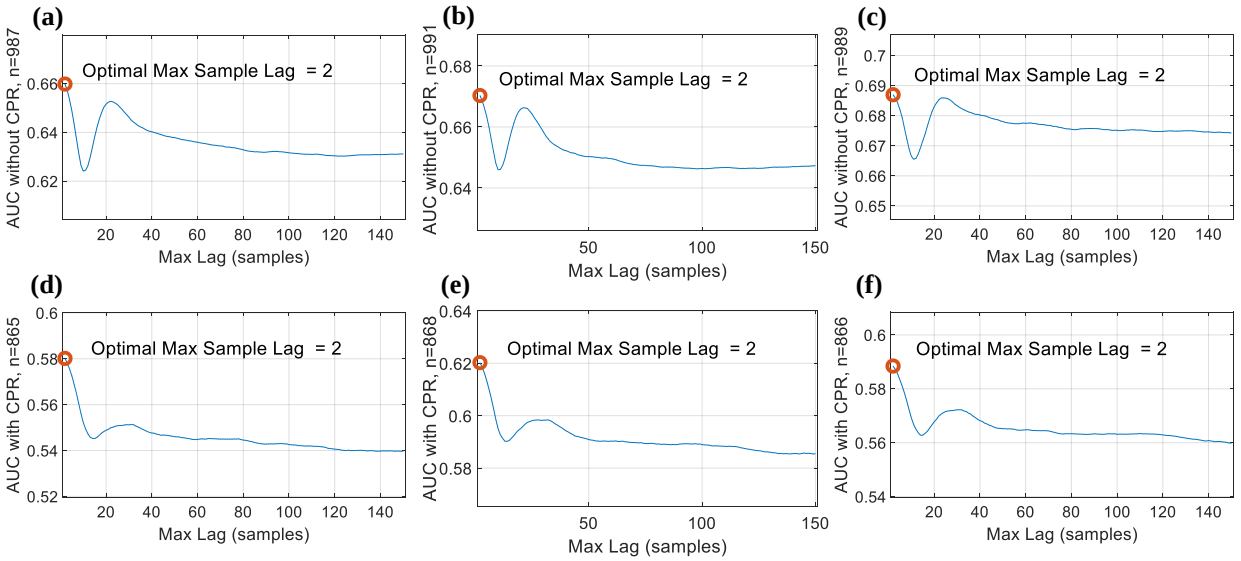

Figure 4.31 Log of Absolute Correlations lag selection
Lag value optimization for predicting survival (a) without and (d) with CCs, return of circulation (b) without and (e) with CCs, and return of rhythm (c) without and (f) with CCs.

4.9.1.3 Combination Model Training: Neural Networks

Neural Networks were first trained for predicting the primary study outcome, survival, using both scaled conjugate gradient and Bayesian regularization training methods to select an optimal gradient descent and training method. For prediction of the primary outcome of survival, Bayesian regularization training produced networks with the highest Pearson correlation between target and output values as well as the highest AUC on training data (Table 4.4). Therefore, we used Bayesian regularization training to implement all final Neural Network models.

Table 4.4 Neural network training method selection
Pilot training results indicate higher performance on training data using Bayesian regularization training versus scaled conjugate gradient training, based on Pearson correlation (R) and areas under receiver operating characteristic curves (AUC) on training data for predicting survival with and without chest compressions (CCs) after optimization of network structures.

	Bayesian regularization	**Scaled conjugate gradient**
Network structure selection method:	100x mean cross-validation error	100x mean cross-validation error
Stopping criteria:	18 consecutive validation failures or convergence	4 consecutive validation failures
Error function:	Mean-squared error plus sum-squared parameters weighted by regularization parameter	Cross-entropy
Training performance for predicting survival without CCs:	R = 0.43 AUC = 0.76	R = 0.42 AUC = 0.75
Training performance for predicting survival with CCs:	R = 0.43 AUC = 0.76	R = 0.38 AUC = 0.73

Selections of final neural network layer and node sizes for each outcome based on mean 100x cross-validation error using Bayesian regularization are shown below (Figure 4.32–Figure 4.34).

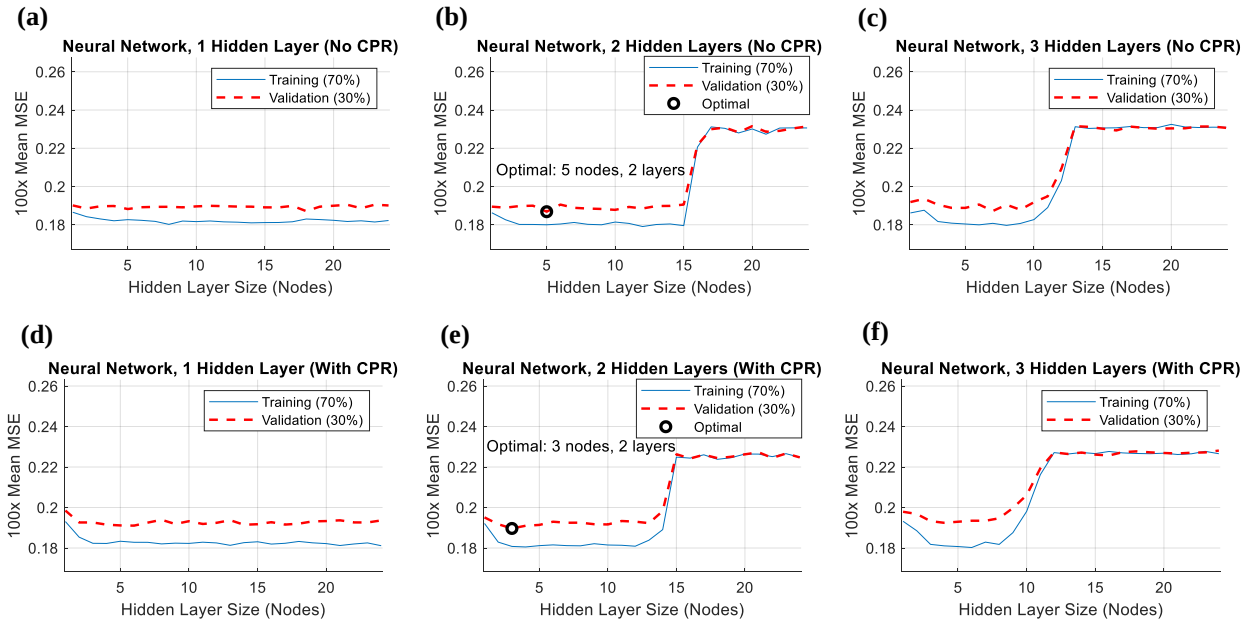

Figure 4.32 Neural Network structure selection for predicting survival
MSE for training$_{tr}$ (training) and training$_{val}$ (validation) cross-validation subsets of overall training data averaged over 100 training iterations versus network size for predicting survival. Results are shown without CCs using (a) one, (b) two, and (c) three hidden layers, and with CCs using (d) one, (e) two, and (f) three hidden layers. Configurations with minimum mean validation error over all 100 training runs are circled. (MSE = mean-squared error.)

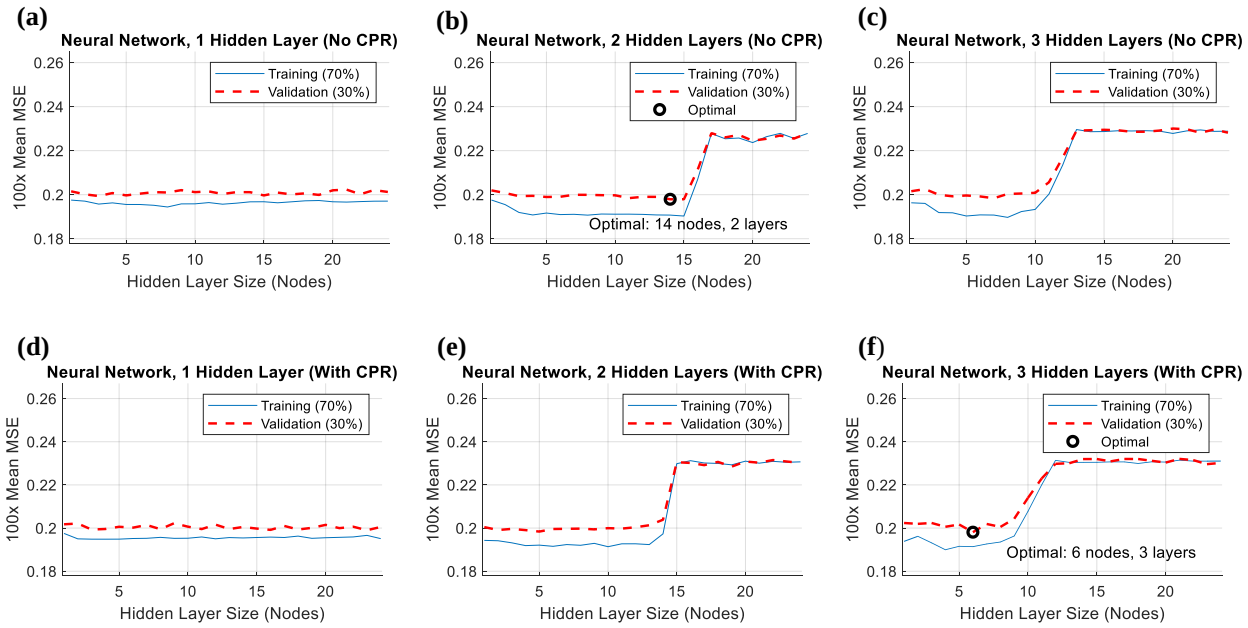

Figure 4.33 Neural Network structure selection for predicting return of circulation
MSE for training$_{tr}$ (training) and training$_{val}$ (validation) cross-validation subsets of overall training data averaged over 100 training iterations versus network size for predicting return of circulation. Results are shown without CCs using (a) one, (b) two, and (c) three hidden layers, and with CCs using (d) one, (e) two, and (f) three hidden layers. Configurations with minimum mean validation error over all 100 training runs are circled. (MSE = mean-squared error.)

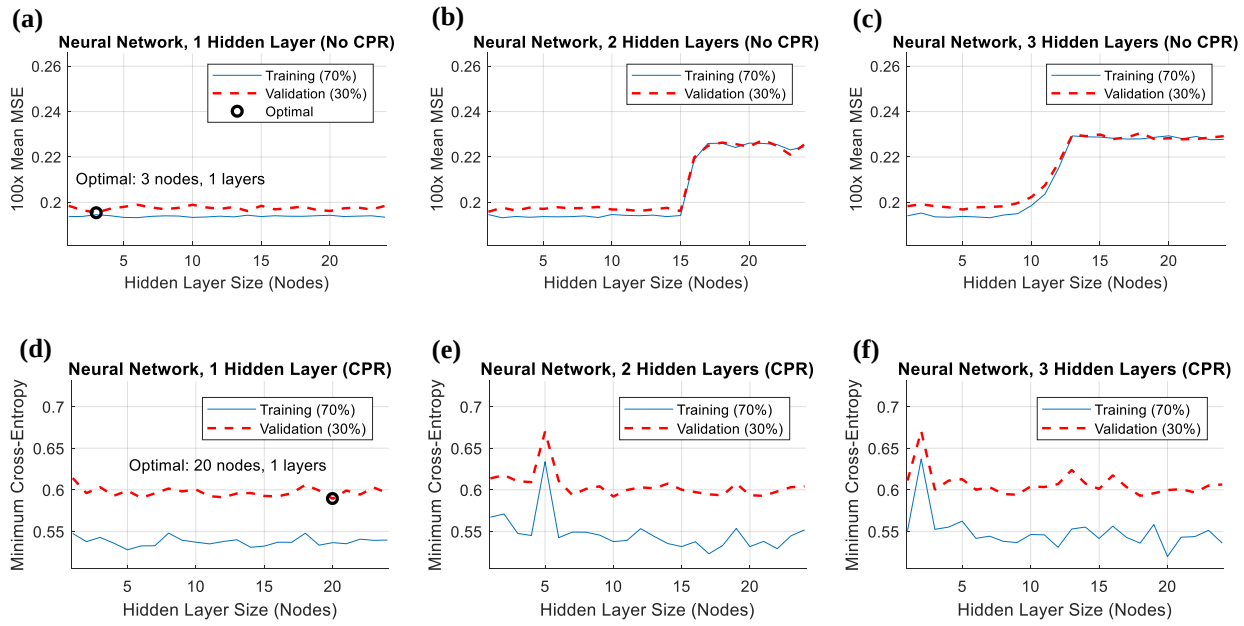

Figure 4.34 Neural Network structure selection for predicting return of rhythm
MSE for training$_{tr}$ (training) and training$_{val}$ (validation) cross-validation subsets of overall training data averaged over 100 training iterations versus network size for predicting return of rhythm. Results are shown without CCs using (a) one, (b) two, and (c) three hidden layers, and with CCs using (d) one, (e) two, and (f) three hidden layers. Configurations with minimum mean validation error over all 100 training runs are circled. (MSE = mean-squared error.)

After selecting optimal network structures, final neural network models were trained for predicting functional survival, return of circulation, and return of rhythm using the optimal network structures with and without CCs. Training and validation error, gradient and sum-squared parameter values (used to compute the regularized mean-squared error cost function), and the number of validation failures (used to stop training) are shown versus training epoch for use without CCs in Figure 4.35 and for use during CCs in Figure 4.36.

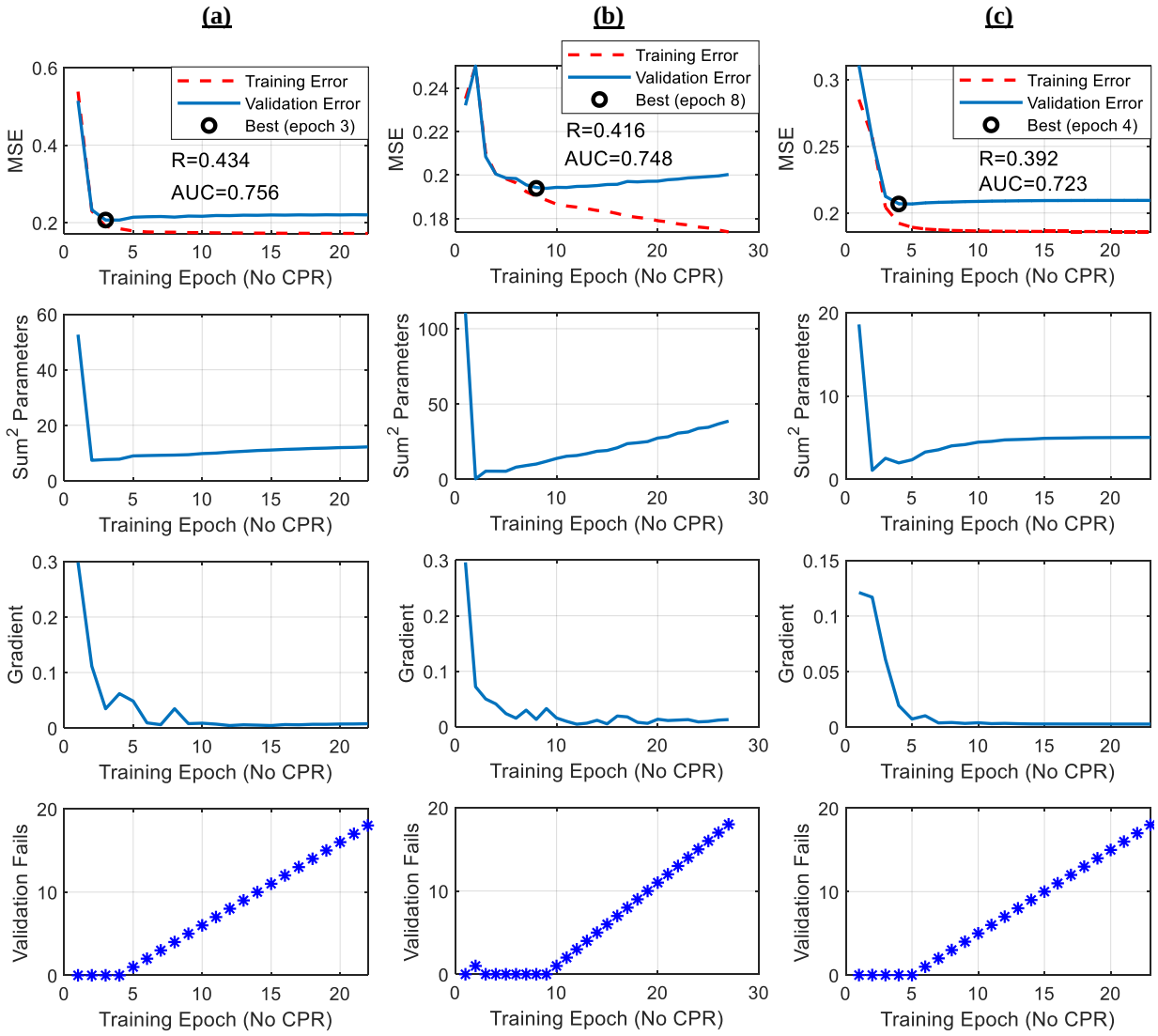

Figure 4.35 Neural Network training results without CCs
Training results for final individual neural network models are shown for (column a) prediction of survival without CCs, (column b) prediction of return of circulation without CCs, and (column c) prediction of return of rhythm without CCs. The top panes in each column illustrate training$_{tr}$ training subset (comprising a random 70% subset of the overall study training data) and training$_{val}$ validation subset (comprising a random 30% subset of the study training data) mean-squared error (MSE) versus training epoch during training of the final models for prediction of each outcome. Selection of the optimal epoch is also shown (circled), and its corresponding Pearson correlation (R) and training AUC displayed.

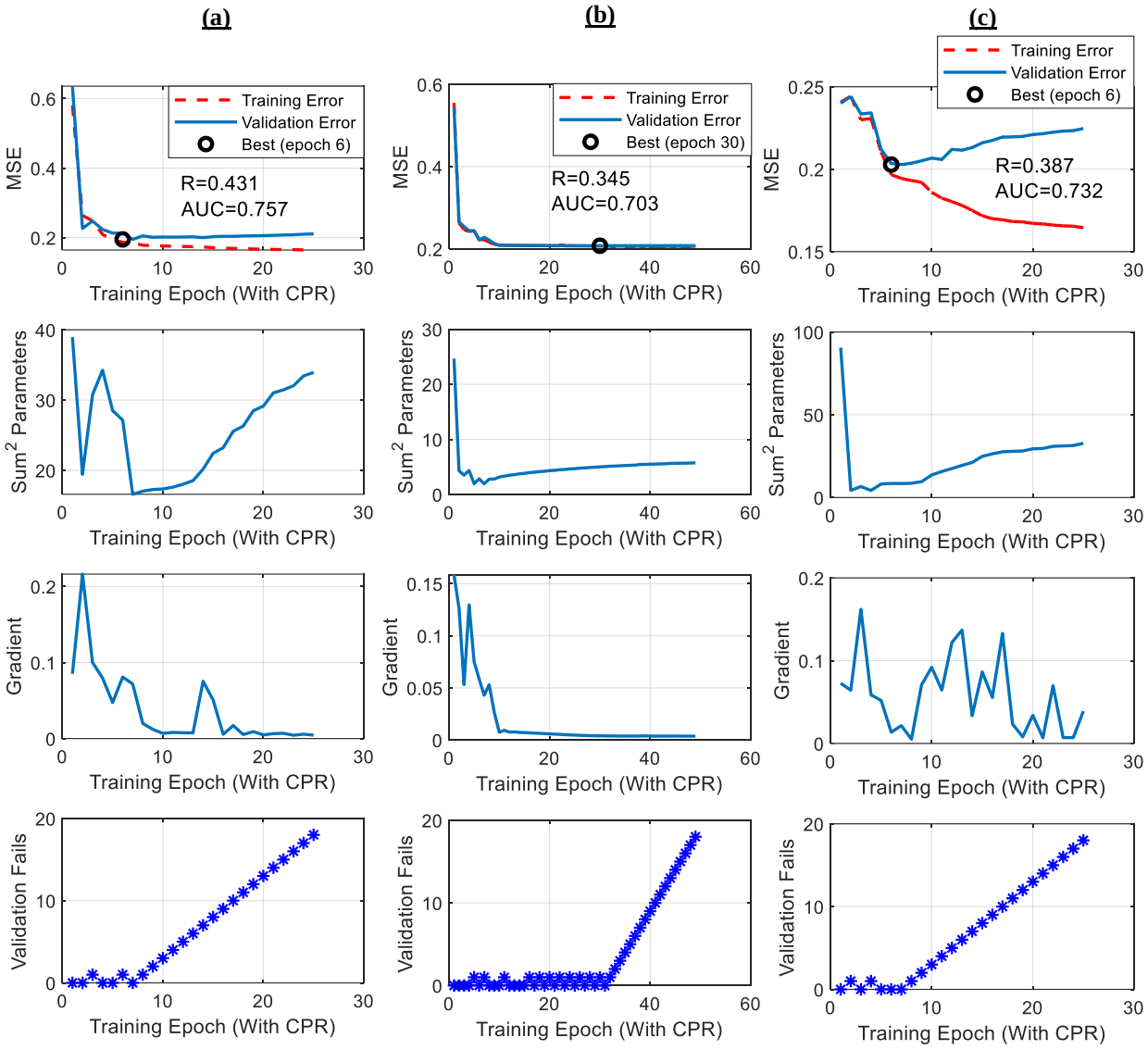

Figure 4.36 Neural Network training results during CCs
Training results for final individual neural network models are shown for (column a) prediction of survival with CCs, (column b) prediction of return of circulation with CCs, and (column c) prediction of return of rhythm with CCs. The top panes in each column illustrate training$_{tr}$ training subset (comprising a random 70% subset of the overall study training data) and training$_{val}$ validation subset (comprising a random 30% subset of the study training data) mean-squared error (MSE) versus training epoch during training of the final models for prediction of each outcome. Selection of the optimal epoch is also shown (circled), and its corresponding Pearson correlation (R) and training AUC displayed.

4.9.1.4 Combination Model Training: Support Vector Machines

Support Vector Machine hyperparameter selections are illustrated below (Figure 4.37).

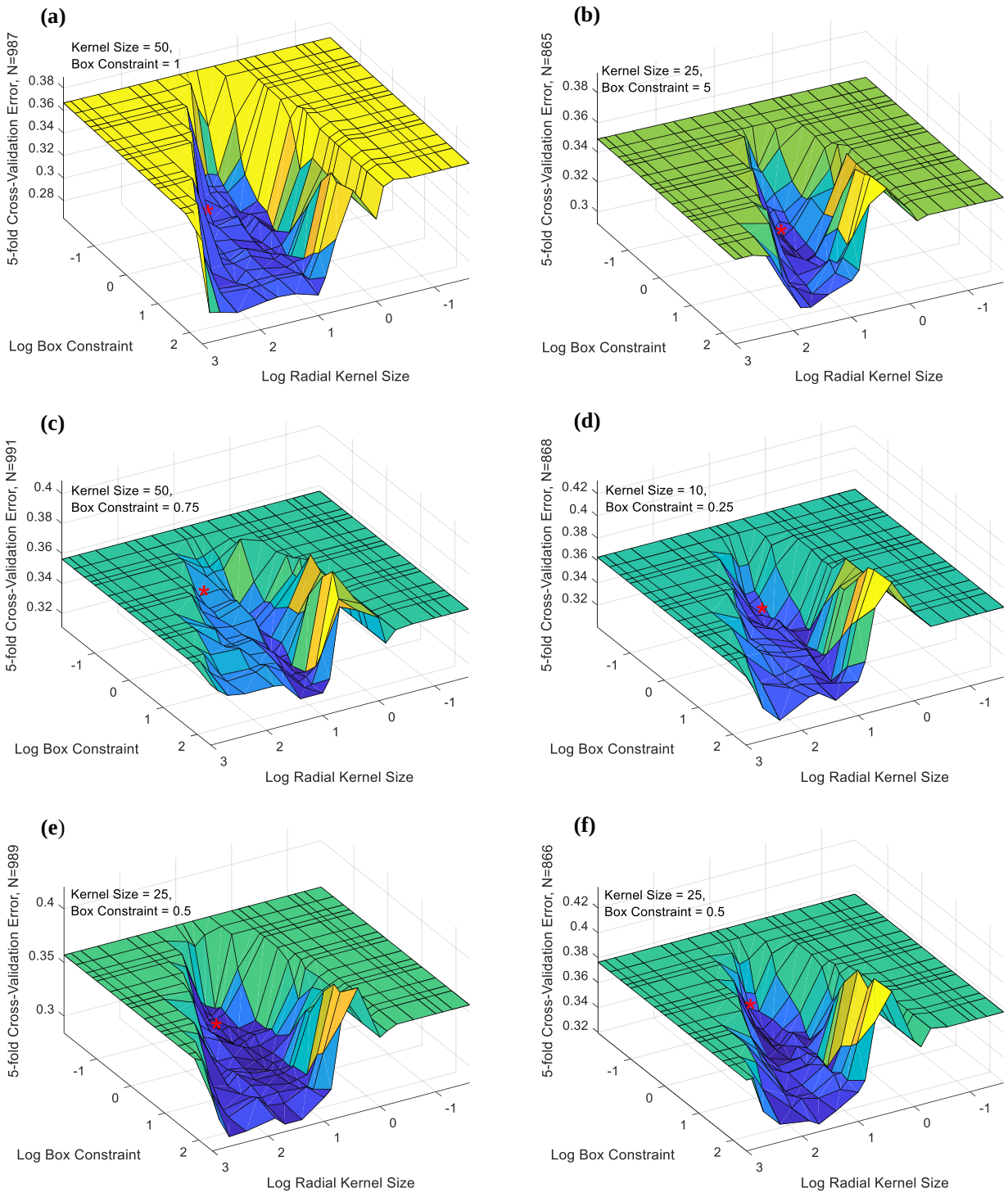

*Indicates final hyperparameter combinations

Figure 4.37 Support Vector Machine hyperparameter selections
Hyperparameter for predicting survival (a) without and (b) with CCs, return of circulation (c) without and (d) with CCs, and return of rhythm (e) without and (f) with CCs.

4.9.2 *Final Parameters*

Final parameter values are shown below in Table 4.5. Parameters optimized to predict functional survival, return of circulation at end of EMS care, and return of rhythm after defibrillation shock, both with CPR CCs and without CCs are shown.

Table 4.5 Waveform measure parameters

Waveform measure parameters derived from training data (460 patients) are shown.

Measure	Survival		Return of Circulation		Return of Rhythm	
	No CPR	**With CPR**	**No CPR**	**With CPR**	**No CPR**	**With CPR**
Amplitude Range[140]	N/A	N/A	N/A	N/A	N/A	N/A
Amplitude Spectrum Area[97]	Range = 6-30 Hz	Range = 6-30 Hz	Range = 5-30 Hz	Range = 6-30 Hz	Range = 1-30 Hz	Range = 4-30 Hz
Angular Velocity[133]	Lag = 2 samples	Lag = 2 samples	Lag = 2 samples	Lag = 2 samples	Lag = 6 samples	Lag = 2 samples
Approximate Entropy[138]	r = 0.375, L = 1	r = 0.25, L = 1	r = 1, L = 1	r = 0.25, L = 1	r = 0.25, L = 1	r = 0.2, L = 1
Centroid Frequency[136]	Range = 1-17 Hz	Range = 2-30 Hz	Range = 1-8 Hz	Range = 2-30 Hz	Range = 1-7 Hz	Range = 2-13 Hz
Centroid Power[139]	Range = 15-30 Hz	Range = 18-30 Hz	Range = 14-30 Hz	Range = 14-30 Hz	Range = 4-25 Hz	Range = 18-30 Hz
Detrended Fluctuation Analysis[104]	Trendline Range = 1.4-2.2	Trendline Range = 1-1.8	Trendline Range = 1.4-2.2	Trendline Range = 1-1.8	Trendline Range = 1.6-2.4	Trendline Range = 1.2-2
Energy[116]	Range = 8-30 Hz	Range = 8-30 Hz	Range = 7-30 Hz	Range = 7-30 Hz	Range = 4-30 Hz	Range = 17-23 Hz
Frequency Ratio[100]	Midpoint = 4 Hz	Midpoint = 5 Hz	Midpoint = 4 Hz	Midpoint = 4 Hz	Midpoint = 3 Hz	Midpoint = 4 Hz
Log of the Absolute Correlations[141]	Max Sample Lag = 2 samples	Max Sample Lag = 2 samples	Max Sample Lag = 2 samples	Max Sample Lag = 2 samples	Max Sample Lag = 2 samples	Max Sample Lag = 2 samples
Logistic Regression[131]	Interaction Terms = 0	Interaction Terms = 0	Interaction Terms = 0	Interaction Terms = 0	Interaction Terms = 0	Interaction Terms = 0
Max Power[68]	Range = 13-30 Hz	Range = 18-30 Hz	Range = 14-30 Hz	Range = 14-30 Hz	Range = 4-30 Hz	Range = 18-30 Hz
Mean Amplitude[140]	N/A	N/A	N/A	N/A	N/A	N/A
Mean Slope[135]	N/A	N/A	N/A	N/A	N/A	N/A
Median Slope[68]	N/A	N/A	N/A	N/A	N/A	N/A
Median Stepping Increment[134]	N/A	N/A	N/A	N/A	N/A	N/A
Neural Network[68]	Layers = 2; Nodes per Layer = 5; Max Validation Fails = 18; Training = Bayesian Regularization	Layers = 2; Nodes per Layer = 3; Max Validation Fails = 18; Training = Bayesian Regularization	Layers = 2; Nodes per Layer = 14 Max Validation Fails = 18; Training = Bayesian Regularization	Layers = 3; Nodes per Layer = 6; Max Validation Fails = 18; Training = Bayesian Regularization	Layers = 1; Nodes per Layer = 3; Max Validation Fails = 18; Training = Bayesian Regularization	Layers = 1; Nodes per Layer = 20; Max Validation Fails = 18; Training = Bayesian Regularization
Peak Amplitude[140]	N/A	N/A	N/A	N/A	N/A	N/A
Peak Frequency[116]	Range = 1-30 Hz	Range = 3-30 Hz	Range = 1-30 Hz	Range = 3-30 Hz	Range = 1-30 Hz	Range = 3-8 Hz
Power Spectrum Analysis[68]	Range = 7-30 Hz	Range = 7-30 Hz	Range = 6-30 Hz	Range = 7-30 Hz	Range = 3-30 Hz	Range = 4-30 Hz
Root Mean Square Amplitude[140]	N/A	N/A	N/A	N/A	N/A	N/A
Signal Integral[139]	N/A	N/A	N/A	N/A	N/A	N/A
Spectral Entropy[142]	Range = 6-30 Hz	Range = 18-22 Hz	Range = 6-30 Hz	Range = 14-30 Hz	Range = 12-30 Hz	Range = 10-30 Hz
Spectral Flatness Measure[116]	Range = 6-30 Hz	Range = 6-30 Hz	Range = 1-30 Hz	Range = 3-28 Hz	Range = 1-24 Hz	Range = 4-27 Hz
Support Vector Machine[101]	Radial Kernel Size = 50; Box Constraint = 1	Radial Kernel Size = 10; Box Constraint = 1	Radial Kernel Size = 50; Box Constraint = 0.75	Radial Kernel Size = 10; Box Constraint = 0.25	Radial Kernel Size = 25; Box Constraint = 0.5	Radial Kernel Size = 25; Box Constraint = 0.5
vRhythm[137]	N/A	N/A	N/A	N/A	N/A	N/A
Wavelet Energy[132]	Range = 10-30 Hz	Range = 13-30 Hz	Range = 7-30 Hz	Range = 9-30 Hz	Range = 4-30 Hz	Range = 6-30 Hz

4.10 Appendix C: Expanded Primary Results

4.10.1 *Receiver Operating Characteristic Curves*

Additional receiver operating characteristic curves are shown in Figure 4.38 and Figure 4.39.

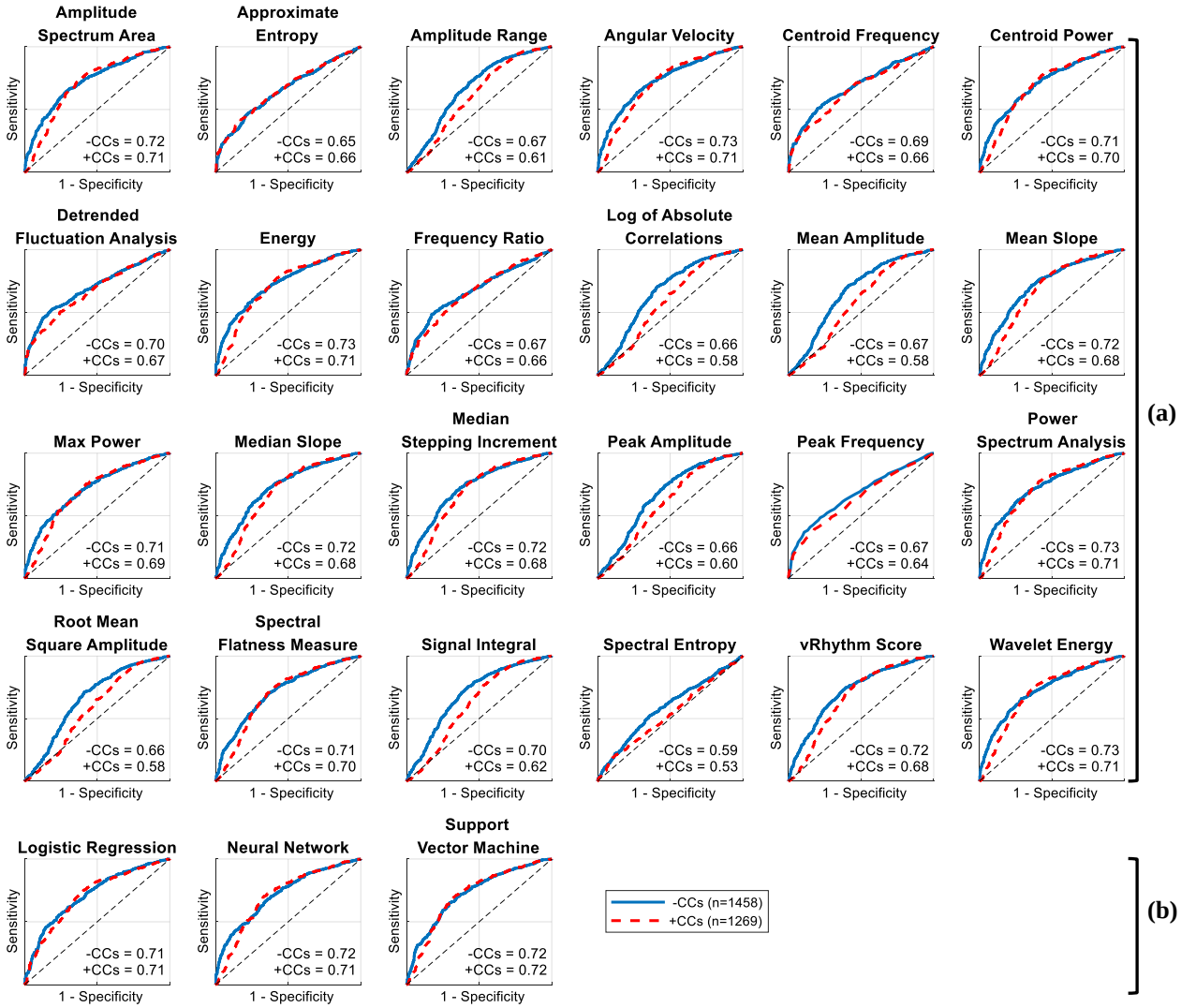

Figure 4.38 Receiver operating characteristic curves for return of circulation
Receiver operating characteristic curves for predicting return of circulation for VF segments from 691 test patients using (a) individual measures and (b) combination measures. (-CCs = without chest compressions, n=1458; +CCs = with chest compressions, n=1269)

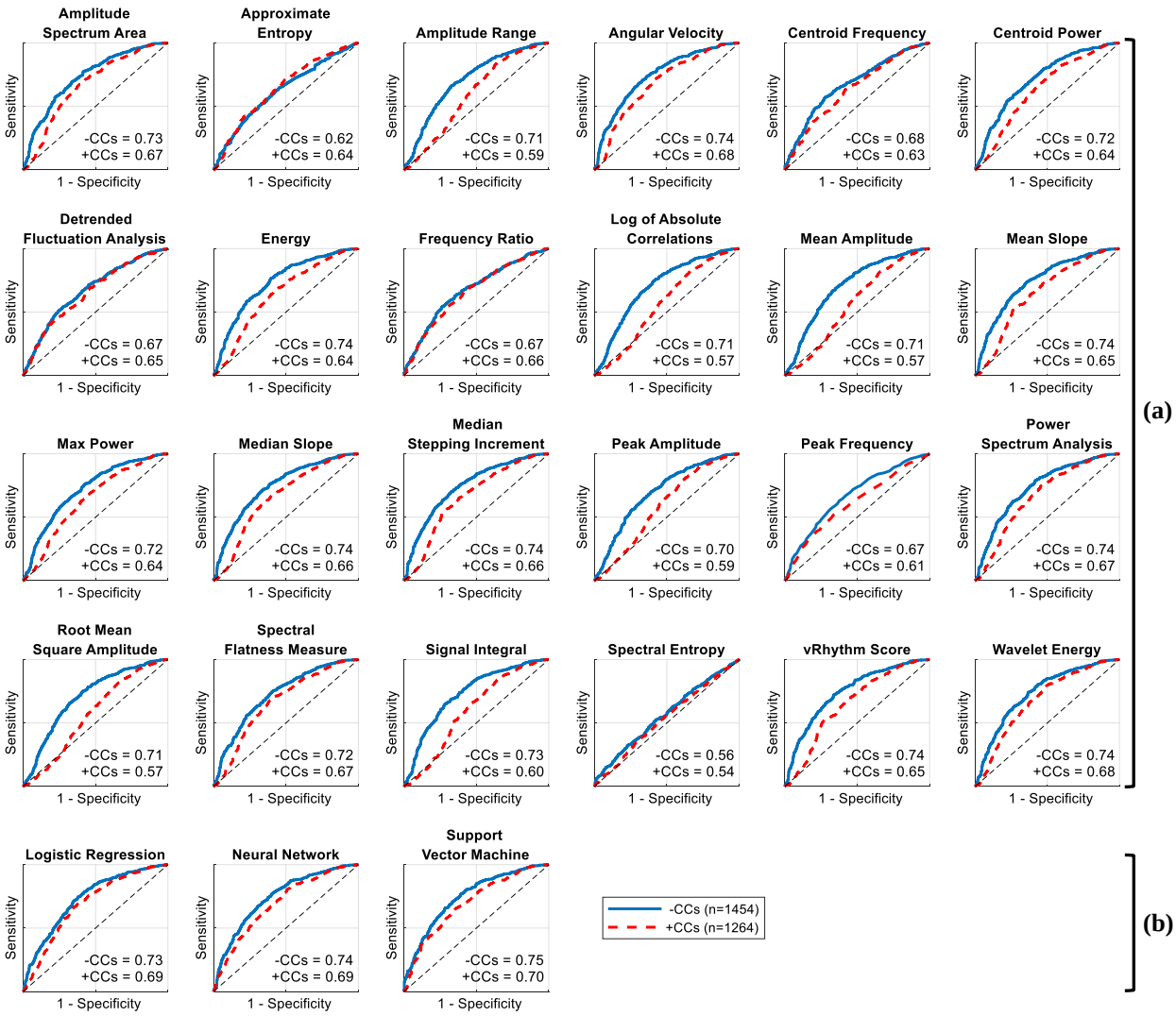

Figure 4.39 Receiver operating characteristic curves for return of rhythm
Receiver operating characteristic curves for predicting return of rhythm after shock for VF segments from 691 test patients using (a) individual measures and (b) combination measures. (-CCs = without chest compressions, n=1454; +CCs = with chest compressions, n=1264.)

4.10.2 *Waveform Measure Quintiles*

Proportions of successful outcome in all waveform measure quintiles for predicting survival, return of circulation, and return of rhythm for test data are shown in Figure 4.40–Figure 4.42.

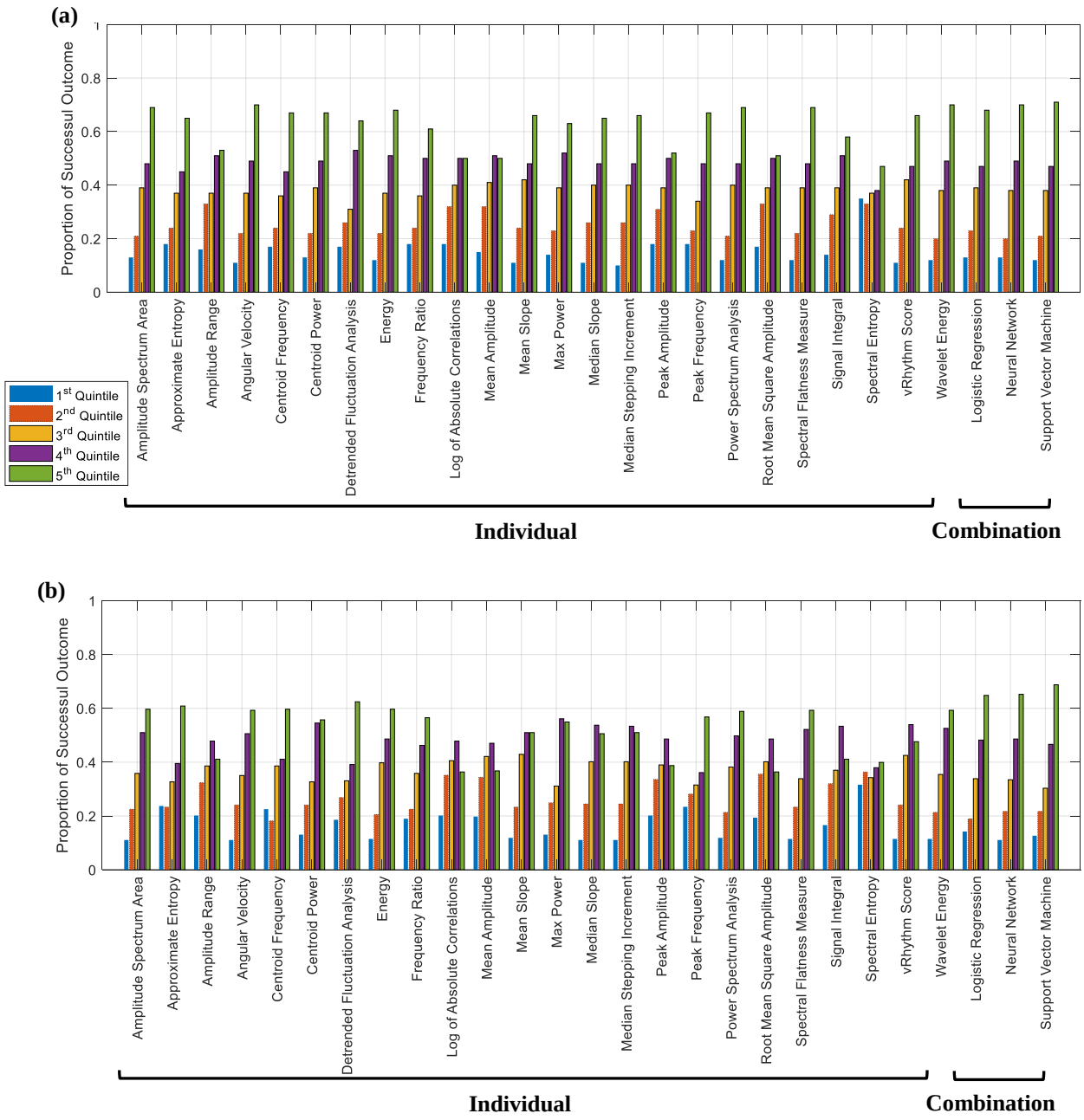

Figure 4.40 Waveform measure quintiles versus functional survival rate
Proportion of functional survival within each waveform measure quintile on VF segments from 691 test patients is shown (a) without CCs (1453 segments) and (b) with CCs (1266 segments). Measures are presented in alphabetical order grouped by individual (left) and combination (right) measures. (-CCs = without chest compressions; +CCs = with chest compressions)

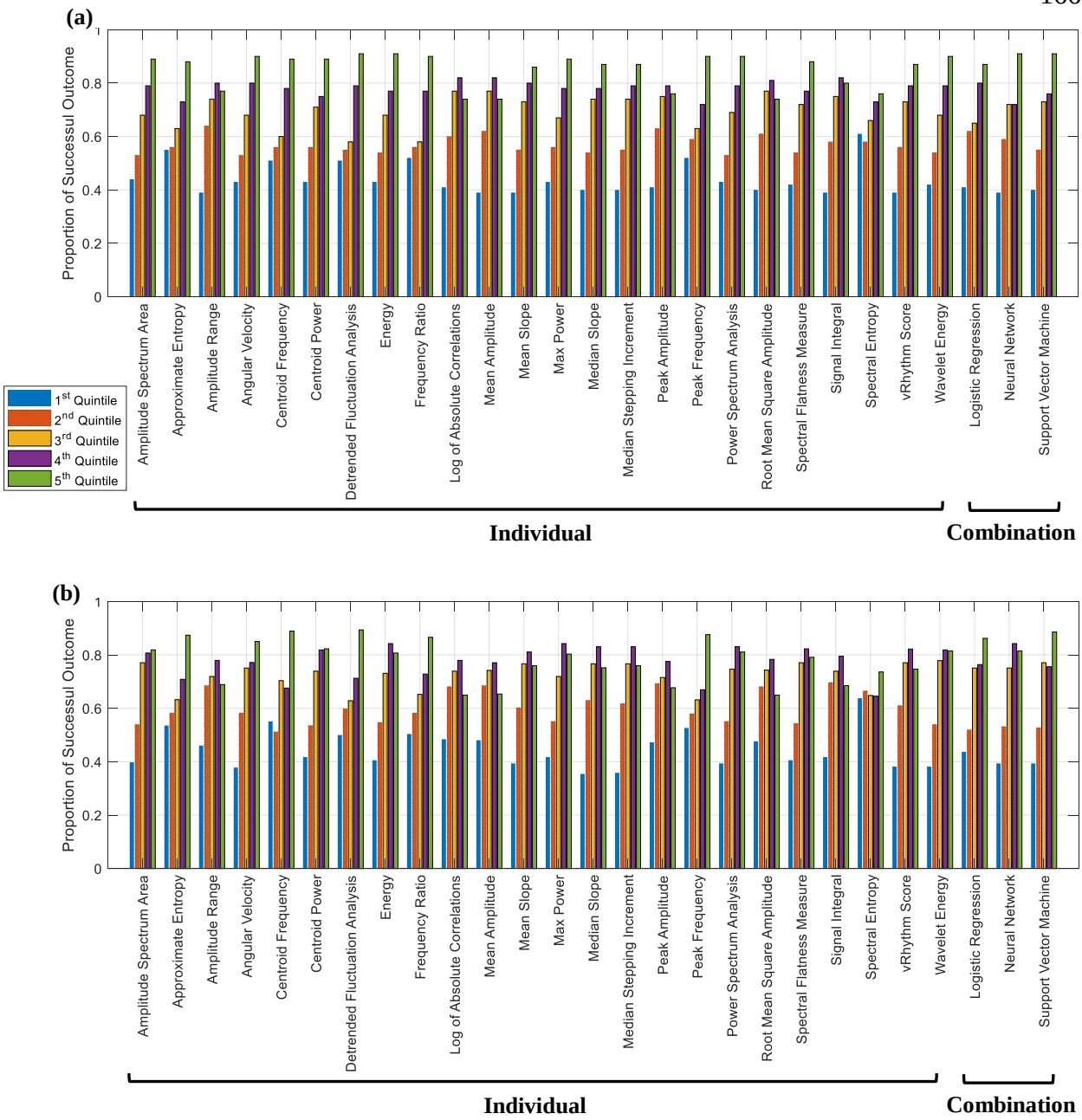

Figure 4.41 Waveform measure quintile versus rate of return of circulation
Proportion of return of circulation within each waveform measure quintile on VF segments from 691 test patients is shown (a) without CCs (1458 segments) and (b) with CCs (1269 segments). Measures are presented in alphabetical order grouped by individual (left) and combination (right) measures. (-CCs = without chest compressions; +CCs = with chest compressions)

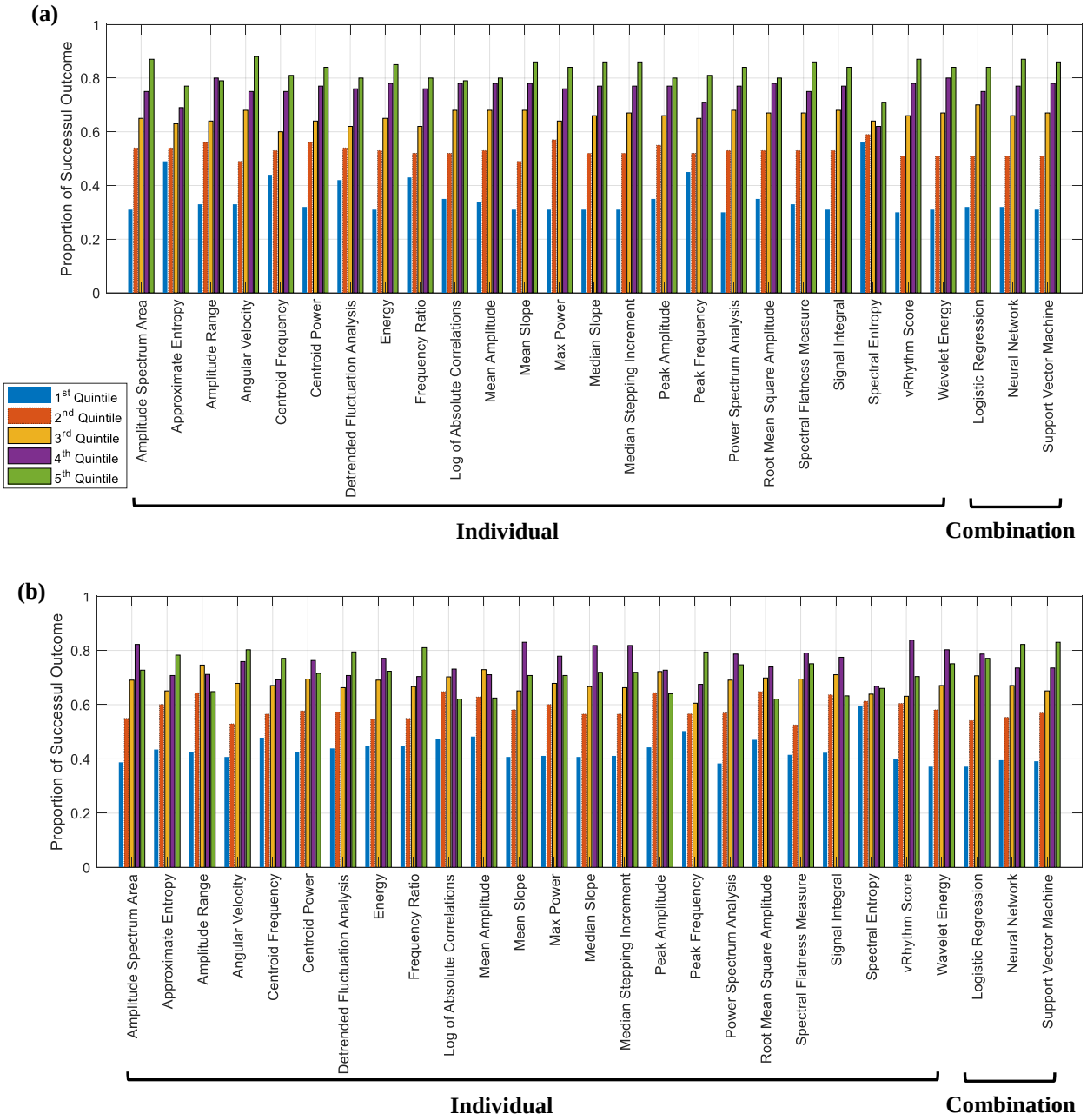

Figure 4.42 Waveform measure quintile versus rate of return of rhythm
Proportion of return of rhythm after shock (i.e. defibrillation success) within each waveform measure quintile on VF segments from 691 test patients is shown (a) without CCs (1454 segments) and (b) with CCs (1264 segments). Measures are presented in alphabetical order grouped by individual (left) and combination (right) measures. (-CCs = without chest compressions; +CCs = with chest compressions)

Quintiles of the measure that generally performed best during CCs, the support vector machine, are shown for predicting primary and intermediate outcomes in Figure 4.43.

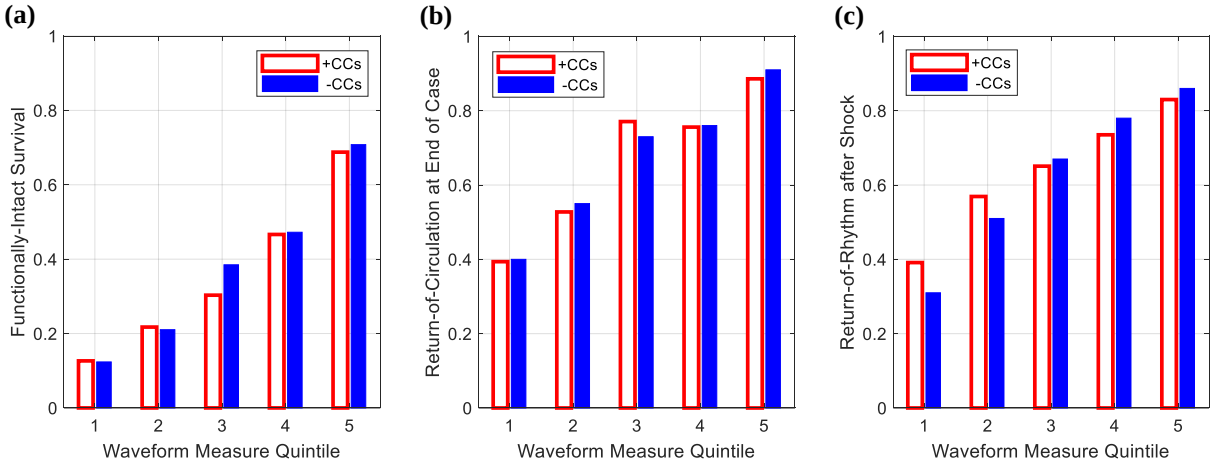

Figure 4.43 Comparison of support vector machine quintiles by outcome
Rates of (a) functional survival, (b) return of circulation at end of case, and (c) return of rhythm after shock versus support vector machine model output quintiles are shown for all VF segments from 691 test patients with chest compressions (+CCs) and without chest compressions (-CCs). Note that due to the fact that VF segments prior to the first four shocks from each patient were collected if available, each patient may be represented by up to four segments with four corresponding waveform measure values (both with or without chest compressions). Therefore, overall patient-wise survival and return of circulation rates may differ from the rate of segment-wise survival and return of circulation rates.

4.11 Appendix D: Intra-cluster Correlation

4.11.1 *Introduction*

In the primary results of the current investigation, we calculated AUC values using standard receiver operating characteristic curve analysis (i.e., the trapezoidal rule) and calculated 95% confidence intervals using stratified bootstrapping.[109,115] Since data was collected from up to the first four shock cycles [when available] from each patient, there may be correlation between multiple shocks sampled from the same patient. In total, our study dataset consisted of 2755 shocks sampled from 1,151 patients. Prediction of return of rhythm, which analyzes a single VF segment (either with or without CCs) to predict outcome of a subsequent shock, may have correlated outcomes (i.e. multiple return of rhythm outcomes) within a single patient. Similarly, prediction

of survival, which independently analyzes a single VF segment prior to each available shock to predict survival, may also have intra-cluster correlation since multiple VF segments share a singular outcome of survival within a given patient.

Therefore, we sought to confirm that our approach was appropriate by recalculating AUC confidence intervals while accounting for potential intra-cluster correlation.

4.11.2 *Methods*

We recalculated AUC values and 95% intervals using the methods of Obuchowski to account for clustering within patients using a resource from the Cleveland Clinic Lerner Research Institute.[146,172] AUC values were evaluated for prediction of return of rhythm after shock and prediction of functional survival. For return of rhythm and survival, our original study results using standard analysis (with 95% confidence intervals calculated using stratified bootstrapping) were then compared to clustered analysis (Obuchowski method) to determine whether clustering effects were significant.[109,115,146,172]

4.11.3 *Results*

Results were similar for predicting functional survival corrected with correction for intra-cluster correlation, as compared to standard analysis (Table 4.6). For predicting return of rhythm after each shock corrected for intra-cluster correlation as compared to standard analysis, results were also similar (Table 4.7).

Table 4.6 Predicting survival with correction for intra-patient clustering
AUC [95% CI] values are presented for prediction of survival using all test data. Results are presented accounting for clustering versus the original bootstrap analysis.

Waveform Measure	Predicting Functional Survival without Chest Compressions		Predicting Functional Survival during Chest Compressions	
	Clustered	*Bootstrap*	*Clustered*	*Bootstrap*
Amplitude Range	0.65 [0.61 0.70]	0.65 [0.63 0.68]	0.60 [0.56 0.65]	0.60 [0.57 0.63]
Amplitude Spectrum Area	0.75 [0.71 0.79]	0.75 [0.73 0.78]	0.72 [0.68 0.76]	0.72 [0.69 0.75]
Angular Velocity	0.75 [0.71 0.79]	0.75 [0.72 0.77]	0.72 [0.68 0.76]	0.72 [0.69 0.75]
Approximate Entropy	0.70 [0.67 0.74]	0.70 [0.68 0.73]	0.67 [0.62 0.71]	0.67 [0.63 0.70]
Centroid Frequency	0.71 [0.68 0.75]	0.71 [0.69 0.74]	0.68 [0.64 0.72]	0.68 [0.65 0.71]
Centroid Power	0.73 [0.70 0.77]	0.73 [0.71 0.76]	0.71 [0.67 0.75]	0.71 [0.68 0.74]
Detrended Fluctuation Analysis	0.72 [0.68 0.75]	0.72 [0.69 0.74]	0.68 [0.64 0.72]	0.68 [0.65 0.71]
Energy	0.75 [0.71 0.79]	0.75 [0.72 0.77]	0.72 [0.68 0.76]	0.72 [0.69 0.75]
Frequency Ratio	0.70 [0.66 0.74]	0.70 [0.67 0.73]	0.68 [0.64 0.72]	0.68 [0.65 0.71]
Log of Absolute Correlations	0.64 [0.60 0.69]	0.64 [0.62 0.67]	0.58 [0.54 0.63]	0.58 [0.55 0.61]
Logistic Regression	0.74 [0.70 0.78]	0.74 [0.71 0.77]	0.73 [0.69 0.77]	0.73 [0.70 0.76]
Max Power	0.73 [0.69 0.77]	0.73 [0.70 0.76]	0.71 [0.67 0.75]	0.71 [0.68 0.74]
Mean Amplitude	0.65 [0.61 0.69]	0.65 [0.62 0.68]	0.58 [0.54 0.63]	0.58 [0.55 0.61]
Mean Slope	0.73 [0.69 0.77]	0.73 [0.70 0.76]	0.69 [0.65 0.73]	0.69 [0.66 0.72]
Median Slope	0.73 [0.69 0.77]	0.73 [0.71 0.76]	0.69 [0.65 0.73]	0.69 [0.67 0.72]
Median Stepping Increment	0.73 [0.69 0.77]	0.73 [0.71 0.76]	0.70 [0.66 0.74]	0.70 [0.67 0.72]
Neural Network	0.75 [0.72 0.79]	0.75 [0.73 0.78]	0.74 [0.70 0.78]	0.74 [0.71 0.77]
Peak Amplitude	0.65 [0.61 0.69]	0.65 [0.62 0.68]	0.59 [0.55 0.64]	0.59 [0.56 0.63]
Peak Frequency	0.71 [0.67 0.74]	0.71 [0.68 0.74]	0.64 [0.60 0.68]	0.64 [0.61 0.67]
Power Spectrum Analysis	0.75 [0.72 0.79]	0.75 [0.73 0.78]	0.72 [0.68 0.76]	0.72 [0.69 0.75]
Root Mean Square Amplitude	0.65 [0.60 0.69]	0.65 [0.62 0.68]	0.58 [0.54 0.63]	0.58 [0.55 0.62]
Signal Integral	0.69 [0.65 0.73]	0.69 [0.67 0.72]	0.63 [0.58 0.67]	0.63 [0.60 0.66]
Spectral Entropy	0.56 [0.52 0.59]	0.56 [0.53 0.59]	0.53 [0.50 0.56]	0.53 [0.50 0.56]
Spectral Flatness Measure	0.75 [0.71 0.79]	0.75 [0.72 0.77]	0.72 [0.68 0.76]	0.72 [0.69 0.75]
Support Vector Machine	0.75 [0.72 0.79]	0.75 [0.73 0.78]	0.75 [0.71 0.79]	0.75 [0.72 0.78]
vRhythm Score	0.73 [0.69 0.77]	0.73 [0.70 0.75]	0.68 [0.64 0.73]	0.68 [0.66 0.71]
Wavelet Energy	0.75 [0.72 0.79]	0.75 [0.73 0.78]	0.73 [0.69 0.77]	0.73 [0.70 0.76]

Table 4.7 Predicting return of rhythm with correction for intra-patient clustering
AUC values [95% confidence intervals] are presented for prediction of return of rhythm after shock using all test data. Results are presented accounting for clustering versus the original bootstrap analysis.

Waveform Measure	Predicting Return of Rhythm without Chest Compressions		Predicting Return of Rhythm during Chest Compressions	
	Clustered	*Bootstrap*	*Clustered*	*Bootstrap*
Amplitude Range	0.71 [0.67 0.74]	0.71 [0.68 0.73]	0.59 [0.55 0.63]	0.59 [0.56 0.63]
Amplitude Spectrum Area	0.73 [0.70 0.76]	0.73 [0.71 0.76]	0.67 [0.64 0.71]	0.67 [0.64 0.70]
Angular Velocity	0.74 [0.72 0.77]	0.74 [0.72 0.77]	0.68 [0.65 0.72]	0.68 [0.65 0.71]
Approximate Entropy	0.62 [0.59 0.66]	0.62 [0.59 0.65]	0.64 [0.61 0.68]	0.64 [0.61 0.67]
Centroid Frequency	0.68 [0.64 0.71]	0.68 [0.65 0.70]	0.63 [0.60 0.67]	0.63 [0.60 0.67]
Centroid Power	0.72 [0.69 0.75]	0.72 [0.69 0.74]	0.64 [0.60 0.67]	0.64 [0.61 0.67]
Detrended Fluctuation Analysis	0.67 [0.64 0.70]	0.67 [0.65 0.70]	0.65 [0.62 0.69]	0.65 [0.62 0.69]
Energy	0.74 [0.71 0.77]	0.74 [0.71 0.76]	0.64 [0.61 0.68]	0.64 [0.61 0.67]
Frequency Ratio	0.67 [0.64 0.70]	0.67 [0.64 0.70]	0.66 [0.62 0.69]	0.66 [0.63 0.69]
Log of Absolute Correlations	0.71 [0.67 0.74]	0.71 [0.68 0.73]	0.57 [0.53 0.61]	0.57 [0.53 0.60]
Logistic Regression	0.73 [0.70 0.76]	0.73 [0.70 0.76]	0.69 [0.65 0.72]	0.69 [0.66 0.72]
Max Power	0.72 [0.69 0.75]	0.72 [0.69 0.75]	0.64 [0.60 0.67]	0.64 [0.61 0.67]
Mean Amplitude	0.71 [0.68 0.74]	0.71 [0.68 0.74]	0.57 [0.53 0.61]	0.57 [0.53 0.60]
Mean Slope	0.74 [0.71 0.77]	0.74 [0.72 0.77]	0.65 [0.62 0.69]	0.65 [0.62 0.69]
Median Slope	0.74 [0.71 0.77]	0.74 [0.72 0.77]	0.66 [0.62 0.70]	0.66 [0.63 0.69]
Median Stepping Increment	0.74 [0.71 0.77]	0.74 [0.72 0.77]	0.66 [0.62 0.70]	0.66 [0.63 0.69]
Neural Network	0.74 [0.71 0.77]	0.74 [0.72 0.77]	0.69 [0.66 0.73]	0.69 [0.66 0.72]
Peak Amplitude	0.70 [0.67 0.73]	0.70 [0.67 0.73]	0.59 [0.55 0.63]	0.59 [0.55 0.62]
Peak Frequency	0.67 [0.64 0.70]	0.67 [0.64 0.70]	0.61 [0.57 0.64]	0.61 [0.58 0.64]
Power Spectrum Analysis	0.74 [0.71 0.77]	0.74 [0.71 0.76]	0.67 [0.64 0.71]	0.67 [0.64 0.70]
Root Mean Square Amplitude	0.71 [0.67 0.74]	0.71 [0.68 0.74]	0.57 [0.53 0.61]	0.57 [0.53 0.60]
Signal Integral	0.73 [0.70 0.76]	0.73 [0.70 0.76]	0.60 [0.56 0.64]	0.60 [0.56 0.63]
Spectral Entropy	0.56 [0.53 0.60]	0.56 [0.53 0.59]	0.54 [0.50 0.57]	0.54 [0.50 0.57]
Spectral Flatness Measure	0.72 [0.69 0.75]	0.72 [0.70 0.75]	0.67 [0.63 0.70]	0.67 [0.63 0.70]
Support Vector Machine	0.75 [0.72 0.78]	0.75 [0.72 0.77]	0.70 [0.67 0.73]	0.70 [0.67 0.73]
vRhythm Score	0.74 [0.71 0.77]	0.74 [0.72 0.77]	0.65 [0.61 0.69]	0.65 [0.62 0.68]
Wavelet Energy	0.74 [0.71 0.77]	0.74 [0.71 0.76]	0.68 [0.64 0.71]	0.68 [0.65 0.71]

4.11.4 *Discussion*

Results for prediction of both outcomes were similar using clustered analysis versus standard analysis. The 95% confidence intervals were marginally expanded after correcting for intra-cluster correlation, but typically remained within +/- 0.01 AUC of the original confidence intervals calculated using bootstrapping. The clustering analysis underweights the sample size used to calculate the AUC variance and resulting confidence interval; hence, the confidence intervals are expanded when the samples per cluster (in this case, VF segments per patient) is increased. Since

each patient in this investigation had a maximum of only four samples (one segment from each of the first four shocks without CCs and one segment from each of the first four shocks with CCs), the clustering effect was not great, the resulting AUC variance was only slightly increased, and the confidence intervals were only slightly affected. Additionally, the clustering analysis likely overestimated clustering effects in some cases, as repeated samples from a single patient across separate shock cycles usually represent separate episodes of VF and may be somewhat independent. Indeed, prior studies of waveform measures typically have not corrected for intra-cluster correlation when reporting results.[65] Furthermore, the actual AUC point estimates are not affected when using this clustering analysis; rather, the confidence intervals alone are increased. Therefore, we conclude that in this investigation, standard analysis of the receiver operating characteristic curve is sufficient, and apart from slightly wider confidence intervals, results are not significantly changed when using established methods to correct for clustering effects.

4.12 Appendix E: Subgroup Analyses

We performed three analyses on subgroups of the study data to determine whether the study results by subgroup were similar to the primary study results overall. These analyses were 1) a subgroup analysis limited to adjacent pairs of VF segments with and without CCs, 2) a subgroup analysis limited to a single VF segment with and without CCs per patient, and 3) a subgroup analysis of data grouped by sampling rate.

4.12.1 *Subgroup Analysis 1: Adjacent VF Pairs*

4.12.1.1 Methods

We performed a subgroup analysis of test VF segments limited to shocks with both an adjacent CC and CC-free segment prior to the same shock to allow a one-to-one comparison of VF segments

with and without CC artifact. This analysis eliminates shock cycles that are represented by only a single VF segment either only with CCs or only without CCs. We calculated AUC values for predicting all outcomes using pairs of adjacent segments with and without CCs, and compared individual AUC values without CCs versus with CCs for each waveform measure using DeLong's method for paired receiver operating characteristic curves.[109,115] We also compared median AUC values with CCs versus without CCs using the Wilcoxon signed-rank test.

4.12.1.2 Results

Of the 691 patients in the test group, there was a subset of 531 patients that had 1088 shocks with adjacent pairs of VF segments with and without CCs prior to each included shock; hence 2176 (80%) of all test segments were paired. Median AUC for predicting functional survival using paired data was 0.73 [range: 0.56-0.76] without CCs and 0.70 [range: 0.53-0.76] during CCs, with a median of AUC differences of 0.03 ($p<0.001$ for difference) (Figure 4.44). Median AUC for predicting return of circulation using paired data was 0.73 [range: 0.61-0.75] without CCs and 0.68 [range: 0.53-0.72] during CCs, with a median of AUC differences of 0.05 ($p<0.001$ for difference) (Figure 4.45). Median AUC for predicting return of rhythm was 0.72 [range: 0.55-0.74] without CCs and 0.65 [range: 0.53-0.70] during CCs, with a median of AUC differences of 0.06 ($p<0.001$ for difference) (Figure 4.46).

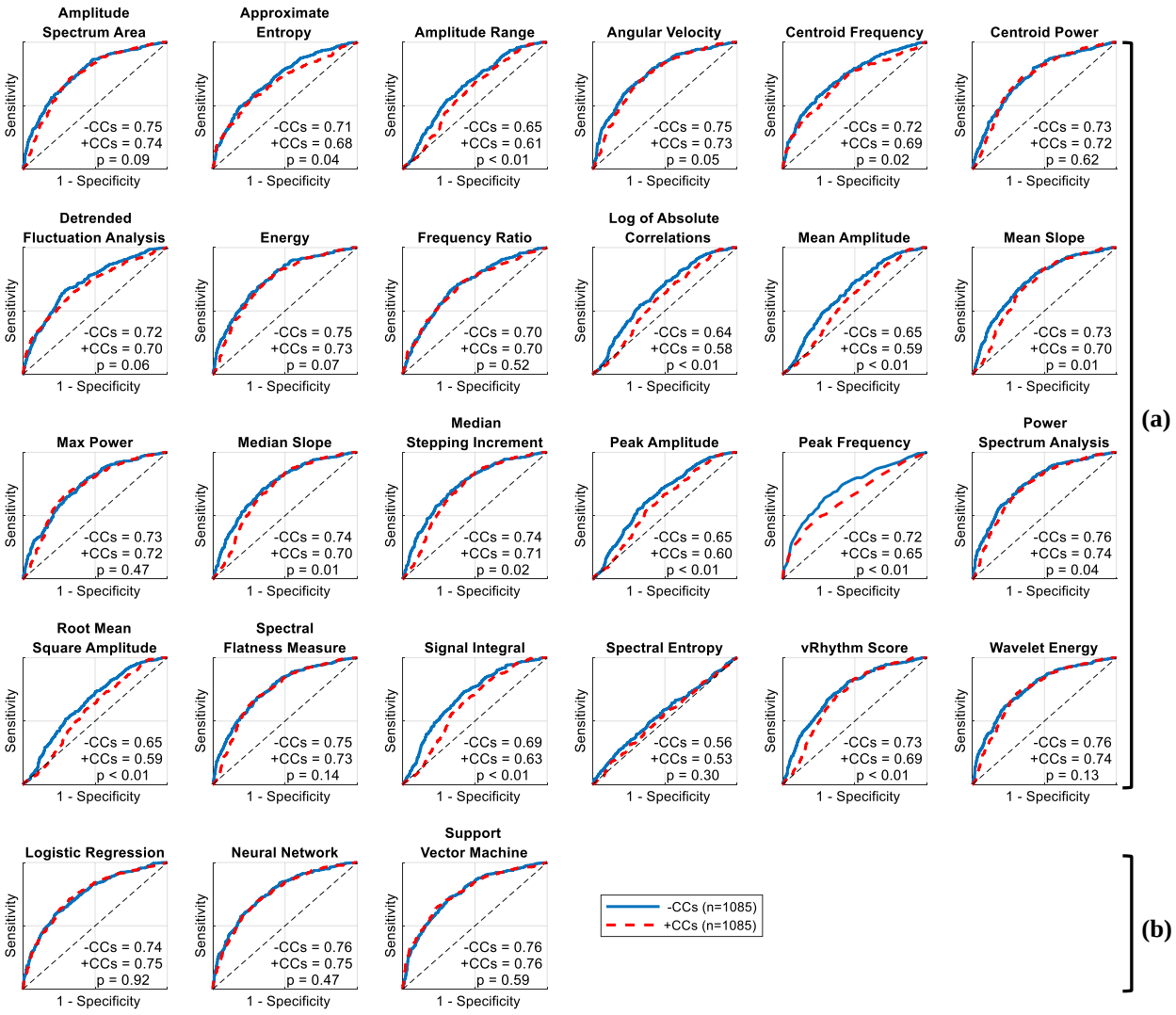

Figure 4.44 AUC values for predicting survival with paired data

AUC values for predicting functional survival using 1085 pairs of VF segments with and without CCs prior to 1085 shocks from test patients (after excluding 3 pairs with unknown survival). P-values are shown for difference in AUC for each measure with CCs versus without CCs. Measures are grouped by (a) individual measures and (b) combination measures. (-CCs = without chest compressions; +CCs = with chest compressions.)

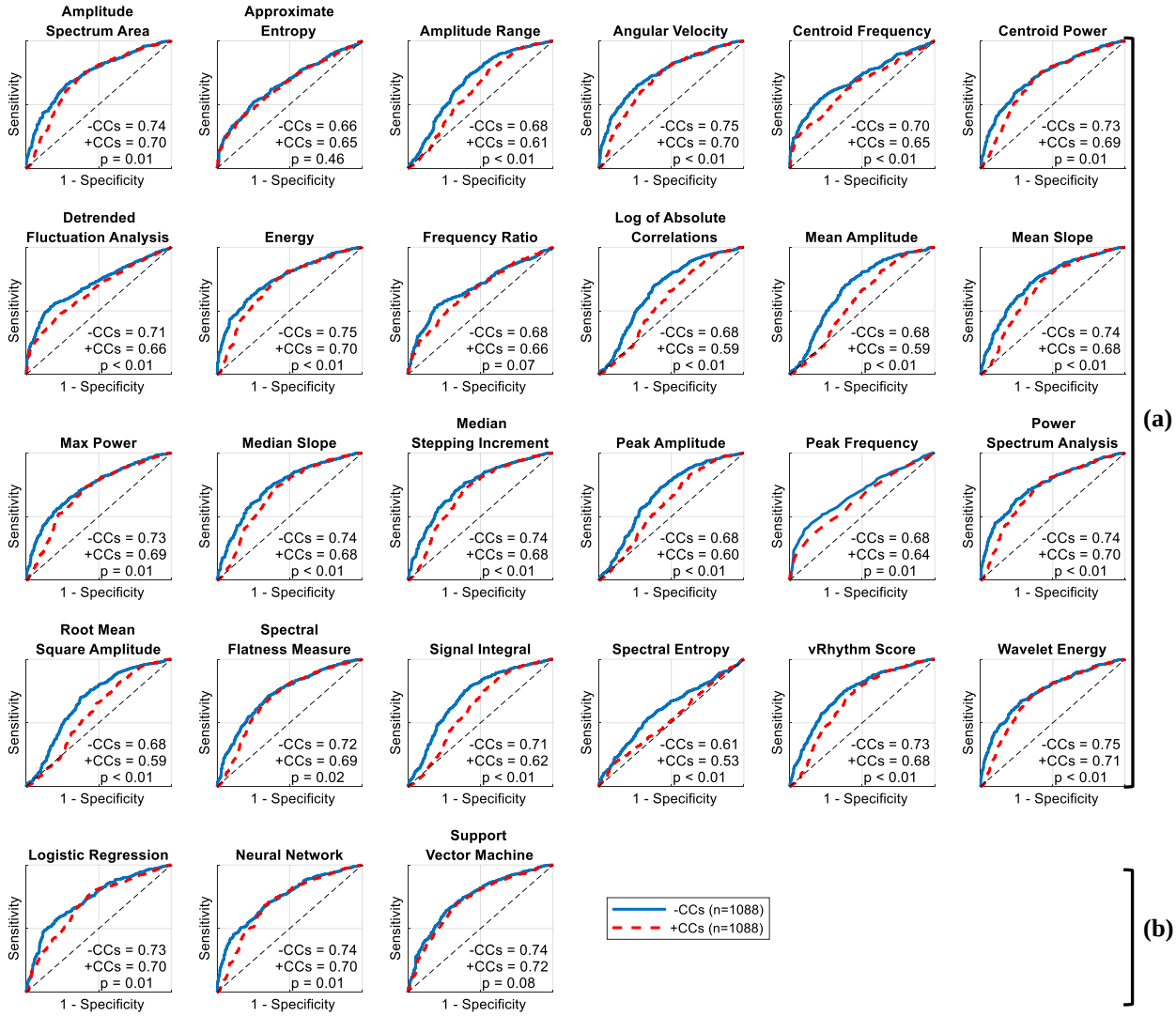

Figure 4.45 AUC values for predicting return of circulation with paired data
AUC values for predicting return of circulation using 1088 pairs of VF segments with and without CCs collected prior to 1088 shocks from test patients. P-values are shown for difference in AUC for each measure with CCs versus without CCs. Measures are grouped by (a) individual measures and (b) combination measures. (-CCs = without chest compressions; +CCs = with chest compressions)

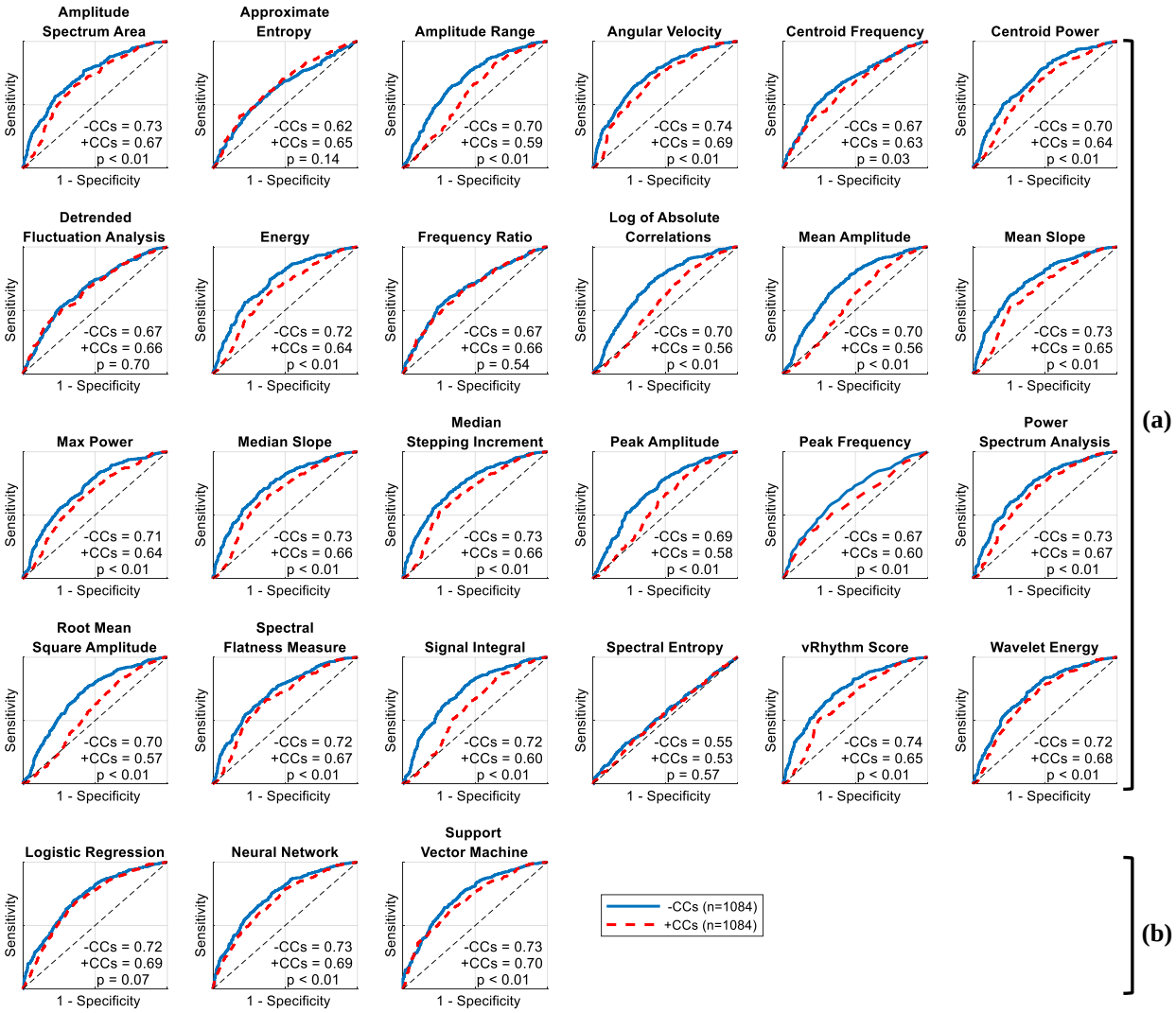

Figure 4.46 AUC values for predicting return of rhythm with paired data
AUC values for predicting return of rhythm using 1084 pairs of VF segments with and without CCs prior to 1084 shocks from test patients (after excluding 4 shocks with indeterminate return of rhythm). P-values are shown for difference in AUC for each measure with CCs versus without CCs. Measures are grouped by (a) individual measures and (b) combination measures. (-CCs = without chest compressions; +CCs = with chest compressions)

Without CCs, median AUC values for prediction of survival, return of circulation, and return-of rhythm using paired data (AUC=0.73, 0.73, and 0.72, respectively) were generally similar to AUC values originally reported using all data (AUC=0.73, 0.71, and 0.72, respectively). With CCs, median AUC values for prediction of survival, return of circulation, and return-of

rhythm using paired data (AUC=0.70, 0.68, and 0.65, respectively) were generally similar to AUC values originally reported using all data (AUC=0.69, 0.68, and 0.65, respectively). Additionally, similar to the original results using all data, using paired data the presence of CC artifact significantly reduced median AUC for predicting both primary and intermediate outcomes ($p<0.001$ for differences in median AUC without CCs versus with CCs for all outcomes).

Results for the best-performing measure during CCs, the Support Vector Machine, were generally similar using paired subgroup data versus the results using all data. For instance, the segments in the lowest Support Vector Machine quintile during CCs corresponded to 12.0% survival for paired data versus 12.7% for all data, and segments in the highest quintile corresponded to survival rates of 71.0% for paired data versus 68.8% for all data (Figure 4.47a). Similar to the primary results, AUC values for predicting all outcomes during CCs remained highest using the Support Vector Machine. Using paired data, AUC for Support Vector Machine prediction of survival was not significantly different without CCs versus with CCs (AUC=0.76 without CCs versus 0.76 with CCs, $p=0.59$ for difference by DeLong's method) (Figure 4.44), which confirms results observed using all (unpaired and paired) data. For predicting intermediate outcomes of return of circulation and return of rhythm using paired data, results were also similar to the original results using all (unpaired and paired) data: Support Vector Machine AUC for predicting return of circulation was marginally reduced, but not significantly, during CCs (AUC= 0.74 without CCs versus 0.72 with CCs, $p=0.08$ for difference) (Figure 4.45), and Support Vector Machine AUC for predicting return of rhythm was significantly reduced during CCs (AUC=0.73 without CCs versus 0.70 with CCs, $p<0.01$ for difference) (Figure 4.46).

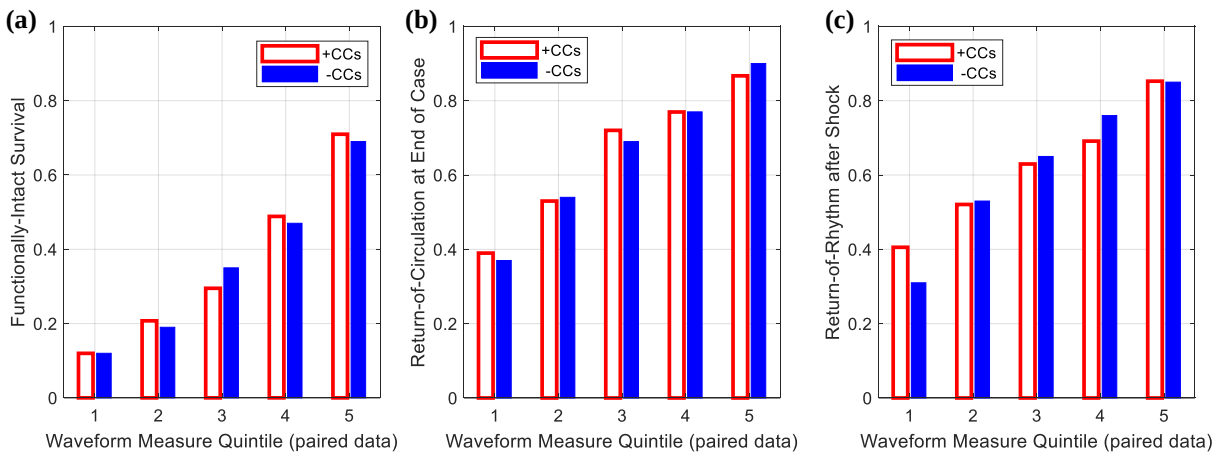

Figure 4.47 Support vector machine quintiles by outcome (paired data)
Rates of (a) functional survival, (b) return of circulation at end of case, and (c) return of rhythm after shock versus support vector machine model output quintiles are shown. Quintiles are limited to the paired adjacent segments subgroup with chest compressions (+CCs) and without chest compressions (-CCs) collected prior to 1088 shocks from 531 test patients.

4.12.1.3 Discussion

Restricting the analysis to paired data resulted in comparable results to using all data. When limiting analysis to adjacent paired segments with and without CCs prior to the same shock, 370 VF segments without CCs were excluded due to a lack of adjacent segment with CCs prior to the same shock, and 181 segments with CCs were excluded due to a lack of an adjacent segment without CCs prior to the same shock. Hence, a total of 551 shock cycles were excluded in the paired subgroup. A greater number of segments without CCs were present in the original dataset since it is sometimes more difficult to obtain a full 5-s VF segment during CCs than without CCs prior to initial shock. Treatment of VF by EMS personnel typically consists of initial CCs followed by a CC pause for initial rhythm analysis, and a subsequent immediate shock once VF is confirmed. However, initially in some cases ECG leads are not attached long enough to obtain a full 5-s VF segment during CCs, whereas the defibrillator's initial rhythm analysis (and concurrent pause in CCs) following the initial period of CCs ensures a period during which a VF segment without CCs

may be collected. Therefore, due to a greater number of exclusions of without-CC segments for pairwise analysis, results using all data versus paired data were more likely to differ without CCs than with CCs. For some specific waveform measures, performance using the paired subgroup was slightly increased versus using all data including unpaired segments. For instance, in predicting survival, Support Vector Machine AUC was 0.75 and 0.75 with and without CCs using all data but 0.76 and 0.76 with and without CCs using paired data. In general, however, limiting the analysis to paired data did not significantly change the overall relative performance of waveform measures, median AUC values, or conclusions of the study.

4.12.2 *Subgroup Analysis 2: Single Segment per Patient*

4.12.2.1 Methods

We analyzed a subset of test VF segments limited to a single segment with CCs and a single segment without CCs from each patient. For this analysis, one single segment (both with and without CCs) from the earliest available shock cycle was used from each patient. These segments were not necessarily adjacent pairs from the same shocks as in the previous subgroup analysis; for example, if the earliest shock cycle for an available segment with CCs was not the same shock cycle as the earliest shock cycle without CCs, both segments were still included, and vice versa.

Using the waveform measure parameters optimized for prediction of survival in the original study analysis, we evaluated prediction of the primary outcome of survival with and without CCs in the single-segment-per-patient subgroup. Similar to the original study analysis, the highest-performing measure with CCs was compared with and without CCs using DeLong's method. Waveform measure quintiles for the highest-performing measure were also tabulated versus rates of survival.

4.12.2.2 Results

After restricting the original test dataset (1639 shock cycles from 691 test patients) to a single VF segment (i.e., single shock cycle) per patient, there were 656 VF segments collected from 656 patients without CCs, and 565 VF segments from 565 patients with CCs (Table 4.8).

Table 4.8 Number of shock cycles sampled per patient
Number of shocks sampled in original study dataset versus the current subgroup analysis

Shock Number	Original Data: Without CCs	Single-Shock Subgroup: Without CCs	Original Data: With CCs	Single-Shock Subgroup: With CCs
1	617	617	356	356
2	403	30	418	193
3	267	5	298	12
4	166	4	194	4
Total	1453	656	1266	565

Overall functional survival for patients in the without-CC subgroup was 40.5% and the survival rate for patients in the with-CC subgroup was 38.4%. Median AUC for the 27 measures was 0.73 [range: 0.59-0.75] without CCs and 0.68 [range: 0.53-0.75] with CCs (median of differences = 0.05, $p<0.001$ for difference) (Figure 4.48). The highest-performing measure during CCs was the Support Vector Machine measure; this measure had similar AUC without CCs (AUC=0.75, 95% CI: 0.72-0.79) versus with CCs (AUC=0.75, 95% CI: 0.71-0.79, p=0.80 for difference in AUC).

Using one segment per patient, the rate of functional survival in the lowest quintile of the Support Vector Machine measure was 11.5% without CCs, as compared to 47.8% in the remaining four upper quintiles without CCs (Figure 4.49). The rate of functional survival in the lowest quintile was 15.0% with CCs, as compared to 44.2% overall in the remaining four upper quintiles with CCs. The rates of functional survival in the highest quintile of the Support Vector Machine measure were 75.6% and 72.6% without CCs and with CCs, respectively.

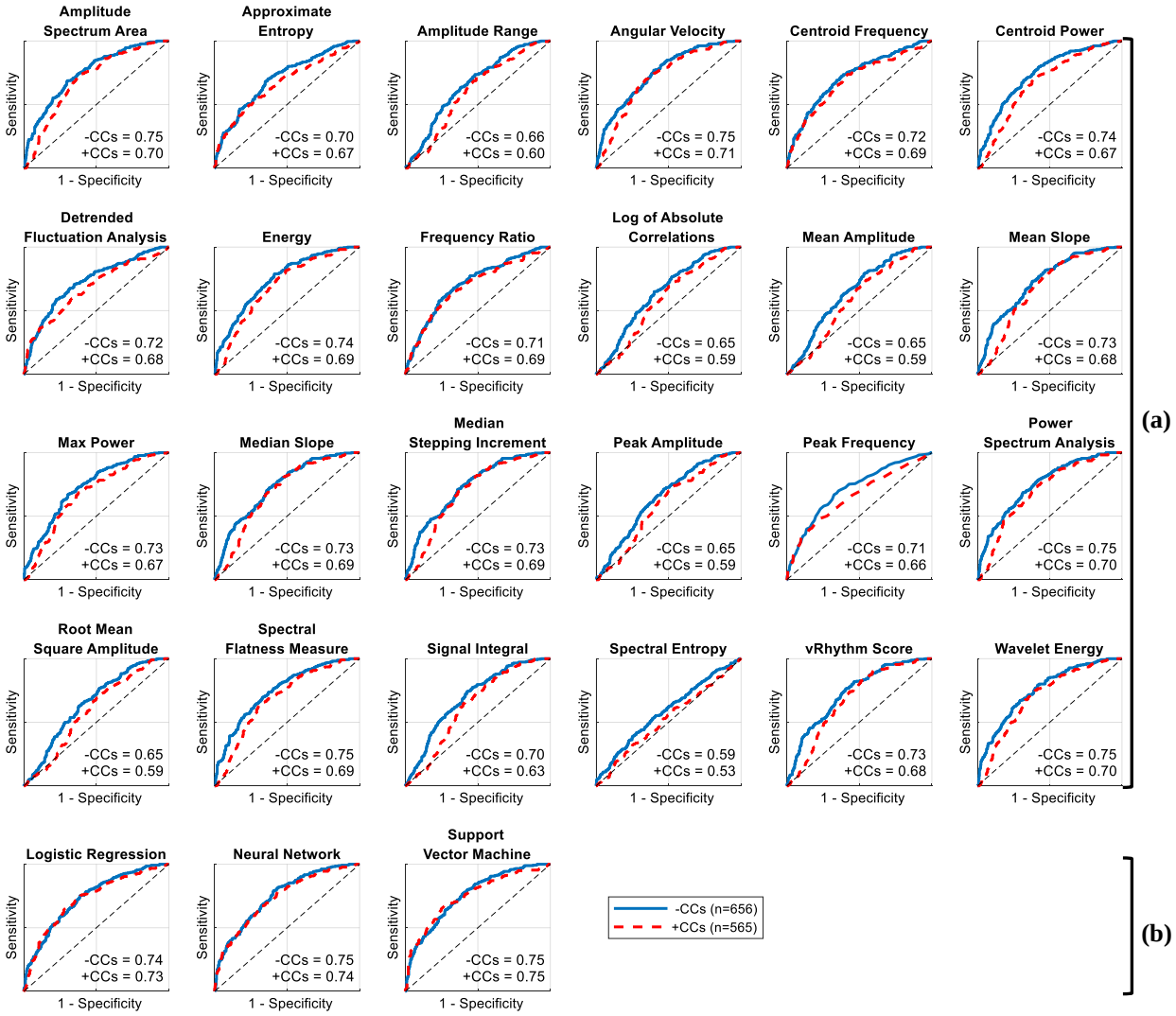

Figure 4.48 AUC values for predicting survival using one shock sample per patient
AUC values for predicting functional survival using 656 segments without CCs from 656 of the 691 test patients, and 565 segments with CCs from 565 of the 691 test patients. Measures are grouped by (a) individual measures and (b) combination measures. (-CCs = without chest compressions; +CCs = with chest compressions)

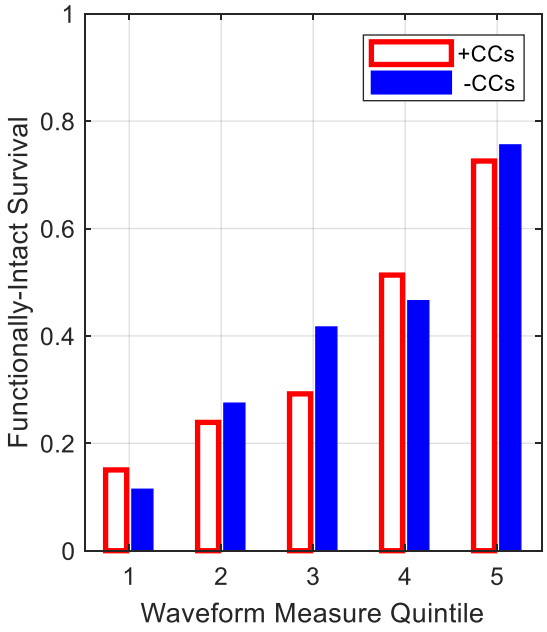

Figure 4.49 Waveform measure quintile versus survival using one sample per patient
Rates of functional survival are shown versus support vector machine quintiles using a subgroup of test data limited to one VF segment per patient without compressions (-CCs, n=656 patients) and one segment with compressions (+CCs, n=565 patients).

4.12.2.3 Discussion

The primary study analyzed multiple shock cycles (each with a corresponding VF segment both without and with CCs when available) to represent each patient. Hence, the results may be correlated, and rates of survival by waveform measure quintile in the primary study results represent the proportion of *segments* that were collected from patients who survived. Since multiple segments may be collected from a single patient, the segment-wise survival rate may differ from the patient-wise survival rate. For instance, in main study test data, 613/1639 (37.4%) of segments were collected from patients who survived, but 283/691 (41.0%) of patients in the test set survived overall. It is expected that segment-wise survival rates may be slightly lower than patient-wise survival rates, as patients with poorer outcomes tend to receive a higher number of shocks (and therefore are represented by more VF segments) than patients with good prognosis.

Therefore, to confirm the primary study results and the ability to identify disparate outcome by waveform measure quintile, we evaluated test data limited to a subgroup of one VF segment from a single shock cycle (both with and without CCs) per patient. We observed that median AUC for predicting survival was similar for the one-segment-per-patient subgroup versus using all segments, both without CCs (median AUC=0.73 in the one-segment-per-patient subgroup versus 0.73 in the primary study group) and with CCs (median AUC=0.68 in the one-segment-per-patient subgroup versus 0.69 in the primary study group). Confirming the primary results, the support vector machine measure using the one-segment-per-patient subgroup remained the highest-performing measure with CCs, and had similar performance with CCs versus without CCs (AUC=0.75 in both cases, p=0.80 for difference). The support vector machine AUC values in the current subgroup analysis are also similar to the AUC values in the primary study (AUC=0.75 in all cases). When the one-segment-per-patient subgroup data was stratified by quintile in the current subgroup analysis, the support vector machine values in the lowest quintile had poor prognosis (12% and 15% survival without and with CCs, respectively), similar to the poor prognosis using all segments as reported in the main results (12% and 13% without and with CCs, respectively). While the survival rates by quintile vary slightly in the one-segment-per-patient subgroup as compared to the analysis using all segments, the subgroup results still confirm the ability of waveform analysis to identify patients with markedly disparate survival rates after limiting analysis to a single 5-s ECG sample per patient. In addition, these results confirm the ability of combination waveform measures to improve prognostic performance for predicting survival during CCs to a performance similar to that observed without CCs.

In both the primary results and the current subgroup, the without-CCs group contained a higher proportion of initial shocks than the with-CCs group (Table 4.8). In the current subgroup

analysis, 617/656 (94%) of the shock cycles without CCs were collected prior to the first shock. This availability of 5-s pauses in CCs prior to initial shock is high to due defibrillator requirements for a hands-off period to allow initial rhythm analysis. However, due to limited availability of extended periods of CCs prior to initial shock as a result of EMS treatment protocol to minimize time to initial shock, only 356/565 (63%) of initial shocks were sampled during CCs. This disparity in shock cycle representation for the with-CCs versus without-CCs groups may account for some observed differences in the with-CCs and without-CCs AUC values. Hence, some comparisons of measures with CCs versus without CCs in the current subgroup analysis may be affected slightly. Overall, however, the current subgroup analysis confirms the primary study results, suggesting that inclusion of multiple segments (and multiple shock cycles) from each patient did not significantly confound the results.

4.12.3 *Subgroup Analysis 3: Low versus High Sampling Rates*

4.12.3.1 Methods

Although all ECG data segments analyzed in the study were resampled to 250 Hz prior to analysis, the ECGs were originally sampled at rates between 125–250 Hz. In the current subgroup analysis, we separated VF segments from the test dataset into higher sampling rate (≥200 Hz) and lower sampling rate (<200 Hz) groups. Waveform measures were calculated using the same parameters used in the main study. We compared median AUC between the two sampling rate groups for predicting the primary study outcome [functional survival] using the Wilcoxon rank-sum test.

4.12.3.2 Results

For test data with known primary study outcome (survival), there were 757 segments without CCs and 556 segments with CCs originally sampled at rates ≥200 Hz. Likewise, there were 696

segments without CCs and 710 segments with CCs originally sampled at rates < 200 Hz. Using higher-sample-rate data, median AUC for waveform measure prediction of functional survival was 0.74 (range: 0.55-0.78) without CCs and 0.72 (range: 0.52-0.77) during CCs. Using lower-sample-rate data, median AUC for waveform measure prediction of functional survival was 0.71 (range: 0.57-0.73) without CCs and 0.68 (range: 0.54-0.74) during CCs.

Median AUC for waveform measure prediction of survival was slightly greater using high sample rate data versus lower sample rate data without CCs (median of AUC differences for high- versus lower sample rate data = 0.03, p=0.002 for difference). Median AUC for prediction of survival was also slightly greater using higher sample rate data with CCs (median of AUC differences versus lower sample rate data = 0.04, p=0.038 for difference).

4.12.3.3 Discussion

We observed slight differences in AUC between high and low sampling rate data. However, it is unclear whether the observed AUC differences were caused by sampling rate or other external factors. The maximum frequency analyzed in the current study was 30 Hz, which is less than half of the Nyquist frequency of the lowest-sampling-rate data; hence, the sampling frequency of all data in the study should be sufficient for calculating all of the study's waveform measures. Other factors may instead have caused differences in AUC. First, since a single device type might be used in specific districts of the study region, it is unknown whether the observed AUC differences are due to device sampling rate or instead due to demographic variables inherent to each geographic district that (by chance) are associated with a specific device type used in that district. For example, a device type used by a district with a dense urban versus rural population could potentially have higher AUC for prognosis due to an increased proportion of early VF resulting from lower response times. Second, AUC differences may also be due to device filter bandwidths

for stored ECG data. The devices in the study had heterogenous ECG filter settings for stored ECG data. Waveform measures optimized to use higher frequency content may not function as well on ECG data filtered with a lower lowpass cutoff. Therefore, a device's filter bandwidth for stored ECG data, which in some cases may be manually adjusted by EMS personnel, may affect the potential for retrospective waveform measure analysis. Third, waveform measures were also not optimized for use on each device type but rather for all devices as a group. Separate optimization for each sampling rate or filter responses may improve performance. Additional controlled investigation would be required to determine the actual underlying cause of the observed AUC differences across sampling rate in the current study. Future investigation should include controlling filter bandwidths for stored ECG data, which can vary by device and user settings but was not taken into account in the current investigation.

4.13 Appendix F: Training versus Test Data

4.13.1 *Introduction*

In the current investigation, patients were randomized into 40% training (n=460) and 60% test (n=691) groups. Since one VF segment was collected with and without CCs prior to the first four shocks when available, patients were each represented by a minimum of one VF segment or as many as eight segments. Therefore, patient randomization into training and test sets could result in disparate performance for either dataset, for instance if patients with aggressive CPR artifact were over- or under-sampled in either the training or test set. Therefore, we investigated whether the training and test datasets were of comparable difficulty by comparing waveform measure performance between training and test sets. We compared performance using a single fixed implementation of a waveform measure described in a prior study to ensure equitable comparisons

across outcomes and CPR state (as the measures used in the current study employed different parameter values depending on outcome and CPR state).

4.13.2 *Methods*

Using all training and test data segments, we calculated the Amplitude Spectrum Area waveform measure from 1-26 Hz as described in a prior study.[65] Use of this previously-published measure (with fixed frequency limits) provides an objective measure of performance and dataset difficulty. We evaluated prediction of two study outcomes (return of rhythm and functional survival) using training and test data, both with and without chest compressions, to determine if the training or test datasets were of similar difficulty.

4.13.3 *Results*

Distribution of Amplitude Spectrum Area waveform measure values and resultant AUC values were generally similar for the training versus test datasets. For predicting the primary outcome of functional survival, AUC values without chest compressions were similar for training (AUC=0.74), test (AUC=0.74), and training and test combined (AUC=0.74). For predicting functional survival during chest compressions, AUC values were also similar for training (AUC=0.70), test (AUC=0.70), and training and test combined (AUC=0.70) (Figure 4.50). (Note that these AUC values, generated using the 1-26 Hz Amplitude Spectrum Area function published previously[65], may vary slightly from the primary study results which used variable frequency limits for Amplitude Spectrum Area.)

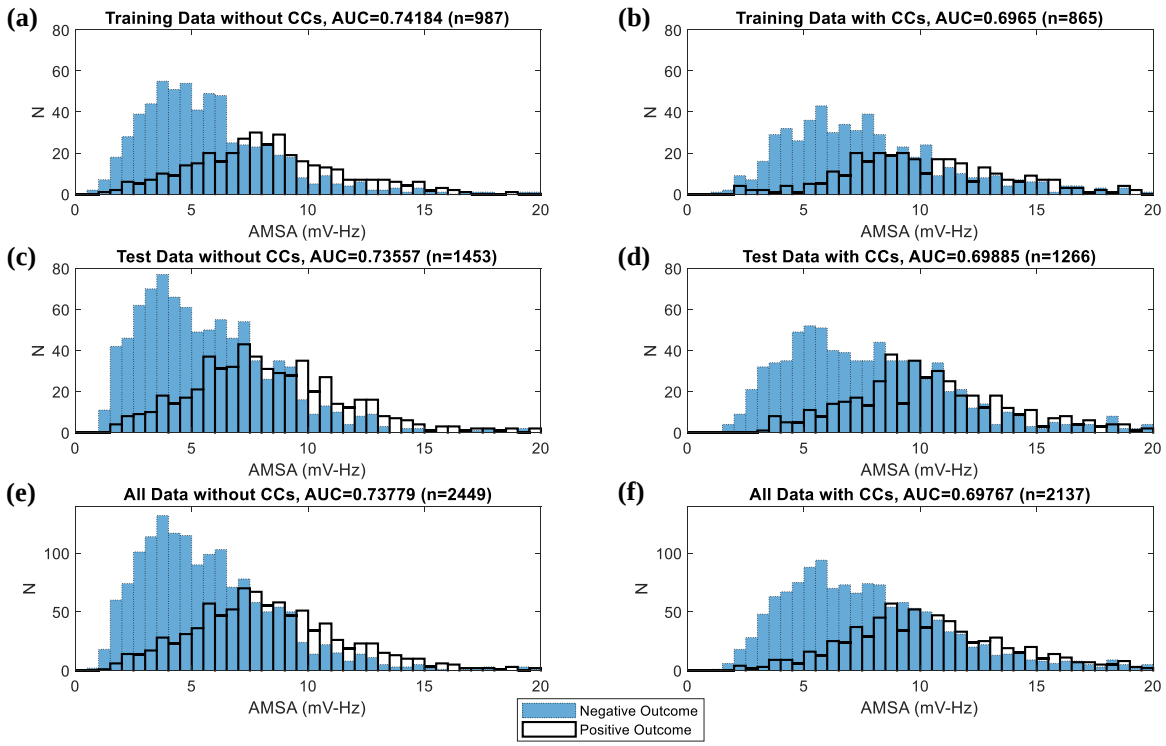

Figure 4.50 Training versus test results for predicting functional survival
Comparison of training versus test dataset AUC for predicting survival with favorable neurologic status, using the 1-26 Hz Amplitude Spectrum Area defined in a prior study. Results are shown for (a) training data without CCs, (b) training data with CCs, (c) test data without CCs, (d) test data with CCs, (e) all data without CCs, (f) all data with CCs. (AUC = area under the receiver operating characteristic curve, CCs = chest compressions.)

For predicting the intermediate outcome of return of rhythm, Amplitude Spectrum Area was slightly lower without CCs for training (AUC=0.71) versus test (AUC=0.73), and training and test combined (AUC=0.73). AUC values for predicting return of rhythm were similar with CCs for training (AUC=0.66), test (AUC=0.66), and training and test combined (AUC=0.66) (Figure 4.51).

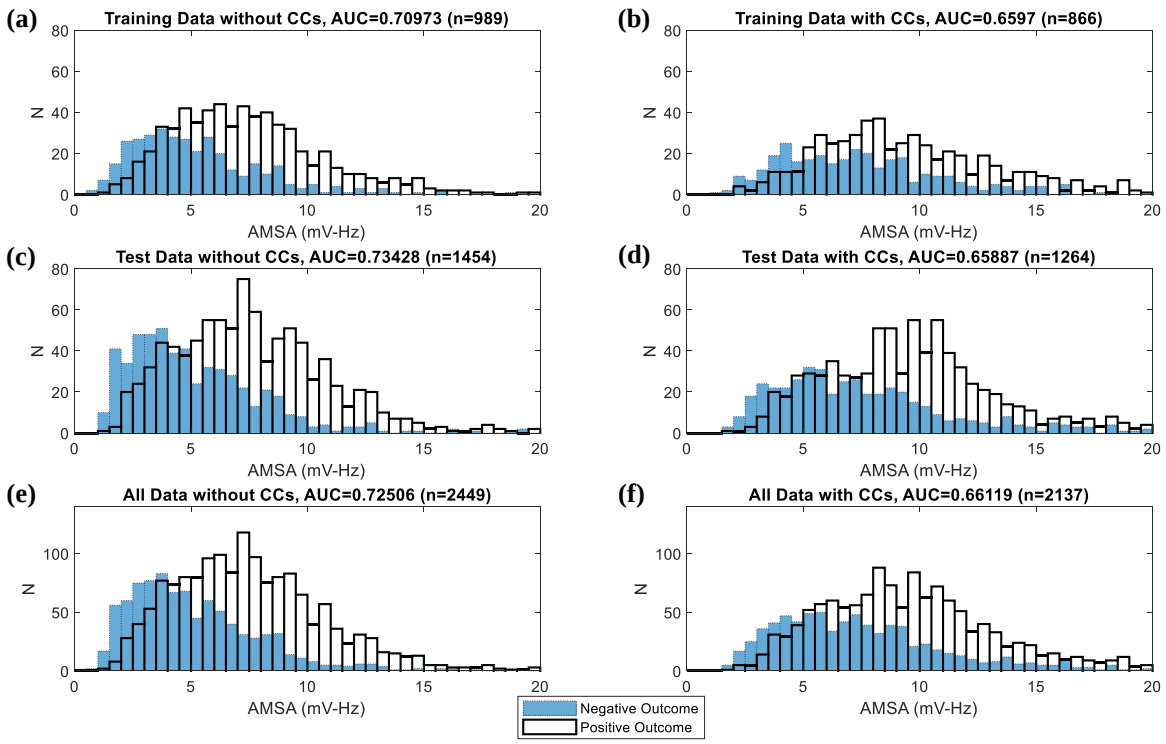

Figure 4.51 Training versus test results for predicting return of rhythm
Comparison of training versus test dataset AUC for predicting return of organized rhythm after shock, using the 1-26 Hz Amplitude Spectrum Area defined in a prior study. Results are shown for (a) training data without CCs, (b) training data with CCs, (c) test data without CCs, (d) test data with CCs, (e) all data without CCs, (f) all data with CCs. (AUC = area under the receiver operating characteristic curve, CCs = chest compressions.)

4.13.4 *Discussion*

For prediction of survival and return of rhythm outcomes, training and test AUC values using an objective waveform measure were similar during CCs (maximum absolute difference <0.0025 AUC). Without CCs, training and test AUC values were fairly comparable but had greater variation (maximum absolute difference <0.025 AUC). Notably, prediction of survival without CCs was lower on test data than training data, and prediction of return of rhythm without CCs was higher on test data than training data.

In comparison to a prior study conducted on a subset of the current dataset, the overall return of rhythm AUC values in the current study using 1-26 Hz Amplitude Spectrum Area are similar to a prior study of the 1-26 Hz Amplitude Spectrum Area collected from shocks 2-4 with and without CCs.[127] Specifically, the prior study results were similar to the current study results, both without CCs (AUC=0.71 in prior study versus 0.73 in the current study) and with CCs (AUC=0.66 in prior study versus 0.66 in the current study). However, others have reported markedly higher overall performance (e.g. AUC=0.83) using the same 1-26 Hz Amplitude Spectrum Area measure used to compute Figure 4.50 and Figure 4.51, indicating that difficulty for predicting outcomes across different patient datasets may vary significantly.[65] Thus the performance of measures can only be relatively compared within a single study (e.g. to determine which measure is more useful compared to other measures), but determination of absolute performance of waveform measures would require evaluation across multiple patient populations.

4.14 Appendix G: High-Pass Cutoff Sensitivity Analysis

4.14.1 *Introduction*

The goal of the primary investigation was to benchmark a comprehensive group of waveform measures and assess their *inherent* ability to predict outcome with and without chest compressions. Hence, we used a wider-band 1-30 Hz, 4th-order Butterworth filter to filter all ECG segments. This filter does not attempt to remove CC artifact. Compression artifact is typically centered at a fundamental frequency of approximately 2 Hz but has higher-frequency harmonics that extend through several multiples of the fundamental frequency (see Figure 3.2) and potentially as high as 20 Hz or more (see Figure 4.2), depending on factors such as chest recoil and impedance

characteristics as well as the amount of transient electrical noise due to physical perturbation of the defibrillator electrodes.[123]

Our prior pilot investigation of two waveform measures during CPR confirmed that predictive performance was marginally improved by using a bandpass filter with a low frequency cutoff of 4 Hz versus without filtering, indicating that even basic bandpass filtering may be useful for removing some chest compression artifact.[127] A challenge to bandpass filtering to remove chest compression artifact is the fact that VF frequencies are concentrated between approximately 2-10 Hz,[68] and are thus attenuated along with chest compression artifact as the filter high-pass cutoff frequency is raised. While prior study has suggested that a high-pass cutoff of approximately 4 Hz is suitable for removing compression artifact while preserving some features of VF, is unknown precisely what filter cutoffs provide the best balance between CC artifact suppression versus preserving VF frequency content useful for waveform analysis.[122,173] We therefore conducted a sensitivity analysis with variable filter cutoffs to determine optimal filter settings in conjunction with each individual waveform measure.

4.14.2 *Methods*

To examine effect of using bandpass filter cutoffs above typical chest compression fundamental frequencies, we incremented the high-pass cutoff of the 4th-order Butterworth ECG filter from 1 Hz to 6 Hz (Figure 4.52). For each filter cutoff setting, all individual waveform measure parameters were re-optimized on the study training data and combination models retrained (Figure 4.53). The parameter and filter combinations resulting in the highest training data AUC for predicting functional survival were selected for each individual measure (Table 4.9). Similar to the primary study methods, we compared median AUC with and without CCs using the Wilcoxon signed-rank test, and we compared the highest performing measure with and without CCs using Delong's

method for unpaired data. We also compared the highest-performing measure from the sensitivity analysis to the highest-performing measure in the primary study using Delong's method for paired data.

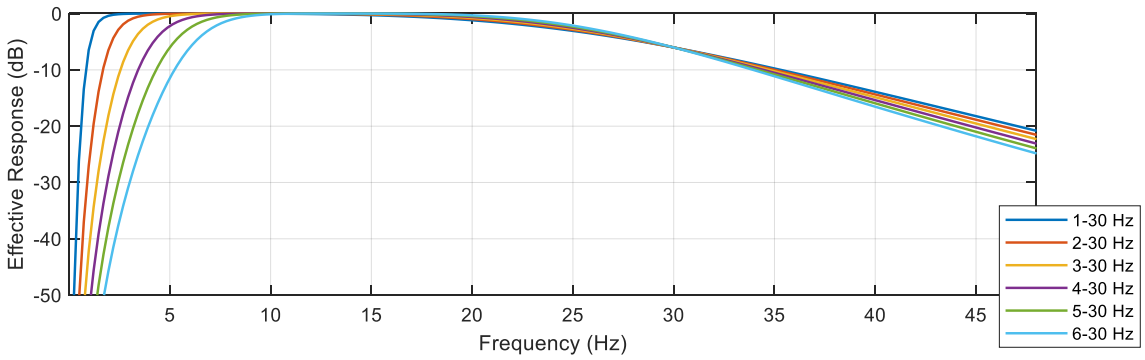

Figure 4.52 ECG bandpass filters
Frequency responses are shown for Butterworth bandpass filters used in the current sensitivity analysis. The frequency responses shown account for the effect of the forwards-backwards zero-phase method used to implement the filters.

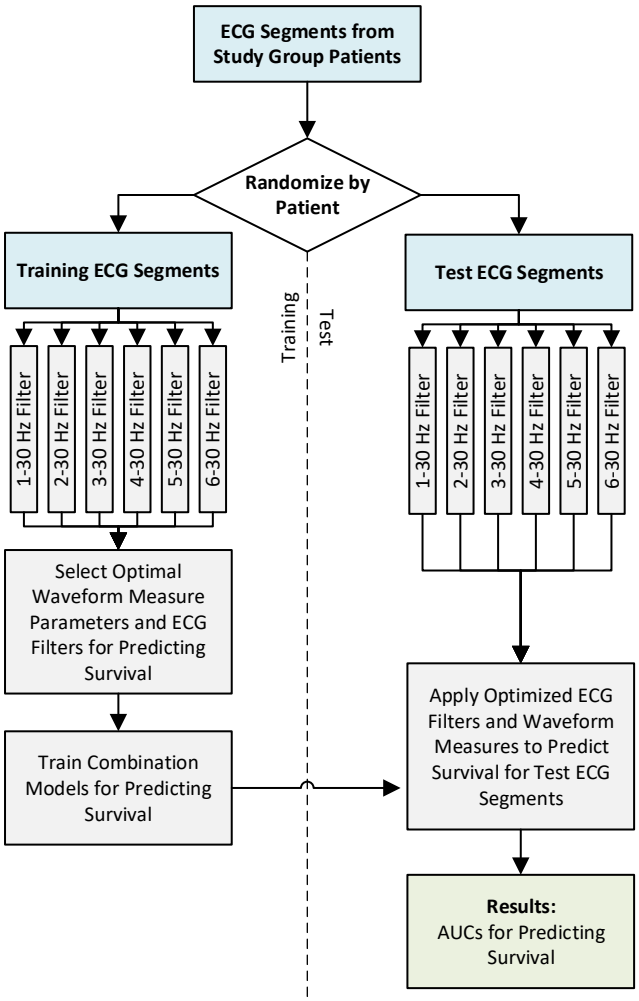

Figure 4.53 Sensitivity analysis training and test process flow
In the current sensitivity analysis, ECG filter cutoffs were varied prior to calculating each individual waveform measure. The filter and parameter combinations resulting in highest AUC were selected for use. (Note that the patient training and test assignments used in the primary study were used in the sensitivity analysis.)

Table 4.9 Waveform measure parameters with variable filter cutoffs

Waveform measure parameter values are shown for use with and without chest compressions (CCs), and were selected in conjunction with the indicated bandpass filter cutoffs. Parameters were automatically selected to maximize AUC for predicting functional survival, using 868 VF segments with chest compressions and 991 VF segments without chest compressions collected prior to 1116 shocks in 460 training patients.

Waveform Measure	**ECG Filter Cutoffs**		**Waveform Measure Parameters**	
	Without CCs	*With CCs*	*Without CCs*	*With CCs*
Amplitude Range[140]	6-30 Hz	6-30 Hz	N/A	N/A
Amplitude Spectrum Area[97]	1-30 Hz	1-30 Hz	Range: 6-30 Hz	Range: 6-30 Hz
Angular Velocity[133]	5-30 Hz	2-30 Hz	Lag: 2 samples	Lag: 2 samples
Approximate Entropy[138]	1-30 Hz	2- 30 Hz	R: 0.375	R: 0.5
Centroid Frequency[136]	1-30 Hz	2-30 Hz	Range: 1-17 Hz	Range: 1-30 Hz
Centroid Power[139]	2-30 Hz	1-30 Hz	Range: 15-30 Hz	Range: 18-30 Hz
Detrended Fluctuation Analysis[104]	1-30 Hz	1-30 Hz	Range: 1.4-2.2	Range: 1-1.8
Energy[116]	1-30 Hz	1-30 Hz	8-30 Hz	8-30 Hz
Frequency Ratio[100]	1-30 Hz	1-30 Hz	Mid Frequency: 4 Hz	Mid Frequency: 5 Hz
Log of the Absolute Correlations[141]	6-30 Hz	6-30 Hz	Lag: 12 samples	Lag: 10 samples
Logistic Regression[131]	N/A	N/A	N/A	N/A
Max Power[68]	4-30 Hz	1-30 Hz	15-30 Hz	18-30 Hz
Mean Amplitude[140]	6-30 Hz	6-30 Hz	N/A	N/A
Mean Slope[135]	6-30 Hz	6-30 Hz	N/A	N/A
Median Slope[68]	1-30 Hz	6-30 Hz	N/A	N/A
Median Stepping Increment[134]	2-30 Hz	5-30 Hz	N/A	N/A
Neural Network[68]	N/A	N/A	Hidden Layers = 1; Nodes/Layer = 3; Max Validation Fails = 18 epochs; Training = Bayesian Regularization	Hidden Layers = 2; Nodes/Layer = 11; Max Validation Fails = 18 epochs; Training = Bayesian Regularization
Peak Amplitude[140]	6-30 Hz	6-30 Hz	N/A	N/A
Peak Frequency[116]	1-30 Hz	2-30 Hz	1-30 Hz	2-30 Hz
Power Spectrum Analysis[68]	1-30 Hz	1-30 Hz	7-30 Hz	7-30 Hz
Root Mean Square Amplitude[140]	6-30 Hz	6-30 Hz	N/A	N/A
Signal Integral[139]	6-30 Hz	6-30 Hz	N/A	N/A
Spectral Entropy[142]	4-30 Hz	5-30 Hz	1-7 Hz	1-10 Hz
Spectral Flatness Measure[116]	1-30 Hz	1-30 Hz	6-30 Hz	6-30 Hz
Support Vector Machine[101]	N/A	N/A	Kernel size: 75 Box constraint: 7.5	Kernel size: 25 Box constraint: 2.5
vRhythm[137]	6-30 Hz	6-30 Hz	N/A	N/A
Wavelet Energy[132]	1-30 Hz	1-30 Hz	10-30 Hz	13-30 Hz

4.14.3 *Results*

Median AUC on test data for predicting survival using measures calculated after filtering ECGs with variable bandpass filters was 0.75 (range 0.62-0.76) without CCs and 0.72 (range 0.59-0.75) with CCs ($p<0.001$ for difference in medians by Wilcoxon signed-rank test) (Figure 4.54). Maximum AUC was achieved by the Support Vector Machine combination measure both without CCs (AUC=0.76, 95% CI 0.73-0.78, n=1453) and with CCs (AUC=0.75, 95% CI 0.72-0.78, n=1266, $p=0.61$ for difference by DeLong's method for unpaired data).

Compared to primary study results which used a fixed 1-30 Hz ECG filter, variable bandpass filter cutoffs in the current sensitivity analysis only slightly improved maximum AUC without CCs (Support Vector Machine AUC=0.76 using variable bandpass filters versus AUC=0.75 with a fixed 1-30 Hz filter, $p=0.001$ for difference by DeLong's method for paired data). Use of variable bandpass filter cutoffs in the current sensitivity analysis did not improve maximum AUC with CCs (Support Vector Machine AUC=0.75 with variable filters versus AUC=0.75 in primary results with a fixed 1-30 Hz filter, $p=0.99$ for difference by DeLong's method for paired data). Median AUC of all measures, however, was improved in the sensitivity analysis versus primary study both without CCs (median AUC=0.75 in sensitivity analysis versus 0.73 in the primary study, $p=0.002$ for difference) and with CCs (median AUC=0.72 in the sensitivity analysis versus 0.69 in the primary study, $p<0.001$ for difference), indicating that even though maximum AUC remained fairly similar in the sensitivity analysis versus primary study, lower-performing measures were improved in the sensitivity analysis.

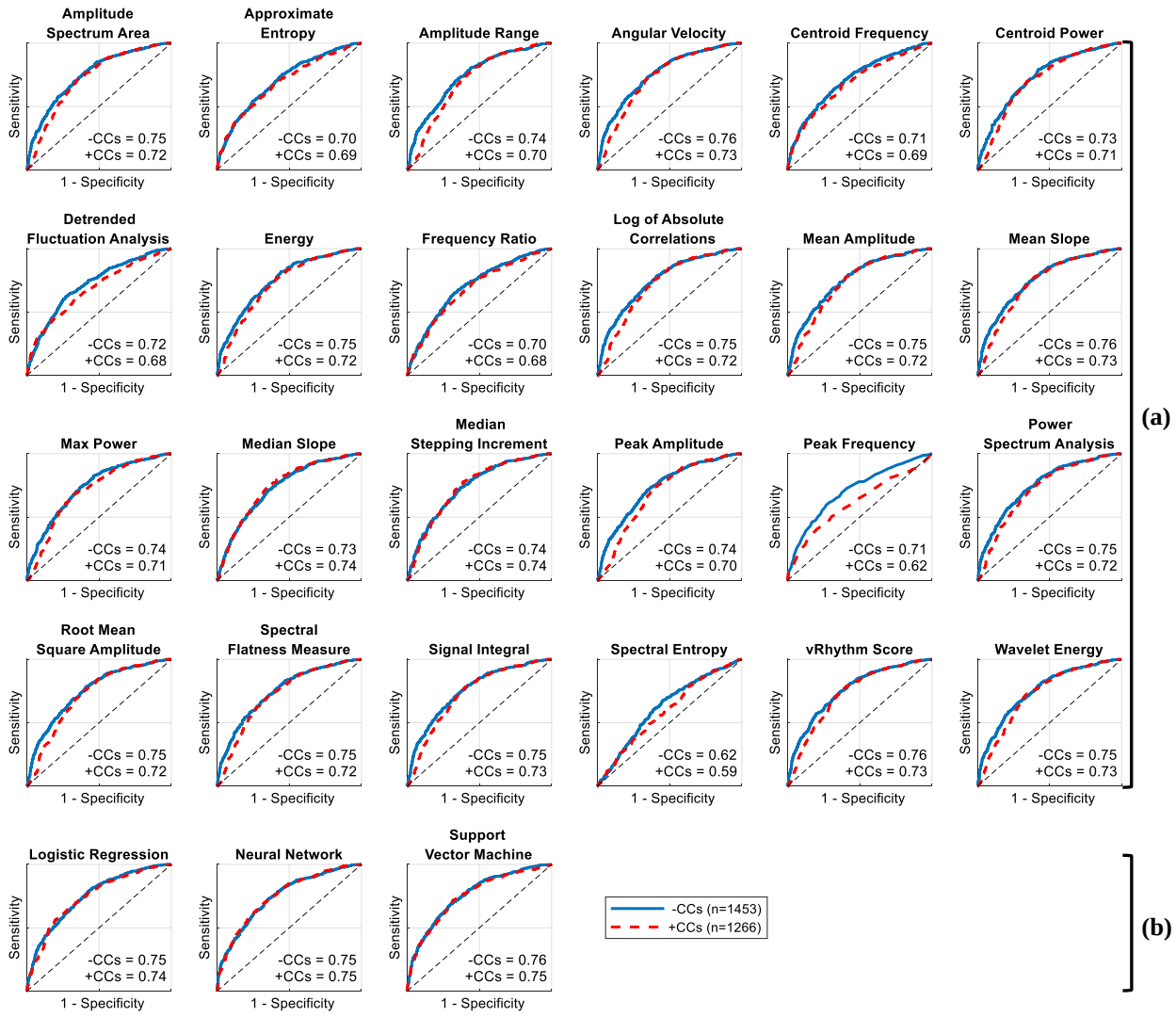

Figure 4.54 AUC values with variable ECG bandpass filters
Receiver operating characteristic curves with AUC values are shown for predicting functional survival on segments from 691 test patients, using waveform measures in conjunction with waveform measure-specific ECG bandpass filters. Measures are sorted by (a) individual measures and (b) machine learning combination measures. (-CCs = without chest compressions; +CCs = with chest compressions)

4.14.4 *Discussion*

Prior investigations have highlighted ability of filtering to remove CC artifact to allow improved ECG analysis during CPR.[44,69] CPR artifact is primarily found at the fundamental frequency of chest compressions (approximately 2 Hz), as well as at lower frequencies caused by ventilations

that are well below the typical dominant VF frequency range of 2-10 Hz.[68] CCs also introduce higher-frequency noise up to 20 Hz due to harmonics and transient effects from properties of the chest, recoil, and other electrical effects caused by mechanical impact.[110,123] Bandpass filtering (as opposed to more-advanced adaptive filtering[123,174] which is outside the scope of this investigation) during CCs may therefore have some, but perhaps limited, benefit due to spectral overlap between the VF signal and CC artifact.[45] Indeed, prior studies have suggested marginal improvement of waveform measure performance during CCs using basic bandpass filters, although performance after artifact suppression using bandpass filters was unable to match CC-free waveform analysis.[43,122]

While the primary goal of the current investigation was limited to assessment of the inherent ability of each measure to predict outcome during CCs (i.e. without additional filtering), in this sensitivity analysis we sought to determine whether maximum AUC could potentially be increased by varying the cutoff frequencies in the ECG filter. We evaluated the effect of incrementing the ECG filter high-pass cutoff frequency in our bandpass filter from 1-6 Hz, sweeping through the fundamental and first two harmonics of CCs. Filter settings and parameters were adjusted for each waveform measure separately to maximize AUC using training data.

We observed that time-domain measures of the ECG (e.g. amplitude), which typically performed poorly in primary study results, were improved using variable filter settings, but performance of measures with adjustable parameters remained similar. Optimal high-pass filter cutoffs for amplitude-based measures were typically 6 Hz (Table 4.9). For example, AUC for Peak Amplitude prediction of survival during CCs was increased from 0.65 (using the 1-30 Hz filter in the primary study) to 0.70 (using the 6-30 Hz filter selected in the sensitivity analysis). This is likely due to the fact that a 6 Hz cutoff (assuming a CPR chest compression rate of approximately

110 compressions per minute) excludes the fundamental and first two harmonic frequencies of CCs. Indeed, after optimizing filter cutoffs on training data, Median Slope actually performed incrementally better *during* CCs than without CCs on test data (AUC = 0.74 with CCs versus 0.73 without CCs, p=0.60 for difference); this result is likely due to selection of a 6-30 Hz filter for use during CCs but a 1-30 Hz filter for use without CCs based on training data. In retrospect, it is reasonable to assume that a filter of 6-30 Hz without CCs would have performed better than the 1-30 Hz filter selected using training data, and that perhaps the cutoffs selected during training were not ideal in all cases due to small variations between training and test data. Therefore, for some time-domain measures, it is possible that removal of frequencies below 6 Hz may thus improve performance not only during CCs but also without CCs as well.

In contrast to time-domain measures, frequency-based measures such as Amplitude Spectrum Area typically performed optimally with the wider filter bandwidth used in the primary study (1-30 Hz) and were largely unchanged in the sensitivity analysis using varied ECG bandpass filter cutoffs. This result is likely due to ability of internal parameters of frequency measures to exclude CC artifact after optimization on training data. After frequency-based measures were optimized on training data, they typically had higher low frequency limits and did not benefit from increased bandpass filter cutoffs. For instance, even when using variable ECG bandpass filter cutoffs, Amplitude Spectrum Area performed optimally with a wide 1-30 Hz ECG bandpass filter in combination with narrower frequency parameter limits of 6-30 Hz.

Bandpass filtering, therefore, can improve measures not previously optimized to ignore CPR artifact, but may only marginally improve performance of the best-performing measures that employ other variable parameters, since optimizing some parameters (e.g. frequency limits) can have an effect similar to basic bandpass filtering. Hence, similar to the primary results, the measure

with the highest AUC for predicting survival in this sensitivity analysis remained the Support Vector Machine, which, similar to the original study results, had similar performance without CCs versus with CCs (p=0.61 for difference). The maximum performance observed during CCs [using Support Vector Machine] in this sensitivity analysis was similar to that observed during CCs in the primary study (p=0.99 for difference), indicating that variable bandpass filters ultimately may not improve maximum performance during CCs. This result is likely due to the fact that the use of optimized frequency ranges in some measures can have an effect similar to bandpass filtering. Variable bandpass filters did however slightly improve maximum performance (i.e., Support Vector Machine AUC) without CCs in the sensitivity analysis (AUC=0.76) versus the primary study (AUC=0.75, p=0.001 for difference), although the difference is slight and significance of the difference is enhanced due to the assumption of correlated receiver operating characteristic curves allowed by DeLong's method for paired data.

Overall, these results suggest that a number of measures, especially poorer-performing (e.g. amplitude-based) measures, are improved by increased bandpass filtering, but that the maximum performance during CCs is not improved using variable bandpass filter cutoffs. Alternative filtering techniques (e.g. adaptive filtering based on the compression rate) may be required for any significant improvement in maximum AUC during compressions.

4.15 Appendix H: Expanded Discussion

4.15.1 *Summary of All Results*

The current investigation compared the performance of twenty-four individual ventricular fibrillation (VF) waveform measures and three machine learning combinations of measures to predict cardiac arrest outcomes. Measures were optimized and evaluated on independent training

and test sets using 5-s VF segments collected prior to 2755 shocks from 1151 patients. Waveform measure performance for predicting the primary study outcome (functional survival) as well as intermediate outcomes (return of circulation at end of EMS care and return of rhythm after defibrillation shock) was evaluated using segments collected both during artifact-free pauses in CPR and during ongoing CCs. In general, we observed the highest performance by combining all individual measures with a support vector machine model. For prediction of the primary outcome of survival on test data, the support vector machine improved performance during CCs was similar to that observed without CCs. When stratified into quintiles, the support vector machine output identified disparate functional survival during ongoing CCs for patients in the lowest quintile (segments corresponding to 13% survival) versus the highest quintile (segments corresponding with 69% survival). Neural Networks also performed similarly, although generally ranking slightly lower than Support Vector Machines in performance.

We confirmed these results using a subgroup limited to adjacent paired VF segments with and without CCs. Results were also confirmed to be similar when controlled for intra-cluster correlation and when limited to a single shock cycle per patient. We conducted a sensitivity analysis using variable ECG bandpass filters to evaluate the effect of filtering CC artifact; in this analysis, varying high-pass cutoffs between 1-6 Hz improved amplitude-based measures, but maximum performance for measures during CCs overall was similar to that observed with the original fixed 1 Hz cutoff frequency.

This study provides a proof-of-concept for using machine learning combinations of waveform measures to maximize waveform measure prognostic performance during CCs, and serves as a comprehensive benchmark of relative waveform measure performance.

4.15.2 *Prior Investigations of Waveform Measures Without Compressions*

A number of waveform measures have been proposed to quantify different characteristics of the VF signal associated with successful outcomes. These VF characteristics indicative of good outcome include higher amplitude, greater high-frequency content, and increased organization. There is a large disparity in performance between different measures, and the true performance of measures is unclear.[34,45,57] Benchmark studies have compared groups of ten to eighteen waveform measures calculated during CC pauses.[42,65,68,88–90] However, waveform measure accuracy remains difficult to ascertain from such studies due to variability in study dataset difficulty and size, inconsistent definitions of successful shock (e.g., termination of VF, return of organized rhythm, return of circulation, survival, or neurologic status), and incomparable performance metrics such as sensitivity and specificity versus receiver operating characteristic curve characteristics.[57,65] In order to fairly assess relative performance, researchers have recommended that multiple measures be tested blindly on the same data using AUC rather than sensitivity/specificity to allow comparison of prognostic performance independent of measure decision boundaries.[42,57] Studies of individual measures, for instance those reporting performance using development data, have reported much higher performance than that observed in subsequent evaluations For example, the Amplitude Spectrum has been reported with a prognostic AUC as low as 0.70 or high as 0.95.[64,111] These inconsistencies highlight the need for the current investigation's comprehensive benchmark of waveform measure performance.

4.15.3 *Prior Investigations of Waveform Measures During Compressions*

Two smaller retrospective studies of measures calculated during CPR have been conducted, but actual AUC values of these measures during CPR were not evaluated and prognostic ability was

not directly compared between CPR and CPR-free groups.[43,122] Hence, in previous investigation we compared a pilot group of measures during CCs versus without CCs, and observed a significant reduction in performance due to CCs; however, the study was limited to two measures. Thus, prior to the current investigation, waveform measure performance during CCs remained generally uncharacterized and it was unclear whether any measures merited further investigation for potential use during CPR.[127]

4.15.4 *Individual Measures*

In the current investigation, we confirmed that individual time-domain, frequency, and complexity-based measures predict functional survival, return of circulation, and return of organized rhythm following shock using VF segments collected with and without CC artifact. While by definition amplitude-based time-domain measures had predefined implementations, other measures required parameter selection. Rather than relying on parameter values published previously, we optimized waveform measure parameters (when possible) to maximize training AUC with and without CCs. Adjustable parameters included time-domain sample lag values, frequency cutoffs, and combination model hyperparameters. Separately optimizing parameters with and without CCs allowed for some measures to partially ignore CC artifact, and to adjust for prediction of different outcomes. For example, Amplitude Spectrum Area has been previously implemented within a frequency range of 1-26 Hz.[65] We observed on training data that without CCs, a similar range of 1-30 Hz maximized AUC for prediction of return of rhythm after shock, but that during CCs, based on training data, frequency limits should be set to 4-30 Hz for predicting return of rhythm and 6-30 Hz for predicting survival (Table 4.5). Increasing the lower frequency limit allowed the function to inherently ignore lower-frequency CC artifact. In contrast, measures that by design lacked adjustable parameters (e.g. time-domain measures of amplitude) tended to

be most corrupted by presence of CCs. For instance, Peak Amplitude (which does not have variable parameters) AUC for predicting survival was reduced by 0.06 during CCs, while Frequency Ratio (which has a variable frequency cutoff parameter) AUC was reduced by only 0.02 during CCs.

Of individual time-domain, frequency-domain, and complexity measures (but excluding combination measures), we observed that Wavelet Energy generally achieved the highest AUC for prediction of survival and return of rhythm with and without CCs. Based on training data, the optimal frequency ranges used to calculate Wavelet Energy ranged between 4-30 Hz (for predicting return of rhythm without CCs) to 13-30 Hz (for predicting survival during CCs), suggesting that mid- and higher-frequency information in the VF waveform is sufficient to assess myocardial metabolic activity and predict survival. Varying the frequency ranges used to calculate Wavelet Energy allowed a balance between including useful VF signal content while ignoring the fundamental and lower harmonic frequencies in CC artifact. Given that the wavelets used in the wavelet transform have a bandwidth extending several Hz to either side of their center frequencies, and in light of the optimal frequency limits using other frequency-domain measures (e.g. 6-30 Hz for Amplitude Spectrum Area and for Spectral Flatness Measure when predicting survival), we estimate that the optimal frequency limits for analysis during CPR lie in the region of approximately 6-30 Hz. (Note that frequency information above 30 Hz may also be useful but was not examined in the current investigation.) Thus, for VF corrupted by CCs, VF information above approximately 6 Hz is useful for evaluating the metabolic state of the myocardium while also ignoring some CC artifact. A relatively accurate prognosis can still even be made using information limited to frequencies above 10 Hz in many cases, indicating that high-frequency activity in the VF waveform alone is sufficient to evaluate patient status. These results confirm a prior study of high-frequency waveform measure analysis of the VF ECG which also demonstrated

optimal prognostic performance using information above a high-pass cutoff of approximately 6 Hz (depending on the specific waveform measure used).[68] With regards to underlying myocardial physiology, such results suggest that the rotation frequency of depolarization rotor(s) may not be the optimal indicator of myocardial amenability to defibrillation, although as observed in the current study, the dominant rotor frequency (e.g. centroid or peak frequency) is still somewhat related to outcome. Instead, properties affecting the sharpness or sustained high-frequency content of the VF waveform may play a more significant role. Whether or not said properties include conduction velocity or the number of smaller reentrant rotors remains unclear.

4.15.5 *Combination Measures*

Previous investigations of logistic regression, neural network, and support vector machine combinations of individual measures calculated from human VF have shown no significant improvement in performance using such combination measures versus individual measures alone.[34,45,68,89] However, no studies have implemented combination models using VF segments collected during ongoing CCs, and thus it was previously unknown whether combination methods were beneficial during CCs. We trained three models previously applied in VF analysis using all individual measures as input features: Logistic regression models, feedforward neural networks, and support vector machines. Hyperparameters for neural network and support vector machine models were optimized using training data prior to training the actual models. We observed that on test data, support vector machine models had the highest AUC values in most cases, and during CCs achieved improved performance versus individual measures. Neural network models had nearly as high performance as support vector machine models, generally ranking second in AUC and also outperforming individual measures.

These results suggest that use of machine learning models able to classify complex patterns and high dimensional combinations of input data in conjunction with a sufficient training dataset (1116 shock cycles from 460 patients in this case) may provide a means to overcome the effects of CC artifact. Performance of machine learning models remains contingent on useful individual measures optimized to function during CCs. Simpler logistic regression models, which did not perform as well as neural networks and support vector machines in our study, may be disadvantaged from not using complex interactions in input features, as we did not implement our logistic models with interaction terms. For instance, as a hypothetical example, while higher amplitudes typically indicate increased likelihood of good outcome, it may be possible that high amplitude with lower amounts of high-frequency content as measured by Amplitude Spectrum Area might indicate decreased likelihood of good outcome; such a relationship could be exploited using a model such as a support vector machine, but not with a simple logistic regression model.

A potentially improved resuscitation treatment strategy could therefore apply VF waveform analysis as a real-time prognostic indicator to rescuers during CCs throughout a resuscitation. Such a strategy would be contingent on accurate rhythm classification during CCs (i.e. to determine if the rhythm is actually VF) in conjunction with VF waveform analysis during CCs. Hence, in prior study we demonstrated a next-generation ECG rhythm diagnostic algorithm that performed rhythm classification without interrupting CCs.[72] Waveform analysis during CCs could thus potentially be performed in conjunction with such a rhythm detection algorithm during CCs, with results displayed to a rescuer as feedback to monitor the effects of therapy or to automatically adjust shock timing. Admittedly, a maximum AUC of 0.75 during CCs (as observed in our primary results) may be insufficient for reliable clinical decision-making in all but extreme cases (i.e. applying differential treatment for patients in the lowest quintile probability for

survival), and thus rather than displaying actual model output probabilities to the rescuer, a more abstracted form of feedback may be more useful. Hence, we stratified waveform measures by quintile and observed that the support vector machine model may be an acceptable candidate for a such a prognostic marker. For example, when a patient is in the lowest or highest quintiles, a rescuer might be informed a patient has exceptionally poor or favorable prognoses. As described in the primary study, differential treatment might then be applied only in these extreme cases, such as delaying shock to apply additional CPR or prioritizing transport to receive interventional treatments in the 'poor' case, or forgoing a scheduled two-minute period of CPR to apply immediate shock in the 'favorable' case.

4.15.6 *Intermediate versus Long-Term Outcomes*

During CCs, we observed that median AUC for waveform measure prediction of the intermediate outcomes of return of rhythm (AUC=0.65) and return of circulation (AUC=0.68) were slightly lower than median AUC for prediction of long-term functional survival (AUC=0.69). Prediction of return of rhythm was also significantly lower during CCs than without CCs for the highest-performing measure (support vector machine AUC=0.75 without CCs versus 0.70 with CCs, p=0.02 for difference), contrasting the results observed for prediction of survival (support vector machine AUC=0.75 without CCs versus 0.75 with CCs, p=0.75 for difference) and prediction of return of circulation (support vector machine AUC=0.72 without CCs versus 0.72 with CCs, p=0.99 for difference). The observed reduction in AUC using the shorter-term outcome of return of rhythm may seem counterintuitive due to the higher number of confounding factors between a more immediate outcome (return of rhythm) versus a medium-term outcome (return of circulation) or a long-term outcome (functional survival). However, the observed results confirm a prior investigation which also demonstrated improved prediction for increasingly longer-term outcome

endpoints.[145] As hypothesized in prior study, these observed increases in AUC for longer-term outcomes may be due to the relative instability of some shorter-term outcomes (such as those based on the ECG rhythm following shock), leading to less reliable prediction for short-term outcome.[145]

Another potential explanation for the difference in AUC between long-term and intermediate outcomes, especially return of rhythm versus survival during CPR, may stem from the specific outcome definitions used. For instance, while interrater reliability for return of rhythm annotation was high, it is possible that manual detection of QRS complexes was incorrect in some cases due to CC artifact in the ECG, preventing reviewers from observing QRS complexes, or conversely, mistaking sharp CC artifact for return of rhythm. Additionally, by definition, our definition of positive return of rhythm may also include clinically-negative pulseless electrical activity. Therefore, even if waveform measures perfectly reflected the metabolic state of the patient, AUC for return of rhythm would be relatively lower due to assigning positive return of rhythm outcome to patients with pulseless QRS complexes and poor clinical prognosis. Similarly, identifying of return of circulation is contingent on physical evaluation of a pulse, which depending on the rescuer's skill or the blood pressure of the patient, may not be as reliable as survival. In contrast to return of rhythm or return of circulation, it is unlikely a patient's survival outcome was recorded incorrectly, making survival a more reliable outcome.

An alternative explanation for the higher prediction of survival observed relative to intermediate outcomes is dataset variability. While prediction of survival was similar for training versus test data using an objective waveform measure (as demonstrated in the sensitivity analysis above), the training and test datasets did indeed exhibit slightly different AUC for predicting return of rhythm without CPR (see Figure 4.51). This may indicate some random heterogeneity in the

dataset across training and test data, and perhaps indicates a potential to compromise the ability of measures to generalize to test data after being tuned using training data.

In addition to differences in AUC across multiple outcome definitions, optimal parameter values were different for prediction of survival versus prediction of return of rhythm and return of circulation. This observation could be due to random variation, or may instead suggest fundamental physiological differences in the relationships between VF morphology, return of rhythm after shock, return of circulation, and long-term neurologic outcome. In general, prediction of survival with functional neurologic status relied more heavily on high-frequency information than prediction of return of rhythm, both with and without CCs (see Table 4.5 and Table 4.9). For example, without CCs, Amplitude Spectrum Area was optimized to 6-30 Hz for predicting survival and 1-30 Hz for predicting return of rhythm. This suggests that while low-frequency (e.g. 1-6 Hz) content of the VF waveform may indicate shorter time since VF onset due to increased electrical coordination and therefore higher probability of immediate electrical return of rhythm, low-frequency VF amplitude may not be as strongly related to long-term survival.[22,58] Low-frequency VF content may simply represent the degree of VF wavefront coordination (i.e. the number of cardiomyocytes contributing to any given depolarization wave) but might be less reflective of the actual metabolic characteristics of the myocardium indicative of likely patient survival such as conduction velocity, amount of infarcted tissue, or effects of myocardial anaerobia such as concentration of adenosine triphosphate, intracellular calcium, or oxygen. In contrast, increased high-frequency activity in the myocardium may indicate a more aerobic state and greater concentration of high-energy phosphates enabling fast conduction, and thus more favorable long-term prognosis overall, regardless if immediate return of rhythm is likely within a given shock cycle. While the underlying physiological mechanisms are unclear, these results could indicate

that electrical return of rhythm, return of circulation, and survival may relate to different characteristics of the VF waveform. Further study may be warranted to determine which outcome definition should be used in order to most effectively guide clinical care.

4.15.7 *Future Directions*

The current results suggest potential for improved waveform analysis during CPR, but as maximum observed AUC was 0.75, current waveform measures alone may be still insufficient to guide clinical care in all but extreme cases. Future study to improve performance could explore development of novel waveform measures designed specifically to function with increased accuracy during CCs. Current waveform measures typically average information over the length of the ECG sample and do not examine time-varying high-frequency morphology. Novel measures based on the time-varying morphology of high frequency content (rather than simply the sum of energy within a high frequency range as with Wavelet Energy), for example, may offer improved performance. More advanced statistical combinations of measures, especially deep learning methods that construct entire features based on training data, may also increase performance. In addition, in spite of the fact that varying bandpass filter cutoffs in our filter sensitivity analysis offered only marginal overall improvement, adaptive filtering based on defibrillator impedance or force channels may offer more precise removal of CC artifact and could potentially improve waveform measure use during CCs.[45,123] Furthermore, the history of prior shock outcomes have already been shown to improve performance when combined with waveform measures, but this technique was not applied in the current investigation as application would be limited to shocks subsequent to initial shocks only.[112,127] Future study incorporating prior shocks with additional signals acquired during resuscitation (such as cerebral perfusion) or use of multi-lead ECGs to compute VF waveform measures could potentially improve overall prediction.

Chapter 5. NOVEL METHOD TO DETECT PRESENCE OF CHEST COMPRESSIONS DURING RESUSCITATION USING TRANSTHORACIC IMPEDANCE

Unpublished by **Coult J**, Blackwood J, Rea T, Kudenchuk P, Kwok H. (Currently under review.)

5.1 ABSTRACT

Objective: Interruptions in chest compressions during treatment of out-of-hospital cardiac arrest are associated with lower likelihood of successful resuscitation. Real-time automated detection of chest compressions may improve CPR administration during resuscitation, and could facilitate application of next-generation ECG algorithms that employ different parameters depending on compression state. In contrast to accelerometer data, transthoracic impedance (TTI) is commonly acquired by defibrillators. We sought to develop and evaluate the performance of a TTI-based algorithm to automatically detect chest compressions. *Methods:* Five-second TTI segments were collected from patients during out-of-hospital cardiac arrest treated by one of four defibrillator models. Segments with and without chest compressions were collected prior to each of the first four defibrillation shocks (when available) from each case. Patients were divided randomly into 40% training and 60% validation groups. From the training segments, we identified spectral and time-domain features of the TTI associated with compressions. We used logistic regression to predict compression state from these features. Performance was measured by sensitivity and specificity in the validation set. The relationship between performance and TTI segment length was also evaluated. *Results:* The algorithm was trained using 1859 segments from 460 training patients. Validation sensitivity and specificity were ≥98% using 2727 segments from 691 validation patients. Validation performance was significantly reduced using segments shorter than

3.2 s. *Conclusions:* A novel method can reliably detect the presence of chest compressions using TTI. These results suggest potential to provide real-time feedback in order to improve CPR performance or facilitate next-generation ECG rhythm algorithms during resuscitation.

5.2 INTRODUCTION

Out-of-hospital cardiac arrest resulting from ventricular fibrillation is a leading cause of death.[3] High-quality cardiopulmonary resuscitation (CPR) is a key treatment that can increase the likelihood of successful resuscitation.[31] High-quality CPR includes near-continuous chest compressions to support circulation, as interruptions in compressions are associated with a lower likelihood of survival.[47,48,175] However, interruptions are common and are attributed to a range of rescuer actions and distractions.[176,177] Therefore, real-time detection of compressions provides an opportunity to prompt rescuers when CPR is interrupted. Moreover, real-time compression detection can inform electrocardiogram (ECG) rhythm analysis algorithms to ensure that the rhythm is analyzed during a CPR-free segment, and could also support next-generation algorithms that attempt rhythm analysis during active CPR by applying parameters based on the current compression state.[72,91,127]

Reliable real-time detection of chest compression metrics during resuscitation can be achieved using an accelerometer sensor placed beneath the rescuers hands on the sternum.[77,178,179] However, many defibrillators due to design or cost constraints are not equipped with an accelerometer. In contrast to accelerometer signals, the transthoracic impedance (TTI) is commonly acquired via the defibrillator electrodes, as this signal is used to confirm proper attachment of electrodes and to calibrate the shock energy delivered to the patient.[92,180,181]

A patient's TTI, which has a typical baseline value between 50–120 Ω, varies with physical changes in the chest that affect conductivity between the defibrillator electrodes.[182] For instance,

during a ventilation, an increase in lung volume will temporarily increase impedance due to the insulating properties of air.[183] Conversely, ejection of blood into the aorta during a pulse will temporarily decrease impedance due to the conductive properties of blood.[92,129,182,184,185] Other changes in chest configuration or lung volume caused by chest compressions will be similarly be reflected as measurable perturbations in TTI.

Prior investigations have described methods to automatically detect compressions using the TTI signal. However, these methods are either limited in classification performance, require prolonged intervals of the TTI signal for optimal analysis, were validated using data from single defibrillator type, or were validated with a modest patient sample size.[73,92–96] Thus, knowledge gaps include a highly-accurate TTI algorithm validated with a large cohort across multiple defibrillator platforms that could be used to provide timely feedback of the chest compression state.

We therefore sought to develop and evaluate a chest compression detection algorithm suitable for an embedded application that could reliably assess compression state across different defibrillator platforms with minimal real-time delay.

5.3 METHODS

5.3.1 *Study Population and Setting*

The study was a retrospective investigation of persons suffering out-of-hospital cardiac arrest between 2005-2015 who presented to the regional Emergency Medical Services (EMS) with an initial arrest rhythm of ventricular fibrillation. During resuscitation, patients were treated in accordance with the American Heart Association guidelines. These guidelines require initial CPR with alternating compressions and ventilations at a ratio of 30:2 followed by compressions

concurrent with ventilations once the patient is intubated, as well as a hands-off pause every two minutes to allow ECG rhythm analysis and defibrillation shock.[31,32] The cohort included patients treated with Physio-Control Lifepak 12, Physio-Control Lifepak 15 (Physio-Control, Redmond, WA), Philips Forerunner 3, or Philips MRx (Philips Healthcare, Bothell, WA) defibrillators. Patients were excluded if they received a shock prior to EMS arrival. Utstein characteristics were tabulated for all patients in the cohort.[128]

In accordance with applicable regulations, this study and waiver of consent were approved by the Research Review Committee of King County Public Health and the Institutional Review Board at the University of Washington Human Subjects Division.

5.3.2 *Data Collection and Processing*

We previously collected the study data for a prior investigation of the ventricular fibrillation ECG.[91] One 5-second TTI segment during chest compressions and one segment without compressions was collected prior to each of the first four defibrillation attempts, when available (Figure 5.1). Presence of compressions was determined via expert review of the TTI and ECG signals during data collection. Prior study has demonstrated the reliability of such manual annotation of chest compressions using the TTI signal.[92] Compressions were defined as present if they occurred during at least 90% of the segment; similarly, compressions were defined as absent if they occurred during less than 10% of the segment. Segments were collected with and without compressions regardless of the presence of ventilations.

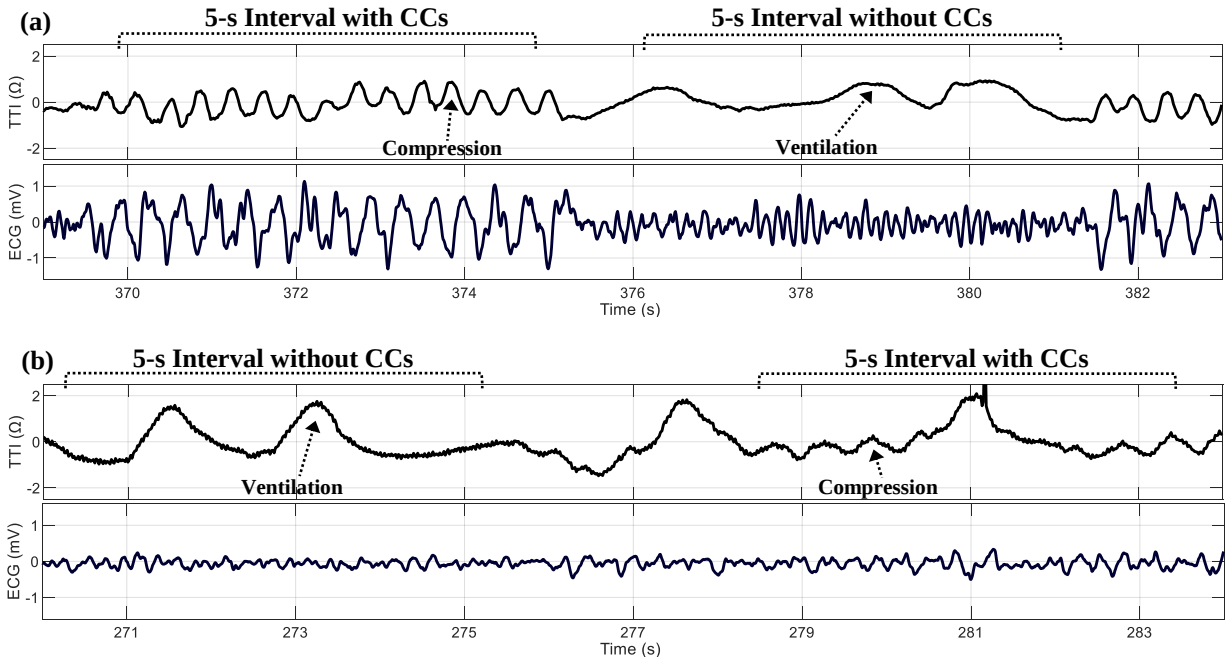

Figure 5.1 Transthoracic impedance segment collection
One 5-s transthoracic impedance segment was collected during CCs and one segment was collected without CCs prior to each of the first four defibrillation shocks. Impedance (concurrent with ventricular fibrillation electrocardiograms) is shown with relatively large CC artifact (a) and relatively small CC artifact (b). Ventilation artifact was frequently present in either compression state. The DC offset of all TTI signals is removed by the defibrillator's bandpass filters. (CC = chest compression, ECG = electrocardiogram, TTI = transthoracic impedance.)

Four defibrillator models with a range of sampling rates were used in this analysis. Lifepak 12 and Lifepak 15 TTI segments were recorded at a rate of 61.038 Hz and resampled at a ratio of 4:1[*], Forerunner 3 segments were recorded at a rate of 100 Hz and resampled at a ratio of 5:2, and MRx segments were recorded at a rate of 200 Hz and resampled at a ratio of 5:4. Each segment was filtered to remove offset, drift, high-frequency noise, and artifact using a 1-10 Hz, 4th-order Butterworth bandpass filter with a forwards-backwards implementation.

[*] Lifepak TTI data were thus analyzed at a rate (250 Hz) slightly higher than their true rate (244 Hz) rather than implementing interpolation methods to resample the date to exactly 250 Hz, in order to test the potential for more-efficient real-world application of the current method.

5.3.3 *Classification Features*

The first classification feature, Median Deviation, describes TTI amplitude and is calculated as

$$Median\ Deviation = \text{median}(s_{0,\ldots k\ldots,K-1}), \tag{5.1}$$

where

$$s_{0,\ldots k\ldots,K-1} = \sqrt{\frac{\sum_{n=1+kW}^{W+kW}\left(|x_n| - \frac{1}{W}\left(\sum_{j=1+kW}^{W+kW}|x_j|\right)\right)^2}{W-1}}, \tag{5.2}$$

$x_{1,\ldots n\ldots,N}$ is the TTI input sample array of length N, n is the sample index, W is the window length (in samples), and the number of windows $K = \text{floor}(N/W)$ (Figure 5.2a).

The second feature, Power Ratio, was designed to describe the relative amount of power in the spectral range associated with chest compressions, and is calculated as

$$Power\ Ratio = \frac{\sum_{m=L_{PR}(M/f_s)}^{H_{PR}(M/f_s)} X_m}{\sum_{m=0}^{L_{PR}(M/f_s)-1} X_m + \sum_{m=1+H_{PR}(M/f_s)}^{(M/2)-1} X_m}, \tag{5.3}$$

where $X_{0,\ldots m\ldots,M-1}$ are the magnitude-squared values of the $M-$point Discrete Fourier Transform of the TTI input signal, m is the frequency index of X, the sampling rate $f_s = 250$ Hz, and L_{PR} and H_{PR} are low and high frequency limits in Hz (Figure 5.2b).

The third feature, Max Power, which was designed to characterize the dominant frequency in spectral range associated with compressions, is defined as

$$Max\ Power = \max(X_m),\ \ \{m \mid L_{MP}(M/f_s) \le m \le H_{MP}(M/f_s)\}, \tag{5.4}$$

where L_{MP} and H_{MP} are low and high frequency limits in Hz (Figure 5.2c).

Prior to computing their Discrete Fourier Transforms, all TTI input segments were zero-padded to a length of $M = 2048$ samples. Parameter optimizations for each feature are illustrated in Figure 5.2d-f.

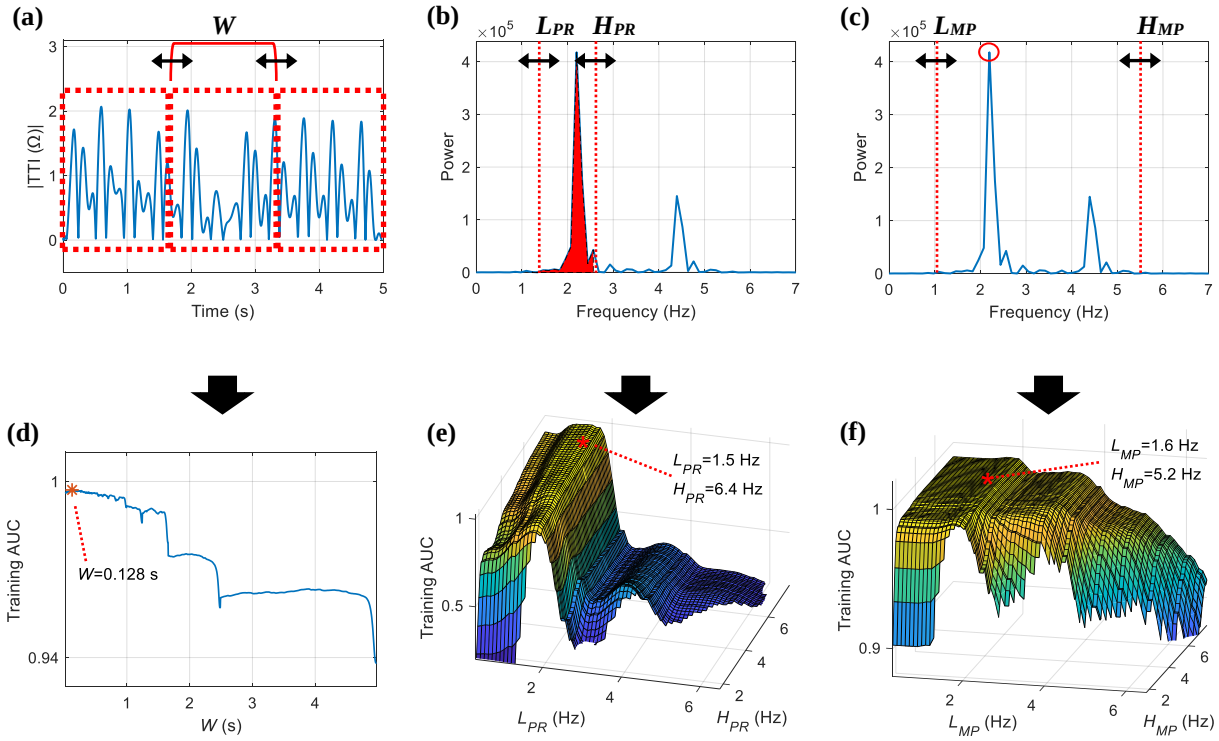

Figure 5.2. Feature calculation and parameter optimization
(a) Absolute TTI signal during CCs. *Median Deviation* is the median of standard deviations within windows of length *W*. (b) TTI power spectrum during CCs. *Power Ratio* is the power within the frequency interval (L_{PR},H_{PR}) divided by the remaining power outside the interval. (c) Example of the TTI power spectrum during CCs. The *Max Power* feature is the maximum power within the interval (L_{MP},H_{MP}). (d) The *Median Deviation* window length *W* is selected to maximize training AUC. (e) The Power Ratio frequency range (L_{PR},H_{PR}) is selected to maximize training AUC. (f) The *Max Power* frequency range (L_{MP},H_{MP}) is selected to maximize training AUC. (AUC = area under the receiver operating characteristic curve, TTI = transthoracic impedance.)

5.3.4 *Classification Model*

To combine the three input features and predict chest compression state, a binary logistic classifier of the following form was used (see section 4.8.4.1 for further background on logistic models):

$$\text{logit}(P_{CC}) = \beta_0 + \beta_1(\textit{Median Deviation}) + \beta_2(\textit{Power Ratio}) + \beta_3(\textit{Max Power}), \quad (5.5)$$

where P_{CC} is the probability of chest compressions and β_{0-3} are the model coefficients.

5.3.5 *Primary Analysis*

Patients were randomly divided into training (40%) and validation groups (60%) for algorithm development and validation. Parameters for individual features and the logistic classification model were trained using the training data. Model performance for chest compression detection was evaluated using the validation dataset and characterized by the AUC. Classification decision thresholds based on the Optimal Operating Point of the training data receiver operating characteristic curves for each defibrillator model were used to determine sensitivity, specificity, and positive predictive value (PPV) for validation data.[186] Data and statistical processing were performed with MATLAB 2018a (The Mathworks, Natick, MA).

5.3.6 *Secondary Analysis*

A shorter TTI input length reduces latency for real-time compression detection, but could result in reduced classification performance. Therefore, we conducted a secondary analysis to determine the relationship between TTI segment length and performance. Training and validation TTI segments were truncated from 5s to 0.2s in increments of 0.6s. Truncation was performed by removing samples from the terminal end of each segment prior to bandpass filtering. At each truncated length, parameters for each of the three classification features were re-optimized and the logistic classifier re-trained on truncated training data. Classification performance on validation data at each truncated length was then compared to the performance using untruncated segments to determine how truncation affected performance. Specifically, we compared AUC values for truncated validation data segments versus the untruncated validation data segments using the DeLong method for correlated receiver operating characteristic curves, and applied an alpha of

0.05 adjusted for multiple comparisons with the Bonferroni correction to determine significance.[115] We then determined the segment length below which performance was significantly reduced compared to the original 5-s analysis.

5.4 RESULTS

Table 5.1 describes the characteristics of the 1151 subjects in the study cohort. A total of 4586 TTI segments were collected from 2755 shock cycles: 1682 (37%) from Lifepak 12 defibrillators, 779 (17%) segments from Lifepak 15 defibrillators, 379 (8%) segments from Forerunner 3 defibrillators, and 1746 (38%) segments from MRx defibrillators.

Table 5.1 Patient characteristics
Characteristics of patients in the study group. (EMS = emergency medical services; IQR = interquartile range.)

Patients, n	1151
Female, n(%)	265(23.0)
Age, median (IQR)	61(52, 72)
Presenting with ventricular fibrillation, n(%)	1151(100)
Cardiac etiology, n(%)	1080(93.8)
Location, n(%)	
Home	707(61.4)
Public	399(34.7)
Nursing Home	45(3.9)
Arrest before EMS arrival, n(%)	1093(95.0)
Witnessed, n(%)	885(76.9)
Bystander cardiopulmonary resuscitation, n(%)	833(72.4)
EMS Response (minutes), median (IQR)	5(4, 6)
Total shocks, median (IQR)	3(2, 6)
Return of spontaneous circulation at end of EMS care, n(%)	817(71.0)
Admit to hospital, n(%)	810(70.4)
Survive to hospital discharge, n(%)	524(45.5)
Survive with cerebral performance category 1 or 2, n(%)	471(40.9)

In the training set of 460 patients, there were 868 segments without chest compressions and 991 segments with compressions. Performance on training data for detecting compressions

was high, with AUC, sensitivity, specificity, and PPV ≥98% (Table 5.2, Figure 5.3). In the validation set of 691 patients, there were 1269 segments without chest compressions and 1458 segments with compressions. Performance on validation data was also high, with AUC, sensitivity, specificity, and PPV ≥98% (Table 5.2, Figure 5.3). Performance was comparable across the four defibrillator models (Table 5.3).

Table 5.2. Algorithm performance
Algorithm performance for detecting CCs is indicated for training and validation data. (AUC = area under the receiver operating characteristic curve, CI = confidence interval, PPV = positive predictive value, TTI = transthoracic impedance.)

	Training	Validation
Patients	460	691
TTI Segments	1859	2727
AUC [95% CI]	0.998 [0.995,0.999]	0.997 [0.993,0.999]
Sensitivity	99.0%	98.8%
Specificity	98.8%	98.8%
PPV	98.6%	98.7%

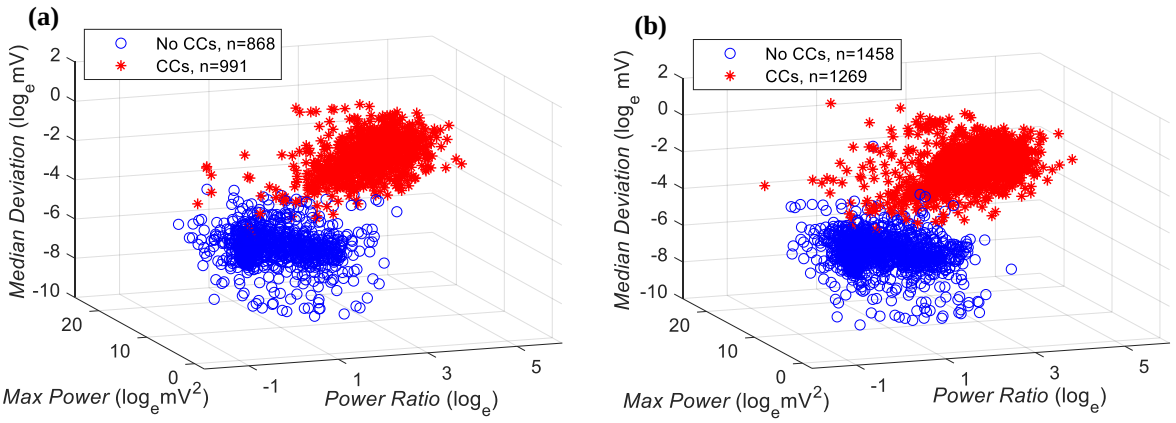

Figure 5.3. Feature scatterplots
(a) Features calculated from training segments. (b) Features calculated from validation segments. (CCs = chest compressions)

Table 5.3. Sensitivity and specificity by model
Performance for detecting compressions on validation data is stratified by defibrillator model.

	Lifepak 12	Lifepak 15	MRx	Forerunner 3
n(%)	974 (35.7%)	439 (16.1%)	1096 (40.2%)	218 (8.0%)
Sensitivity	99.3%	100.0%	98.3%	95.8%
Specificity	98.3%	98.8%	99.1%	100.0%

In our secondary analysis, performance on validation data was significantly decreased (AUC=0.92, sensitivity=87%, specificity=86%) as length was truncated from the original length of 5.0 s to the shortest length of 0.2 s (Figure 5.4). Compared to the full length of 5.0 s, input lengths below 3.2 s had a significantly-reduced AUC.

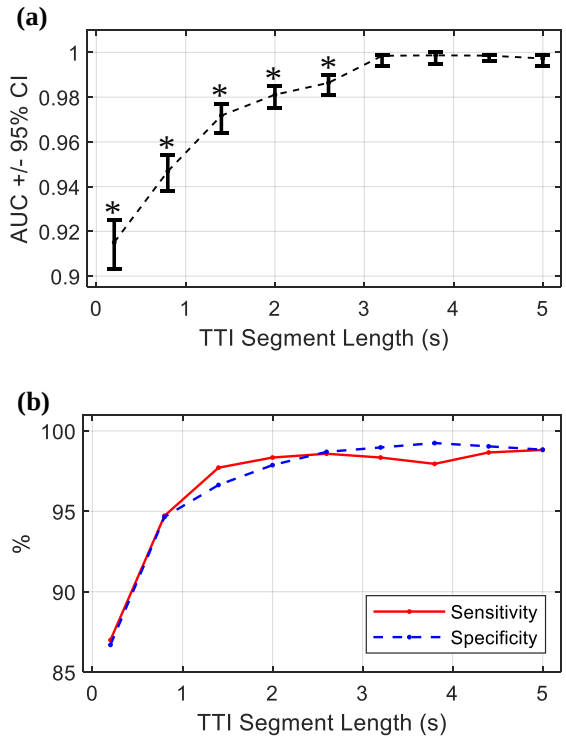

*significant difference versus AUC at 5 s (p<0.006)

Figure 5.4. Secondary analysis with varied input length
(a) Validation AUC versus TTI segment length. (b) Validation sensitivity and specificity versus TTI segment length. (AUC = area under the receiver operating characteristic curve, CI = confidence interval, TTI = transthoracic impedance.)

5.5 DISCUSSION

In this investigation of 1151 persons suffering out-of-hospital cardiac arrests, we demonstrate a novel method to detect the presence of chest compressions using the TTI signal. High performance (AUC, sensitivity, and specificity ≥98%) was observed using TTI segments ranging from 3.2 – 5 s in length. Performance was robust across a variety of defibrillator platforms. These results demonstrate potential to use TTI as a ubiquitous strategy for automated, computationally-efficient detection of the real-time compression state during resuscitation.

High-quality, minimally-interrupted CPR is an important link in the 'chain of survival' for treatment of cardiac arrest.[3,31,32] Outcomes may be improved by minimizing pauses in chest compressions and prompting rescuers to provide hands-on-compressions throughout resuscitation.[47,176] Moreover, while current ECG rhythm diagnostic algorithms require CPR pause for analysis, there is increasing interest in rhythm analysis during active compressions so as to continuously inform ECG rhythm status during uninterrupted CPR.[39,44,45,73] Some experimental algorithms designed to assess the ECG rhythm during CPR apply parameter and filter settings depending on the presence of compressions and thus require accurate classification of the real-time compression state.[91,123,127,187]

Commercially-available defibrillator review software has a reported sensitivity of 94% and PPV of 90% for annotating individual chest compressions using TTI.[92] Other prior methods to detect compressions have demonstrated sensitivity and specificity values ranging from 94–97%.[93–96] In a recent investigation, we demonstrated a method (accuracy=0.98%) for identifying presence of compressions by TTI using hidden Markov modeling.[73] However, this Markov method integrates repeated analysis buffers from continuous TTI signals that precede the analyzed segment and so may not perform optimally on isolated segments. Ideally, a TTI method to actively guide

CPR administration or to inform ECG algorithms of the compression state would achieve high performance across a range of defibrillator platforms using isolated TTI segments.

In the current investigation we describe a method to detect compressions using a combination of time- and frequency-domain features derived from isolated TTI segments. High classification performance was observed using validation data. We hypothesize that the observed performance was enabled by the use of both frequency- and amplitude-based features, in contrast to prior methods which are limited to time-domain techniques (such as detecting individual compression peaks).[93–95] In the current method, frequency cutoffs selected using a large training dataset allow inclusion of characteristics indicative of compressions while excluding other phenomena. For example, the optimized range for evaluation of the *Power Ratio* feature was 1.5 – 6.4 Hz, which inherently excludes perturbations such as low-frequency ventilations or high-frequency artifact that might otherwise cause false positives using time-domain amplitude alone (Figure 5.5). Notably, assuming a typical compression rate of approximately 100-120 compressions per minute as specified in guidelines, the optimized range for *Power Ratio* would generally include the fundamental and first two harmonic frequencies of chest compressions (such as observed in Fig. 5d) while the optimal range for *Max Power* (1.6 – 5.2 Hz) would tend to include only the fundamental and first harmonic. Likewise, the optimal window length for calculation of *Median Deviation* (0.13 s) indicates that short-term (i.e. higher-frequency) amplitude information may be more robust against artifact such as ventilations, with use of the median operation excluding any singular transient artifacts (such as the artifact in Figure 5.1b at 281 s).

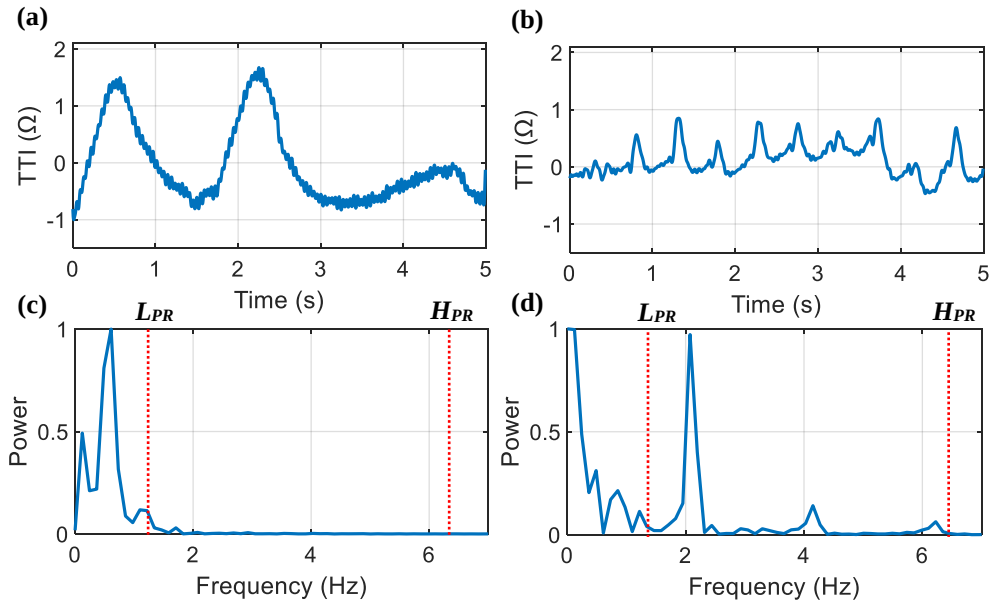

Figure 5.5. Example of *Power Ratio* of ventilations versus compressions
(a) TTI segment without CCs during ventilations. (b) TTI segment during CCs without ventilations. (c) Power spectrum of ventilation artifact exhibits low relative power in the optimized Power Ratio interval (L_{PR},H_{PR}), suggesting the absence of CCs. (d) Power spectrum of CCs has increased relative power in the optimized Power Ratio interval (L_{PR},H_{PR}), suggesting the presence of CCs. For illustrative purposes, power spectra in this example are normalized and TTI segments are unfiltered. (CCs = chest compressions, TTI = transthoracic impedance.)

The study cohort includes data from multiple device types. The majority of prior studies have used data collected from a single defibrillator model type to develop and evaluate TTI-based chest compression detection algorithms, and it is unclear whether these algorithms are generalizable to other sampling rates or other devices.[73,93–95] Hence, the current investigation includes TTI data sampled at rates ranging from 61-200 Hz collected from four different device models. To maximize inter-device compatibility, TTI data was homogenized by resampling and bandpass filtering, and feature calculation was limited to frequencies well within the smallest sampling bandwidth. The use of heterogenous sampling rates in conjunction with a relatively large validation dataset of 691 patients suggests that the current results have the potential to generalize to other devices and populations.

We conducted a secondary analysis using a range of TTI input segment lengths. The TTI length required for accurate analysis directly affects the real-time delay for detection of the current compression state. For instance, ideally rescuer prompts of chest compression interruption could be issued almost instantaneously depending on the circumstance so as to enable timely feedback. However, more-immediate compression state detection may result in a potential decrement in performance as the TTI segment is shortened. Prior studies have not evaluated the relationship between TTI segment length and chest compression detection performance.[73,92–95] We observed that the current method maintained consistently high performance (i.e., sensitivity and specificity ≥ 98%) using segment lengths as short as 3.2 s, and that performance was steadily but only moderately reduced (i.e., sensitivity and specificity ≥ 95%) as length was reduced from 3 s to 0.8 s. While the optimal trade-off between analysis length and performance is uncertain, these results highlight the potential to adapt the current method to different applications based on performance and latency requirements.

5.6 LIMITATIONS

This study has limitations. We used TTI segments during which chest compressions were present (or absent) for a minimum of 90% of that interval, and we did not include more-heterogeneous segments (such as those that might be collected during analysis of an entire continuous arrest) which may have a greater misclassification rate. Individual chest compressions were not singularly identified as in other investigations; rather, the investigation was limited to prediction of an overall presence of compressions for each input segment. However, this limitation allowed inclusion of robust frequency-based classification features. The study was conducted in a region with well-trained EMS personnel; therefore, the quality of chest compressions may be more consistent and easier to detect than that in other systems. The cohort was limited to patients presenting to EMS

with an initial rhythm of ventricular fibrillation, which may limit generalizability across patient populations. In addition, TTI segments were collected during episodes of ventricular fibrillation and not during other ECG rhythms present during attempted resuscitation (i.e. non-shockable rhythms).[91] However, results of a supplemental validation were similar using TTI segments collected during non-shockable ECG rhythms from a random subset of validation patients (Appendix A). Lastly, the study was retrospective; ideally results should be confirmed in a prospective investigation in another system.

These limitations should be considered in the context of this study's strengths. Specifically, the study used a large human cohort to independently train and validate an algorithm with potential to improve CPR application and ECG rhythm diagnosis during resuscitation from cardiac arrest.

5.7 Conclusion

This investigation demonstrates a method to reliably identify the presence of chest compressions using a combination of time- and frequency-domain features of the TTI signal. Overall performance was relatively high compared to prior methods, and robust using TTI segments as short as 3.2 s across multiple defibrillator platforms. Thus, the current method has potential to provide timely prompts for rescuer CPR and inform ECG rhythm diagnostic algorithms of the real-time compression state.

5.8 Acknowledgements

MATLAB code for comparisons of correlated receiver operating characteristic curves by the DeLong method was provided by John W Pickering (University of Otago, Christchurch, New Zealand). Informative discussions regarding compression detection were conducted in conjunction

with Chenguang Liu (Philips Healthcare, Bothell, WA). This work was supported in part by grants provided to the University of Washington by the Washington State Life Sciences Discovery Fund, Philips Healthcare, and the National Institute of Biomedical Imaging and Bioengineering of the National Institutes of Health (T32EB001650). The content of this work is solely the responsibility of the authors and does not represent the views of the funding organizations, Public Health – Seattle & King County, Philips Healthcare, or Physio-Control.

5.9 Appendix A: Validation During Organized Rhythm

5.9.1 *Introduction*

The primary study evaluated a method to detect chest compressions (CCs) using a dataset of transthoracic impedance (TTI) segments collected during periods of ventricular fibrillation prior to defibrillation shock. However, the primary study did not evaluate the effect of cardiac rhythm type on detection of CCs using TTI. Presence of a pulse may cause regular perturbations visible in TTI at frequencies similar to CCs, and thus may confound detection of CCs using TTI.[129] Therefore as a supplemental validation to confirm ability to detect CCs during a non-shockable cardiac rhythm, we evaluated performance for detecting CCs using a supplemental validation set of TTI segments collected during intervals with organized rhythm visible in the electrocardiogram (ECG).

5.9.2 *Methods*

Following each of the first four defibrillation shocks from random subset of 25% the study validation patients, one 5-s TTI segment was collected during CCs and one segment was collected without CCs during periods in which QRS complexes were visible in the ECG (Figure 5.6).

Performance of the CC detection model was then evaluated on these additional validation segments using the parameters and classification thresholds selected in the primary study.

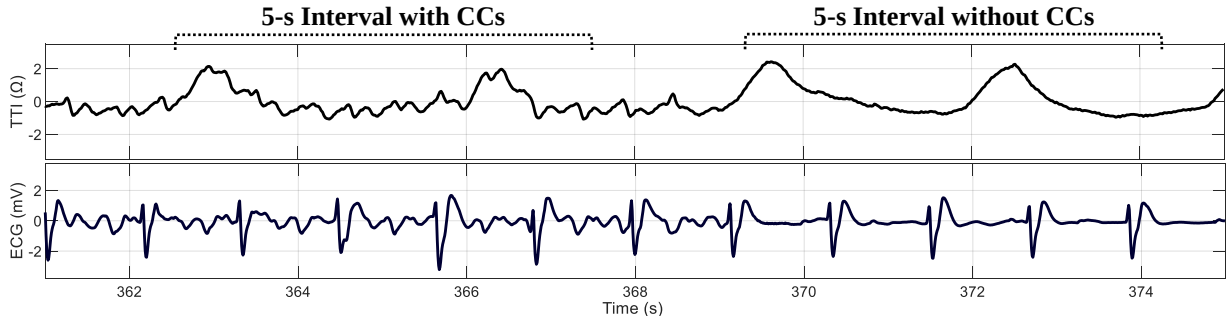

Figure 5.6: Collection of supplemental validation segments during organized rhythm
One 5-s TTI segment was collected with and without CCs from a random 25% subset of validation patients during intervals with QRS complexes visible in the ECG. (CCs = chest compressions; ECG = electrocardiogram; TTI = transthoracic impedance.)

5.9.3 *Results*

Performance for detection of CCs using the supplemental TTI segments collected during organized cardiac rhythms was similar to the primary study results (Table 5.4), suggesting that organized ECG rhythm does not significantly confound ability of the algorithm to detect CCs.

Table 5.4. Results for TTI segments collected during organized rhythm
Results for detecting CCs using TTI segments collected during Non-Shockable Organized rhythms from a random subset of 25% the study validation patients. Results are presented next to main study results for comparison. (AUC = area under the receiver operating characteristic curve; CCs = chest compressions; CI = confidence interval; PPV = positive predictive value; TTI = transthoracic impedance.)

	Supplemental Validation Results	**Main Study Validation Results**
Rhythm Visible in ECG	Organized Rhythm	Ventricular Fibrillation
Validation Patients	173 (25%)	691 (100%)
TTI Segments with CCs	297	1269
TTI Segments without CCs	197	1458
Total TTI Segments	494	2727
AUC [95% CI]	1.000 [0.998,1.000]	0.997 [0.993,0.999]
Sensitivity	99.7%	98.8%
Specificity	98.0%	98.8%
PPV	98.7%	98.7%

Chapter 6. NOVEL METHOD TO PREDICT DEFIBRILLATION OUTCOME WITHOUT INTERRUPTING CHEST COMPRESSIONS

Unpublished by **Coult J**, Blackwood J, Kudenchuk P, Kwok H, Rea T. (Preliminary results of this work were presented at the American Heart Association Resuscitation Science Symposium, November 10-11 2018, Chicago, IL, USA.)

6.1 ABSTRACT

Background: Out-of-hospital ventricular fibrillation (VF) cardiac arrest is a leading cause of death. Quantitative measures of the VF electrocardiogram (ECG) predict myocardial amenability to therapy and thus provide opportunity to guide treatment during resuscitation, but have traditionally required chest compression (CC) interruption to allow analysis. A recent prior study demonstrated improved waveform measure performance during continuous CCs using machine learning to combine existing measures. However, overall performance during CCs as measured by area under the receiver operating characteristic curve (AUC) remained modest, and prediction of return of sinus rhythm following shock was significantly reduced during CCs. We therefore sought to determine whether a novel method designed for use both during and without CCs could further improve prediction of patient outcome over the best-performing method from recent previous investigation. *Methods:* We used a previously-described dataset of 5-s VF ECG segments with and without CC artifact collected from N=1151 patients. Using data from training patients (n=460), ten quantitative VF waveform features and three categorical features were designed to predict survival and return of rhythm. Parameters were optimized with and without CCs separately. CCs were detected automatically using chest impedance. An adaptive ECG filter based on CC frequency was applied to remove compression artifact. Features were combined using a series of support vector machine and logistic models. Prognostic performance was evaluated using data

from validation patients (n=691). *Results:* AUC (95% CI) for predicting survival was 0.753 (0.725-0.781) during CCs and 0.762 (0.737-0.788) without CCs (p=0.63 for difference). AUC (95% CI) for predicting return of rhythm was 0.741 (0.714-0.768) during CCs and 0.773 (0.750-0.797) without CCs (p=0.10 for difference). Compared to the prior best-performing method from a previous investigation, performance using the current method for predicting survival was not significantly improved during CCs (AUC increase=0.005, p=0.60) and without CCs (AUC increase=0.008, p=0.21). However, performance for predicting return of rhythm was significantly improved during CCs (AUC increase=0.042, p<0.001) and without CCs (AUC increase=0.028, p<0.001). *Conclusion:* A novel method designed to function during CCs demonstrated significantly-improved prediction of return of rhythm both with and without CCs. These results suggest potential for improved assessment of patient status during uninterrupted CCs.

6.2 Background and Significance

Out-of-hospital cardiac arrest caused by ventricular fibrillation (VF) results in approximately 50,000 deaths per year in the United States.[3] VF is a cardiac arrhythmia characterized by the presence of self-perpetuating waves of cardiomyocyte depolarizations manifesting as chaotic high-frequency activity in the electrocardiogram (ECG).[18] Cessation of coordinated ventricular contraction during VF results in a lethal loss of blood flow. Treatment of VF consists of electrical defibrillation to reinstate organized rhythm as well as continuous cardiopulmonary resuscitation (CPR) and vasopressors to sustain perfusion.[31]

Current resuscitation treatment by Basic Life Support and Advanced Cardiovascular Life Support providers follows a fixed algorithmic protocol based on a two-minute CPR cycle. In this protocol the ECG is analyzed once electrodes are attached, shock is applied immediately if VF is detected, and CPR is then administered. CPR is subsequently paused every two minutes to allow

repeated ECG analysis and shock.[31,32] However, this approach is applied regardless of the patient's underlying physiologic status. Under the current approach, a significant portion of defibrillation attempts fail, and depending on shock energy delivered, these repeated failed shocks may cause myocardial tissue damage and should be avoided.[188,189] Given the current shock failure rate and the disparities in VF survival (ranging from approximately 3% to over 40%) across different systems, there may be potential for improvement over the current one-size-fits-all algorithmic approach by modifying treatment based on real-time patient status.[3,28,31,49] For example, while applying immediate shock after VF onset typically results in successful conversion to organized rhythm, shocks applied to prolonged VF that has not been treated with CPR (e.g. such as during an initially-unwitnessed out-of-hospital arrest) are typically unsuccesful.[34,35] These shock failures are due in part to the metabolically-compromising effects of myocardial ischemia during VF, which reduces the ability of the heart to autonomously pace into a viable organized rhythm following defibrillation.[190] Studies have demonstrated improved outcomes by delaying initial shock to allow CPR prior to defibrillation if the myocardium is assumed to be metabolically compromised. Specifically, when a patient has sustained >4-5 minutes of untreated VF, temporarily delaying initial shock for several minutes to perfuse myocardial tissue using CPR and vasopressor medications prior to defibrillation may improve shock success over the current approach of early defibrillation.[35,40,41,191] However, modifying treatment based on the assumed duration of untreated VF is problematic due to the fact that time since VF onset is difficult to assess in the out-of-hospital setting.

Rather than inferring the state of the myocardium based on assumed VF duration, direct assessment of myocardial physiology may offer a better means to inform defibrillation-versus-CPR priority and potentially improve shock success and survival.[45] Patients with a high likelihood

of successful shock may warrant the current practice of immediate defibrillation, while patients with poor prognosis and predicted shock failure may benefit from delayed defibrillation to allow an interim period of CPR and medication.[34,56] Indeed, the 2015 American Heart Association Advanced Cardiac Life Support summary states that continuously monitoring patient physiology during resuscitation provides important information about a patient's response to real-time therapy such as CPR, and that real-time monitors of patient physiology could potentially be used in real time to optimize administration of therapy.[31] Thus, adjusting treatment based on automated feedback that directly reflects a patient's individual physiology over the course of resuscitation may improve outcomes.

Quantitative measures of the VF waveform describe ECG characteristics such as amplitude, frequency, and complexity.[45,62,88] These waveform measures predict defibrillation success and reflect the metabolic state of the myocardium, making them a potential candidate to monitor patient physiology during resuscitation and adjust shock timing to maximize defibrillation success.[22,45,60,65] Furthermore, since measures can be calculated using ECG segments only seconds in length,[114] they offer a potential means by which to instantaneously gauge the quality of resuscitative treatments such as CPR or specific medications,[192,193] with their trajectory over time also potentially informing rescuers whether or not such treatments are being administered effectively over the course of resuscitation.[86]

Chest compression artifact during CPR obscures the ECG. Artifact is primarily introduced through mechanical disturbance of the electrode-skin interface, but artifacts may also be caused by electrical and impedance changes from compression of the thorax or by transient cardiomyocyte depolarizations induced by physical compression impacts on myocardial tissue.[44,126,194] Thus, CPR pause is required for optimal ECG analysis including calculation of waveform measures.[34,39,43–

[45,67] However, pauses in chest compressions result in rapid loss of perfusion pressure, and even short pauses can negatively affect patient outcomes; for example one study estimates an 18% decrease in survival for every additional 5-s pre-defibrillation pause.[31,46,47,55,195] An ideal VF waveform measure would assess a patient's status during uninterrupted CPR without any reduction in prognostic performance.[45] Prior investigations of VF waveform measures during CPR have been limited to a small number of studies that did not directly compare prognostic performance with versus without CPR; thus, while there is consensus that CPR pause is required for ECG analysis in general, the true effect of compression artifact on prognostic measures of the VF waveform has been largely unknown.[68,111,122]

Therefore in a recent benchmark study of current VF waveform prognostic measures, we demonstrated that most measures are significantly confounded by compression artifact.[91] Furthermore, we demonstrated that optimizing individual measures for use during compressions and combining them using a support vector machine model allowed improved prediction of survival in the presence of compression artifact. This improved prediction was enabled in part through use of parameters and machine learning models optimized separately with and without compressions; however, presence of chest compressions was annotated manually rather than automatically, and it is unknown whether waveform measure calculation blinded to the presence of compressions under real-world conditions would achieve similar performance. In addition, we observed that while similar prediction of survival could be achieved during chest compressions versus without compressions, prediction of the more immediate outcome of return of organized rhythm following defibrillation was still significantly reduced by compression artifact. Furthermore, even without artifact performance overall was only moderate, calling into question the potential for clinical application. Therefore in spite of recent advances, there is a need for a

novel, improved algorithm that can achieve high prognostic performance and is not significantly compromised during chest compressions.[45,56]

To improve prognostic analysis during resuscitation, additional categorical variables could potentially be used in conjunction with ECG-based measures of the VF waveform. In a recent prior study, we demonstrated that return of organized rhythm following a shock is associated with increased likelihood of subsequent shock success, and can thus be leveraged to improve waveform measure analysis of subsequent shocks following initial shock.[127] Use of such a variable would require detection of return of rhythm in the ECG to determine prior shock success. Hence, in additional related study, we demonstrated accurate ECG rhythm identification during chest compressions using wavelet-based features; this classification algorithm in theory could be used by an automated defibrillator to detect return of rhythm following shock and thus enable incorporation of shock success into a potential VF-waveform-based prognostic algorithm.[72] However, incorporation of this binary categorical variable would be limited, as it can only be applied to analysis of repeated shocks following the initial shock. It is therefore unclear whether incorporation of such a variable would offer an overall benefit to a prognostic algorithm designed to predict response to all shocks.

In addition to using a patient's prior response to shock to improve prognosis in combination with features of the VF waveform, Utstein variables such as witnessed status, age, sex, response time, and bystander CPR are also significantly associated with patient outcome and may be useful in improving prediction of patient outcomes.[102,128] However, while incorporating a patient's Utstein characteristics could improve a prognostic algorithm in retrospective analysis, a majority of Utstein variables may not be immediately known or easily incorporated into a defibrillator during treatment of out-of-hospital cardiac arrest in real time. Thus, a potential strategy

incorporating Utstein-like variables that could be easily entered into a defibrillator during resuscitation would be limited to one or two binary variables obvious to rescuers at the scene of the arrest (e.g. sex).

Active removal of chest compression artifact from the ECG may enable improved prognosis during CPR. Much investigation has been conducted with regards to filtering compression artifact from the ECG, with a recent review citing over 120 studies related to the subject.[123] The focus of such investigations, however, has been in the application of improving ECG rhythm classification during compressions (rather than predicting patient outcomes as in the current investigation). A general consensus is that techniques for the removal of compression artifact can partially – but not completely – reduce the negative effects of artifact on such ECG classification algorithms.[44] Compression artifact, which can have transient effects up to 20 Hz but is primarily located in the first few compression harmonics between 1-6 Hz, is difficult to remove from VF signals because the artifact overlaps the typical 3-8 Hz spectral range of VF.[54,122,123]

In a recent pilot investigation, we demonstrated that fixed-frequency (4 Hz) high-pass filtering to remove the fundamental and first compression harmonic can significantly improve waveform measure prediction of two representative waveform measures during compressions, although filtered performance was still significantly reduced compared to compression-free analysis (see Figure 3.7. AUC for filtered and unfiltered data with and without CPR).[127] In subsequent recent investigation, we demonstrated improved waveform measure performance during chest compressions by varying high-pass frequency cutoffs for individual measures rather than selecting filter cutoffs *a priori*; in this previous investigation, many measures demonstrated optimal performance using a 6 Hz high-pass cutoff frequency (see Table 4.9 Waveform measure parameters with variable filter cutoffs).[91] These prior results confirm that removal of the

fundamental and first two harmonics of compressions may be useful versus simply removing the fundamental compression frequency (assuming the guidelines-based compression rate of 100-120 compressions per minute). Adaptive filtering may offer even greater benefit than such fixed-frequency high-pass filters, but as adaptive filters have not previously been applied in conjunction with VF waveform prognostic algorithms, it is unknown whether prognostic performance during compressions would actually be improved through use of an adaptive filter.[39,54,123,150,196] In general, prior investigations have observed that adaptive filters informed by a second reference channel outperform filters based on the ECG alone; these results suggest that incorporation of a reference signal (such as chest impedance) may be beneficial for application of an adaptive in the current investigation over simply filtering based on ECG characteristics alone.[123,182]

In the current investigation, we therefore sought to develop a novel prognostic algorithm and to determine whether this novel algorithm can improve prediction of patient outcomes both with and without chest compressions under real-world constraints. We hypothesized that integration of novel VF waveform measures, categorical variables, and adaptive filtering would significantly improve prediction of outcomes over the performance of prior prognostic methods.

6.3 METHODS

6.3.1 *Overview and Experimental Design*

We sought to determine whether a novel prognostic algorithm designed specifically for use during chest compressions would achieve improved prediction of patient outcomes. We hypothesized that a novel algorithm would demonstrate increased prediction when compared against best-performing prognostic methods identified in our previous benchmark investigation.[91]

First, using training data, an adaptive filter was designed to remove compression artifact (Figure 6.1). Training data was then used to develop features of the filtered and unfiltered VF ECG, and to identify binary categorical variables associated with patient outcomes. VF features and binary variables were combined using machine learning models to predict outcome. To determine whether the algorithm improved performance over existing methods, we selected the highest-performing method from our prior benchmark study of current waveform measures to serve as a reference.[91] Using validation data, we then compared the novel method against the best-performing previous existing method, and determined whether the novel algorithm significantly improved prediction of patient outcome. To better understand how such an algorithm would perform under real-world conditions, we constrained the algorithm during validation by blinding it to the presence of chest compressions and limiting input information to what would feasibly be available at the current point of analysis.

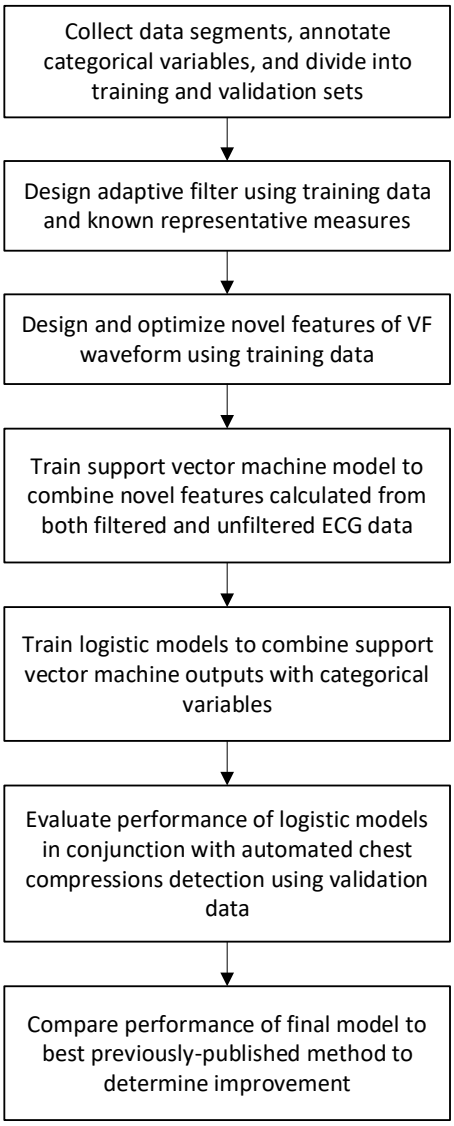

Figure 6.1 Algorithm design process
The current investigation sought to design a novel prognostic algorithm and determine whether the algorithm achieved improved prediction of patient outcomes during chest compressions compared to prior methods. (ECG = electrocardiogram, VF = ventricular fibrillation)

To characterize the relative utility of the individual ECG features employed by the novel algorithm described in this investigation, the prognostic performance of each feature was also evaluated individually on validation data. Furthermore, to serve as a reference for the relative difficulty of the study data versus data used across other studies, an established well-characterized measure (the Amplitude Spectrum Area) was evaluated on validation data.[65,97]

6.3.2 *Study Population and Setting*

The study population consisted of out-of-hospital cardiac arrest patients presenting to emergency medical services (EMS) with an initial rhythm of VF from 2005-2015 in King County, WA (excluding Seattle) that had complete defibrillator recordings available. The cohort included patients treated with Lifepak 12, Lifepak 15 (Physio-Control, Redmond, WA), Forerunner 3, and HeartStart MRx (Philips Healthcare, Bothell, WA) automated biphasic defibrillators. Patients were excluded if they were treated by a public access or police defibrillator prior to EMS arrival or were age <18. The study system employs a two-tiered 9-1-1 response, with emergency medical technician firefighters trained in basic life support followed by paramedics trained in advanced cardiovascular life support. The system implements American Heart Association resuscitation treatment guidelines.[31] The system maintains a data registry of out-of-hospital cardiac arrests that includes Utstein characteristics, clinical outcomes, medications, and defibrillator downloads which contain audio, ECG, and chest impedance data.[128]

This study and waiver of informed consent were approved by the Research Review Committee of King County Public Health and the Institutional Review Board at the University of Washington Human Subjects Division.

6.3.3 *Dataset*

We collected the study data previously for a prior study of VF waveform measures.[91] The data included 5-s ECG and transthoracic impedance (TTI) segments concurrently collected through the 2-lead paddle electrodes during periods of VF. When available, one VF segment was collected during chest compressions and one segment was collected without compressions immediately prior

to the first four defibrillation shocks. Presence of chest compressions and VF were confirmed by expert review of the TTI and ECG signals (Figure 6.2).

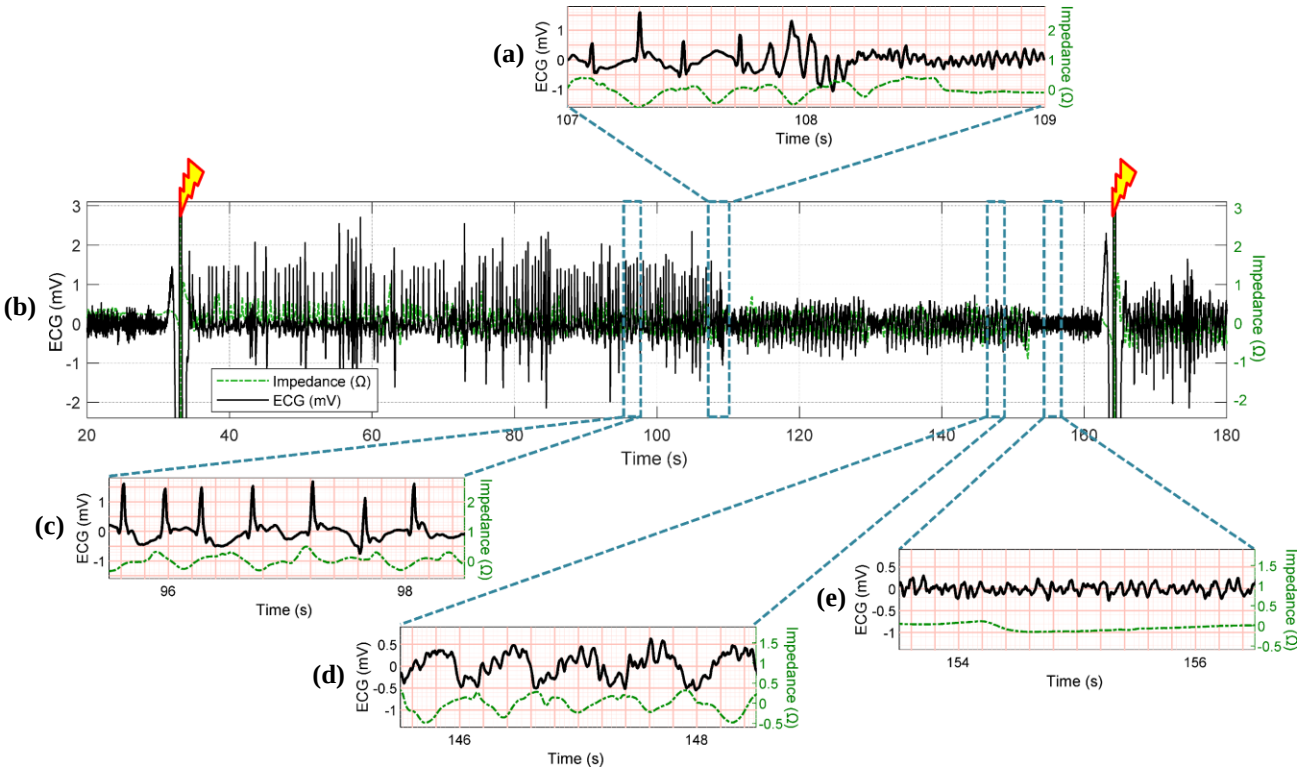

Figure 6.2 ECG examples
(a) Reentry (onset of VF). (b) Overview plot with defibrillation shocks illustrated at approximately 35 s and 165 s. (c) Return of organized rhythm following the first shock. (d) VF during chest compressions prior to the second shock. (e) VF without chest compressions prior to the second shock. Baseline offset of all signals has been removed for display. (ECG = electrocardiogram, VF = ventricular fibrillation.)

As described previously, after data collection and exclusions, the final study cohort included 1151 patients with usable data during the study period (Table 6.1).[91] The randomized training (40%) and validation (60%) division of the cohort patients performed in the prior investigation was preserved to allow direct comparison of validation results between the current and prior study (Figure 6.3).

Table 6.1 Patient characteristics
Characteristics of the patients in the study group.

Characteristic	n
Patients, n	1151
Female, n(%)	265(23.0)
Age, median (IQR)	61(52, 72)
Presenting with ventricular fibrillation, n(%)	1151(100)
Cardiac etiology, n(%)	1080(93.8)
Location, n(%)	
Home	707(61.4)
Public	399(34.7)
Nursing Home	45(3.9)
Arrest before EMS arrival, n(%)	1093(95.0)
Witnessed, n(%)	885(76.9)
Bystander cardiopulmonary resuscitation, n(%)	833(72.4)
EMS Response (minutes), median (IQR)	5(4, 6)
Total shocks, median (IQR)	3(2, 6)
Return of spontaneous circulation at end of EMS care, n(%)	817(71.0)
Admit to hospital, n(%)	810(70.4)
Survive to hospital discharge, n(%)	524(45.5)
Survive with cerebral performance category 1 or 2, n(%)	471(40.9)
Median estimated chest compression rate (IQR)*	112/min (95, 128)

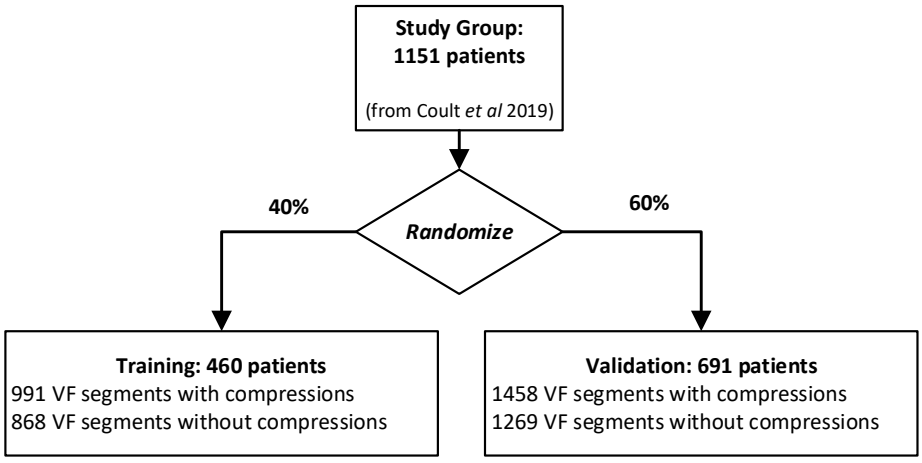

Figure 6.3 Study dataset
5-s VF ECG segments were collected from the study group patients

* Estimated chest compression rate for the study group patients was calculated based on the frequency of the greatest peak between 1.1–2.9 Hz in the upsampled spectra of the 5-s transthoracic impedance segments.

6.3.4 *Data Pre-Processing*

Because ECG and TTI signals used in this investigation were acquired from four different defibrillator models, all signal data were homogenized by resampling signals to 250 Hz and applying bandpass filters. Forerunner 3 ECG segments were collected at 200 Hz and resampled at a ratio of 5:4, and Forerunner 3 TTI segments were collected at 100 Hz and resampled at a ratio of 5:2. MRx ECG segments were collected at 250 Hz, and MRx TTI segments were collected at 200 Hz and resampled at a ratio of 5:4. Lifepak 12 and Lifepak 15 ECG segments were collected at 125 Hz and resampled at a ratio of 2:1, and Lifepak TTI segments were collected at 61.038 Hz and resampled at a ratio of 4:1. (Lifepak TTI segments were thus converted to a true rate of 244.152 Hz but analyzed at 250 Hz rather than interpolating to the signal to exactly 250 Hz. We have previously demonstrated this procedure to be sufficient for the purpose of detecting the presence of chest compressions in Chapter 5.)

While defibrillators internally acquire and analyze ECG signals at higher bandwidths (e.g. the Association for the Advancement of Medical Instrumentation specifies a 0.05-150 Hz diagnostic bandwidth), the bandwidth for stored data may be lower. As Forerunner 3 ECG data are collected in an unfiltered state, all raw Forerunner 3 ECG data were high-pass filtered at 0.5 Hz using a 2^{nd}-order Butterworth bandpass filter with forwards-backwards implementation to remove drift. MRx ECG data was collected raw but was assumed to be pre-filtered (by the device itself) to a maximum bandwidth of 0.15-40 Hz, and Lifepak ECG data was collected raw and assumed pre-filtered at a maximum bandwidth of 1.3-30 Hz. The exact bandwidth for exported MRx and Lifepak data are not explicitly listed in documentation, but reportedly the data have a bandwidth as narrow as 1.3-23 Hz or as wide as 0.05-40 Hz.[197–199] All TTI data were filtered from 1-10 Hz using a 4^{th}-order Butterworth bandpass filter with forwards-backwards implementation.

High-frequency information in the ECG is related to patient outcome and may offer a means to extract information above frequencies dominated by chest compression artifact, but high-frequency content is also prone to artifact.[44,68,91] Therefore, filtered and unfiltered ECG segments were both analyzed in this investigation in order to ensure inclusion of potentially useful high-frequency information (e.g. 30–40 Hz) in unfiltered ECGs while also allowing parallel analysis of filtered ECGs. Following resampling but prior to additional bandpass filtering, a copy of all unfiltered ECG data was saved for parallel analysis. ECG segments were then filtered from 1-30 Hz using a 4th-order Butterworth filter with forwards-backwards implementation to reduce transient artifacts, high-frequency noise, and drift (Figure 6.4). The mean value of each filtered and unfiltered ECG segment was also removed prior to subsequent analysis.

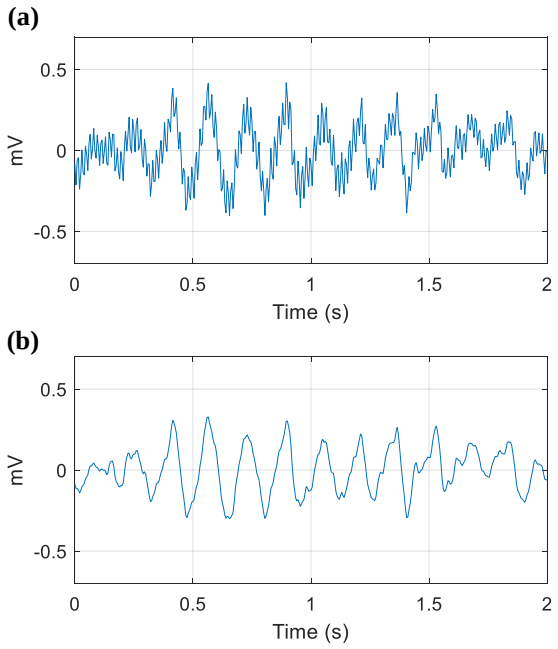

Figure 6.4 Example of powerline noise
(a) Original Forerunner 3 ECG with 60 Hz noise. (b) Forerunner 3 ECG after bandpass filtering.

6.3.5 *Study Outcomes*

Two patient outcomes were evaluated in the current investigation. Successful long-term outcome was defined as functional survival with a Cerebral Performance Category of 1 or 2.[107,108] Successful short-term outcome was return of rhythm after a defibrillation attempt, defined as a return of organized rhythm visible in the ECG for with a rate of >12 QRS complexes per minute following shock (see Figure 6.2).[127] Annotation of return of rhythm after shock in a random subset of 18% of the study patients by two reviewers had 93% agreement.[91]

6.3.6 *Algorithm*

We designed a novel algorithm to predict patient outcome based on information that could be obtained during treatment of a VF arrest and feasibly implemented in a defibrillator (Figure 6.5). Given a 5-s, 250 Hz ECG input segment with concurrent chest impedance, the algorithm computes 10 continuous features using both filtered and unfiltered ECGs (resulting in 20 total features), combines these 20 features in a support vector machine, and incorporates the support vector machine output with three categorical variables using logistic models to predict a final probability of positive patient outcome. The algorithm was restricted to analysis of inputs that would be available in real time during a resuscitation to demonstrate potential real-world application. For example, during validation, presence of chest compressions was determined automatically based on impedance, and incorporation of categorical variables such as prior return of organized rhythm was limited to information available up to the current point of analysis.

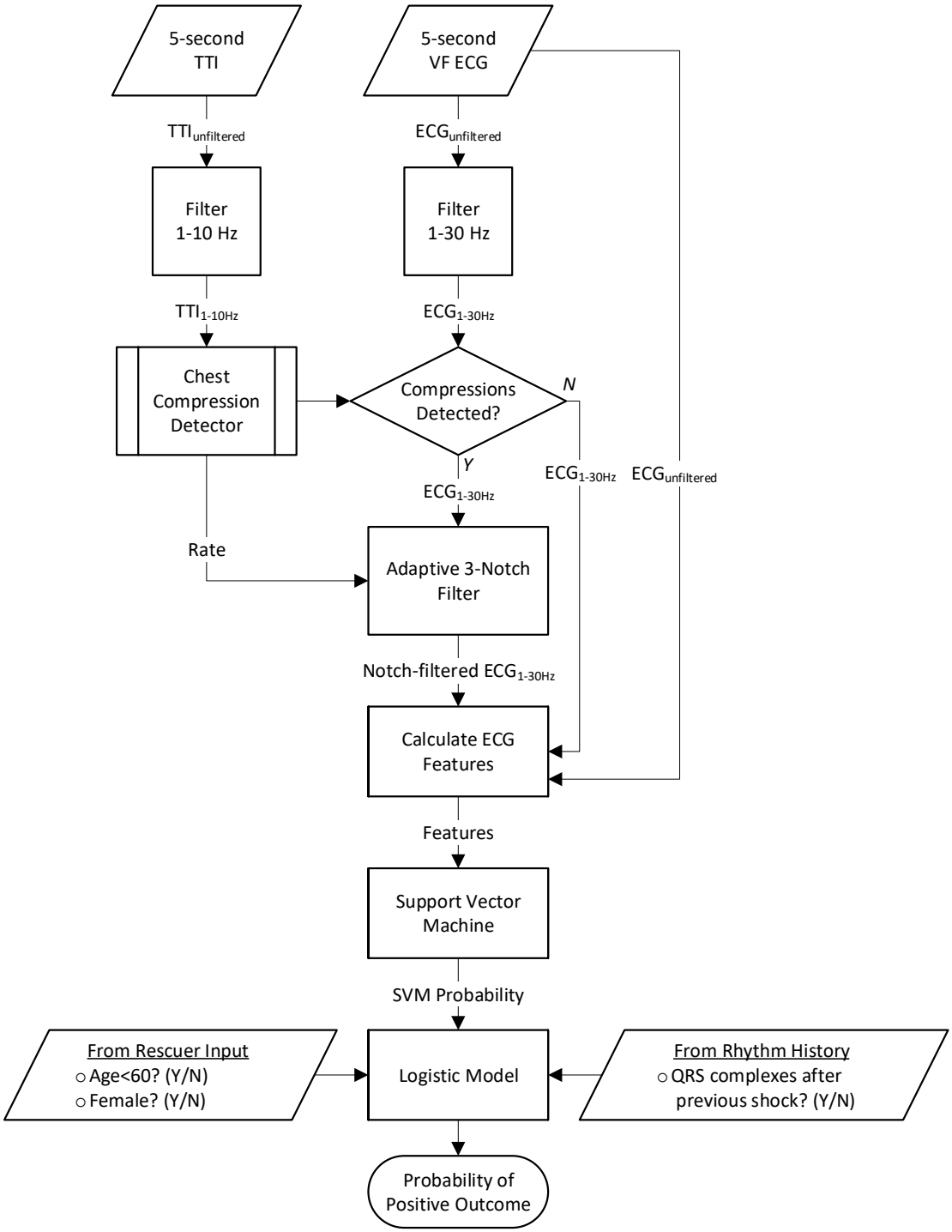

Figure 6.5 Novel prognostic algorithm overview
Novel algorithm incorporating electrocardiogram (ECG) and transthoracic impedance (TTI) signals to calculate novel features, apply adaptive filtering, and incorporate available categorical variables to predict patient outcome based on a 5-s buffer.

6.3.7 *Chest Compression Detection*

We applied an automated TTI-based chest compression detection function described previously (see Chapter 5). The detector accepts a 5-s TTI segment and predicts presence of chest compressions using a logistic regression model to combine time- and frequency-domain TTI features. While the presence of compressions in training data was annotated manually, we blinded the algorithm to the compression state during validation; hence, the compression state of each validation segment (and whether to apply feature and model parameters designed for use with versus without compressions) was determined by the compression detection algorithm.

6.3.8 *Adaptive Filter*

The novel algorithm included an adaptive notch filter that, during validation, was applied to bandpass-filtered ECG segments when compressions were automatically identified (Figure 6.5). Hence, to simulate real-world conditions, if an ECG segment without compressions was erroneously predicted to be undergoing chest compressions, the notch filter was applied to that segment in spite of any potential detriment and vice versa. Following the rationale of Gong et al., we implemented the adaptive filter based on the fundamental compression frequency f_{cc} in the TTI signal spectrum.[174] Deviating from the methods of Gong et al., we selected the estimated compression frequency f_{cc} as the frequency of the maximum peak within a predefined frequency range of the TTI spectrum. Although resuscitation guidelines dictate a target chest compression rate between 100-120 compressions per minute, rates can potentially vary widely by rescuer.[31,77] Therefore we conservatively assumed a maximum chest compression range of 66–174 compressions per minute, and thus selected the corresponding peak in the TTI spectrum between 1.1–2.9 Hz to determine estimated f_{cc}. Then, as the true frequency resolution in the ECG is greater

than that of the TTI by a factor of 2 to 4 depending on the device, f_{cc} was adjusted to match the exact compression peak frequency in the ECG spectrum within a tolerance of +/- 0.3 Hz of the original estimated compression frequency from the TTI spectrum. A series of Butterworth notch filters was then applied to the ECG using forward-backwards implementation and centered at frequencies f_{cc}, $2f_{cc}$, and $3f_{cc}$ to remove the fundamental and first two harmonic frequencies of compression artifact (Figure 6.6). Filter notch frequencies were based on multiples of the compression fundamental rather than individually adjusted to compression harmonic peak frequencies observed in the ECG spectrum, as dominant VF rotor frequencies are typically centered at approximately 3-8 Hz and may overlap (and thus hinder precise detection of) the first and second compression harmonics.[17,18,54,200] Filter parameters (notch bandwidth = 0.55 Hz, filter order = 2, number of notches = 3) were selected empirically by varying parameters to maximize training AUC for predicting survival using a representative group of waveform measures.

We confirmed significant utility of the final filter implementation on training data by calculating AUC values for predicting outcomes with three representative measures before versus after applying the notch filter (Table 6.2).

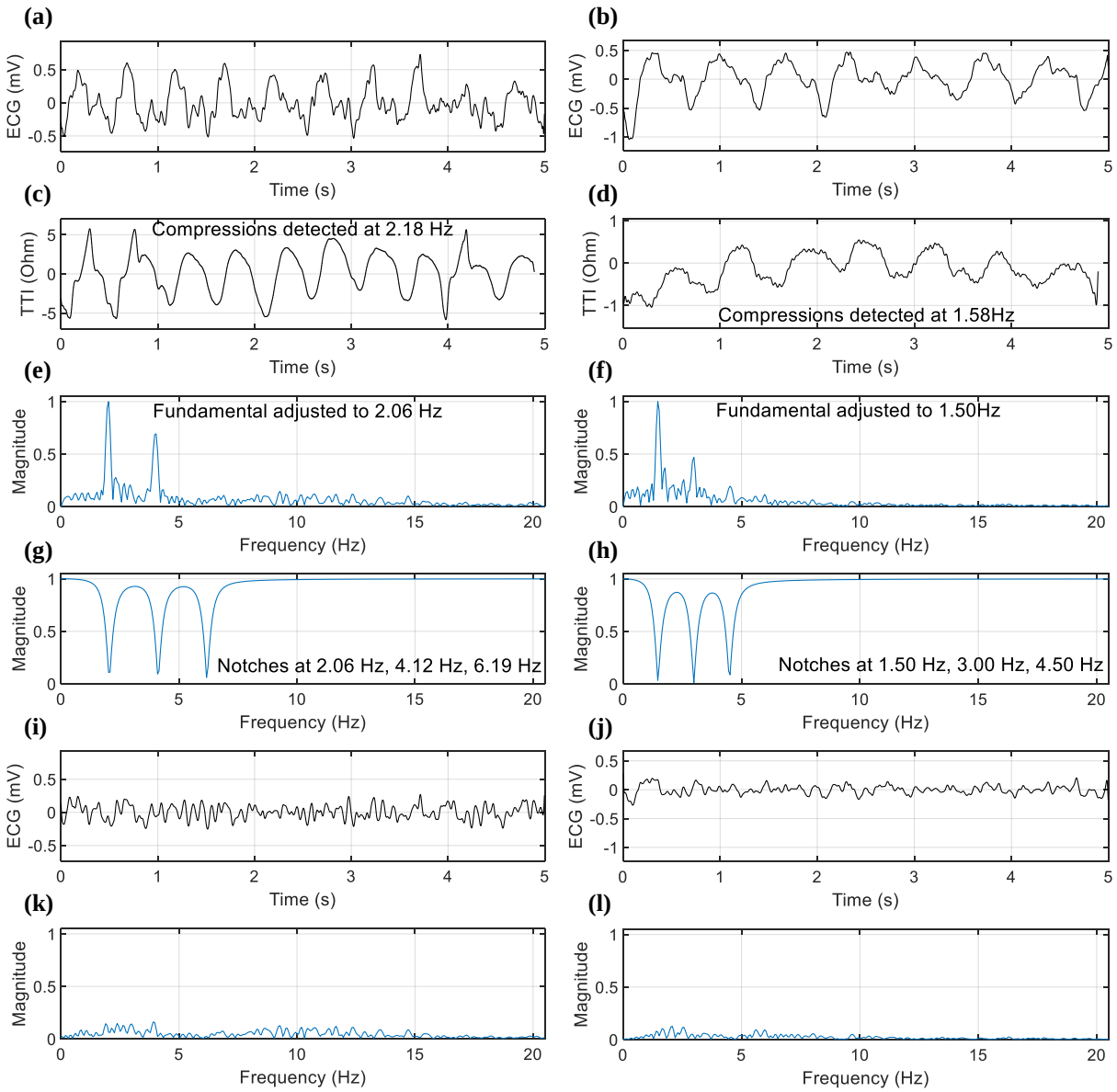

Figure 6.6 Adaptive filter description

(a,b) VF ECG segments during compressions following 1-30 Hz preprocessing filter. (c,d) Compressions detected in impedance; estimated compression fundamental based on impedance spectra is displayed. (e,f) Spectra of ECG during compressions displayed with final adjusted estimated compression frequency values based on upsampled spectra of ECG. (g,h) Filter response based on estimated compression fundamental frequency. (i,j) Filtered ECGs following notch filter confirm removal of the majority of compression artifact. (k,l) Spectra of filtered ECGs confirm removal of the majority of compression artifact.

Table 6.2 Adaptive filter benefit during compressions (training data)
Representative waveform measure AUC values for predicting patient outcomes on training data (460 patients) with chest compression artifact are presented for the adaptive filter versus without the adaptive filter. Significance of AUC increase is calculated as p-value for difference between AUC values with adaptive filtering versus without filtering. (AMSA = amplitude spectrum area, AUC = area under the receiver operating characteristic curve, RMS = root mean square.)

Measure	AUC for predicting survival			AUC for predicting return of rhythm		
	With filter	Without filter	Difference	With filter	Without filter	Difference
Peak Amplitude[140]	0.641	0.598	p<0.001	0.634	0.614	p=0.044
RMS Amplitude[140]	0.655	0.583	p<0.001	0.645	0.590	p<0.001
$AMSA_{1\text{-}26Hz}$[65,97]	0.707	0.698	p=0.010	0.669	0.660	p=0.009

6.3.9 *Amplitude Features and Parameter Selections*

VF amplitude may be related to the size of depolarization waves in the ventricular myocardium and the number of cells contributing to any given wave (see section 4.8.1), with higher VF amplitude generally associated with greater likelihood of defibrillation success. During VF, local areas in the myocardium depolarize synchronously in three-dimensional spiral and vortex waves, with the contractions becoming less coordinated over time as the functional units of contraction decrease in size and increase in number.[10,11,57,201] Thus early investigation by Weaver et al. demonstrated that higher-amplitude coarse VF (suggesting a relatively high amount of spatiotemporal organization) was associated with increased likelihood of conversion to organized rhythm following shock, while lower-amplitude fine VF (suggesting a relatively low amount of spatiotemporal organization) most often resulted in asystole when shocked.[140] However, as demonstrated previously (see section 4.15.4), prediction of outcome based on VF amplitude is severely confounded by voltage changes caused during chest compressions, challenging potential integration of amplitude features in a prognostic algorithm designed to limit chest compression interruption.

In the current investigation, we designed two amplitude-based features of the VF signal. To improve performance and allow these features to avoid transient chest compression artifact, we calculated the median of the amplitude in a sliding window to exclude spurious high-amplitude values. To allow the features to avoid low-frequency compression and ventilation artifact, we optimized window lengths to limit analysis to short periods within the signal (hence ignoring lower-frequency fluctuations). Specifically, the *Sliding Deviation* of VF ECG amplitude was calculated as

$$Sliding\ Deviation = \text{median}(s_{0,\ldots k\ldots,K}), \tag{6.1}$$

where

$$s_{0,\ldots k\ldots,K} = \sqrt{\frac{\sum_{n=k}^{k+W_{SD}-1}\left(|x_n| - \frac{1}{W_{SD}}\left(\sum_{n=k}^{k+W_{SD}-1}|x_n|\right)\right)^2}{W_{SD}-1}}, \tag{6.2}$$

W_{SD} is the window length (in samples), $x_0,\ldots,x_n,\ldots,x_{N-1}$ are N zero-mean ECG voltage samples collected during 5 seconds of VF, and $K = N - W_{SD} - 1$. Similarly, we calculated the *Sliding Peak* amplitude as

$$Sliding\ Peak = \text{median}(p_{0,\ldots k\ldots,K}), \tag{6.3}$$

where

$$p_{0,\ldots k\ldots,K} = \max|x_n|, \ \ \{n \mid k \le n < k + W_{SP}\}, \tag{6.4}$$

W_{SP} is the window length, and $K = N - W_{SP} - 1$ (Figure 6.7).

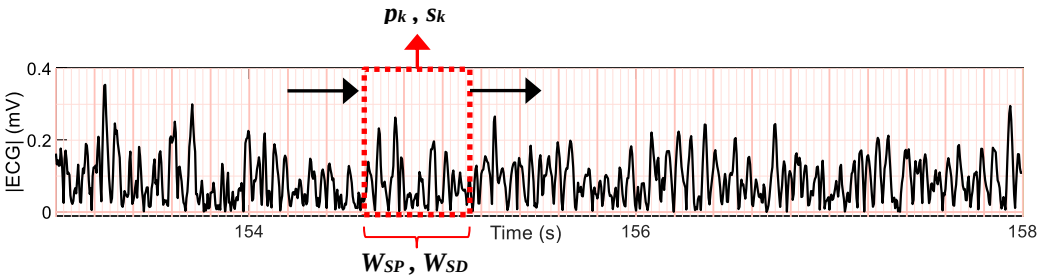

Figure 6.7 Amplitude-based ECG features
Median of standard deviation and peak amplitudes are calculated within sliding variable-length windows for *Sliding Deviation* and *Sliding Peak*.

We selected W_{SD} and W_{SP} to maximize training AUC for predicting survival and return of rhythm. Optimizations were performed with and without compressions and for filtered and unfiltered ECG segments separately (Figure 6.8, Figure 6.9).

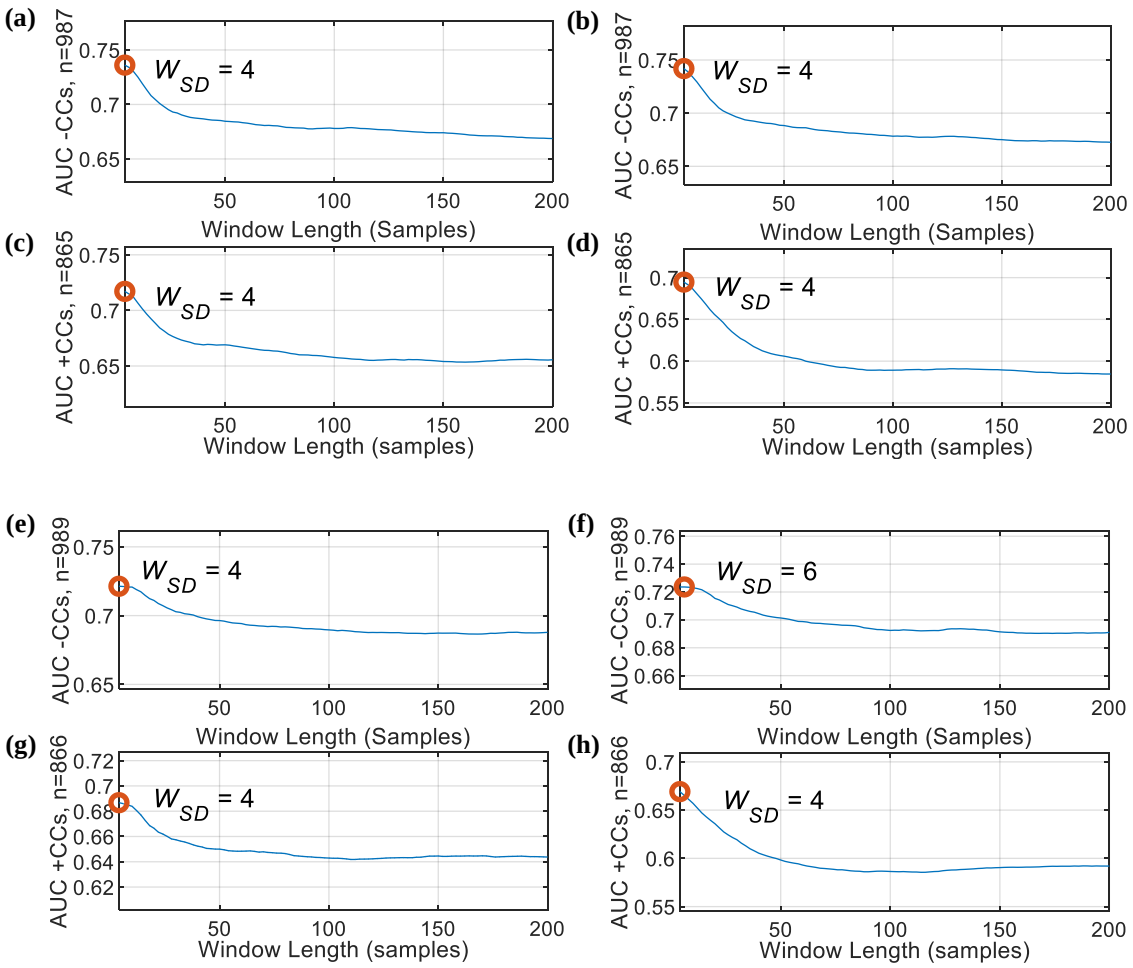

Figure 6.8 *Sliding Deviation* parameter selection
Parameter selections for W_{SD} based on training data for prediction of (a) survival -CCs, (b) survival -CCs using unfiltered data, (c) survival +CCs, (d) survival +CCs using unfiltered data, (e) return of rhythm -CCs, (f) return of rhythm -CCs using unfiltered data, (g) return of rhythm +CCs, (h) return of rhythm +CCs using unfiltered data. Minimum allowable x-value is W = 4 samples. (-CCs = without chest compressions, +CCs = with chest compressions.)

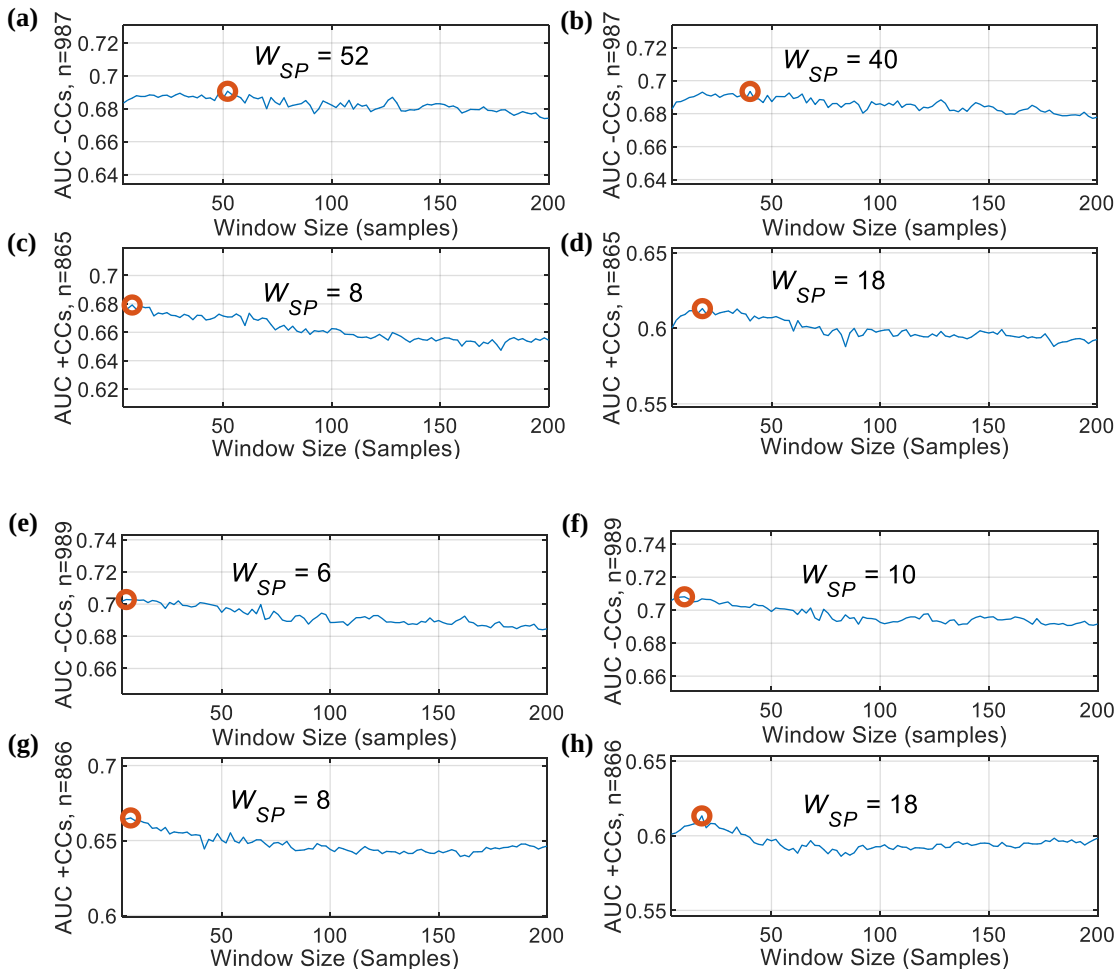

Figure 6.9 *Sliding Peak* parameter selection
Parameter selections for W_{SP} based on training data for prediction of (a) survival -CCs, (b) survival -CCs using unfiltered data, (c) survival +CCs, (d) survival +CCs using unfiltered data, (e) return of rhythm -CCs, (f) return of rhythm -CCs using unfiltered data, (g) return of rhythm +CCs, (h) return of rhythm +CCs using unfiltered data. Minimum allowable x-value is W = 4 samples. (-CCs = without chest compressions, +CCs = with chest compressions.)

6.3.10 *Wavelet Entropy Features and Parameter Selections*

The complex Morlet wavelet $\psi(t)$ can be described as a sinusoid with a Gaussian envelope; i.e., $\psi(t) = \pi^{-1/4} \exp(\mathrm{i}2\pi f_0 t) \exp(-t^2/2)$, given time t and base frequency $f_0 = \sqrt{1/(2\ln 2)}$.[154] The mother wavelet $\psi(t)$ can be scaled to specific center frequencies using a scale factor, a, and computing $\psi(t/a)$. Convolving an input signal $x_0, \ldots, x_n, \ldots, x_{N-1}$ and a wavelet with known center

frequency in discrete time therefore performs a transformation similar to a bandpass filter, producing output coefficients w_n, where index n in the wavelet coefficient output vector corresponds to the sampling index n of the input x (after truncation following convolution to align the two signals) (see section 4.8.2.2). Multiple wavelets with known center frequencies f_j (with j indicating frequency index and f typically spaced logarithmically in Hz) can be convolved with an input x to produce a matrix of values $|w_{n,j}|$ at sampling indices n and frequency indices j to construct a spectrogram of x (Figure 6.10). Such wavelet-based time-frequency transforms are considered to have superior temporal resolution compared to traditional time-frequency methods such as the short-time Fourier transform.[42]

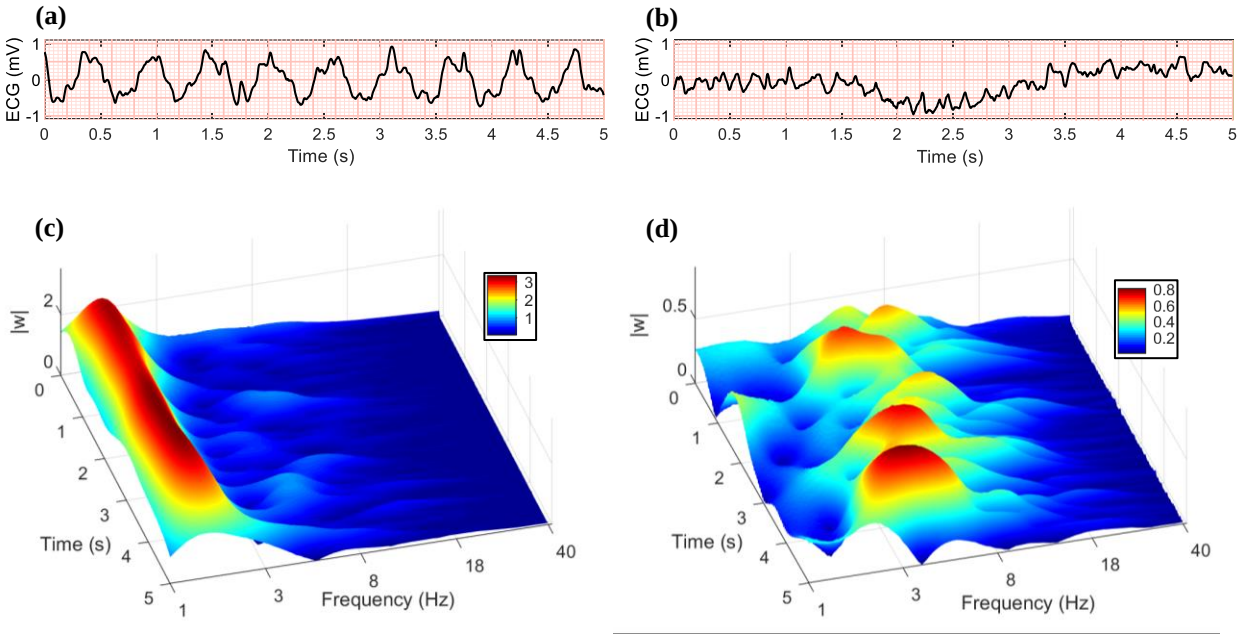

Figure 6.10 Wavelet spectrograms of VF with and without CPR
Example of VF segments collected adjacent to each other prior to the same shock with compressions (a) and without compressions (b). Compression artifact is visible in (a) as large oscillations in the ECG which obscure the VF, and the low-frequency drift in (b) is due to an artificial respiration. Spectrograms are shown for the VF with compressions in (c) and without compressions in (d). While VF content is between approximately 3-10 Hz in both spectrograms and has a similar magnitude (with $|w|$ approximately = 0.5), the compression fundamental at approximately 2 Hz in (c) is relatively much larger than the VF signal content (chest compression $|w|$ = approximately 2.5), rendering the VF content difficult to visualize.

Prior investigations have demonstrated methods to predict defibrillation outcomes by designing features derived from wavelet transforms of the VF ECG.[88,117,132,154,192] These investigations were limited to analysis without chest compression artifact. In subsequent investigation, we demonstrated that during chest compressions, high-frequency energy in the wavelet transform as described by Endoh et al. exhibited superior performance during chest compressions as compared to other individual features of the VF waveform.[88,91] However, simply computing the total energy within a defined frequency range of the wavelet transform (as in Endoh et al.) ignores time-dependent behavior that could otherwise be exploited. Hence, in the current investigation we sought to design features of the VF wavelet transform that describe time-variant

and frequency-variant properties of the transform, and to incorporate variable parameters in such a way to allow ECG features to ignore potential chest compression artifact after optimization on training data.

Shannon originally described a measurement of entropy that can be used to quantify the presence of unpredictable values and estimate information content.[202] Forms of the Shannon Entropy, $-\sum P_x \log_2 P_x$ (for P_x = probability of discrete value of x), have been applied to analysis of a variety of time-domain signals (such as electroencephalograms) as well as to analysis of these signals' respective Fourier and wavelet transforms.[203,204] An example applied to distributions of arbitrary signals is shown in Figure 6.11. With regards to prediction of defibrillation success, entropy-based features have been primarily been calculated directly from the time-domain ECG.[88,90,104,142,143,158] Entropy-like features to predict defibrillation outcome have also been calculated from wavelet transforms of the VF ECG. Specifically, Shandilya et al. calculated Shannon entropies within multiple frequencies of the wavelet spectrogram, while Watson et al. calculated an entropy feature from a single frequency in the wavelet spectrogram.[42,99,101,205] However, these prior studies have not calculated entropy features during chest compressions, and it was previously unknown whether the presence of compression artifact would confound entropy methods.

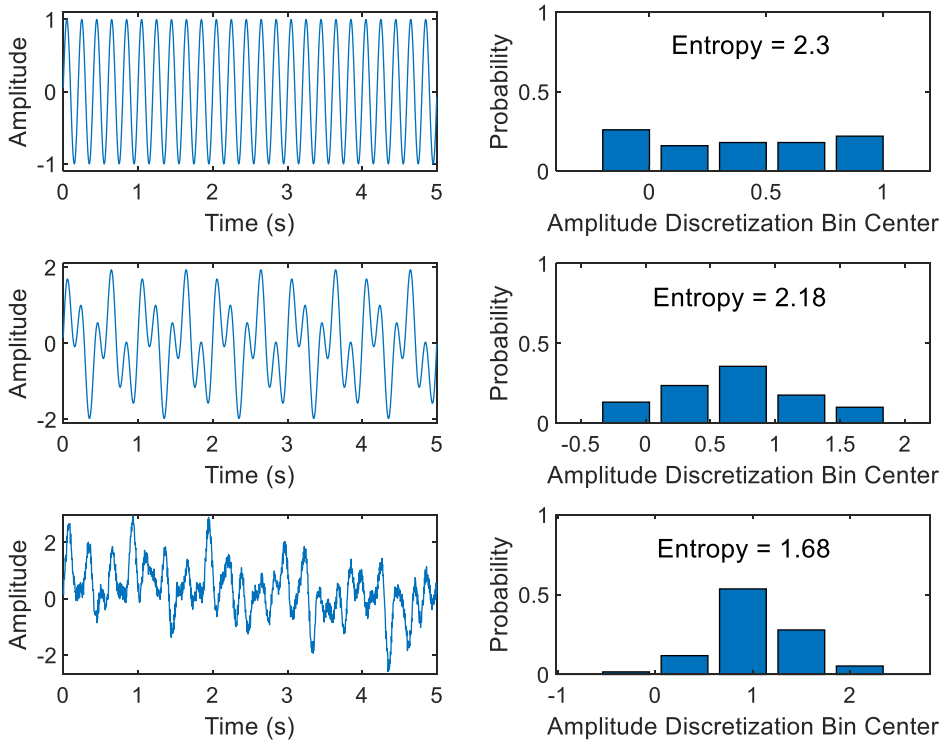

Figure 6.11 Shannon Entropy examples
Synthesized arbitrary sinusoidal signals with increasing numbers of sinusoids and noise (left) and the corresponding entropy values calculated from their probability distributions discretized into 5 bins (right). Signals with a flat distribution of discrete value ranges have higher entropy.

In the current investigation, we designed four features of the VF ECG related to likelihood of positive shock outcome using the Shannon equation to describe characteristics of the magnitude VF wavelet transform coefficients $\left|w_{n,j}\right|$. We designed the *Interfrequency Entropy* to quantify the time-varying spectral distribution as it evolves over the length of the VF segment. In contrast to prior wavelet-based entropy methods,[101,205] we calculated *Interfrequency Entropy* as the median of entropy values at each timepoint of the wavelet spectrogram using variable magnitude probability bin resolutions and variable low frequency cutoffs. Specifically,

$$Interfrequency\ Entropy = \text{median}(h_{0,\ldots n,\ldots N-1}), \tag{6.5}$$

where

$$h_{0,\ldots n,\ldots .N-1} = -\sum_{b=1}^{B} P_{n,b}\left(\log_2 P_{n,b}\right), \tag{6.6}$$

P_n is the probability distribution of the magnitude wavelet coefficients $\left|w_{n,j}\right|$ at sample index n between frequency indices $j_{low} \le j \le j_{hi}$ (corresponding to the frequency range $[f_{low}, f_{hi}]$ in Hz), B is the number of discretizations (bins) in the probability distribution, b is the probability bin index, and N is the sample length of the original ECG input (Figure 6.12). While increased h in *Interfrequency Entropy* is associated with positive outcomes when applied across a wide frequency range, we observed that analysis limited to high frequency content (i.e. above approximately 10 Hz) counterintuitively results in low h being associated with positive outcomes. Therefore, to describe the distribution of high-frequency content at each timepoint in the wavelet spectrogram, we also calculated the *High-Frequency Entropy* as the inverse of the median of h, or

$$\textit{High-Frequency Entropy} = -\text{median}(h_{0,\ldots n,\ldots .N-1}), \tag{6.7}$$

where similarly,

$$h_{0,\ldots n,\ldots .N-1} = -\sum_{b=1}^{B} P_{n,b}\left(\log_2 P_{n,b}\right). \tag{6.8}$$

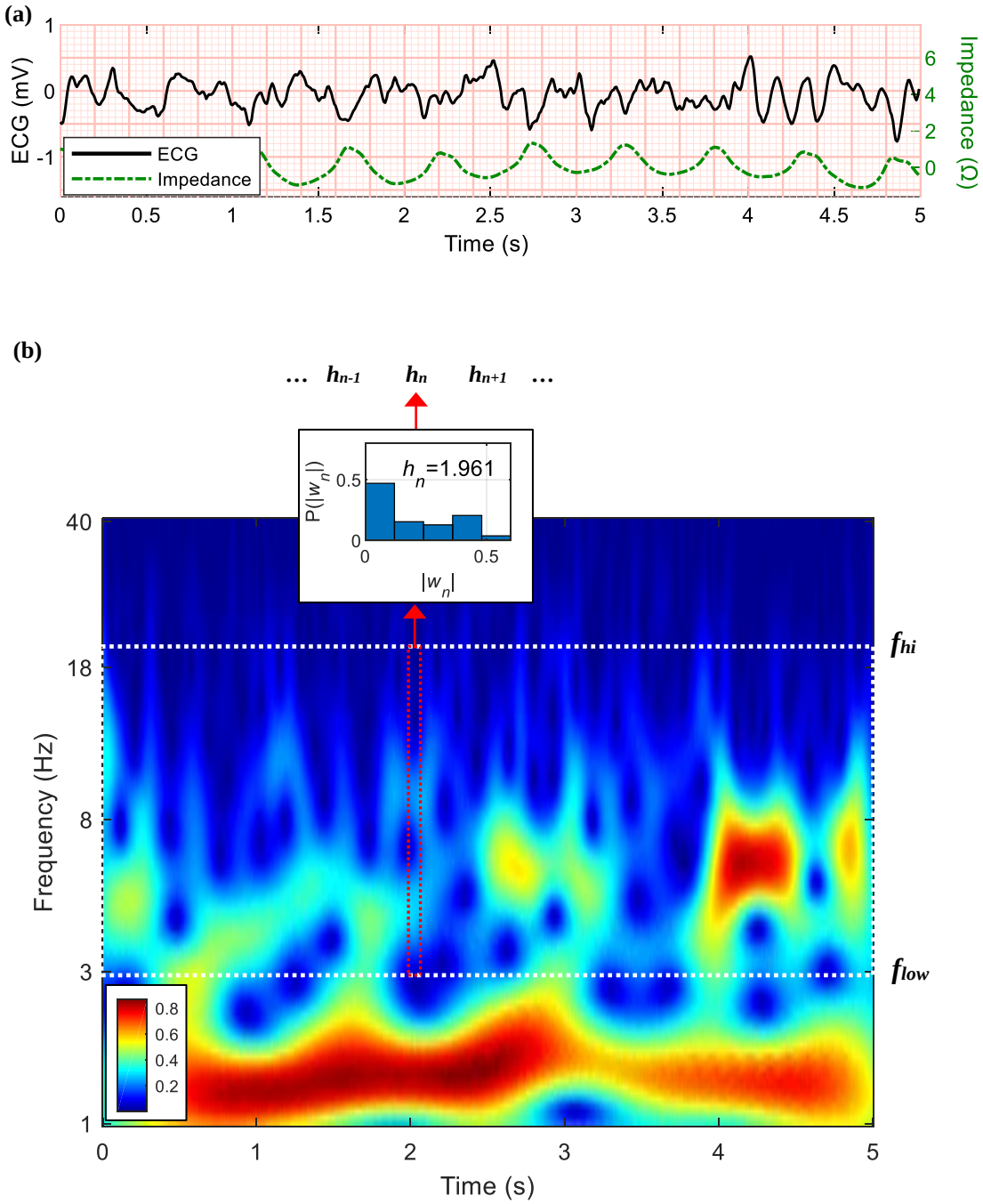

Figure 6.12 ***Interfrequency Entropy*** **and** ***High-Frequency Entropy***
(a) VF ECG during compressions with compressions confirmed in the impedance. (b) Spectrogram of VF during compressions with compression fundamental band visible at approximately 1.5 Hz. To calculate entropy features, the spectrogram is evaluated between variable frequency limits f_{low}-f_{hi} to calculate probability distributions P_n and generate h_n at for sample index. In this illustration, f_{low} is indicated at 3 Hz, which ignores the chest compression fundamental band below f_{low}.

Shannon-like entropy functions describe probability distributions normalized to a total area of 1 by definition; thus, information related to the overall amplitude of original signal is lost. For instance, *Interfrequency Entropy* above is calculated from the distribution of wavelet coefficient magnitudes within a range of frequencies at each timepoint, but the probability distribution of the coefficient magnitudes is normalized such that the absolute scale of the values are not accounted for (e.g., as in Figure 6.11, the actual x-values in the distributions are not used to calculate h). As we demonstrated in prior investigation after expanding on the methods of Endoh et al., however, the total energy in specific frequency ranges of the wavelet transform (particularly in higher frequencies) is strongly related to patient outcome during ongoing chest compressions and may offer additional information useful in conjunction with entropy.[88,91] Therefore, deviating from the methods of Endoh et al. which calculate the integral of spectrogram magnitudes within fixed frequency ranges, we applied the Shannon entropy equation directly to the spectrogram magnitude values in both the time and frequency directions within variable frequency ranges. Specifically, we calculated the *Shannon Energy* to describe the energy content at each frequency index j across all time indices n, and the *Interfrequency Shannon Energy* to describe the energy content within each time sample n in the spectrogram across all frequency indices j. We applied the median operation in *Shannon Energy* to allow the function to ignore outliers in frequency caused by noise that may occur within narrow frequency ranges (such as regular compressions or other persistent noise). We applied the median operation in *Interfrequency Shannon Energy* to allow the function to ignore transient artifact outliers in time (such as severe individual compressions or transient motion artifact). We defined the *Shannon Energy* as

$$Shannon\ Energy = \text{median}(g^{SE}_{j_{low},\ldots j,\ldots j_{hi}}), \tag{6.9}$$

where

$$g^{SE}{}_{j_{low},\ldots j,\ldots j_{hi}} = -\sum_{n=0}^{N-1} \left| w_{n,j} \right| \left(\log_2 \left| w_{n,j} \right| \right), \tag{6.10}$$

$w_{n,j}$ are the wavelet coefficients at frequency indices j and time sample indices n, j_{low} and j_{hi} are the low and high frequency index limits corresponding to an analysis frequency range (in Hz) $[f_{low}, f_{hi}]$, and N is the number of n time samples in the wavelet transform coefficients $w_{n,j}$ (Figure 6.13). We also calculated the *Interfrequency Shannon Energy* as

$$\textit{Interfrequency Shannon Energy} = \text{median}(g^{ISE}{}_{0,\ldots n,\ldots N-1}), \tag{6.11}$$

where

$$g^{ISE}{}_{0,\ldots n,\ldots N-1} = -\sum_{j=j_{low}}^{j_{hi}} \left| w_{n,j} \right| \left(\log_2 \left| w_{n,j} \right| \right). \tag{6.12}$$

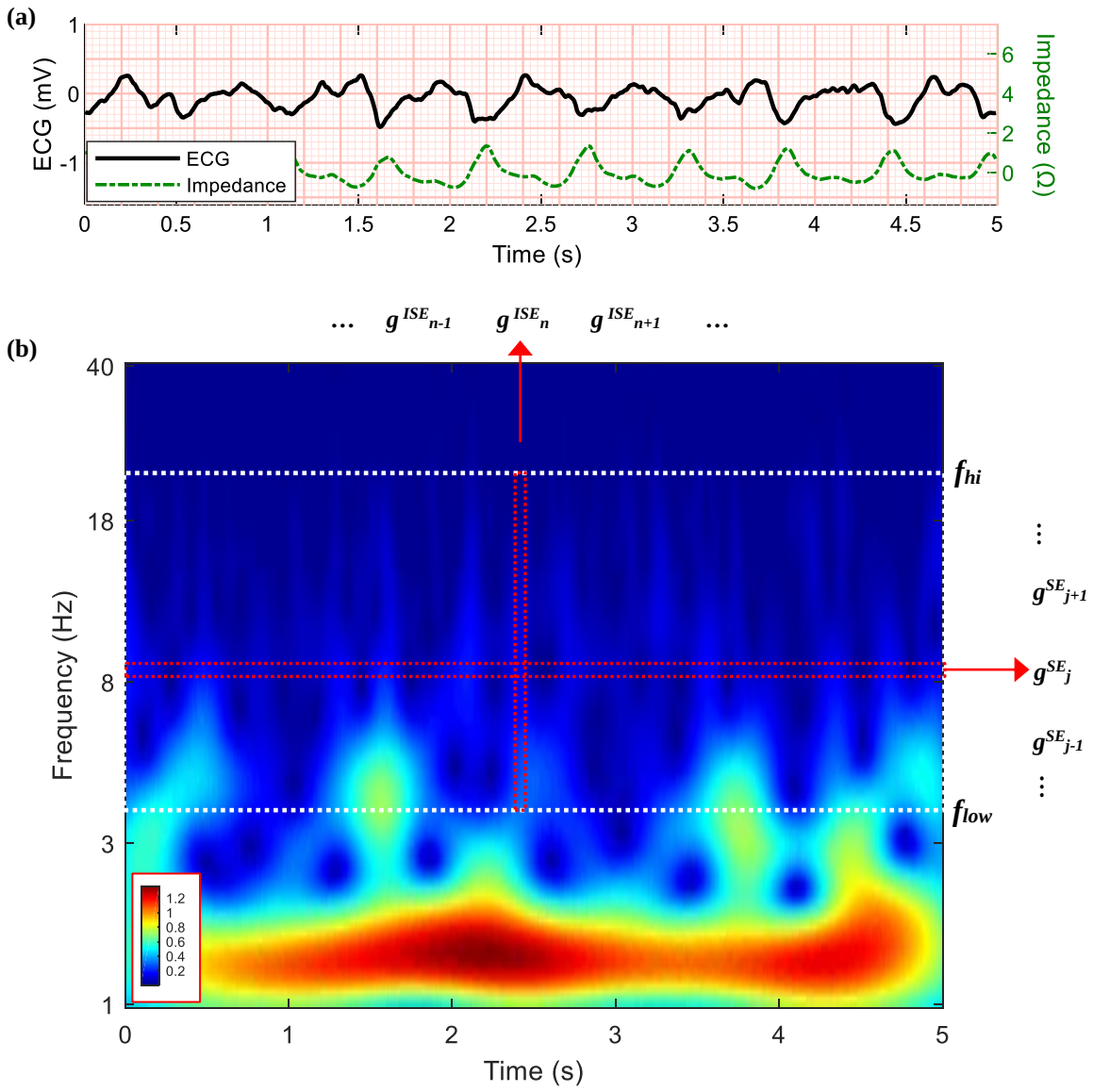

Figure 6.13 *Shannon Energy* and *Interfrequency Shannon Energy*
(a) VF ECG during compressions, with compressions confirmed in the impedance. (b) Spectrogram of VF during compressions with the compression fundamental band visible at approximately 1.5 Hz. To calculate features, the spectrogram is evaluated between variable frequency limits f_{low}-f_{hi} to calculate *Shannon Energy* as the median of g^{SE} at each frequency and the *Interfrequency Shannon Energy* as the median of g^{ISE} at each time sample.

We optimized parameters in the four entropy-like functions described above to maximize performance with and without chest compressions using training data. To optimize *Interfrequency Entropy* and *High-Frequency Entropy*, we varied the low frequency limits of analysis and the

number of bins in the probability distributions used to calculate entropy. Specifically, in order to allow an inherent avoidance of low-frequency chest compression artifact, we varied the lowest frequency limit f_{low} (in Hz) corresponding to low frequency limit index j_{low}, and ignored frequencies in the wavelet transform below this threshold. The high frequency limit f_{hi} was set equal to the upper bandwidth limit of the signal (f_{hi} = 30 Hz for filtered data and f_{hi} = 40 Hz for unfiltered data). Furthermore, while the number of probability bins used to calculate ECG entropy has typically been chosen arbitrarily in prior investigations (e.g. on the order of 10—30 bins), we varied the number of discretization bins B to determine optimal bin resolutions.[101,142,204] To improve ability of the function to generalize, we simplified the function by limiting the maximum B to eight. In contrast to *Interfrequency Entropy* and *High-Frequency Entropy*, the *Shannon Energy* and *Interfrequency Shannon Energy* are calculated directly from the wavelet transform coefficients and do not employ probability distributions; thus, for these functions, we varied both the low and high frequency limits defining the range of analysis $[f_{low}, f_{hi}]$ to determine the optimal corresponding frequency index limits j_{low} and j_{hi} to evaluate these functions. Varying both upper and lower frequency limits allowed these functions to avoid potential high-frequency noise and to reduce the effect of low-frequency compression artifact. Parameter optimizations for all four Shannon-based wavelet features are shown below in Figure 6.14 – Figure 6.17. Parameters were selected to maximize training AUC. When optimizing both $[f_{low}, f_{hi}]$, the widest frequency range corresponding to an AUC within +/- 0.005 of the maximum AUC was selected to prevent overfitting to local maxima in the AUC optimization surface.

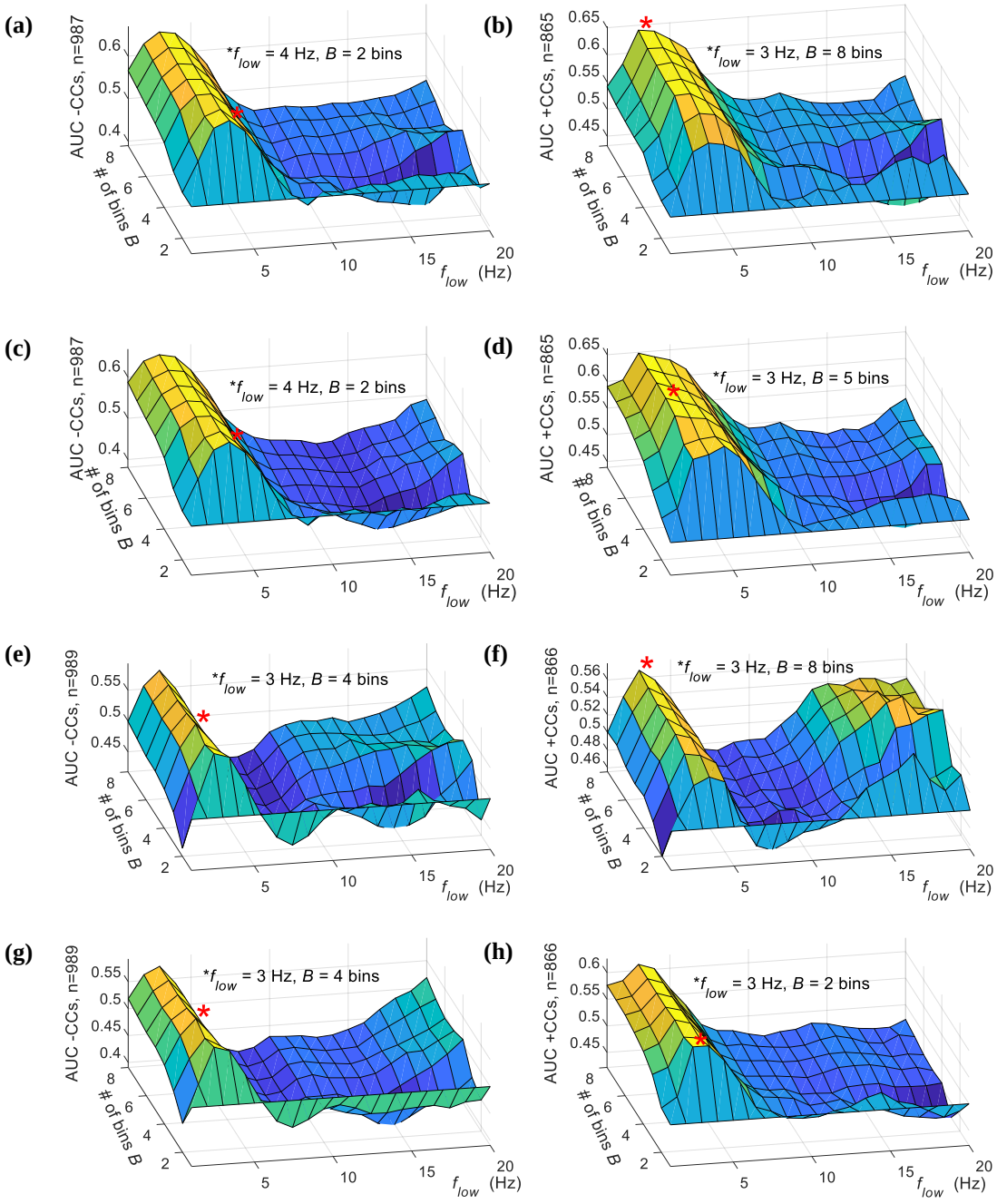

Figure 6.14 *Interfrequency Entropy* parameter selection
Parameter selections based on training data area under the receiver operating characteristic curve (AUC) for *Interfrequency Entropy* for predicting survival using filtered data (a) without compressions (-CCs) and (b) with compressions (+CCs), for predicting survival using unfiltered data (c) -CCs and (d) +CCs, for predicting return of rhythm using filtered data (e) -CCs and (f) +CCs, and for predicting return of rhythm using unfiltered data (g) -CCs and (h) +CCs.

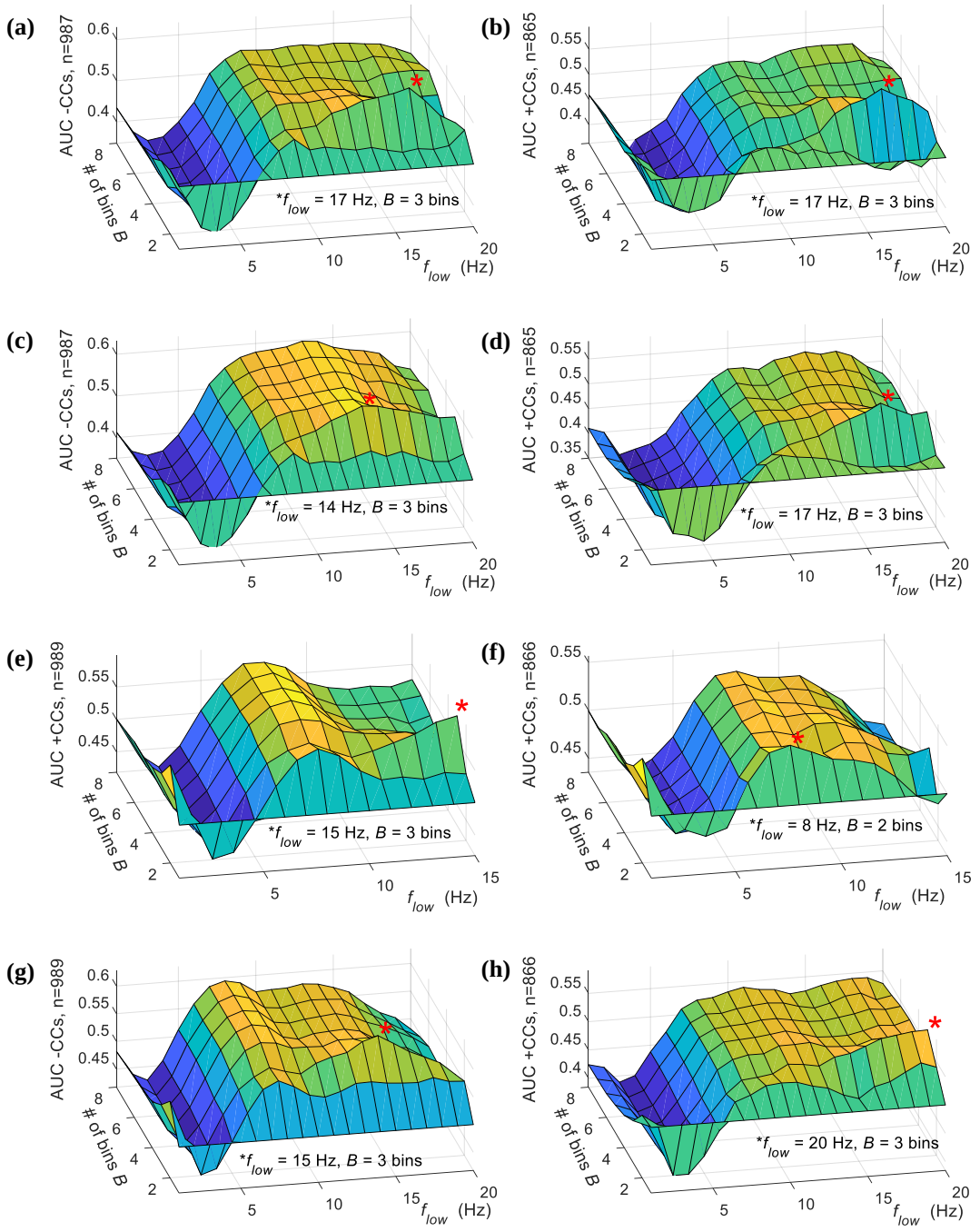

Figure 6.15 *High-Frequency Entropy* parameter selection
Parameter selections based on training data area under the receiver operating characteristic curve (AUC) for *High-Frequency Entropy* for predicting survival using filtered data (a) without compressions (-CCs) and (b) with compressions (+CCs), for predicting survival using unfiltered data (c) -CCs and (d) +CCs, for predicting return of rhythm using filtered data (e) -CCs and (f) +CCs, and for predicting return of rhythm using unfiltered data (g) -CCs and (h) +CCs.

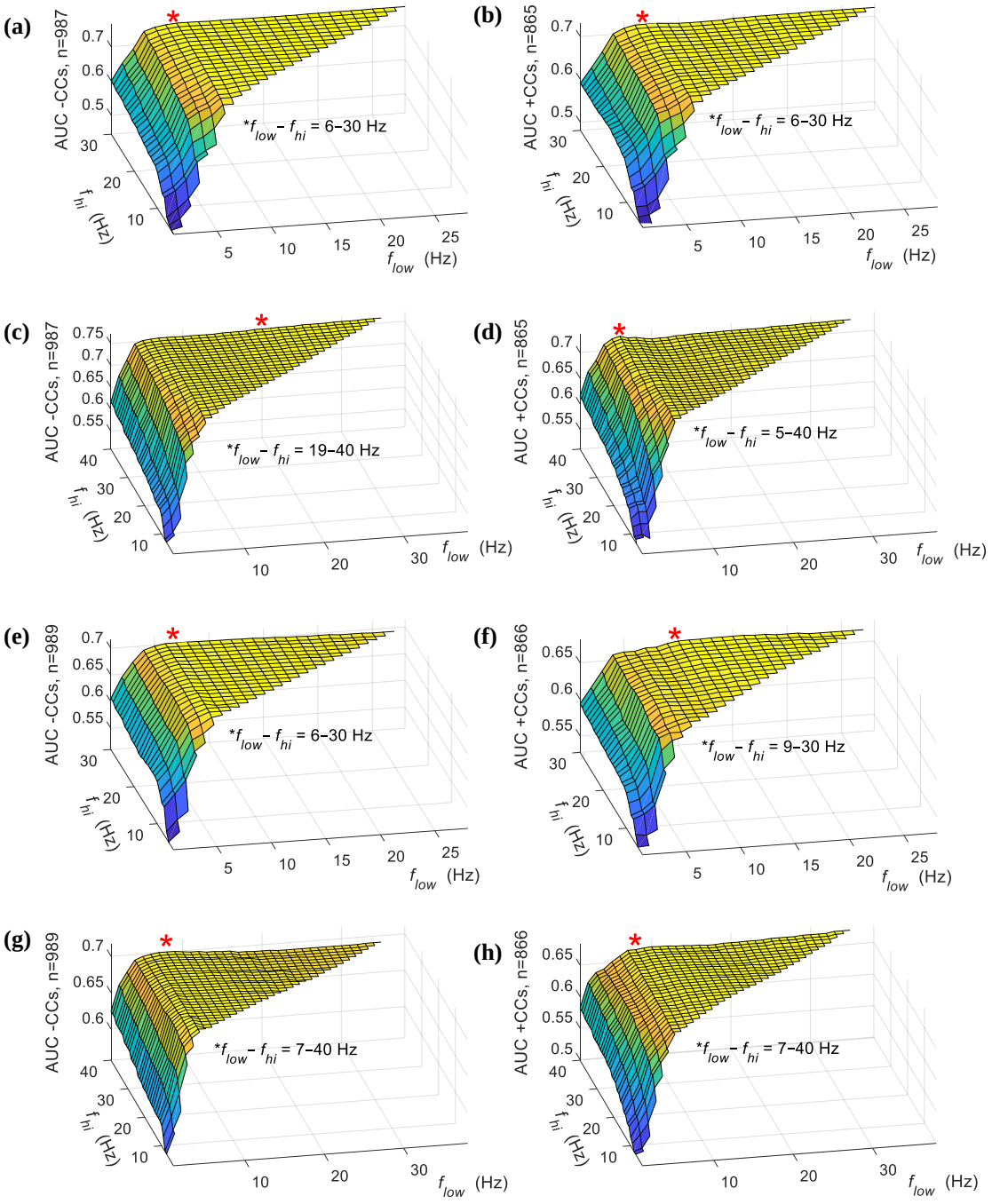

Figure 6.16 *Shannon Energy* parameter selection
Parameter selections based on training data area under the receiver operating characteristic curve (AUC) for *Shannon Energy* for predicting survival using filtered data (a) without compressions (-CCs) and (b) with compressions (+CCs), for predicting survival using unfiltered data (c) -CCs and (d) +CCs, for predicting return of rhythm using filtered data (e) -CCs and (f) +CCs, and for predicting return of rhythm using unfiltered data (g) -CCs and (h) +CCs.

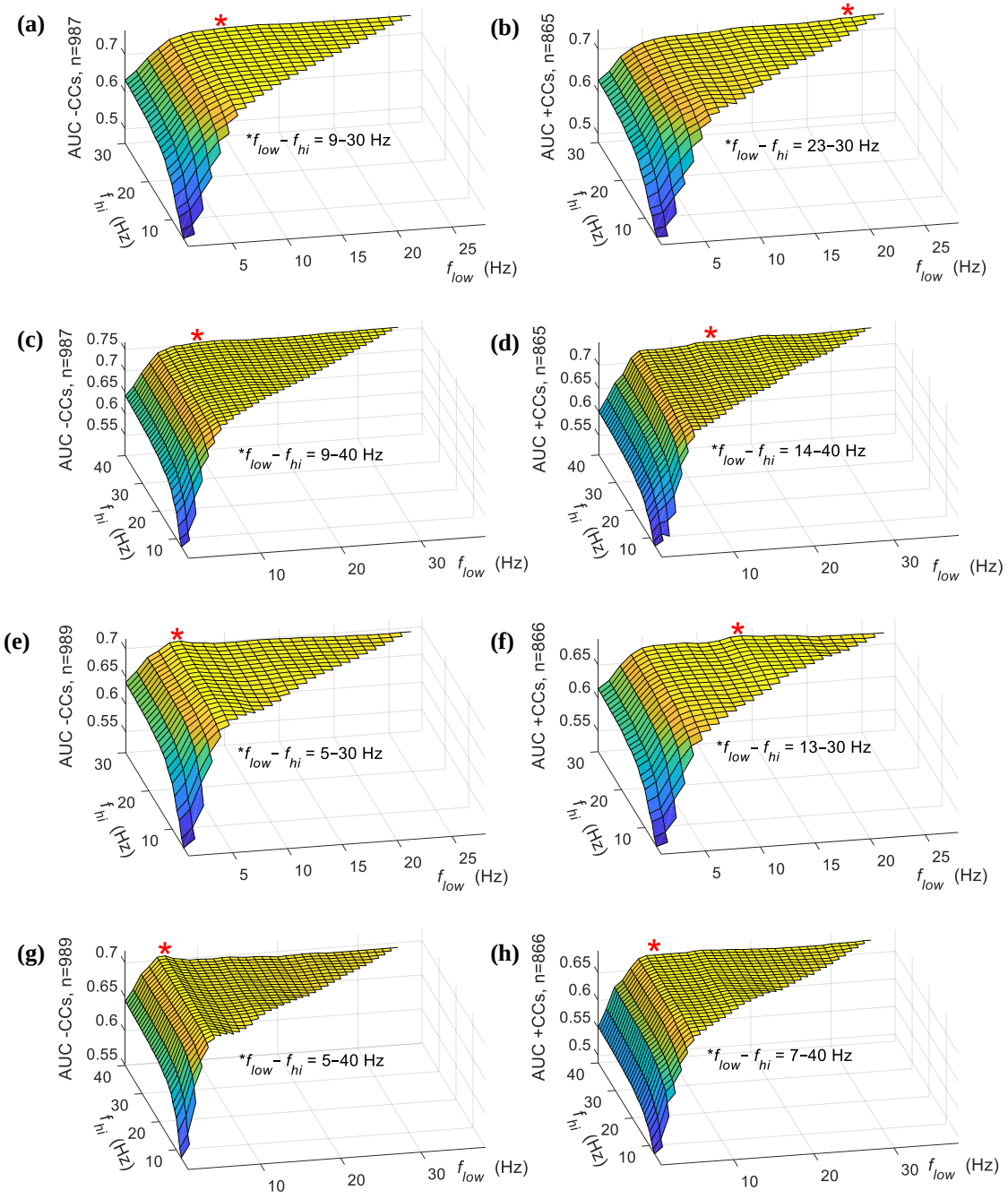

Figure 6.17 *Interfrequency Shannon Energy* parameter selection
Parameter selections based on training data area under the receiver operating characteristic curve (AUC) for *Interfrequency Shannon Energy* for predicting survival using filtered data (a) without compressions (-CCs) and (b) with compressions (+CCs), for predicting survival using unfiltered data (c) -CCs and (d) +CCs, for predicting return of rhythm using filtered data (e) -CCs and (f) +CCs, and for predicting return of rhythm using unfiltered data (g) -CCs and (h) +CCs.

6.3.11 *Dominant Frequency Features and Parameter Selections*

Brown et al. first demonstrated an association between the median frequency in the VF Fourier spectrum and VF duration, with VF frequency observed to decrease as ischemia persists in the myocardium and the likelihood of successful defibrillation is reduced.[7] Further metrics to describe the dominant frequency in the Fourier spectrum of the VF signal, such as centroid power and peak frequency, also have been proposed by Brown et al. and Eftestol et al.[116,136] However, such methods are limited by the Fourier spectrum and do not account for variations over time. Watson et al. therefore subsequently proposed improved wavelet spectrogram-based estimators of mean and peak frequency in the VF signal to account for variations in frequency over time.[42]

In the current investigation we characterized the dominant frequency in the VF ECG calculated from the wavelet spectrogram. To provide an alternative descriptor of dominant frequency in contrast to prior methods such as those proposed by Watson et al., we optimized a specific frequency cutoff indicative of robust VF physiology and calculated the proportion of time the dominant VF frequency exceeded the cutoff. Specifically, we calculated the wavelet *Maxima Fraction* as

$$Maxima\ Fraction = \frac{\sum_{n=0}^{N-1} \sigma_n}{N}, \tag{6.13}$$

where to determine σ_n at each sample index $0,...n...,N-1$,

$$\sigma_n = \begin{cases} 1 & \text{if } m_n > f_c \\ 0 & \text{if } m_n \le f_c \end{cases}, \tag{6.14}$$

given

$$m_n = \arg\max_f (|w_n|), \tag{6.15}$$

where $w_{n,f}$ are the wavelet transform coefficients at sample indices n across frequencies f (in Hz) and f_c is a frequency threshold parameter. Hence, the *Maxima Fraction* can be understood as the proportion of time the dominant VF frequency m_n in the spectrogram exceeds f_c (Figure 6.18). To further describe the overall dominant frequency of the VF signal we also calculated the *Mean Maxima,* the average dominant frequency (in Hz) over the course of the input signal, as

$$Mean\ Maxima = \frac{1}{N}\sum_{n=0}^{N-1} m_n\,, \tag{6.16}$$

where again,

$$m_n = \arg\max_f \left(\left|w_{n,f}\right|\right), \tag{6.17}$$

and $w_{n,f}$ are the wavelet transform coefficients at sample indices n and frequencies f (Figure 6.18).

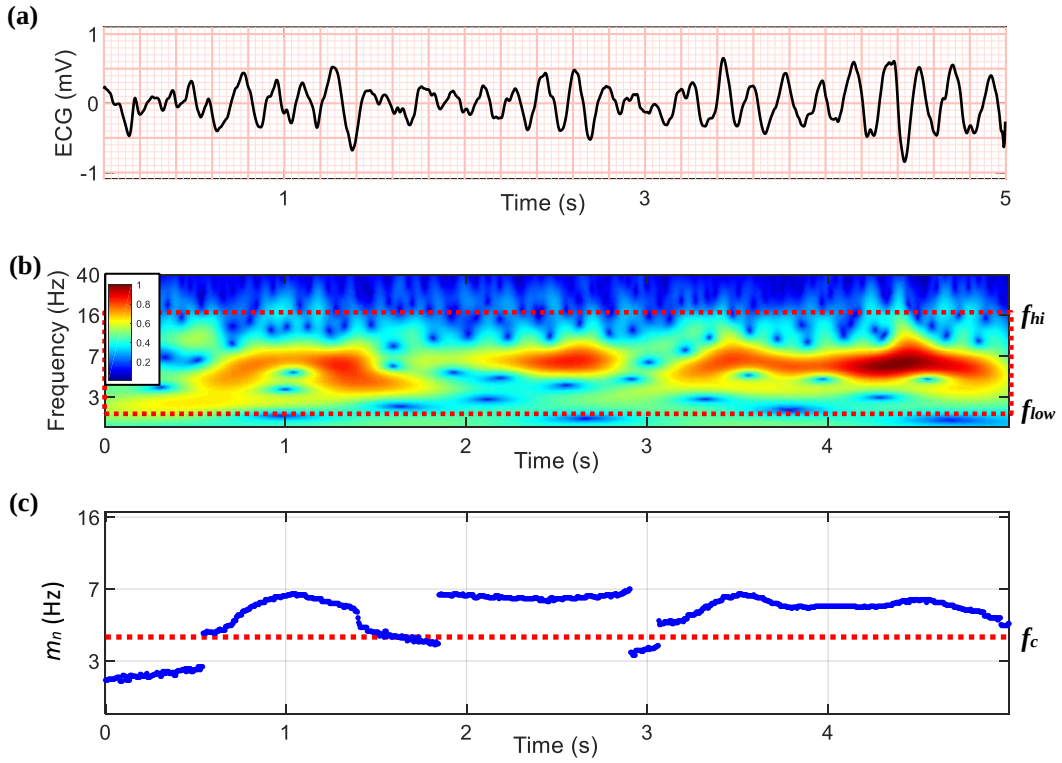

Figure 6.18 *Maxima Fraction* and *Mean Maxima* example
(a) VF ECG without chest compressions. In this example, the VF signal has a good prognosis (i.e. large amplitude and higher fundamental frequency) and resulted in return of rhythm after subsequent shock. (b) Spectrogram of VF during compressions normalized to a maximum of 1. (c) Maxima m_n at each time sample relative to the variable threshold f_c indicative of good prognosis. The time-series maxima m_n represent the dominant frequency of the signal.

We varied parameters for *Maxima Fraction* and *Mean Maxima* to optimize performance with and without compressions (Figure 6.19 and Figure 6.20). Specifically, the frequency threshold value f_c indicative of robust VF (see Figure 6.18c) in *Maxima Fraction* was varied to maximize AUC on training data. The frequency range [f_{low}, f_{hi}] (see Figure 6.18b) for evaluation of the *Mean Maxima* was optimized to allow the function to ignore potential low-frequency chest compression artifact and high-frequency noise. When optimizing [f_{low}, f_{hi}], the widest frequency range corresponding to an AUC within +/- 0.005 of the maximum AUC was selected to prevent overfitting to local AUC maxima.

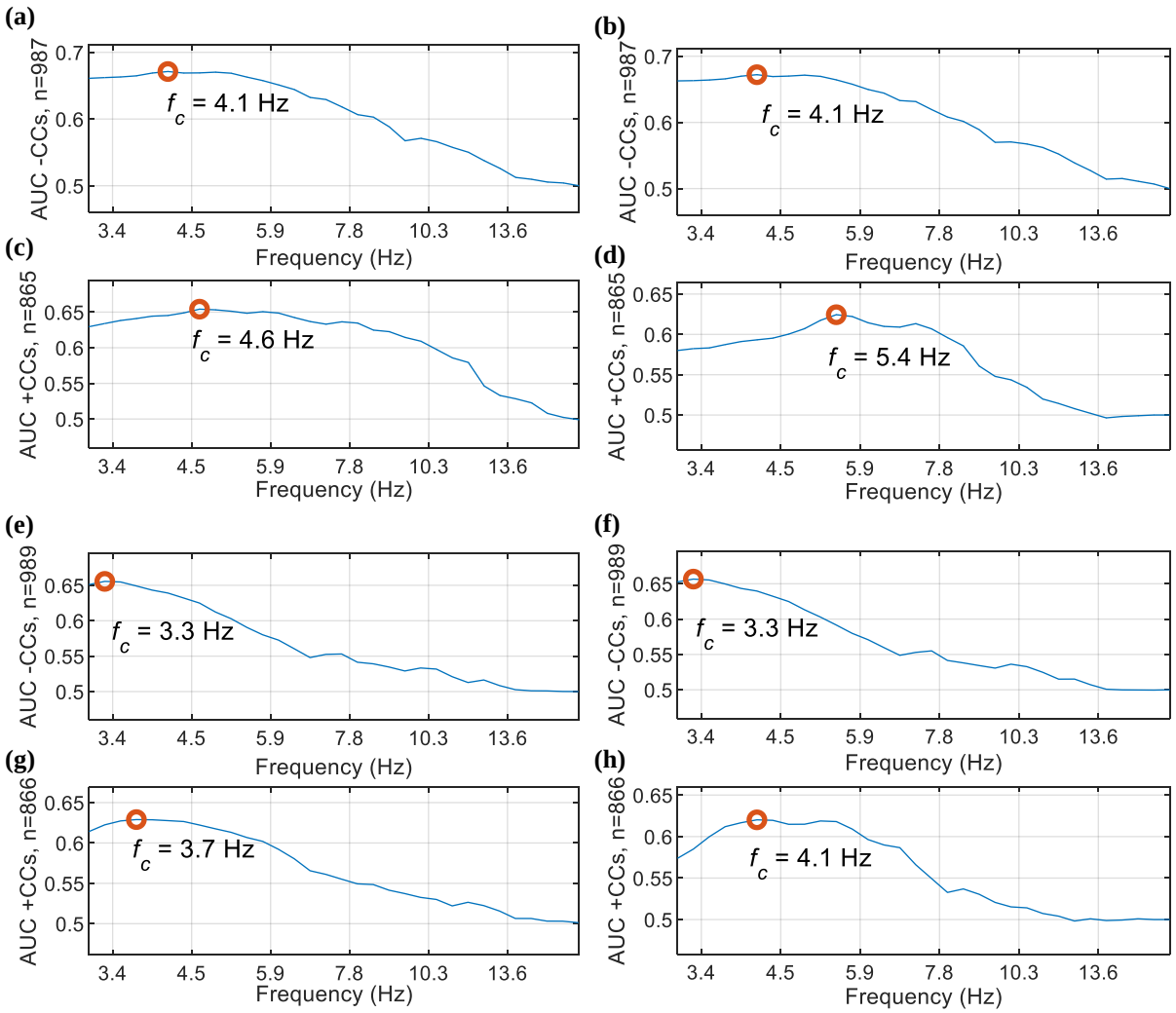

Figure 6.19 *Maxima Fraction* parameter selection
Selections of the frequency cutoff f_c indicative of VF with good prognosis are illustrated based on training AUC. Results are shown for (a) predicting survival -CCs using filtered data, (b) predicting survival -CCs using unfiltered data, (c) predicting survival +CCs using filtered data, (d) predicting survival +CCs using unfiltered data, (e) predicting return of rhythm -CCs using filtered data, (f) predicting return of rhythm -CCs using unfiltered data, (g) predicting return of rhythm +CCs using filtered data, and (h) predicting return of rhythm +CCs using unfiltered data. (AUC = area under receiver operating characteristic curve, -CCs = without chest compressions, +CCs = with chest compressions.)

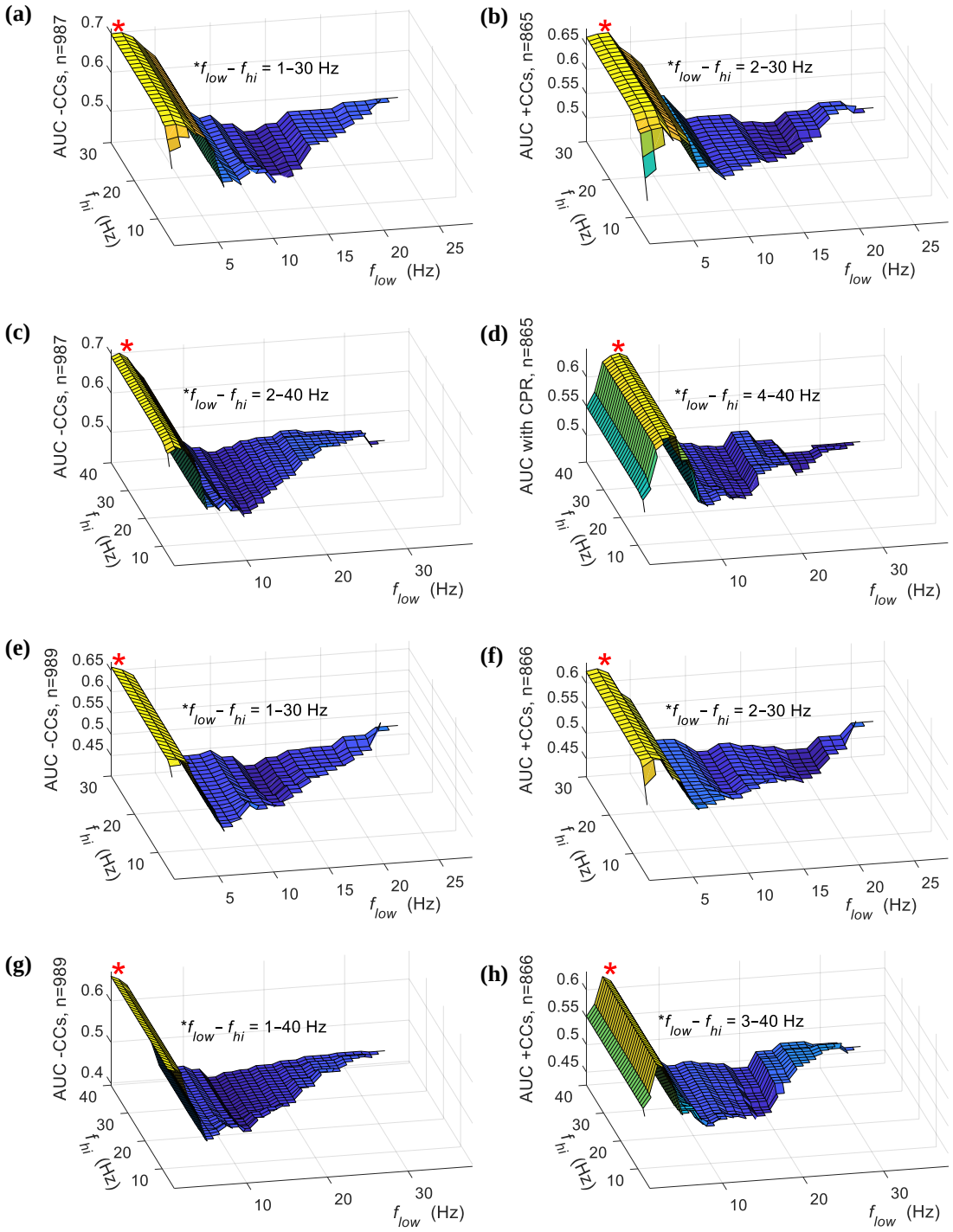

Figure 6.20 *Mean Maxima* parameter selection
Mean Maxima frequency ranges f_{low}–f_{hi} are selected using AUC on training data. Results are shown for predicting survival using filtered data (a) -CCs and (b) +CCs, for predicting survival using unfiltered data (c) -CCs and (d) +CCs, for predicting return of rhythm using filtered data (e) -CCs and (f) +CCs, and for predicting return of rhythm using unfiltered data (g) -CCs and (h) +CCs. (AUC = area under the receiver operating characteristic curve, -CCs = without chest compressions, +CCs = with chest compressions.)

6.3.12 *Short-Time Fourier Transform Features and Parameter Selections*

The short-time Fourier transform can be computed by evaluating the discrete Fourier transform of windowed segments of the input signal to provide a time-varying representation of the signal's spectrum. The general discrete form is $X(m,\omega)=\sum_{n} x_n w_{n-m} e^{-j\omega n}$, given slow-time index m (where m is the index of the current window), time-domain input x_n with sampling index n, window w, and discretized frequency ω. The Morlet wavelet transforms employed in the previous sections provide excellent temporal and frequency separation, and are therefore considered superior to short-time Fourier transforms for the purpose of ECG analysis and feature extraction.[42,154] Therefore, in the current investigation, to complement the wavelet-based features which employed a fixed temporal resolution, we calculated coarse short-time Fourier transforms with variable window sizes to provide an alternative representation of the VF signal with spectral content averaged over longer time segments (in contrast to wavelet transforms).

We derived two features of the VF ECG using relatively low-resolution short-time Fourier transforms calculated within box windows with no window overlap. The *Short-Time Deviation* was calculated as

$$\textit{Short-Time Deviation} = \text{median}(s_{0,\ldots m\ldots,M-1}), \tag{6.18}$$

where

$$s_m = \sqrt{\frac{1}{(j_{hi}-j_{low})}\sum_{j=j_{low}}^{j_{hi}} (X_{m,j}-\bar{X}_m)^2}, \tag{6.19}$$

X_m are the root-magnitude values of the discrete Fourier transform at window index m normalized to a maximum of 1, the frequency indices j for $j_{low} \le j \le j_{hi}$ correspond to the range

of frequencies $[f_{low}, f_{hi}]$ (in Hz) selected for analysis, $\bar{X}_m$ designates the mean of X_m at a single window index m between frequency indices $j_{low} \le j \le j_{hi}$, and M is the short-time window length in samples (Figure 6.21).

To describe the change in the VF spectrum and to quantify the similarities of the magnitude profiles over time between different frequencies, we calculated the *Correlation Component* from the correlation between time profiles at each frequency index in the short-time Fourier transform. As described above, $X_{m,j}$ represents the root-magnitude at time window index m and frequency index j. We calculated the correlation matrix R of size JxJ comparing the short-time Fourier transform root-magnitude profiles across all m at between all possible pairs of frequencies j, where the frequency indices j are between frequency index limits $j_{low} \le j \le j_{hi}$ corresponding to frequency limits $[f_{low}, f_{hi}]$, the number of frequency bins analyzed $J = j_{hi} - j_{low} + 1$, and R represents the matrix of correlations between the vectors X_j of spectral magnitudes over time at each frequency index j. Thus,

$$R = \begin{pmatrix} r(X_{j_{low}}, X_{j_{low}}) & \cdots & r(X_{j_{low}}, X_{j_{hi}}) \\ \vdots & \ddots & \vdots \\ r(X_{j_{hi}}, X_{j_{low}}) & \cdots & r(X_{j_{hi}}, X_{j_{hi}}) \end{pmatrix}, \tag{6.20}$$

where $r(X_{j_1}, X_{j_2})$ represents the Pearson correlation between the time-series root magnitude profiles at frequency indices j_1 and j_2 (Figure 6.21). Then, to reduce the dimensionality of R to a small number of values orthogonally describing the variation in the correlation matrix and thus enable use of a single variable to represent the interfrequency similarity, the *Correlation Component* is calculated as

$$Correlation\ Component = p_c, \tag{6.21}$$

where p_c is equal to the c^{th} principal component of the correlation matrix R.

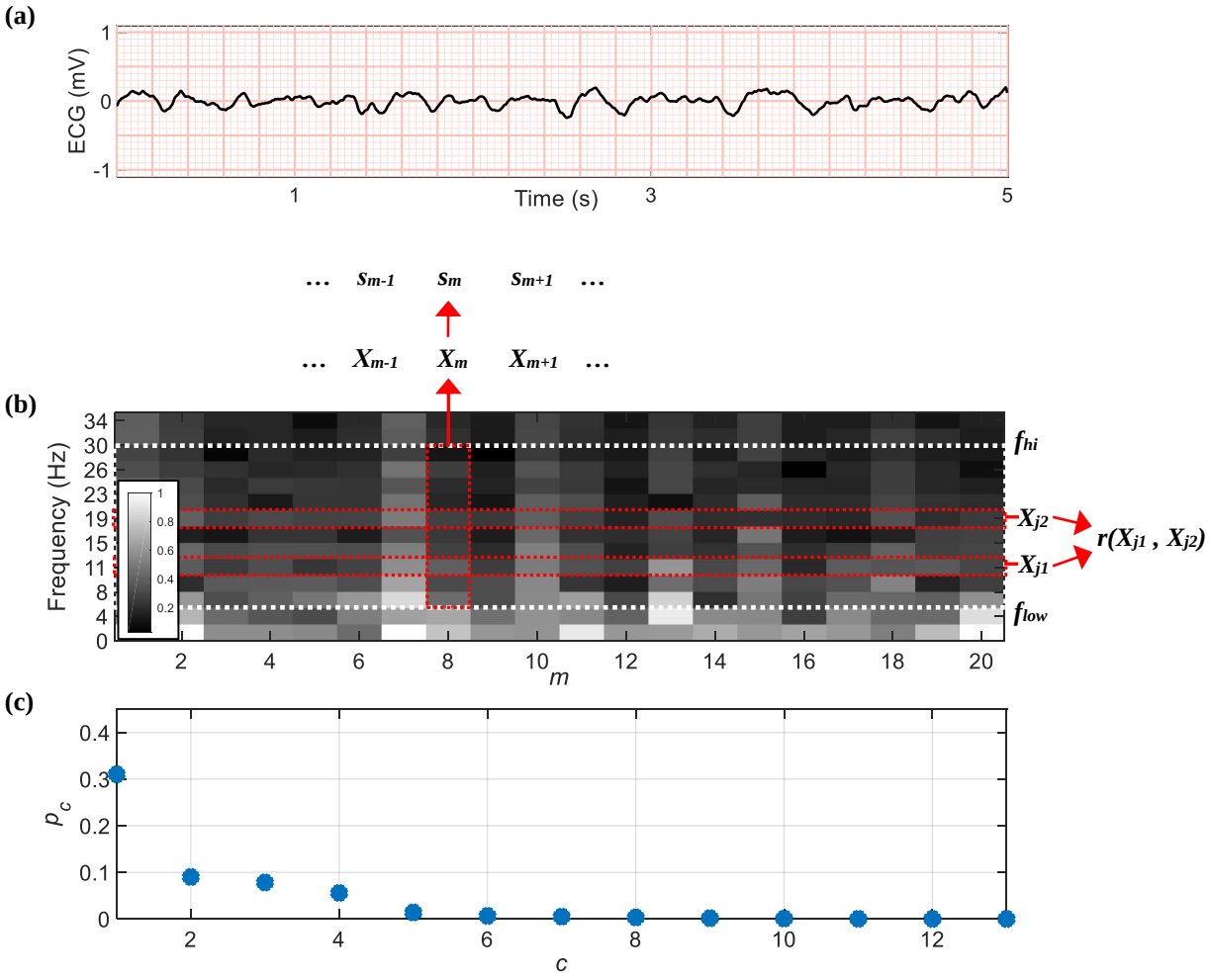

Figure 6.21 *Short-Time Deviation* and *Correlation Component* example
(a) VF without chest compressions. In this example (in contrast to Figure 6.18a), the VF signal has a poor prognosis (i.e. lower amplitude and frequency) and did not result in return of rhythm after subsequent shock. (b) Low-resolution short-time Fourier transform of VF without compressions with M = 20. (c) Principal component values of the Pearson correlation matrix calculated from X_m.

We selected parameters to optimize the prognostic performance of *Short-Time Deviation* and *Correlation Component*. In contrast to our wavelet features which employed variable frequency limits, frequency limits for calculation of both functions were fixed at [f_{low}, f_{hi}] = [5 Hz, 40 Hz] to avoid low-frequency chest compression artifact. The *Correlation Component*

parameter c was selected as $c = 2$. Window sizes M were varied to maximize AUC on training data (Figure 6.22, Figure 6.23). The frequency resolution for evaluation of *Short-Time Deviation* was increased proportionally to the window size, while the frequency resolution for evaluation of *Correlation Component* was fixed at 2.5 Hz.

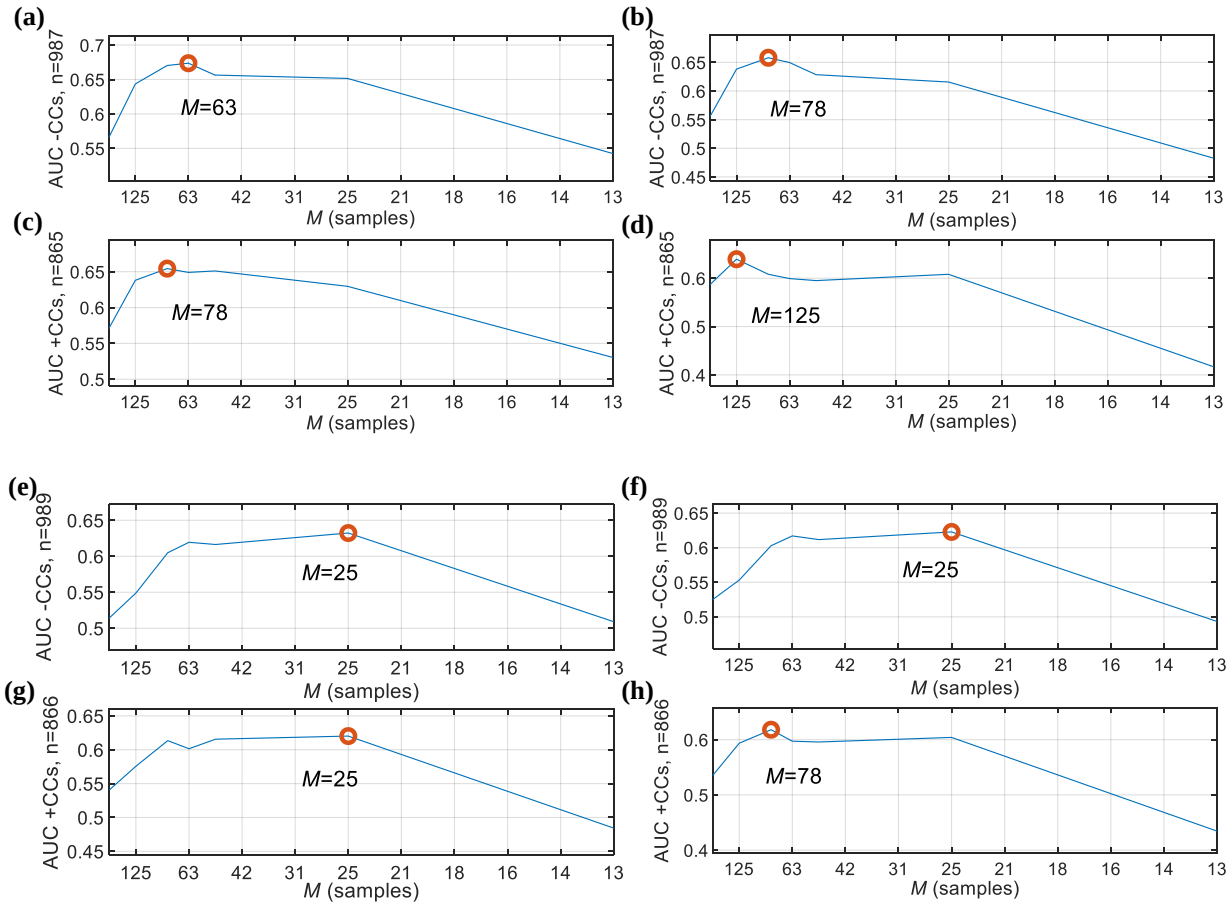

Figure 6.22 *Short-Time Deviation* parameter selection
Selections of window size *M* are illustrated based on training AUC. Results are shown for (a) predicting survival -CCs using filtered data, (b) predicting survival -CCs using unfiltered data, (c) predicting survival +CCs using filtered data, (d) predicting survival +CCs using unfiltered data, (e) predicting return of rhythm -CCs using filtered data, (f) predicting return of rhythm -CCs using unfiltered data, (g) predicting return of rhythm +CCs using filtered data, and (h) predicting return of rhythm +CCs using unfiltered data. (AUC = area under receiver operating characteristic curve, -CCs = without chest compressions, +CCs = with chest compressions.)

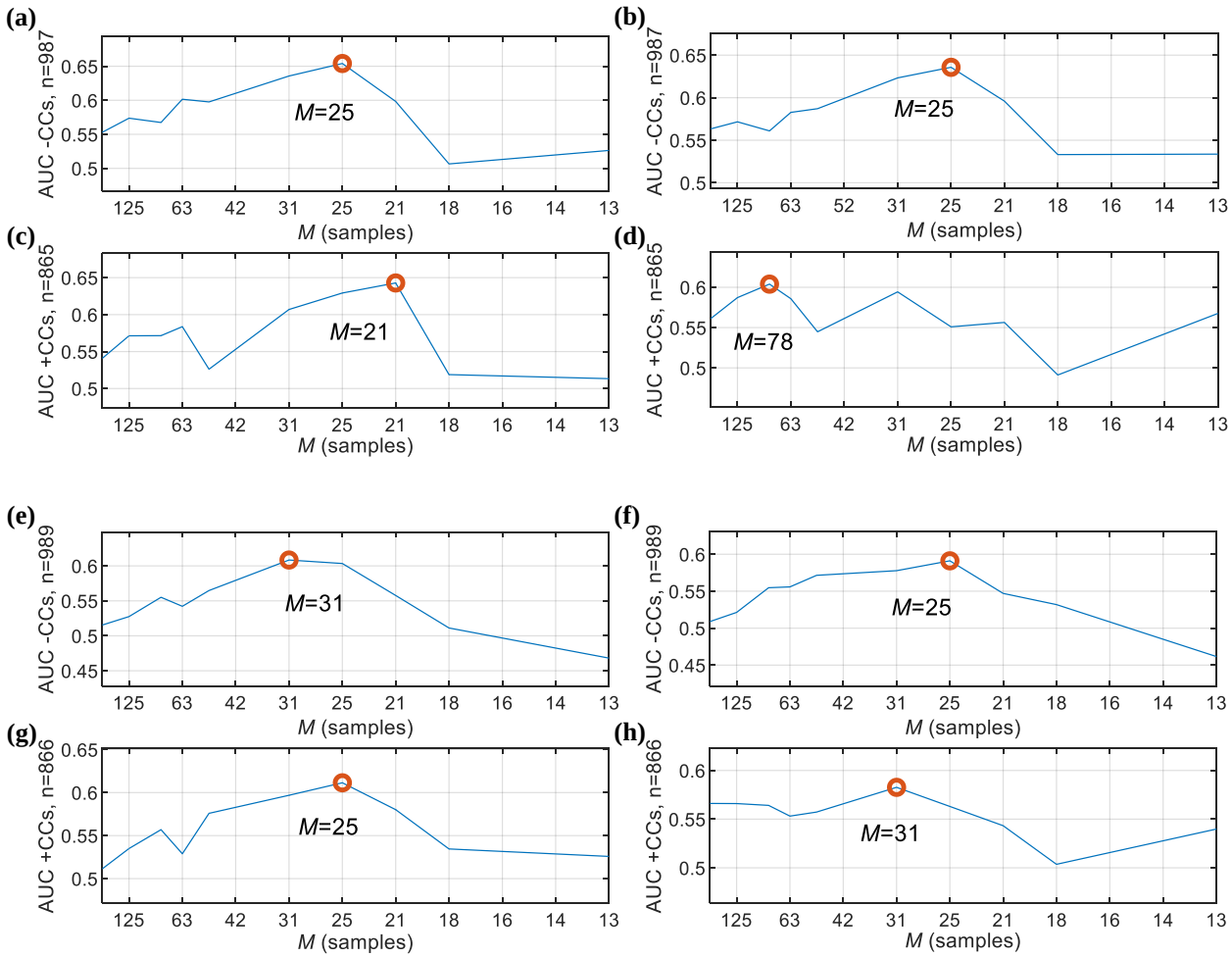

Figure 6.23 *Correlation Component* parameter selection
Selections of window size *M* are illustrated based on training AUC. Results are shown for (a) predicting survival -CCs using filtered data, (b) predicting survival -CCs using unfiltered data, (c) predicting survival +CCs using filtered data, (d) predicting survival +CCs using unfiltered data, (e) predicting return of rhythm -CCs using filtered data, (f) predicting return of rhythm -CCs using unfiltered data, (g) predicting return of rhythm +CCs using filtered data, and (h) predicting return of rhythm +CCs using unfiltered data. (AUC = area under receiver operating characteristic curve, -CCs = without chest compressions, +CCs = with chest compressions.)

6.3.13 *Support Vector Machine Model*

Support vector machines are binary classifiers that discriminate classes of data using the principle of a maximally-separating hyperplane defining the boundaries between classes. The class of an unknown $N-$dimensional input x_{input} is predicted based on its position relative to the separating hyperplane, where N is the number of input features. The hyperplane itself is defined by T training points (support vectors) x_t which support the classification boundaries in the $N-$dimensional feature space. Furthermore, the support vectors can be mapped to a higher-dimensional feature space using a kernel function K to allow construction of a hyperplane in this higher-dimensional space that may provide improved separation than a discriminant in the $N-$dimensional feature space.[164,171] In effect, such a classifier can be considered as evaluating the sum of similarities between unknown inputs x_{input} and known support vector training points x_t (and the associated training class assignments $y_t \in \{-1,1\}$). The sign of the summation of similarities determines the position of the unknown point versus the decision boundary and indicates the class prediction. Specifically, the output of a support vector machine employing a kernel function is of the form

$$f(x) = \text{sign}\left(\sum_{t=1}^{T} y_t \alpha_t K(x_{input}, x_t) + w_0 \right), \tag{6.22}$$

where α_t are model parameters and w_0 is a constant. While a variety of kernel functions K are available to evaluate similarity between a known sample and unknown sample, we selected the radial (Gaussian) kernel which in effect allows nonlinear boundaries and enables model regularization through adjustment of a kernel parameter. Using the radial kernel, the similarity between $N-$dimensional arbitrary samples *a* and *b* is evaluated by

$K(a,b) = \exp(-\gamma \sum_{j=1}^{N} \left(a_j - b_j\right)^2)$, where γ is a positive constant that controls the size of the gaussian curve used to evaluate similarity (thus affecting the smoothness of the decision boundary). The objective function minimized during training is of the form $\frac{1}{2}\|w\|^2 + C\left(\sum_{t=1}^{T} \xi_t\right)$, where w represents parameter weights, the slack variable ξ represents the degree of misclassification for each training point (i.e. support vector), and the slack penalty C (also referred to as box constraint) is a constant that controls the relative weight of the misclassification error during minimization. To perform model regularization and control the bias-variance tradeoff during training, both the kernel size γ and box constraint C hyperparameter constants may be adjusted. The majority of prior VF prognosis studies that employ support vector machines held a fixed $C = 1$ and adjust only γ; this is likely due the fact that most studies lack sufficient data to allow optimization of multiple hyperparameters on training data.[89,144] Further discussion on support vector machine methods are provided in section 4.8.4.4.

In the current investigation, we trained support vector machine models to predict patient outcome using ten novel features of the VF ECG (Figure 6.24). To improve the normality of the input feature and model posterior probability distributions, we employed natural logarithm and logit transformations, respectively. Models were trained for use with compressions and without compressions separately, and were also trained for predicting survival and return of rhythm separately. (Hence one of four separate support vector machine models were used depending on presence of compressions and the definition of positive outcome.) We optimized both kernel size γ and box constraint C hyperparameters using training data by performing a grid search of 5-fold cross-validation error values versus hyperparameter values (Figure 6.25). Due to the fact that the data samples in this study were difficult to classify and exhibit a relatively large overlap, we

underfit the model to improve generalizability. Using a regularization technique that we introduced previously,[91] a tolerance error value τ was applied during support vector machine training such that during the grid search of error versus hyperparameter values, we determined the maximum γ and minimum C subject to the constraint $\tau \geq \left| error_{\gamma,C} - \min(error) \right|$, where $error_{\gamma,C}$ represents the cross-validation error at a particular (γ, C) combination, and $\min(error)$ represents the minimum observed error over all hyperparameter combinations. In effect, this procedure slightly increased kernel size and slightly reduced box constraint (thus increasing bias and reducing variance to improve generalizability) while maintaining an overall cross-validation error within a small tolerance of the minimum observed error in the search grid. Because the scale of the hyperparameters was not comparable, different tolerances were selected for each hyperparameter. Specifically, the minimum C was selected such that $\tau_C \geq \left| error_{\gamma,C} - \min(error) \right|$, and then the maximum γ was selected holding C fixed such that $\tau_\gamma \geq \left| error_{\gamma,C} - \min(error) \right|$. We used τ_C = 0.035 for data without compressions, τ_C = 0.035/2 for data with compressions (as compression-artifacted data had increased class overlap), and τ_γ = 0.003. An alternative explanation of this procedure is provided in section 4.8.4.5.

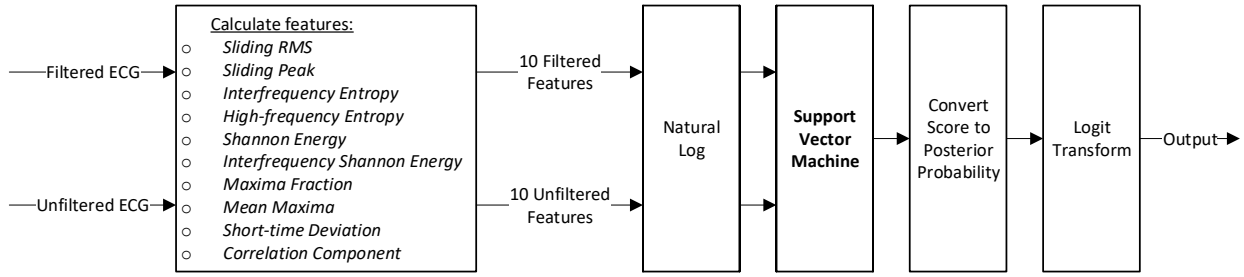

Figure 6.24 Support vector machine model
The process for computing support vector machine output from ECG input data is illustrated.

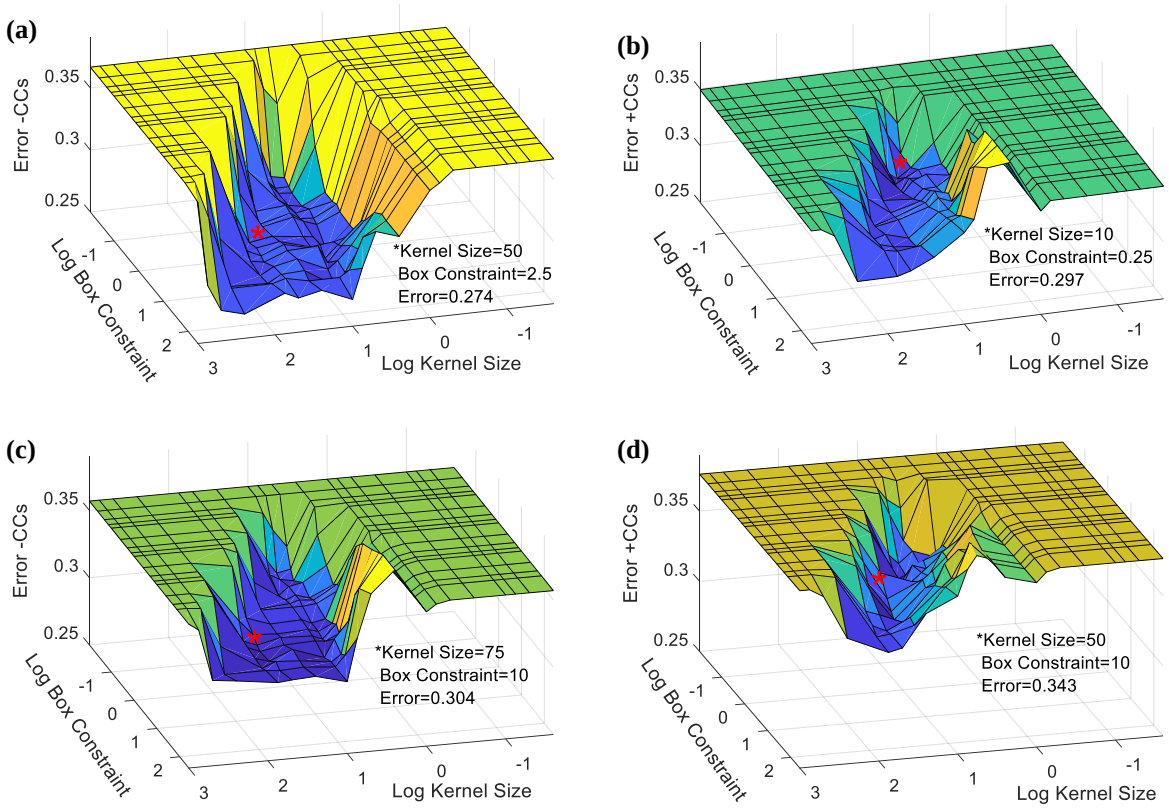

Figure 6.25 Support vector machine hyperparameter selection
Box constraint and kernel size values (C and γ respectively) were selected to minimize 5-fold cross validation error using training data. The final values (indicated by *) are selected as the minimum box constraint and maximum kernel sizes with a final error value within the error tolerance τ values. Results are shown for the models to (a) predict survival -CCs, (b) predict survival +CCs, (c) predict return of rhythm -CCs, and (d) predict return of rhythm +CCs. (-CCs = without chest compressions, +CCs = with chest compressions.)

6.3.14 *Binary Features*

Studies have demonstrated that within a resuscitation, successive conversions of VF to organized rhythm are correlated; hence, if a prior shock resulted in return of rhythm following shock, subsequent shocks are also more likely to result in return of rhythm.[106,112] Therefore in recent study, we demonstrated that for repeated shocks, waveform measures analyzed in combination with prior return of rhythm improved prognostic performance during chest compressions.[127] While current defibrillators still require CPR pause for accurate rhythm classification, in recent study we

also demonstrated accurate identification of VF, organized, and asystolic rhythms during uninterrupted compressions.[72,74] Therefore for the sake of the current investigation, we assumed that rhythm classification had been continuously ongoing during chest compressions and that the presence of QRS complexes (i.e. organized rhythm) up to the current point of analysis was known regardless of whether they occurred during compressions. For the subset of VF segments collected prior to the second, third, and fourth shocks, we thus included *Prior ROR* as a binary variable indicating whether the previous shock resulted in return of rhythm.

Utstein characteristics of a patient are significantly related to outcomes but may not be known at the scene of an arrest.[102] We therefore assumed that on-scene rescuers could determine only two Utstein-like characteristics of the patient during treatment (i.e. through visual examination of the patient or the patient's identification) and enter these as two binary variables into a defibrillator during resuscitation. The two characteristics included are *Sex* (sex = female) and *Age* (age < 60). We hypothesized that addition of these categorical variables would improve prediction of patient outcomes when combined with analysis of the VF waveform.

6.3.15 *Logistic Classification Models*

Logistic regression classifiers were used to produce the final output probability for the algorithm (see section 4.8.4.1 for further background on logistic models). For a given 5-s input segment, these models combine the continuous support vector machine output with binary categorical variables to produce posterior probabilities that represent the likelihood of positive outcome. Different versions of the logistic models were applied in the algorithm depending on the availability of categorical variables and which variables demonstrated significant association with specific outcomes on training data. Variables that were not significantly associated with a particular outcome (as observed on training data) were not included in the final logistic model for

predicting that particular outcome. For instance, prior to initial shocks, *Prior ROR* is unknown by definition and is thus not included for analysis of initial shocks, and for prediction of return of rhythm, *Age* and *Sex* were not used as they were not significantly associated with likelihood of return of rhythm (Table 6.3, Table 6.4).

Table 6.3 Logistic model variable descriptions
Summary of variables employed in the final logistic models

Logistic Model Input Variable	Description
Prior ROR	Did the prior defibrillation attempt result in return of rhythm in the ECG (only available for shocks 2-4)? (1 = yes, 0 = no)
Age	Is patient age <60? (1 = yes, 0 = no)
Sex	Is the sex of the patient female? (1 = yes, 0 = no)
*Age*Sex*	Product of Age and Sex. (1 = female and age<60, 0 = otherwise)
SVM	Support vector machine combination of 10 features calculated from filtered VF segments and 10 features calculated from unfiltered VF segments. (Continuous probability of positive outcome.)

Table 6.4 Odds ratios for individual variables on training data
Univariate odds (95% confidence interval) of positive outcome on training data (460 patients). Training data segments were separated into subgroups with and without chest compressions. Odds for continuous variables were standardized. (-CCs = without chest compressions, +CCs = with chest compressions, n = number of training segments, SVM = support vector machine.)

Variable	Odds of Functional Survival		Odds of Return of rhythm	
	-CCs (n=987)	+CCs (n=865)	-CCs (n=989)	+CCs (n=866)
Binary:				
Prior ROR†	2.84 (1.96-4.12)*	2.29 (1.62-3.24)*	4.61 (3.21-6.63)*	4.23 (3.01-5.93)*
Age	1.71 (1.32-2.22)*	1.80 (1.36-2.22)*	1.02 (0.78-1.32)	0.86 (0.66-1.14)
Sex	1.04 (0.76-1.42)	1.22 (0.87-1.71)	1.16 (0.85-1.59)	1.26 (0.89-1.77)
Age×Sex	2.34 (1.51-3.63)*	2.51 (1.56-4.05)*	1.48 (0.92-1.38)	1.23 (0.75-2.01)
Continuous:				
SVM	2.68 (2.29-3.14)*	2.31 (1.98-2.71)*	2.36 (2.02-2.74)*	2.12 (1.81-2.48)*

*Odds significantly greater than 1
†Limited to segments with known values (i.e. prior to shocks 2-4 only)

The final logistic models to predict probability of survival $P_{survive}$ and probability of return-of rhythm P_{rhythm} were therefore of the form

$$P_{survive} = \begin{cases} g\left(\beta_0 + \beta_1(SVM) + \beta_2(Age) + \beta_3(Sex) + \beta_4(Age \times Sex)\right) & \text{if } shock = 1 \\ g\left(\beta_0 + \beta_1(SVM) + \beta_2(Age) + \beta_3(Sex) + \beta_4(Age \times Sex) + \beta_5(Prior\ ROR)\right) & \text{otherwise} \end{cases} \quad (6.23)$$

and

$$P_{rhythm} = \begin{cases} g\left(\beta_0 + \beta_1(SVM)\right) & \text{if } shock = 1 \\ g\left(\beta_0 + \beta_1(SVM) + \beta_2(Prior\ ROR)\right) & \text{otherwise} \end{cases} \quad (6.24)$$

where the logistic function $g(z) = \frac{1}{1+e^{-z}}$, *shock* represents the current shock cycle, and β are the logistic regression parameters.

6.3.16 *Statistical Methods and Data Processing*

Performance for prediction of positive outcome was characterized by AUC. Significance of differences between AUC values for correlated receiver operating characteristic curves, as well as 95% confidence intervals, were evaluated using the DeLong method.[115] Differences in uncorrelated AUC values were compared using the Robin extension of the DeLong method for unpaired data.[109] Alpha level to determine statistical significance was 0.05. Odds ratios were calculated based on univariate logistic regression coefficients. Odds ratios for continuous variables were standardized by calculating odds after removing the mean and scaling the variable to a standard deviation of 1.

Data processing was performing using MATLAB 2018a (The Mathworks, Natick, MA) and RStudio Desktop 1.1.383 (RStudio, Boston, MA).

6.4 RESULTS

The final novel prognostic algorithm significantly predicted functional survival and return of rhythm on training data. Specifically, training AUC for predicting survival was 0.78 without

compressions and 0.75 with compressions. Training AUC for predicting return of rhythm was 0.75 without compressions and 0.73 with compressions.

The final prognostic algorithm significantly predicted functional survival and return of rhythm after shock using validation data. Specifically, validation AUC for predicting survival was 0.76 without compressions and 0.75 with compressions (p=0.63 for difference) (Figure 6.26, Table 6.5). Validation AUC for predicting return of rhythm was 0.77 without compressions and 0.74 with compressions (p=0.10 for difference) (Figure 6.26).

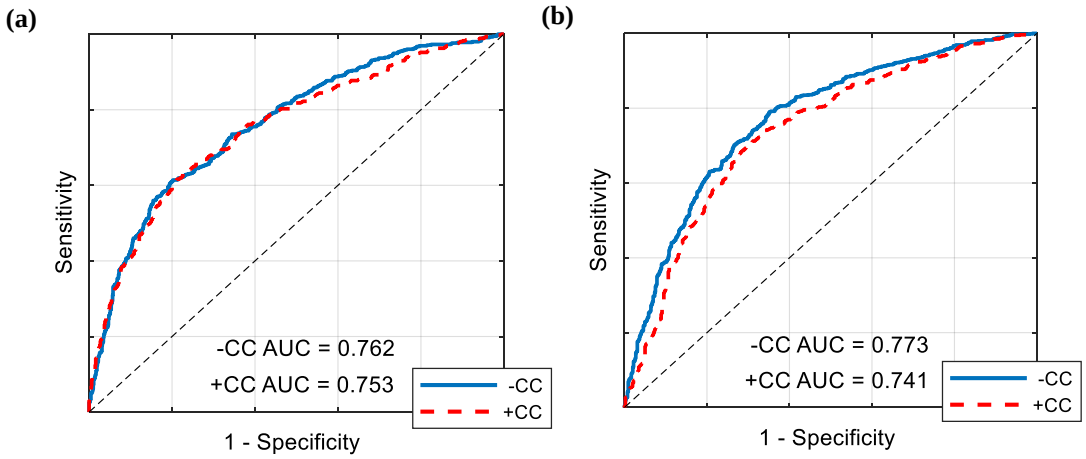

Figure 6.26 Validation receiver operating characteristic curves for novel method
Receiver operating characteristic curve values are shown for predicting (a) survival and (b) return of rhythm in 691 validation patients. (AUC = area under receiver operating characteristic curve, -CC = without chest compressions, +CC = with chest compressions.)

The best-performing previously-published method selected for comparison against the current novel method on validation data was termed the *SVM*$_{24}$ algorithm (denoting the support vector machine combination of 24 existing measures optimized for use during compressions), which we demonstrated in previous investigation.[91] Compared to *SVM*$_{24}$ on the validation dataset, the novel method did not demonstrate improved prediction of survival, but did demonstrate significantly-improved prediction of return of rhythm (Table 6.5).

Table 6.5 Validation AUC values for novel method versus best existing method
AUC (95% confidence interval) values on validation data for the novel prognostic algorithm versus the best-performing prior method (SVM_{24}). AUC increase indicates improvement in AUC using the novel method versus the SVM_{24} method. (AUC = area under the receiver operating characteristic curve, -CCs = without chest compressions, +CCs = with chest compressions.)

	Predicting Survival		**Predicting Return of Rhythm**	
Compression State	-CCs	+CCs	-CCs	+CCs
Novel Method AUC	0.762 (0.736-0.789)	0.753 (0.724-0.782)	0.773 (0.750-0.797)	0.741 (0.714-0.768)
SVM_{24} AUC	0.754 (0.727-0.781)	0.748 (0.719-0.777)	0.745 (0.721-0.770)	0.699 (0.670-0.727)
AUC Increase	0.008	0.005	0.028	0.042
P-value for Change	p=0.21	p=0.60	p<0.001	p<0.001

On validation data, the 10 novel features evaluated individually from both filtered ECGs and unfiltered ECGs were predictive of survival (Table 6.6) and return of rhythm (Table 6.7). As a reference to represent relative difficulty of the dataset, the previously-described amplitude spectrum area measure calculated from bandpass-filtered ECGs (without adaptive filtering) was also predictive of survival (AUC = 0.74 without compressions, AUC = 0.70 with compressions) and return of rhythm (AUC = 0.73 without compressions, AUC = 0.66 with compressions).[65]

Table 6.6 Validation AUC values for individual features (survival)
AUC values for individual ECG features calculated using filtered and unfiltered VF segments from 691 validation patients are reported. Note that while filtered features without compressions employed a 1-30 Hz bandpass filter, filtered features with compressions were applied after bandpass filtering and adaptive notch filtering to remove compression artifact (only if compressions were detected by the compression detection algorithm).

Feature	**Without Chest Compressions**		**With Chest Compressions**	
	1-30 Hz	Unfiltered	1-30 Hz + Notch	Unfiltered
Sliding Deviation	0.728	0.734	0.728	0.694
Sliding Peak	0.670	0.687	0.686	0.613
Interfrequency Entropy	0.679	0.678	0.633	0.677
High-Frequency Entropy	0.573	0.598	0.587	0.559
Shannon Energy	0.753	0.748	0.736	0.741
Interfrequency Shannon Energy	0.752	0.754	0.732	0.740
Wavelet Maxima	0.711	0.716	0.686	0.684
Wavelet Maxima Fraction	0.703	0.702	0.684	0.665
Short-Time Deviation	0.708	0.674	0.667	0.661
Correlation Component	0.632	0.603	0.638	0.585

Table 6.7 Validation AUC values for individual features (return of rhythm)
AUC values for individual ECG features calculated using filtered and unfiltered VF segments from 691 validation patients are reported. Note that while filtered features without compressions employed a 1-30 Hz bandpass filter, filtered features with compressions were applied after both bandpass filtering and adaptive notch filtering to remove compression artifact (only if compressions were detected by the compression detection algorithm).

Feature	Without Chest Compressions		With Chest Compressions	
	1-30 Hz	Unfiltered	1-30 Hz + Notch	Unfiltered
Sliding Deviation	0.744	0.743	0.687	0.652
Sliding Peak	0.723	0.721	0.669	0.580
Interfrequency Entropy	0.606	0.606	0.568	0.634
High-Frequency Entropy	0.567	0.612	0.559	0.524
Shannon Energy	0.730	0.724	0.670	0.669
Interfrequency Shannon Energy	0.734	0.738	0.678	0.690
Wavelet Maxima	0.683	0.681	0.637	0.641
Wavelet Maxima Fraction	0.675	0.676	0.646	0.653
Short-Time Deviation	0.667	0.658	0.618	0.647
Correlation Component	0.641	0.587	0.601	0.572

6.5 DISCUSSION

In this retrospective investigation of out-of-hospital ventricular fibrillation arrest, we demonstrate a novel algorithm designed to evaluate patient status during CPR using a combination of adaptive filtering, ECG features, and categorical variables. We sought to determine whether such an algorithm could provide improved prognostic performance during chest compressions versus the best-performing method described in current literature (which was evaluated in our previous benchmark investigation). Using validation data, we observed that the novel algorithm significantly improved prediction of defibrillation success as defined by return of rhythm after shock. However, prediction of survival was only incrementally greater and was not significantly improved. These results suggest potential for improved real-time assessment of patient myocardial physiology to guide treatment during resuscitation without requiring chest compression interruption.

VF is characterized by depolarization waves in the myocardium which overtake the pacing from the sinoatrial node, preventing coordinated contraction of the ventricles and causing a lethal cessation of blood flow.[18] During VF, the myocardium is in a metabolically demanding state that rapidly depletes high-energy phosphate concentrations, deteriorates transmembrane potentials, and increases intracellular calcium due to lack of blood flow to the cardiac tissue.[4,122] Conversion of VF to a coordinated, perfusing rhythm is possible through electrical defibrillation, but likelihood of successful defibrillation is reduced the longer it takes to administer a shock.[56] The early stage of VF has been termed by some as the 'electrical phase', referring to need for immediate electrical defibrillation within 1-4 minutes of reentry.[124,206] However, after VF continues to persist untreated and the metabolic state of the myocardium becomes increasingly compromised, chest compressions (which can provide up to one third of normal cardiac output) prior to shock can improve the chance of successful defibrillation by partially reperfusing myocardial tissue.[34] This stage of VF (between approximately 4-10 minutes after reentry) has been termed by some as the 'circulatory phase' to indicate the need for perfusion prior to defibrillation in cases where VF has persisted without treatment.[124,206] In practice, when using VF duration as a surrogate for the state of the myocardium, patients who have undergone VF for less than approximately 4-5 minutes should be shocked immediately, whereas patients in prolonged VF may be assumed to be metabolically compromised and should receive CPR and vasopressor medication to improve the condition of the myocardium prior to shock.[35,40,206] Unfortunately, as use of time since VF onset is a difficult metric to implement in an out-of-hospital setting and no alternative direct measure of patient myocardial physiology has been widely accepted, current protocol simply dictates immediate initial defibrillation followed by 2-minute defibrillation-CPR cycles regardless of the underlying condition of the patient's myocardium.[31]

Multiple measures of the VF metabolic state have thus been proposed to prioritize the application of defibrillation, CPR, and medications. However, such measures have been designed and evaluated using VF ECGs free of chest compression artifact and their performance during real-world CPR has been largely unknown, challenging the idea that such measures could be applied continuously during resuscitation.[43,45,57] Hence we recently evaluated the performance of 27 measures during chest compressions, and observed that machine learning combinations of individual measures had the highest performance during compressions, although overall performance remained modest (e.g. AUC=0.70 to predict return of rhythm during CPR), suggesting that such measures may still be insufficient to guide clinical care during resuscitation without interrupting chest compressions to allow analysis.[91] Therefore in the current investigation, we sought to design an improved prognostic method designed specifically to function during uninterrupted CPR chest compressions, and to determine whether such a method would improve prediction of outcomes compared to best-performing prior methods.

We designed an adaptive filter based on the frequency of compressions detected in the TTI signal in order to reduce the effect of chest compression artifact in the ECG and improve subsequent ECG feature calculation. All ECGs were bandpass-filtered to remove drift and high-frequency noise, and the adaptive filter was only applied after bandpass filtering if compressions were automatically detected in the chest impedance (see Chapter 5 for a further description of the compression detection algorithm). Because the spectral content of VF is primarily between approximately 3-8 Hz and compression artifacts can affect frequencies spanning the low-frequency compression fundamental to high-frequency harmonic and transient artifacts (2-20 Hz), it is difficult to remove compression artifact from the ECG without compromising useful prognostic characteristics of the VF signal.[18,110,123] We observed that during chest compressions, lower-

frequency compression artifacts could indeed be removed by the adaptive filter while still preserving much of the VF ECG signal, and that a group of representative measures was significantly improved by the adaptive filter using training data. (As a qualitative example, Figure 6.27 compares adjacent VF segments with and without compressions; after adaptive filtering, the VF during compressions has a similar appearance to the compression-free segment.) These results in consideration with the validation performance of individual features (Table 6.6) suggest that the adaptive filter is useful for improving amplitude-based VF analysis during compressions; however, improvement by filtering is minimal for wavelet-based time-frequency features which inherently exclude low-frequency artifact.

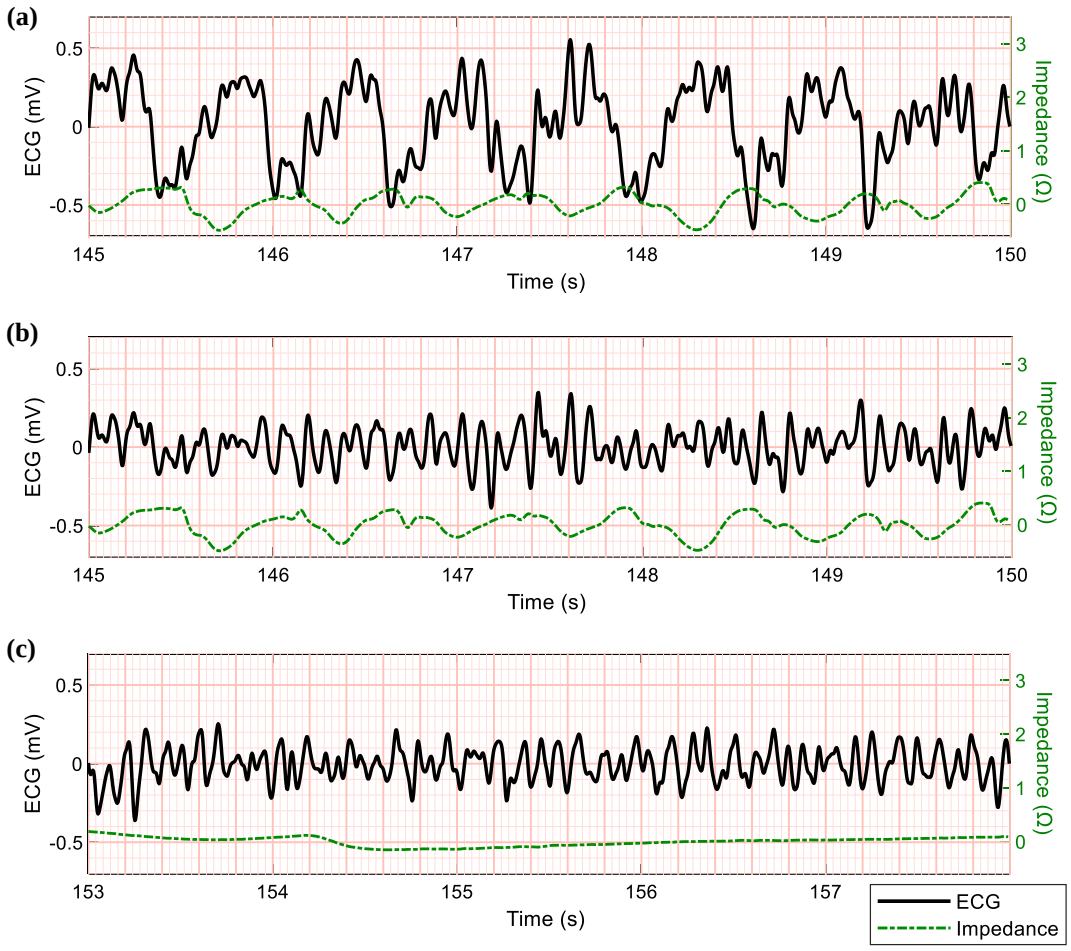

Figure 6.27 Filtered VF during compressions versus VF without compressions
(a) VF ECG during chest compressions before application of the adaptive notch filter. (b) VF ECG during chest compressions after application of the adaptive notch filter. (c) VF ECG without chest compressions collected 3 seconds after the end of the segment in (a). The VF without artifact in (c) has a similar appearance to the notch-filtered VF with artifact in (b), although some residual high-frequency artifacts are still visible in (b) (e.g. at 147.8 s and 149.4 s).

Myocardial ischemia during VF reduces the conduction velocity of cardiomyocytes and causes increased risk of afterdepolarizations.[4] Thus as VF persists, the VF ECG changes from a coarse high-amplitude appearance with larger low-frequency oscillations a to a lower-amplitude, finer appearance.[8,9,110,122] While early, robust VF does have a qualitatively coarse appearance with large lower-frequency oscillations due to larger rotor wavefronts,[104] the amount of high frequency content (e.g. sharpness) in coarse VF may also be greater and the fundamental rotor frequencies

higher; hence, studies of VF frequency have observed a significant overall decrease in median and dominant VF frequency over time as ischemia progresses.[8,9,110] As VF degrades from an early coarse state to a finer, more anaerobic state, it also becomes more disorganized and chaotic over time and can be characterized using entropy and nonlinear dynamics metrics.[10,11,90,101,104,143,207] We sought to quantify these phenomena through evaluation of ten features of ECG amplitude, time-frequency entropy and energy, dominant frequency, and time-frequency self-similarity. The features were designed with variable parameters optimized on training data with and without compressions to allow each feature to minimize the effects of compression artifact.

Two VF features were developed based on ECG amplitude: *Sliding Deviation* and *Sliding Peak*. Both had relatively high performance without compressions but were significantly affected by compression artifact. The optimal analysis window size was as short as 16 ms during compressions, and while the optimal length even without compressions was longer it did not exceed 72 ms. For instance, within a window size of 72 ms, full-period oscillations at approximately ≥14 Hz may be observed, and since both amplitude functions operate on the absolute-value, zero-mean ECG (i.e. negative fluctuations below baseline are translated to positive fluctuations, thus doubling the occurrence of positive peaks), a full period of rotors resulting from a native ≥7 Hz source may theoretically be observed within such a window size. These observations suggest that high-frequency amplitude in VF is predictive of patient outcome and that lower-frequency amplitude fluctuations (i.e. below approximately 7 Hz) in the waveform, while useful, may be ignored to reduce the effect of chest compression artifact in amplitude-based analysis.

Four features were designed based on forms of the Shannon equation applied to the wavelet spectrogram: *Interfrequency Entropy*, *High-Frequency Entropy*, *Shannon Energy*, and

Interfrequency Shannon Energy. These features incorporate the median operation to exclude spurious behavior within specific frequency bands or at specific time points. *Interfrequency Entropy* and *High-Frequency Entropy* features were calculated from probability distributions of spectrogram magnitudes across frequencies. The wider-band *Interfrequency Entropy* functioned optimally with a low frequency cutoff of approximately 3-4 Hz both with and without CPR. This result suggests that having evenly-distributed magnitudes across a wide range of frequencies (indicating that VF contains both low- and high-frequency content, perhaps due to strong fundamental rotor concurrent with sharp oscillations or high-frequency fibrillation) indicates a good prognosis as compared to smoother VF containing only low-frequency content. Prior studies of various entropy metrics of the VF signal have confirmed similar observations of higher entropy values indicating better prognosis.[90,143] However, we also observed that when frequency ranges were optimized for maximum prediction based on inverse entropy across frequency magnitude distributions, the optimal frequency ranges for analysis were approximately 15-40 Hz. This result suggests that when limited to high frequencies alone, presence of dominant or persistent behavior in narrow high-frequency bands, rather than an even distribution of spectral content, is also indicative of good prognosis and may be related to metabolic characteristics such as higher conduction velocities require to sustain higher-frequency rotors and fibrillation in the myocardium.

Shannon Energy and *Interfrequency Shannon Energy* had similar formulations to entropy measures but were calculated using the Shannon equation applied directly to the non-normalized wavelet transform coefficient magnitudes. Prediction was higher on unfiltered data in spite of the adaptive filter used in filtered data. This result is due to the utility of the higher-frequency information in the unfiltered data, as unfiltered data had a bandwidth up to 40 Hz versus a 30 Hz in filtered data. Increased energy was associated with positive outcome, and frequency limits for

analysis ranged from a low cutoff of 5-20 Hz to a high cutoff of 40 Hz depending on the specific outcome or compression state. The two Shannon energy features had the most robust performance during compressions of any individual metrics in the current investigation (e.g. AUC=0.74 for *Shannon Energy* prediction of survival during compressions using unfiltered data). These results suggest that increased high-frequency energy (between approximately 10-40 Hz) in the VF waveform is a superior indicator of good prognosis. As a qualitative example, Figure 6.28 illustrates VF with good prognosis versus poor prognosis, with intratemporal normalization applied to their spectrograms (i.e. normalized to the maximum at each time sample) to allow visual comparison of relative frequency content at each timepoint.

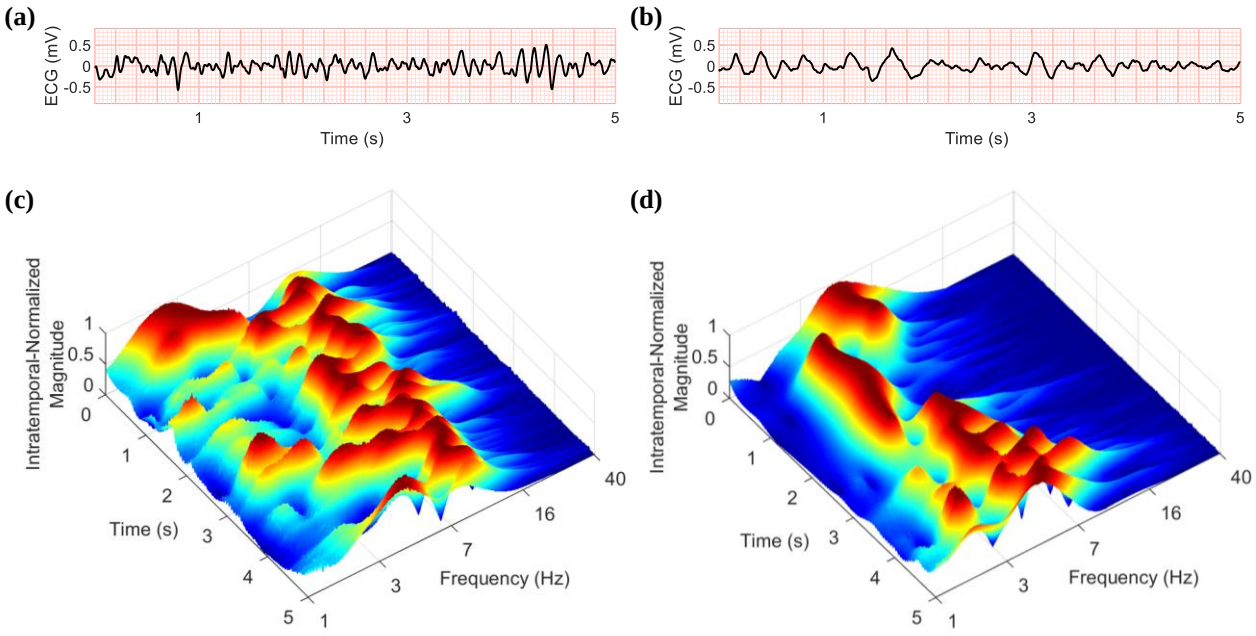

Figure 6.28 Good versus poor prognosis with intratemporal normalization
In general, a greater relative amount of high-frequency activity is indicative of robust VF. (a) VF with good prognosis (i.e. the subsequent defibrillation resulted in return of rhythm) without chest compressions. (b) VF with poor prognosis (i.e. the subsequent defibrillation did not result in return of rhythm) without chest compressions. (c) Wavelet spectrogram of VF with good prognosis, with intratemporal normalization to emphasize dominant frequency. (d) Wavelet spectrogram of VF with poor prognosis, also with intratemporal normalization.

Two features to describe the dominant frequency of the VF signal over time were designed: *Maxima Fraction* and *Mean Maxima.* Prior Fourier-based methods have estimated the dominant, peak, centroid, and median frequency in the VF signal averaged over the entire length of the signal, as higher VF frequency is associated with time since reentry and likelihood of successful outcome.[7,20,88,110,136] Rather than estimating dominant frequency averaged over a single Fourier transform which averages frequency content over the entire input segment, *Maxima Fraction* and *Mean Maxima* both track the VF frequency with the greatest magnitude over the length of the input segment using the wavelet spectrogram. *Maxima Fraction* evaluated the proportion of time the VF frequency exceeded a threshold indicative of robust physiology and good prognosis; this dominant frequency threshold was determined using training data and ranged from 3.3-5.4 Hz (depending on CPR, filtering, and outcome). While the exact VF dynamics in humans are uncertain, one prevailing theory is that VF is largely driven by a dominant self-sustaining mother rotor of depolarizing ventricular cardiomyocytes, while others theorize the presence of multiple smaller self-perpetuating rotors.[14,17,18] Regardless, our results indicate that a dominant frequency (whether from a single rotor or multiple contributing rotors) above approximately 3.3-5.4 Hz is indicative of good prognosis, while a dominant frequency below this range is associated with poor prognosis and may be related to factors that reduce likelihood of successful shock, such as prolonged ischemia and reduced conduction velocity. In contrast to *Maxima Fraction*, the *Mean Maxima* did not derive a specific threshold defining robust VF but instead optimized frequency ranges for evaluation of dominant frequency to allow exclusion of CPR artifact. Optimal frequency ranges selected on training data for calculation of *Mean Maxima* were wide (e.g. 1-40 Hz) in the absence of compression artifact, and slightly narrower during compressions (with low frequency limits between 2-4 Hz) in order to avoid chest compression artifact. Notably, in contrast to energy and

entropy features which functioned with relatively high performance using only high frequencies (i.e. ≥10 Hz), *Mean Maxima* required mid-frequency content between 4-10 Hz for accurate analysis, and had poor performance when limited to high-frequency content only. This result is likely due to the fact that since most human VF is between 3-8 Hz, evaluation of dominant frequency is only useful when describing the fundamental rotor frequency but not for evaluating the sharpness and high frequency content in the signal; thus, dominant frequency analysis is not useful for VF prognosis when evaluated only at high frequencies. Therefore, in contrast to energy measures, estimation of dominant frequency is also likely more susceptible to artifact during chest compressions due to the overlap of compression harmonics with dominant VF frequencies.

Two features were designed to evaluate similarities between the spectra within short-time Fourier transforms of the VF signal: *Short-Time Deviation* and *Correlation Component*. *Short-Time Deviation* evaluated the median flatness of the Fourier magnitudes over short windows of the input signal as described by their standard deviations. A higher median standard deviation of spectral magnitudes indicated a good prognosis, suggesting that the presence of relatively prominent or fewer rotors in the ventricular myocardium increases the likelihood of successful defibrillation, and more chaotic electrical activity lacking prominent spectral peaks may indicate prolonged VF. These results confirm prior observations that the lack of spectral flatness is a useful predictor of myocardial receptiveness to defibrillation.[116,208] *Correlation Component* evaluated similarities across time profiles between different frequencies. This function may be able to detect sharper oscillations indicative of robust VF that span a wider spectral range (e.g. a dominant rotor with fast conduction velocity). However, utility of this feature was low, suggesting that simply comparing the time-series profiles across frequency bands is not a strong prognostic indicator.

We used a support vector machine model to combine individual features into a single metric. Prior investigations have combined multiple VF waveform measures using support vector machine models in attempts to improve performance over individual measures.[89,101,144,209] Results of these prior studies are mixed, with the majority of studies not demonstrating an obvious advantage of support vector machines over individual measures, likely due to limited data and the use of fixed (rather than optimized) box constraint values. Additionally, these studies were limited to analysis without chest compressions, and do not address the potential for analysis during chest compressions. Hence in recent study, we demonstrated improved performance relative to individual features using support vector machines during chest compressions (although maximum performance remained modest).[91] These prior results suggest that given adequate training data, support vector machines are an ideal way to combine multiple features of the VF ECG, especially during CPR. Therefore, in the current investigation, we used support vector machines with radial kernels to combine 20 individual ECG features (10 from filtered data and 10 from unfiltered data) into a single probability value. Different models were trained for prediction of survival and return of rhythm, both with and without compressions. When trained without hyperparameter optimization, support vector machines can easily overfit and thus fail to generalize. Therefore, we adjusted both the kernel and box constraint hyperparameters, and using a novel technique, searched for optimum hyperparameter combinations within error tolerance values relative to minimum error. This process allowed the model to be trained for maximum robustness and generalizability. Of the features employed in the current investigation, some functioned optimally using filtered data (e.g. amplitude features) while others functioned optimally using unfiltered data (e.g. energy features). Use of the support vector machine model enabled the ideal relative contributions of all filtered and unfiltered features and exclusion of less useful features. Specifically, use of the radial

kernel enabled separation of data in higher-dimensional feature space, which we hypothesized leveraged optimal combinations of input features based on our training data.[167,169,171] Unfortunately, unlike models such as logistic regression or neural networks, support vector machine models are not easily-interpretable; thus, the actual relative contributions of individual input features in our models is unknown.

We included three binary variables to provide additional information to the algorithm useful for predicting patient outcomes: *Prior ROR* (previous defibrillation success), *Sex* (sex=female), and *Age* (age<60). While *Prior ROR* was significantly predictive of long-term survival and successful electrical defibrillation as defined by return of rhythm, *Sex* and *Age* were significantly associated with survival but not with successful defibrillation. Overall, use of these three variables improved prognostic performance over use of ECG-based features alone. Notably, *Prior ROR* provided an exceptional benefit to overall prediction of return of rhythm versus using ECG-based features alone, even though *Prior ROR* was only known for a subset of the data (i.e. segments collected prior to shocks 2-4). However, inclusion of *Sex, Age,* and *Prior ROR* in a prognostic algorithm requires assumptions. For accurate detection of *Prior ROR*, the defibrillator would theoretically be required to continuously analyze the ECG rhythm to detect a short period of QRS complexes following shock, regardless of whether this rhythm occurred during ongoing chest compressions. While current defibrillators do not implement rhythm classification during CPR, we recently demonstrated a read-through-CPR ECG algorithm in prior investigation, and thus made an assumption in the current study that a next-generation defibrillator would employ such an algorithm.[72] Indeed, two leading defibrillator manufacturers have recently conducted pilot studies demonstrating rhythm analysis during chest compressions; hence the assumption that a next-generation defibrillator can classify ECG rhythms during compressions is reasonable.[74,75] We

also assumed that the rescuers would be able to determine whether the patient was female sex and whether the patient was aged less than 60, either based on the patient's identifying documents or by visual inspection, and that this information could be entered into a defibrillator at the onset of a resuscitation (such as while the defibrillator pads were being attached).

We used logistic regression to combine the support vector machine probability (which describes the VF ECG waveform) with binary categorical patient characteristics to produce a final probability of positive outcome. As *Prior ROR* is by definition unknown prior to initial shock but is known for shocks delivered thereafter, two variations of the final logistic models (one which includes *Prior ROR* and one that does not) were implemented depending on the current shock cycle. While we have demonstrated utility of *Prior ROR* in a prior study for analysis of shocks 2-4 during CPR, it was unknown whether such a feature applied to a prognostic algorithm designed to analyze all shocks (including shocks with unknown *Prior ROR*) would ultimately provide any overall benefit.[127] Thus in the current study, to evaluate AUC for validation data, posterior probabilities for versions of the model to predict initial shock outcome (which do not incorporate *Prior ROR*) and for versions of the model to predict subsequent shock outcome (which do incorporate *Prior ROR*) were mapped to a shared probability scale as would be required in a real-world setting. These classification probabilities mapped to the shared probability scale were used to produce a single receiver operating characteristic curve to represent the combined performance across all shocks, as illustrated in Figure 6.26.

In this investigation, different versions of the novel algorithm were trained and evaluated to predict outcome with and without CPR. Specifically, each CPR state was analyzed with different filtering, ECG feature parameters, and logistic combination models. Prediction of survival was only marginally greater without compressions versus with compressions ($p=0.61$), and while

prediction of return of rhythm had a moderately higher AUC without compressions versus with compressions, this difference was also not significant (p=0.10). Thus, performance with and without CPR was fairly similar and not statistically different, but AUC point estimates remained moderately higher without CPR. (It should be noted that because the CPR and CPR-free data were not paired, an unpaired test was used to compare performance with and without compressions; it is possible that evaluation using a paired dataset would yield a statistically-significant difference.) These results suggest that while chest compression artifact overall may have a slight negative impact on the novel method (more so for prediction of return of rhythm), analysis may be performed with or without chest compressions without a severe reduction in AUC.

We developed separate versions of the novel prognostic method in the current investigation to predict different patient outcomes: One version employed feature and model parameters optimized for prediction of survival, while the other version was optimized to predict return of rhythm. Other studies have evaluated prediction of a variety of outcomes including return of circulation or survival to hospital admission; however there is not a consensus as to which definition of good patient outcome is superior.[145] It is possible that using a model designed to predict survival may have different practical applications compared to a model designed to predict return of rhythm. When assessing the effect of medications or resuscitation therapies such as brain cooling, for instance, a prognostic algorithm predictive of neurologically-intact survival could potentially provide a better metric by which to assess the real-time effect of these therapies. In contrast, as defibrillation shock is intended to convert ventricular fibrillation to an organized rhythm in the heart and is not intended to directly treat other organs such as the brain, an algorithm designed to predict electrical return of rhythm might perhaps be preferred to guide shock timing. While the optimal configuration and application for predicting one outcome versus another is

hypothetical and requires further study, these results highlight the potential for the algorithm to predict different outcomes in order to guide specific types of therapy.

To determine whether the novel algorithm described in this investigation exhibited improved prognostic performance compared to prior methods, we selected the best-performing method from our prior benchmark of 27 existing methods (termed the SVM_{24} method) for comparison. Comparing performance of both methods on our validation data using a paired test, the novel algorithm exhibited significantly-improved prediction of return of rhythm versus SVM_{24} (AUC increase = 0.03 and 0.04 without and with chest compressions respectively, $p<0.001$ for increases). However, performance was not significantly improved for predicting survival (although there was a marginal increase in AUC). We hypothesize that these results were enabled in part through the use of optimized ECG-based features calculated in parallel from unfiltered ECGs (which allowed increased high-frequency information, thus improving wavelet features) and adaptive-filtered ECGs (which have reduced compression artifact, thus improving amplitude features). In addition, incorporating the categorical variables of *Age*, *Sex*, and *Prior ROR* provided further benefit; without these categorial variables (especially *Prior ROR*), the novel algorithm may not have significantly out-performed SVM_{24} which was based solely on isolated ECG segments without incorporating information available from the ECG history. These results were observed in spite of use of a chest compression detection function for the novel method (rather than manual annotation) to simulate real-world conditions. While the prior SVM_{24} method and the novel method both apply specific parameters depending on chest compression state, the reported performance of SVM_{24} was evaluated on validation segments with the presence of compressions pre-annotated which may have inflated the true real-world performance of the SVM_{24} method. The novel method, however, was evaluated blinded to the presence of chest compressions, and applied specific

parameters and filter settings based on automatic detection of compressions in the chest impedance. These results suggest that the novel method has greater potential than SVM_{24} for real-world application than may be indicated by AUC values alone.

To assess the relative difficulty of our validation data in comparison to data collected in other studies, we evaluated a well-established measure that has been characterized in a number of prior investigations. As the overall difficulty of datasets across studies can vary, the relative performance of measures described elsewhere versus measures described in the current investigation can be difficult to ascertain. Indeed, there is consensus that lack of a standardized dataset by which to gauge VF waveform algorithms is a major shortcoming in the field of VF waveform analysis.[56,57] However, in lieu of a standardized dataset, evaluating the relative performance of a predefined measure with highly-characterized performance can provide a means by which to indirectly compare different measures across studies when a direct side-by-side comparison is not possible. Therefore as a reference, we calculated the well-characterized amplitude spectrum area measure using our validation data.[97,98] Prior comprehensive benchmark studies multiple waveform measures have reported amplitude spectrum area AUC values of 0.83, 0.81, and 0.88 without compressions, as compared to 0.74 in the current investigation.[65,89,90] This result indicates that the current study dataset is relatively difficult, or conversely, that study data from other investigations was subject to selection bias (e.g. excluding noisy or unusual samples). It is also possible that the current study data is more difficult to analyze due to inclusion of signals with heterogenous original filter responses and sampling rates which in turn may have slightly different optimal ECG waveform measure thresholds indicative of good prognosis. Indeed, in prior investigation of the current study data, we confirmed a significant reduction in prognostic AUC due to use of ECG segments from devices with heterogenous sampling rates (see section 4.12.3).

In spite of modest overall performance however, the AUC values for the novel method demonstrated in the current study were greater than the AUC for amplitude spectrum area; for example, AUC=0.75 versus AUC=0.70 respectively ($p<0.001$ for difference) for predicting survival during chest compressions. By comparison, one recent study described a measure (the *Signal Integral*) with a high reported AUC of 0.95 during chest compressions; however, the same study also reported an amplitude spectrum area AUC of 0.95 during compressions.[111] The AUC values from the *Signal Integral* study suggest that in spite of a high absolute AUC for the *Signal Integral* measure, relative performance of the *Signal Integral* is likely less than measures observed to out-perform the amplitude spectrum area (such as the novel method described in the current study). Overall, therefore, we conclude that the current study dataset is comparatively difficult versus data collected in other studies, and that while relative performance of measures evaluated on the current study data can allow comparisons between those specific measures, comparisons of AUC values observed in the current investigation versus those in other studies must be considered in light of the difficulty of the particular dataset.

6.6 LIMITATIONS

The study data contained 5-s VF ECG segments collected during ongoing compressions, which in some instances may be difficult to classify as VF due to compression artifact in the ECG. Hence, the segments could potentially contain other rhythms such as asystole or weak organized rhythms mistakenly annotated as VF due to chest compression artifact. To determine utility of the novel method during compressions, the performance of the method was compared to a best-performing previous method as determined by a prior benchmark investigation. It is unknown whether other previous methods that have not been compared would have superior performance. The current investigation used data collected from four different defibrillator models with heterogenous

hardware-based filtering bandwidths and sampling rates, which may reduce overall AUC for waveform measures. However, the results therefore highlight the cross-platform applicability of the algorithm demonstrated in this study. The results of the current study were retrospective, and the potential for improved patient care using a prognostic algorithm is hypothetical. Prospective evaluation in a clinical setting would ultimately be required to determine whether a prognostic algorithm could improve patient survival.

6.7 CONCLUSION

A novel prognostic algorithm demonstrated improved prediction of return of rhythm and equivalent prediction of survival during chest compressions as compared to prior methods. The novel algorithm's observed prognostic performance was enabled through a combination of adaptive filtering, optimized ECG features, and categorical variables. These results suggest potential for real-time evaluation of patient status during uninterrupted chest compressions in order to monitor the effects of therapy and to optimize timing of defibrillation. Future investigation to leverage continuous ECG data (rather than isolated 5-s segments as in the current investigation) in conjunction with techniques such as deep learning may offer opportunity for further-improved prognostic analysis.

6.8 ACKNOWLEDGEMENTS

Chenguang Liu (Philips Healthcare, Bothell, WA) provided the suggestion to analyze the unfiltered ECG in addition to (and in parallel with) with the filtered ECG. Dawn Jorgensen, Stacy Gehman, and Vijay Tadipatri (Philips Healthcare, Bothell, WA) provided additional insights on Philips defibrillator data processing. MATLAB code to calculate p-values for comparing correlated receiver operating characteristic curves was provided by John W Pickering (University

of Otago, Christchurch, New Zealand). This work was supported in part by grants provided to the University of Washington by the Washington State Life Sciences Discovery Fund, Philips Healthcare, the Laerdal Foundation, and the National Institute of Biomedical Imaging and Bioengineering of the National Institutes of Health (T32EB001650). The content of this work is solely the responsibility of the authors and does not represent the views of the funding organizations, Public Health Seattle and King County, or Philips Healthcare.

Chapter 7. SUMMARY

7.1 KEY FINDINGS OF SPECIFIC AIMS

These investigations indicate potential for improved defibrillator-guided treatment of out-of-hospital ventricular fibrillation cardiac arrest. Our observations suggest that patient status (as represented by likelihood of positive clinical outcome) can – to a limited degree – be automatically monitored in real time during resuscitation without requiring CPR interruption for analysis. This estimate of patient status may be useful for guiding application of therapy and monitoring the effects of treatments in real time.

7.1.1 *Aim 1: Evaluate potential for VF prognosis during short CPR pauses.*

In Aim 1 (Chapter 2), we observed that two representative measures of the ventricular fibrillation ECG predicted patient outcomes when calculated from input segments as short as 0.2 s. A significant loss in performance was observed using segments as short as approximately ≤0.8-1.8 s depending on the specific measure and outcome evaluated. These results indicate a limited potential to assess patient status during incidental chest compression pauses throughout resuscitation. However, given the potential loss in prognostic performance (depending on buffer size) and ability to only intermittently apply measures when CPR is paused, ideally patient status would be assessed continuously during uninterrupted CPR.

7.1.2 *Aim 2: Determine whether incorporating prior shock outcome improves VF waveform measure prediction of subsequent outcomes during CPR.*

In Aim 2 (Chapter 3), we observed that CPR artifact significantly reduces the performance of two representative measures of the VF waveform, but that performance of these measures is

significantly improved during CPR when combined with the outcome of the previous shock (e.g. AUC increase from 0.68 to 0.74 during CPR). These results suggest that when predicting outcome of repeated shocks (i.e. the second, third, or fourth shock cycles), incorporating ECG rhythm history – specifically whether sinus rhythm occurred after a previous defibrillation attempt – can significantly improve performance.

7.1.3 *Aim 3: Characterize existing waveform measures and determine whether combining multiple measures improves performance during CPR.*

In Aim 3 (Chapter 4), we observed that individual existing measures of the VF waveform are compromised by the presence of CPR artifact even after optimizing parameters (such as frequency limits) to mitigate the effect of chest compression artifact. We also observed that a best-performing machine learning combination of individual measures exhibited near-equivalent prediction of survival with CPR versus without CPR (AUC = 0.75 in both cases) while also demonstrating superior performance relative to individual measures. However, prediction of return of rhythm was still reduced with CPR (AUC = 0.70) versus without CPR (AUC = 0.75) using this best-performing machine learning combination. These results that suggest machine learning combinations of individual features, when trained on CPR-corrupted data and CPR-free data separately, offer superior potential to assess patient status throughout resuscitation without requiring CPR pause for analysis.

7.1.4 *Aim 4: Develop impedance-based chest compression detection function.*

In Aim 4 (Chapter 5), we observed that a function designed to detect presence of chest compressions using the transthoracic impedance signal had high performance on validation data (sensitivity and specificity $\geq$ 98%). The performance of this function exceeded that of prior

methods and was validated using a relatively large patient cohort, suggesting broad applicability across platforms. This function could therefore enable use of next-generation ECG algorithms that apply different parameters depending on the chest compression state.

7.1.5 *Aim 5: Determine whether a novel prognostic algorithm improves assessment of patient status during CPR.*

In Aim 5 (Chapter 6), we observed that a novel algorithm to assess patient status during CPR exhibited improved prognostic performance when compared to the best-performing existing methods identified in Aim 3. Specifically, using a combination of adaptive filtering, novel features of the ECG optimized for using during compressions, and categorical variables assumed to be available during resuscitation, the novel algorithm demonstrated significantly-improved prediction of the patient's likelihood of return of sinus rhythm after defibrillation (e.g. AUC = 0.74 during CPR for the novel method versus AUC = 0.70 for the best-performing previous method). However, prediction of survival was only marginally improved versus the best-performing prior method (AUC = 0.75 for both the novel algorithm and prior method during CPR). The novel method was applied in conjunction of the automatic compression detector described in Aim 4, indicating potential for use under real-world constraints. These results indicate that adaptive filtering, historical and categorical variables, and features that exploit the organization of high-frequency content in the ECG can be leveraged to provide superior prediction of return of rhythm after shock. Such a method could thus potentially enable real-time assessment of a patient's myocardial status during resuscitation without requiring chest compression pause for analysis, and hence be used to prioritize the application of CPR, medications, and defibrillation.

7.2 CONCLUSIONS

Current protocol for defibrillator-guided resuscitation from out-of-hospital ventricular fibrillation arrest follows a one-size-fits all approach. This protocol administers shock, CPR, and medications using a predefined sequence of treatments regardless of the patient's underlying myocardial metabolic status. Under the current approach, survival from VF arrest is poor. However, survival might be improved by the application of algorithms that inform patient-specific therapy and reduce interruptions in CPR. In these retrospective investigations of VF cardiac arrests, we have demonstrated concepts suggesting potential to improve patient survival through (1) application of algorithms to advise treatment based on real-time patient status and by (2) minimizing interruptions in CPR during the use of these algorithms. These results contribute to a larger overall effort by researchers towards an ideal defibrillator-guided resuscitation protocol that includes continuous CPR, continuous rhythm classification, and continuous patient-specific therapy.

7.3 FUTURE DIRECTIONS

7.3.1 *Surrogate Data*

A major limitation to investigations of the human VF waveform during out-of-hospital cardiac arrest is the limited availability of data. Studies of the VF waveform in humans are generally limited to datasets on the order of 50-100 patients, hindering potential application of data-driven machine learning or deep learning techniques in all but the largest studies.[57] Methods to generate surrogate VF segments synthesized based on characteristics of real VF segments may offer opportunity to expand dataset size and enable machine learning techniques in studies where sample size would otherwise be prohibitive. Common methods to generate surrogate signals include techniques based on manipulation of the discrete Fourier transform of an original signal to create

similar surrogates statistically independent from the original signal.[210,211] However, such techniques have not been applied to the human ECG in investigations of VF waveform analysis.

As a proof-of-concept to demonstrate potential to generate surrogate VF ECG segments based on actual VF segments, we modified Fourier-transform-based surrogate methods to generate synthetic ECG segments based on original ECG segments.[210] Specifically, to generate a surrogate signal in the Fourier domain, we first calculated the discrete Fourier transform of the original ECG. We then preserved the magnitude response of the original ECG but generated a random normal distribution of surrogate phase values with a standard deviation equal to that of the original phase distribution. After performing the inverse Fourier transform to convert the surrogate signal to the time domain, we scaled the final surrogate ECG voltages by the ratio of standard deviations of the original and surrogate ECG voltages. Visual inspection of the surrogate ECG signals suggest that such methods may indeed merit investigation for increasing VF dataset sample size (Figure 7.1). Future investigation is required to determine the potential benefit of such methods.

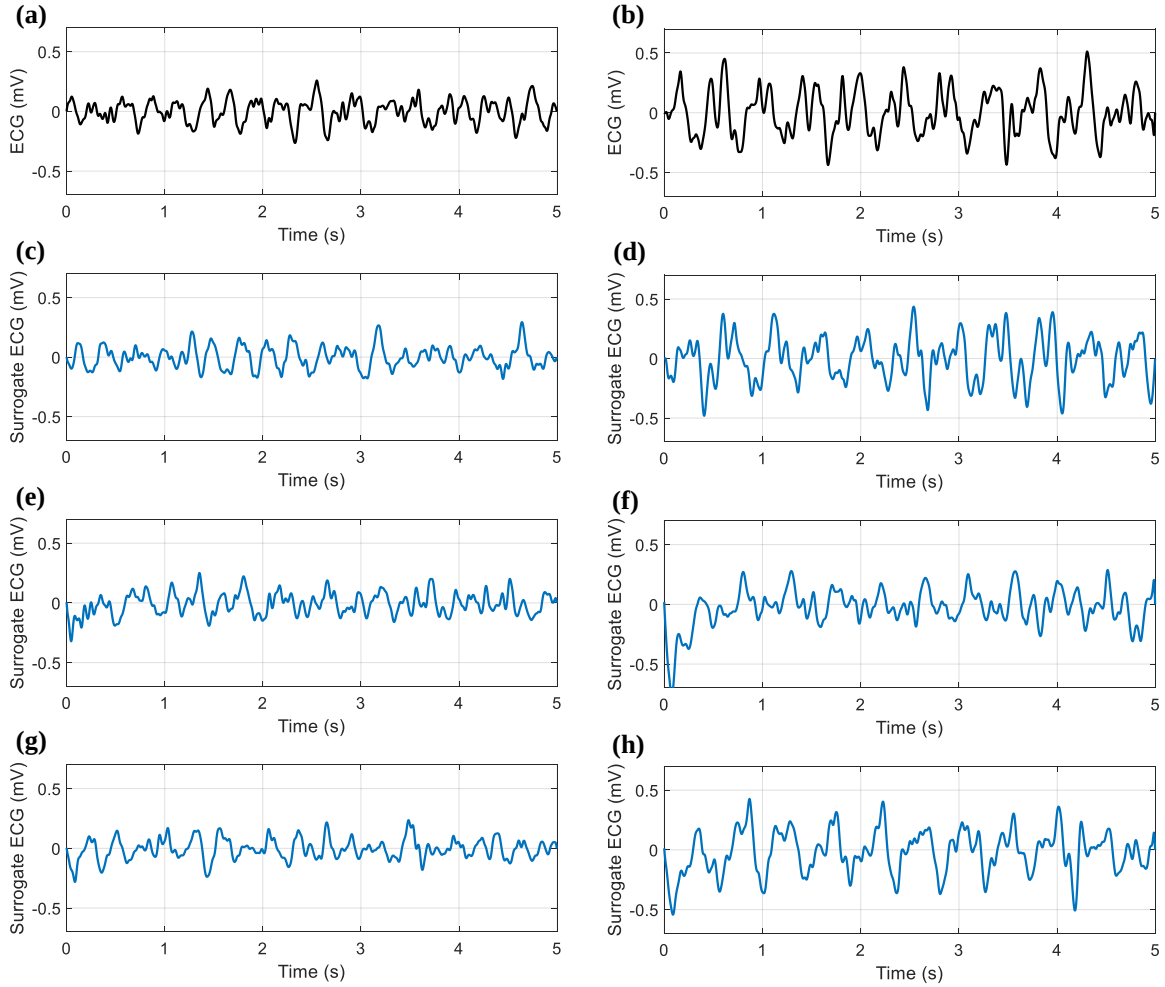

Figure 7.1 Pilot example of surrogate VF ECGs
(a) Original VF ECG segment without chest compressions. (b) Original VF ECG segment during chest compressions. (c,e,g) Surrogate VF segments synthesized based on phase randomizations of original VF ECG without compressions. (d,f,h) Surrogate VF segments synthesized based on phase randomizations of original VF ECG during compressions. (ECG = electrocardiogram, VF = ventricular fibrillation.)

7.3.2 *Deep Learning*

While recent investigations of prognostic VF algorithms have demonstrated improved performance using machine learning techniques such as support vector machines and neural networks, a limitation of such methods is that input features must be designed and trained manually, and may not optimally-describe characteristics of the VF ECG indicative of good

outcome.[91,209] Deep learning (e.g. convolutional neural networks) may offer potential for improved ECG analysis by classifying images of the ECG spectrogram. Using transfer learning, convolutional neural networks may be pre-trained on extremely large image datasets to develop a basic set of robust image classification features and filters. By adapting a pre-trained network (such as *ResNet* or *GooLeNet*) to classify ECG spectrogram images, improved performance may be possible given a large enough ECG training dataset to retrain the final layers of a pre-trained network and adapt the network for ECG spectrogram classification.[212] While convolutional neural networks are a relatively new technique and have not yet been applied to VF waveform prognosis,[209] several recent studies have demonstrated high performance in ECG classification using such methods.[213,214] Therefore, future investigation of convolutional neural networks (whether applying pre-trained networks or training new networks from scratch) is warranted and may offer potential for improved VF waveform analysis.

7.3.3 *Prospective Evaluation of Waveform-Guided Treatment During CPR*

Prospective evaluation of a VF waveform prognostic algorithm to guide clinical care without interrupting chest compressions is ultimately required to confirm utility of such an algorithm. One prior prospective investigation of VF-waveform-analysis-guided treatment has been conducted but this investigation required chest compression pause for waveform evaluation. In this prospective study, no significant improvement in survival outcomes was observed using waveform analysis to guide initial defibrillation timing, although the waveform measure trajectory over the course of arrest was observed to be related to patient outcome.[66] However, prognostic performance of the waveform method applied in the prospective investigation (vRhythm, see section 4.4.2) was modest and survival rates were low. Another prospective trial is also currently underway which applies the amplitude spectrum area measured during pauses in chest compressions to inform the

priority of CPR versus defibrillation (Clinical Trial Identifier NCT03237910). However, use of the modest-performing amplitude spectrum area waveform measure, and the requirement to analyze the ECG only during pauses in chest compressions (rather than continuously) may similarly reduce the benefit of this prospective waveform-guided treatment trial. An improved prognostic algorithm designed to function continuously during uninterrupted chest compressions in order to inform the exact time at which a defibrillation should be administered (such as the novel method proposed in Chapter 6) may ultimately be required for any observable survival benefit. Ideally, any ECG analysis (i.e. rhythm classification or VF waveform analysis) should be conducted during uninterrupted chest compressions, and compression pause only prompted once a shock is likely to be successful based on the quality of the VF rather than applying shocks to all VF regardless of the likelihood of shock success.[45]

Chapter 8. ABSTRACTS FROM CO-AUTHORED WORKS

Relevant investigations by group members or collaborators that I provided assistance with are represented below by their respective abstracts. My investigative role is indicated. For the interested reader, DOI links to the full manuscripts are provided.

8.1 Relationship Between VF Waveform Measure Change and Survival

Full manuscript published as: Schoene P, **Coult J**, Murphy L, Fahrenbruch C, Blackwood J, Kudenchuk P, Sherman L, Rea T. Course of quantitative ventricular fibrillation waveform measure and outcome following out-of-hospital cardiac arrest. *Heart Rhythm* 2014; 11:230-236. https://doi.org/10.1016/j.hrthm.2013.10.049

Investigative role: Data collection assistance, data processing assistance.

Background: Quantitative measures of the ventricular fibrillation waveform at the outset of resuscitation are associated with survival. However, little is known about the course of these measures during resuscitation and how this course is related to outcome. *Objective:* The purpose of this study was to determine how waveform measures change over the course of resuscitation and whether these changes might be used to guide resuscitation. *Methods:* We evaluated 390 persons treated by emergency providers following out-of-hospital ventricular fibrillation arrest. We assessed the ventricular fibrillation waveform using the amplitude spectrum area (AMSA) from the defibrillator's continuous electrocardiogram measured before each of the first three shocks. We used logistic regression to evaluate the relationship of AMSA and the change in AMSA with favorable neurologic survival as determined by the Cerebral Performance Category at hospital discharge. *Results:* Of the 390 patients who received an initial shock, 273 required a second shock and 210 required a third shock. The mean (standard deviation) for AMSA was 9.64 mV-Hz (0.52)

for the 873 total shock cycles. $AMSA_1$ measured before the first shock was strongly associated with favorable neurologic survival (odds ratio [OR] 3.40, 95% confidence interval [CI] [2.48, 4.66] for 1 SD change). We observed a similar relationship for second-shock $AMSA_2$ (OR 3.53, 95% CI [2.42, 5.14]) and third-shock $AMSA_3$ (OR 3.10, 95% CI [2.03, 4.73]). The median change in AMSA was 0.24 mV-Hz for $\Delta AMSA_{1-2}$ and 0.21 mV-Hz for $\Delta AMSA_{2-3}$. A positive median change in AMSA between shocks was associated with favorable neurologic survival (OR 1.44, 95% CI [1.16, 1.80] for $\Delta AMSA_{1-2}$ and OR 1.31, 95% CI [1.01, 1.71] for $\Delta AMSA_{2-3}$). *Conclusion*: Given their prognostic and dynamic qualities, quantitative waveform measures may provide an effective real-time strategy to guide individual treatment and improve survival.

8.2 Relationship Between VF Waveform Measures and Ischemic Causes of Arrest

Full manuscript published as: Hidano D, **Coult J**, Blackwood J, Farenbruch C, Kwok H, Kudenchuk P, Rea T. Ventricular fibrillation waveform measures and the etiology of cardiac arrest. *Resuscitation* 2016; 109:71-75.
https://doi.org/10.1016/j.resuscitation.2016.10.007

Investigative role: Data collection assistance, data processing assistance, study design assistance.

Background: Early determination of the acute etiology of cardiac arrest could help guide resuscitation or post-resuscitation care. In experimental studies, quantitative measures of the ventricular fibrillation waveform distinguish ischemic from non-ischemic etiology. *Methods:* We investigated whether waveform measures distinguished arrest etiology among adults treated by EMS for out-of-hospital ventricular fibrillation between January 1, 2006-December 31, 2014. Etiology was classified using hospital information into three exclusive groups: acute coronary syndrome (ACS) with ST elevation myocardial infarction (STEMI), ACS without ST elevation (non-STEMI), or non-ischemic arrest. Waveform measures included amplitude spectrum area

(AMSA), centroid frequency (CF), mean frequency (MF), and median slope (MS) assessed during CPR-free epochs immediately prior to the initial and second shock. Waveform measures prior to the initial shock and the changes between first and second shock were compared by etiology group. We a priori chose a significance level of 0.01 due to multiple comparisons. *Results:* Of the 430 patients, 35% (n=150) were classified as STEMI, 29% (n=123) as non-STEMI, and 37% (n=157) with non-ischemic arrest. We did not observe differences by etiology in any of the waveform measures prior to shock 1 (Kruskal Wallis Test) (p=0.28 for AMSA, p=0.07 for CF, p=0.63 for MF, and p=0.39 for MS). We also did not observe differences for change in waveform between shock 1 and 2, or when the two acute ischemia groups (STEMI and non-STEMI) were combined and compared to the non-ischemic group. *Conclusion:* This clinical investigation suggests that waveform measures may not be useful in distinguishing cardiac arrest etiology.

8.3 Relationship Between VF Waveform Measures and Chronic Health Conditions

Full manuscript published as: Dumas F, **Coult J**, Blackwood J, Kudenchuk P, Cariou A, Rea T. The association of chronic health status and survival following ventricular fibrillation cardiac arrest: Investigation of a primary myocardial mechanism. *Resuscitation* 2019; 137:190-196. https://doi.org/10.1016/j.resuscitation.2019.02.018

Investigative role: Data collection assistance, data processing assistance.

Introduction: Quantitative waveform measures are a surrogate of the acute physiological status of the myocardium and predict survival following ventricular fibrillation out-of-hospital cardiac arrest (OHCA). We investigated whether the amplitude spectrum area (AMSA) waveform measure mediates the adverse relationship between increasing burden of chronic health conditions and lower likelihood of survival. *Methods*: We performed a cohort investigation of persons >=18 years who suffered ventricular fibrillation OHCA between 2008-2015 in a metropolitan emergency

medical service (EMS) system. The count of chronic health conditions was determined using the Charlson Comorbidity Index (CCI). AMSA was calculated just prior to the initial shock. We used multivariable logistic regression to assess the relationship between CCI and survival-to-discharge in models first without and then with AMSA to determine the extent to which AMSA attenuated the CCI-survival association. *Results*: Of the 716 eligible patients, 422/716 (59%) had at least one chronic health condition; 21.8% with one, 19.6% with two, 10.3% with 3, and 7.3% with ≥4. Survival-to-discharge was 45% (324/716). In the multivariable model adjusted for traditional Utstein characteristics, increasing CCI was associated with lower odds of survival (odds ratio (OR) (95% confidence interval) = 0.82 [0.72, 0.93] for each additional chronic health condition). The addition of AMSA to the model only modestly attenuated the CCI-survival association (OR=0.85 [0.74,0.98]). *Conclusion*: The waveform measure AMSA – a surrogate for the physiological status of the myocardium – mediated only a modest portion of the association between increasing burden of chronic health conditions and lower likelihood of survival following ventricular fibrillation OHCA.

8.4 Characterization of Chest Compression Duty Cycle

Full manuscript published as: Johnson B, **Coult J**, Fahrenbruch C, Blackwood J, Sherman L, Kudenchuk P, Sayre M, Rea T. Cardiopulmonary resuscitation duty cycle in out-of-hospital cardiac arrest. *Resuscitation* 2015; 87:86-90.
https://doi.org/10.1016/j.resuscitation.2014.11.008

Investigative role: Data collection assistance, data processing assistance.

Background: Duty cycle is the portion of time spent in compression relative to total time of the compression–decompression cycle. Guidelines recommend a 50% duty cycle based largely on animal investigation. We undertook a descriptive evaluation of duty cycle in human resuscitation, and whether duty cycle correlates with other CPR measures. *Methods:* We calculated the duty

cycle, compression depth, and compression rate during EMS resuscitation of 164 patients with out-of-hospital ventricular fibrillation cardiac arrest. We captured force recordings from a chest accelerometer to measure ten-second CPR epochs that preceded rhythm analysis. Duty cycle was calculated using two methods. Effective compression time (ECT) is the time from beginning to end of compression divided by total period for that compression–decompression cycle. Area duty cycle (ADC) is the ratio of area under the force curve divided by total area of one compression–decompression cycle. We evaluated the compression depth and compression rate according to duty cycle quartiles. *Results:* There were 369 ten-second epochs among 164 patients. The median duty cycle was 38.8% (SD = 5.5%) using ECT and 32.2% (SD = 4.3%) using ADC. A relatively shorter compression phase (lower duty cycle) was associated with greater compression depth (test for trend <0.05 for ECT and ADC) and slower compression rate (test for trend <0.05 for ADC). Sixty-one of 164 patients (37%) survived to hospital discharge. *Conclusion:* Duty cycle was below the 50% recommended guideline, and was associated with compression depth and rate. These findings provide rationale to incorporate duty cycle into research aimed at understanding optimal CPR metrics.

8.5 Detection of Chest Compressions Using Impedance

Full manuscript published as: Kwok H, **Coult J**, Liu C, Blackwood J, Kudenchuk P, Rea T, Sherman L. An accurate method for real-time chest compression detection from the impedance signal. *Resuscitation* 2016; 105:22-28.
https://doi.org/10.1016/j.resuscitation.2016.04.023

Investigative role: Feature design assistance.

Objective: Real-time feedback improves CPR performance. Chest compression data may be obtained from an accelerometer/force sensor, but the impedance signal would serve as a less costly, universally available alternative. The objective is to assess the performance of a method which

detects the presence/absence of chest compressions and derives CPR quality metrics from the impedance signal in real time at 1 s intervals without any latency period. *Methods:* Defibrillator recordings from cardiac arrest cases were divided into derivation (N = 119) and validation (N = 105) datasets. With the force signal as reference, the presence/absence of chest compressions in the impedance signal was manually annotated (reference standard). The method classified the impedance signal at 1 s intervals as Chest Compressions Present, Chest Compressions Absent or Indeterminate. Accuracy, sensitivity and specificity for chest compression detection were calculated for each case. Differences between method and reference standard chest compression fractions and rates were calculated on a minute-to-minute basis. *Results*: In the validation set, median accuracy was 0.99 (IQR 0.98, 0.99) with 2% of 1 s intervals classified as Indeterminate. Median sensitivity and specificity were 0.99 (IQR 0.98, 1.0) and 0.98 (IQR 0.95, 1.0), respectively. Median chest compression fraction error was 0.00 (IQR −0.01, 0.00), and median chest compression rate error was 1.8 (IQR 0.6, 3.3) compressions per minute. *Conclusion*: A real-time method detected chest compressions from the impedance signal with high sensitivity and specificity and accurately estimated chest compression fraction and rate. Future investigation should evaluate whether an impedance-based guidance system can provide an acceptable alternative to an accelerometer-based system.

8.6 Rhythm Classification During Chest Compressions

Full manuscript published as: Kwok H, **Coult J**, Drton M, Rea T, Sherman L. Adaptive rhythm sequencing: A method for dynamic rhythm classification during CPR. *Resuscitation* 2015; 91:26-31. https://doi.org/10.1016/j.resuscitation.2015.02.031

Investigative role: Feature design assistance.

Objective: The accuracy of methods that classify the cardiac rhythm despite CPR artifact could potentially be improved by utilizing continuous ECG data. Our objective is to compare three approaches which use identical ECG features and differ only in their degree of temporal integration: (1) static classification, which analyzes 4-s ECG frames in isolation; (2) "best-of-three averaging," which takes the average of three consecutive static classifications successively; and (3) "adaptive rhythm sequencing," which uses hidden Markov models to model ECG segments as rhythm sequences. *Methods:* Defibrillator recordings from 95 out-of-hospital cardiac arrests were divided into training and test sets. Each method classified the rhythm as asystole, organized rhythm or shockable rhythm throughout the recordings. Classifications were compared to the gold standard of physician review. The primary outcome was accuracy during CPR, which was estimated using a generalized linear mixed-effects model. *Results:* In the training set, accuracies during CPR were 0.89 (95% CI 0.85, 0.92), 0.92 (95% CI 0.89, 0.94) and 0.97 (95% CI 0.95, 0.98) for the static, best-of-three averaging and adaptive rhythm sequencing methods, respectively. The corresponding results in the test set were 0.92 (95% CI 0.86, 0.96), 0.94 (95% CI 0.89, 0.97), and 0.97 (95% CI 0.94, 0.99). Of the dynamic methods, only adaptive rhythm sequencing was significantly more accurate than static classification in the training ($p < 0.001$) and test ($p = 0.03$) sets. *Conclusion:* In a continuous monitoring setting, adaptive rhythm sequencing was significantly more accurate than static rhythm classification during CPR.

8.7 Relationship Between Rhythm Sequence and Survival

Full manuscript published as: Bhandari S, Doan J, Blackwood J, **Coult J**, Kudenchuk P, Sherman L, Rea T, Kwok H. Rhythm profiles and survival after out-of-hospital ventricular fibrillation cardiac arrest. *Resuscitation* 2018; 125:22-27.
https://doi.org/10.1016/j.resuscitation.2018.01.037

Investigative role: Data processing assistance.

Objective: Treatment protocols for cardiac arrest rely upon rhythm analyses performed at two-minute intervals, neglecting possible rhythm changes during the intervening period of CPR. Our objective was to describe rhythm profiles (patterns of rhythm transitions during two-minute CPR cycles) following attempted defibrillation and to assess their relationship to survival. *Methods:* The study included out-of-hospital cardiac arrest cases presenting with ventricular fibrillation from 2011 to 2015. The rhythm sequence was annotated during two-minute CPR cycles after the first and second shocks of each case, and the rhythm profile of each sequence was classified. We calculated absolute survival differences among rhythm profiles with the same rhythm at the two-minute check. *Results:* Of 569 rhythm sequences after the first shock, 46% included a rhythm transition. Overall survival was 47%, and survival proportion varied by rhythm at the two-minute check: ventricular fibrillation (46%), organized (58%), and asystole (20%). Survival was similar between profiles which ended with an organized rhythm at the two-minute check. Likewise, survival was similar between profiles with asystole at the two-minute check. However, in patients with ventricular fibrillation at the two-minute check, survival was twice as high in those with a transient organized rhythm (69%) compared to constant ventricular fibrillation (32%) or transient asystole (28%). *Conclusion:* Rhythm transitions are common after attempted defibrillation. Among patients with ventricular fibrillation at the subsequent two-minute check, transient organized rhythm during the preceding two-minute CPR cycle was associated with favorable survival, suggesting distinct physiologies that could serve as the basis for different treatment strategies.

Chapter 9. LIST OF CONTRIBUTIONS FROM THIS WORK

9.1 PLANNED PUBLICATIONS

1. **Coult J**, Blackwood J, Rea T, Kudenchuk P, Kwok H. A novel method to predict defibrillation outcomes during chest compressions. [Chapter 6; planned.]
2. **Coult J**, Blackwood J, Rea T, Kudenchuk P, Kwok H. A method to detect chest compression state using transthoracic impedance. [Chapter 5; currently under review.]

9.2 PUBLICATIONS

1. Dumas F, **Coult J**, Blackwood J, Kudenchuk P, Cariou A, Rea T. The association of chronic health status and survival following ventricular fibrillation cardiac arrest: Investigation of a primary myocardial mechanism. *Resuscitation* 2019; 137:190-196. doi:10.1016/j.resuscitation.2019.02.018
2. **Coult J**, Blackwood J, Sherman L, Rea T, Kudenchuk P, Kwok H. Ventricular fibrillation waveform analysis during chest compressions to predict survival from cardiac arrest. *Circulation: Arrhythmia and Electrophysiology* 2019; 12(1):1-10. doi:10.1161/CIRCEP.118.006924
3. Bhandari S, Doan J, Blackwood J, **Coult J**, Kudenchuk P, Sherman L, Rea T, Kwok H. Rhythm profiles and survival after out-of-hospital ventricular fibrillation cardiac arrest. *Resuscitation* 2018; 125:22-27. doi:10.1016/j.resuscitation.2018.01.037
4. **Coult J**, Kwok H, Sherman L, Blackwood J, Kudenchuk P, Rea T. Ventricular fibrillation waveform measures combined with prior shock outcome predict defibrillation success during cardiopulmonary resuscitation. *Journal of Electrocardiology* 2018; 51:99-106. doi:10.1016/j.jelectrocard.2017.07.016
5. **Coult J**, Sherman L, Kwok H, Blackwood J, Kudenchuk P, Rea T. Short ECG segments predict defibrillation outcome using quantitative waveform measures. *Resuscitation* 2016; 109:16-20. doi:10.1016/j.resuscitation.2016.09.020
6. Hidano D, **Coult J**, Blackwood J, Farenbruch C, Kwok H, Kudenchuk P, Rea T. Ventricular fibrillation waveform measures and the etiology of cardiac arrest. *Resuscitation* 2016; 109:71-75. doi:10.1016/j.resuscitation.2016.10.007

7. Kwok H, **Coult J**, Liu C, Blackwood J, Kudenchuk P, Rea T, Sherman L. An accurate method for real-time chest compression detection from the impedance signal. *Resuscitation* 2016; 105:22-28. doi:10.1016/j.resuscitation.2016.04.023
8. Kwok H, **Coult J**, Drton M, Rea T, Sherman L. Adaptive rhythm sequencing: A method for dynamic rhythm classification during CPR. *Resuscitation* 2015; 91:26-31. doi: 10.1016/j.resuscitation.2015.02.031
9. Johnson B, **Coult J**, Fahrenbruch C, Blackwood J, Sherman L, Kudenchuk P, Sayre M, Rea T. Cardiopulmonary resuscitation duty cycle in out-of-hospital cardiac arrest. *Resuscitation* 2015; 87:86-90. doi:10.1016/j.resuscitation.2014.11.008
10. Schoene P, **Coult J**, Murphy L, Fahrenbruch C, Blackwood J, Kudenchuk P, Sherman L, Rea T. Course of quantitative ventricular fibrillation waveform measure and outcome following out-of-hospital cardiac arrest. *Heart Rhythm* 2014; 11:230-236. doi:10.1016/j.hrthm.2013.10.049

9.3 Patent Cooperation Treaty (PCT) Patent Applications Submitted

1. Kwok H, **Coult J,** Sherman L. METHODS AND DEFIBRILLATORS UTILIZING HIDDEN MARKOV MODELS TO ANALYZE ECG AND/OR IMPEDANCE SIGNALS. Intl. Pub. No. WO 2016/081879 A1. (Abandoned.)
2. Ramachandran A, **Coult J,** Sherman L, Kudenchuk P. APPARATUSES AND METHODS FOR DETERMINING WHETHER CARDIOPULMONARY RESUSCITATION IS BEING CONDUCTED BASED ON AN IMPEDANCE SIGNAL. Intl. Pub. No. WO 2015/200813 A1. (Abandoned.)
3. Ramachandran A, Sherman L, **Coult J,** Kudenchuk P, Chin A, Neils C. APPARATUSES AND METHODS FOR CLASSIFICATION OF ELECTROCARDIOGRAM SIGNALS DURING CARDIOPULMONARY RESUSCITATION. Intl. Pub. No. WO 2015/051280 A1. (Abandoned.)
4. **Coult J,** Neils C, Eisenberg M, Rea T, Kudenchuk P, Sherman L. SYSTEMS AND METHODS FOR ANALYZING ELECTROCARDIOGRAMS TO DETECT VENTRICULAR FIBRILLATION. Intl. Pub. No. WO 2013/003852 A1. (Abandoned.)

9.4 CONFERENCE ABSTRACTS

1. **Coult J**, Sherman L, Blackwood J, Kwok H, Kudenchuk P, Rea T. A Novel Method to Predict Survival from Ventricular Fibrillation Arrest During Chest Compressions. *Circulation* 2018;138:A309. Presented at the American Heart Association Resuscitation Science Symposium, November 10-11 2018, Chicago, IL, USA.
2. Liu C, Gehman S, Jorgenson D, Lyster T, **Coult J**, Eisenberg M, Kudenchuk P, Rea T, Sherman L. A Shock Advisory Algorithm to Analyse through Chest Compressions for Reducing Interruptions during Cardiopulmonary Resuscitation. *Resuscitation* 2017;Vol 119; S1:e6. Presented at Congress of the European Resuscitation Council, September 28-30 2017, Freiburg, Germany.
3. **Coult J**, Sherman L, Kwok H, Kudenchuk P, Blackwood J, Rea T. AMSA Combined with Prior Shock Outcome Predicts Defibrillation Success During CPR. *Circulation* 2016; 134:A20568. Presented at the American Heart Association Resuscitation Science Symposium, Nov 12-16 2016, New Orleans, LA, USA.
4. Dumas F **Coult J**, Blackwood J, Kudenchuk P, Cariou A, Sherman L, Rea T. Amplitude Spectrum Area (AMSA) and Outcome: Role of Utstein and Comorbidities Factors. *Circulation* 2016; 134:A20568. Presented at the American Heart Association Resuscitation Science Symposium, Nov 12-16 2016, New Orleans, LA, USA.
5. Liu C, Gehman S, Jorgenson D, Lyster T, **Coult J**, Eisenberg M, Kudenchuk P, Rea T, Sherman L. Sequential Shock – No Shock Algorithm to Reduce Interruption during Cardiopulmonary Resuscitation. *Circulation* 2016; 134:A19355. Presented at the American Heart Association Resuscitation Science Symposium, Nov 12-16 2016, New Orleans, LA, USA.
6. Kwok H, **Coult J**, Sherman L, Blackwood J, Kudenchuk P, Rea T. A Method for Real-time CPR Detection from the Thoracic Impedance Signal. *Circulation* 2015; 132:A17882. Presented at the American Heart Association Resuscitation Science Symposium, November 7-11 2015, Orlando, FL, USA.
7. Kwok H, **Coult J**, Blackwood J, Kudenchuk P, Sherman L, Rea T. An Accurate Method for Automated Rhythm Classification during CPR. *Circulation* 2015; 132:A18877. Presented at

the American Heart Association Resuscitation Science Symposium, November 7-11 2015, Orlando, FL, USA.

8. Ramachandran AR, **Coult J**, Kudenchuk P, Blackwood J, Sherman L, Rea T. Detection of Chest Compressions using Transthoracic Impedance. *Circulation* 2015; 132:A18955. Presented at the American Heart Association Resuscitation Science Symposium, November 7-11 2015, Orlando, FL, USA.
9. Rea T, Johnson B, **Coult J**, Fahrenbruch C, Blackwood J, Sherman L, Kudenchuk P, Sayre M. Cardiopulmonary Resuscitation Duty Cycle in Out-of-Hospital Cardiac Arrest. *Circulation* 2014; 130:A290. Presented at the American Heart Association Resuscitation Science Symposium, November 15-19 2014, Chicago, IL, USA.
10. Schoene P, Murphy L, Sherman L, **Coult J**, Blackwood J, Fahrenbruch C, Rea T. Descriptive analysis of ventricular fibrillation waveform progression and its relationship to survival. *Journal of Investigative Medicine* 2013; 61:4. Presented at the Western Regional Meeting of the American Federation for Medical Research, January 24 2013, Carmel, CA.

Chapter 10. BIBLIOGRAPHY

1. Benjamin EJ, Virani SS, Callaway CW, Chamberlain AM, Chang AR, Cheng S, Chiuve SE, Cushman M, Delling FN, Deo R, de Ferranti SD, Ferguson JF, Fornage M, Gillespie C, Isasi CR, et al. Heart Disease and Stroke Statistics—2018 Update: A Report From the American Heart Association. *Circulation* 2018;137:E67–E492. doi:10.1161/CIR.0000000000000558.
2. Mozaffarian D, Benjamin EJ, Go AS, Arnett DK, Blaha MJ, Cushman M, Das SR, de Ferranti S, Després J-P, Fullerton HJ, Howard VJ, Huffman MD, Isasi CR, Jiménez MC, Judd SE, et al. Executive Summary: Heart Disease and Stroke Statistics - 2016 Update: A Report From the American Heart Association. *Circulation* 2016;133:447–454. doi:10.1161/CIR.0000000000000350.
3. Rea TD, Eisenberg MS, Sinibaldi G, White RD. Incidence of EMS-treated out-of-hospital cardiac arrest in the United States. *Resuscitation* 2004;63:17–24. doi:10.1016/j.resuscitation.2004.03.025.
4. Klabunde RE. Cardiovascular Physiology Concepts. 2nd ed. 2012.
5. Jalife J, Delmar M, Anumonwo J, Berenfeld O, Kalifa J. Basic Cardiac Electrophysiology for the Clinician. 2nd ed. Wiley-Blackwell; 2009.
6. Dubin D. Rapid Interpretation of EKG's. 6th ed. COVER; 2000.
7. Brown C, Dzwonczyk R. Estimating the duration of ventricular fibrillation. *Ann Emerg Med* 1989;18:1181–1185.
8. Brown CG, Dzwonczyk R, Martin DR. Physiologic measurement of the ventricular fibrillation ECG signal: estimating the duration of ventricular fibrillation. *Ann Emerg Med* 1993;22:70–74.
9. Dzwonczyk R, Brown CG, Werman HA. The median frequency of the ECG during ventricular fibrillation: its use in an algorithm for estimating the duration of cardiac arrest. *IEEE Trans Biomed Eng* 1990;37:640–646. doi:10.1109/10.55668.
10. Hastings HM, Evans SJ, Quan W, Chong ML, Nwasokwa O. Nonlinear dynamics in ventricular fibrillation. *Proc Natl Acad Sci U S A* 1996;93:10495–10499.
11. Gray RA, Pertsov AM, Jalife J. Spatial and temporal organization during cardiac fibrillation. *Nature* 1998;392:75–78.

12. ten Tusscher KHWJ, Mourad a, Nash MP, Clayton RH, Bradley CP, Paterson DJ, Hren R, Hayward M, Panfilov a V, Taggart P. Organization of ventricular fibrillation in the human heart: experiments and models. *Exp Physiol* 2009;94:553–562. doi:10.1113/expphysiol.2008.044065.
13. Weiss JN, Qu Z, Chen PS, Lin SF, Karagueuzian HS, Hayashi H, Garfinkel A, Karma A. The dynamics of cardiac fibrillation. *Circulation* 2005;112:1232–1240. doi:10.1161/CIRCULATIONAHA.104.529545.
14. Jalife J. Ventricular Fibrillation: Mechanisms of Initiation and Maintenance. *Annu Rev Physiol* 2000;62:25–50. doi:10.1146/annurev.physiol.62.1.25.
15. Nolan JP, Soar J. Defibrillation in clinical practice. *Curr Opin Crit Care* 2009;15:209–215. doi:10.1097/MCC.0b013e32832931cb.
16. Khan MG. Rapid ECG Interpretation. 1st ed. W.B. Saunders Company; 1997.
17. Nash MP, Mourad A, Clayton RH, Sutton PM, Bradley CP, Hayward M, Paterson DJ, Taggart P. Evidence for Multiple Mechanisms in Human Ventricular Fibrillation. *Circulation* 2006;114:536–542. doi:10.1161/CIRCULATIONAHA.105.602870.
18. Ten Tusscher KHWJ, Hren R, Panfilov A V. Organization of Ventricular Fibrillation in the Human Heart. *Circ Res* 2007;100:e87-101. doi:10.1161/CIRCRESAHA.107.150730.
19. Lawson BA, Burrage K, Burrage P, Drovandi CC, Bueno-Orovio A. Slow Recovery of Excitability Increases Ventricular Fibrillation Risk as Identified by Emulation. *Front Physiol* 2018;9:1–19. doi:10.3389/fphys.2018.01114.
20. Reed MJ, Clegg GR, Robertson CE. Analysing the ventricular fibrillation waveform. *Resuscitation* 2003;57:11–20. doi:10.1016/S0300-9572(02)00441-0.
21. Indik JH, Allen D, Gura M, Dameff C, Hilwig RW, Kern KB. Utility of the ventricular fibrillation waveform to predict a return of spontaneous circulation and distinguish acute from post myocardial infarction or normal swine in ventricular fibrillation cardiac arrest. *Circ Arrhythm Electrophysiol* 2011;4:337–343. doi:10.1161/CIRCEP.110.960419.
22. Salcido DD, Menegazzi JJ, Suffoletto BP, Logue ES, Sherman LD. Association of intramyocardial high energy phosphate concentrations with quantitative measures of the ventricular fibrillation electrocardiogram waveform. *Resuscitation* 2009;80:946–950. doi:10.1016/j.resuscitation.2009.05.002.
23. Indik JH, Donnerstein RL, Hilwig RW, Zuercher M, Feigelman J, Kern KB, Berg MD,

Berg R a. The influence of myocardial substrate on ventricular fibrillation waveform: a swine model of acute and postmyocardial infarction. *Crit Care Med* 2008;36:2136–2142. doi:10.1097/CCM.0b013e31817d798c.

24. Sherman LD, Niemann JT, Rosborough JP, Menegazzi JJ. The effect of ischemia on ventricular fibrillation as measured by fractal dimension and frequency measures. *Resuscitation* 2007;75:499–505. doi:10.1016/j.resuscitation.2007.05.019.
25. Neumar RW, Brown CG, Van Ligten P, Hoekstra J, Altschuld RA, Baker P. Estimation of myocardial ischemic injury during ventricular fibrillation with total circulatory arrest using high-energy phosphates and lactate as metabolic markers. *Ann Emerg Med* 1991;20:222–229. doi:10.1016/S0196-0644(05)80927-8.
26. Kudenchuk PJ, Brown SP, Daya M, Rea T, Nichol G, Morrison LJ, Leroux B, Vaillancourt C, Wittwer L, Callaway CW, Christenson J, Egan D, Ornato JP, Weisfeldt ML, Stiell IG, et al. Amiodarone, Lidocaine, or Placebo in Out-of-Hospital Cardiac Arrest. *N Engl J Med* 2016;374:1711–1722. doi:10.1056/NEJMoa1514204.
27. Berg R a, Hemphill R, Abella BS, Aufderheide TP, Cave DM, Hazinski MF, Lerner EB, Rea TD, Sayre MR, Swor R a. Part 5: Adult Basic Life Support: 2010 American Heart Association Guidelines for Cardiopulmonary Resuscitation and Emergency Cardiovascular Care. *Circulation* 2010;122:S685-705. doi:10.1161/CIRCULATIONAHA.110.970939.
28. Abrams HC, McNally B, Ong M, Moyer PH, Dyer KS. A composite model of survival from out-of-hospital cardiac arrest using the Cardiac Arrest Registry to Enhance Survival (CARES). *Resuscitation* 2013;84:1093–1098. doi:10.1016/j.resuscitation.2013.03.030.
29. Plank G, Leon LJ, Kimber S, Vigmond EJ. Defibrillation depends on conductivity fluctuations and the degree of disorganization in reentry patterns. *J Cardiovasc Electrophysiol* 2005;16:205–216. doi:10.1046/j.1540-8167.2005.40140.x.
30. Link MS, Atkins DL, Passman RS, Halperin HR, Samson RA, White RD, Cudnik MT, Berg MD, Kudenchuk PJ, Kerber RE. Part 6: electrical therapies: automated external defibrillators, defibrillation, cardioversion, and pacing: 2010 American Heart Association Guidelines for Cardiopulmonary Resuscitation and Emergency Cardiovascular Care. *Circulation* 2010;122:S706-19. doi:10.1161/CIRCULATIONAHA.110.970954.
31. Link MS, Berkow LC, Kudenchuk PJ, Halperin HR, Hess EP, Moitra VK, Neumar RW,

O'Neil BJ, Paxton JH, Silvers SM, White RD, Yannopoulos D, Donnino MW. Part 7: Adult Advanced Cardiovascular Life Support. *Circulation* 2015;132:S444–S464. doi:10.1161/CIR.0000000000000261.

32. Kleinman ME, Brennan EE, Goldberger ZD, Swor RA, Terry M, Bobrow BJ, Gazmuri RJ, Travers AH, Rea T. Part 5: Adult Basic Life Support and Cardiopulmonary Resuscitation Quality. *Circulation* 2015;132:S414–S435. doi:10.1161/CIR.0000000000000259.
33. Kudenchuk PJ, Cobb LA, Copass MK, Cummins RO, Doherty AM, Fahrenbruch CE, Hallstrom AP, Murray WA, Olsufka M, Walsh T. Amiodarone for Resuscitation after Out-of-Hospital Cardiac Arrest Due to Ventricular Fibrillation. *N Engl J Med* 1999;341:871–878. doi:10.1056/NEJM199909163411203.
34. Strohmenger H-U. Predicting defibrillation success. *Curr Opin Crit Care* 2008;14:311–316. doi:10.1097/MCC.0b013e3282fc9a9c.
35. Niemann JT, Cairns CB, Sharma J, Lewis RJ. Treatment of prolonged ventricular fibrillation. Immediate countershock versus high-dose epinephrine and CPR preceding countershock. *Circulation* 1992;85:281–287. doi:10.1161/01.CIR.85.1.281.
36. Nakahara S, Tomio J, Nishida M, Morimura N, Ichikawa M, Sakamoto T. Association Between Timing of Epinephrine Administration and Intact Neurologic Survival Following Out-of-hospital Cardiac Arrest in Japan: A Population-based Prospective Observational Study. *Acad Emerg Med* 2012;19:782–792. doi:10.1111/j.1553-2712.2012.01387.x.
37. Cummins RO, Ornato JP, Thies WH, Pepe PE. Improving survival from sudden cardiac arrest: the "chain of survival" concept. A statement for health professionals from the Advanced Cardiac Life Support Subcommittee and the Emergency Cardiac Care Committee, American Heart Association. *Circulation* 1991;83:1832–1847. doi:10.1161/01.CIR.83.5.1832.
38. Peberdy MA, Ornato JP. Post-resuscitation care: is it the missing link in the Chain of Survival? *Resuscitation* 2005;64:135–137. doi:10.1016/j.resuscitation.2004.09.015.
39. Ruiz de Gauna S, Irusta U, Ruiz J, Ayala U, Aramendi E, Eftestøl T. Rhythm Analysis during Cardiopulmonary Resuscitation: Past, Present, and Future. *Biomed Res Int* 2014;2014:1–13. doi:10.1155/2014/386010.
40. Cobb LA, Fahrenbruch CE, Walsh TR, Copass MK, Olsufka M, Breskin M, Hallstrom

AP. Influence of cardiopulmonary resuscitation prior to defibrillation in patients with out-of-hospital ventricular fibrillation. *JAMA* 1999;281:1182–1188.

41. Wik L, Hansen TB, Fylling F, Steen T, Vaagenes P, Auestad BH, Steen PA. Delaying defibrillation to give basic cardiopulmonary resuscitation to patients with out-of-hospital ventricular fibrillation. *JAMA* 2003;289:1389–1395.
42. Watson JN, Uchaipichat N, Addison PS, Clegg GR, Robertson CE, Eftestol T, Steen P a. Improved prediction of defibrillation success for out-of-hospital VF cardiac arrest using wavelet transform methods. *Resuscitation* 2004;63:269–275. doi:10.1016/j.resuscitation.2004.06.012.
43. Neurauter A, Eftestøl T, Kramer-Johansen J, Abella BS, Wenzel V, Lindner KH, Eilevstjønn J, Myklebust H, Steen PA, Sterz F, Jahn B, Strohmenger H-U. Improving countershock success prediction during cardiopulmonary resuscitation using ventricular fibrillation features from higher ECG frequency bands. *Resuscitation* 2008;79:453–459. doi:10.1016/j.resuscitation.2008.07.024.
44. Li Y, Tang W. Techniques for artefact filtering from chest compression corrupted ECG signals: Good, but not enough. *Resuscitation* 2009;80:1219–1220. doi:10.1016/j.resuscitation.2009.09.003.
45. Affatato R, Li Y, Ristagno G. See through ECG technology during cardiopulmonary resuscitation to analyze rhythm and predict defibrillation outcome. *Curr Opin Crit Care* 2016;22:199–205. doi:10.1097/MCC.0000000000000297.
46. Yu T, Weil MH, Tang W, Sun S, Klouche K, Povoas H, Bisera J. Adverse Outcomes of Interrupted Precordial Compression During Automated Defibrillation. *Circulation* 2002;106:368–372. doi:10.1161/01.CIR.0000021429.22005.2E.
47. Cheskes S, Schmicker RH, Christenson J, Salcido DD, Rea T, Powell J, Edelson DP, Sell R, May S, Menegazzi JJ, Van Ottingham L, Olsufka M, Pennington S, Simonini J, Berg R a., et al. Perishock Pause. *Circulation* 2011;124:58–66. doi:10.1161/CIRCULATIONAHA.110.010736.
48. Brouwer TF, Walker RG, Chapman FW, Koster RW. Association Between Chest Compression Interruptions and Clinical Outcomes of Ventricular Fibrillation Out-of-Hospital Cardiac Arrest. *Circulation* 2015;132:1030–1037. doi:10.1161/CIRCULATIONAHA.115.014016.

49. Kudenchuk PJ, Cobb LA, Copass MK, Olsufka M, Maynard C, Nichol G. Transthoracic Incremental Monophasic Versus Biphasic Defibrillation by Emergency Responders (TIMBER). *Circulation* 2006;114:2010–2018. doi:10.1161/CIRCULATIONAHA.106.636506.

50. Gold LS, Fahrenbruch CE, Rea TD, Eisenberg MS. The relationship between time to arrival of emergency medical services (EMS) and survival from out-of-hospital ventricular fibrillation cardiac arrest. *Resuscitation* 2010;81:622–625. doi:10.1016/j.resuscitation.2010.02.004.

51. Simpson PM, Goodger MS, Bendall JC. Delayed versus immediate defibrillation for out-of-hospital cardiac arrest due to ventricular fibrillation: A systematic review and meta-analysis of randomised controlled trials. *Resuscitation* 2010;81:925–931. doi:10.1016/j.resuscitation.2010.04.016.

52. Association AH. 2005 American Heart Association guidelines for cardiopulmonary resuscitation and emergency cardiovascular care: Part 3: Defibrillation. *Circulation* 2005;112:III-17-III24. doi:10.1161/CIRCULATIONAHA.105.166473.

53. Ristagno G, Mauri T, Cesana G, Li Y, Finzi A, Fumagalli F, Rossi G, Grieco N, Migliori M, Andreassi A, Latini R, Fornari C, Pesenti A, Bozzola M, Pagliosa A, et al. Amplitude spectrum area to guide defibrillation. *Circulation* 2015;131:478–487. doi:10.1161/CIRCULATIONAHA.114.010989.

54. Eilevstjønn J, Eftestøl T, Aase SO, Myklebust H, Husøy JH, Steen PA. Feasibility of shock advice analysis during CPR through removal of CPR artefacts from the human ECG. *Resuscitation* 2004;61:131–141. doi:10.1016/j.resuscitation.2003.12.019.

55. Kramer-Johansen J, Edelson DP, Abella BS, Becker LB, Wik L, Steen PA. Pauses in chest compression and inappropriate shocks: A comparison of manual and semi-automatic defibrillation attempts. *Resuscitation* 2007;73:212–220. doi:10.1016/j.resuscitation.2006.09.006.

56. Li Y, Tang W. Optimizing the timing of defibrillation: the role of ventricular fibrillation waveform analysis during cardiopulmonary resuscitation. *Crit Care Clin* 2012;28:199–210. doi:10.1016/j.ccc.2011.10.013.

57. Callaway CW, Menegazzi JJ. Waveform analysis of ventricular fibrillation to predict defibrillation. *Curr Opin Crit Care* 2005;11:192–199.

58. Snyder DE, White RD, Jorgenson DB. Outcome prediction for guidance of initial resuscitation protocol: Shock first or CPR first. *Resuscitation* 2007;72:45–51. doi:10.1016/j.resuscitation.2006.05.018.

59. Sherman LD, Niemann JT, Rosborough JP, Menegazzi JJ. The effect of ischemia on ventricular fibrillation as measured by fractal dimension and frequency measures. *Resuscitation* 2007;75:499–505. doi:10.1016/j.resuscitation.2007.05.019.

60. Olasveengen TM, Eftestøl T, Gundersen K, Wik L, Sunde K. Acute ischemic heart disease alters ventricular fibrillation waveform characteristics in out-of hospital cardiac arrest. *Resuscitation* 2009;80:412–417. doi:10.1016/j.resuscitation.2009.01.012.

61. Bonnes JL, Keuper W, Westra SW, Zegers ES, Oostendorp TF, Brouwer MA, Smeets JLRM. Characteristics of ventricular fibrillation in relation to cardiac aetiology and shock success: A waveform analysis study in ICD-patients. *Resuscitation* 2015;86:95–99. doi:10.1016/j.resuscitation.2014.10.003.

62. Li Y, Bisera J, Weil MH, Tang W. An algorithm used for ventricular fibrillation detection without interrupting chest compression. *IEEE Trans Biomed Eng* 2012;59:78–86. doi:10.1109/TBME.2011.2118755.

63. Ristagno G, Li Y, Fumagalli F, Finzi A, Quan W. Amplitude spectrum area to guide resuscitation—A retrospective analysis during out-of-hospital cardiopulmonary resuscitation in 609 patients with ventricular fibrillation cardiac arrest. *Resuscitation* 2013;84:1697–1703. doi:10.1016/j.resuscitation.2013.08.017.

64. Indik JH, Conover Z, McGovern M, Silver AE, Spaite DW, Bobrow BJ, Kern KB. Association of amplitude spectral area of the ventricular fibrillation waveform with survival of out-of-hospital ventricular fibrillation cardiac arrest. *J Am Coll Cardiol* 2014;64:1362–1369. doi:10.1016/j.jacc.2014.06.1196.

65. Firoozabadi R, Nakagawa M, Helfenbein ED, Babaeizadeh S. Predicting defibrillation success in sudden cardiac arrest patients. *J Electrocardiol* 2013;46:473–479. doi:10.1016/j.jelectrocard.2013.06.007.

66. Freese JP, Jorgenson DB, Liu P-Y, Innes J, Matallana L, Nammi K, Donohoe RT, Whitbread M, Silverman R a, Prezant DJ. Waveform Analysis–Guided Treatment Versus a Standard Shock-First Protocol for the Treatment of Out-of-Hospital Cardiac Arrest Presenting in Ventricular Fibrillation. *Circulation* 2013;128:995–1002.

doi:10.1161/CIRCULATIONAHA.113.003273.

67. Ayala U, Irusta U, Ruiz J, Eftestøl T, Kramer-Johansen J, Alonso-Atienza F, Alonso E, González-Otero D. A Reliable Method for Rhythm Analysis during Cardiopulmonary Resuscitation. *Biomed Res Int* 2014;2014:1–11. doi:10.1155/2014/872470.
68. Neurauter A, Eftestøl T, Kramer-Johansen J, Abella BS, Sunde K, Wenzel V, Lindner KH, Eilevstjønn J, Myklebust H, Steen PA, Strohmenger H-U. Prediction of countershock success using single features from multiple ventricular fibrillation frequency bands and feature combinations using neural networks. *Resuscitation* 2007;73:253–263. doi:10.1016/j.resuscitation.2006.10.002.
69. Lo M-T, Lin L-Y, Hsieh W-H, Ko PC-I, Liu Y-B, Lin C, Chang Y-C, Wang C-Y, Young VH-W, Chiang W-C, Lin J-L, Chen W-J, Ma MH-M. A new method to estimate the amplitude spectrum analysis of ventricular fibrillation during cardiopulmonary resuscitation. *Resuscitation* 2013;84:1505–1511. doi:10.1016/j.resuscitation.2013.07.004.
70. Coult J. Development of an algorithm to identify shockable and non-shockable electrocardiogram signals. University of Washington, 2011.
71. Coult J, Neils C, Eisenberg M, Rea TD, Kudenchuk PJ, Sherman L. Systems and Methods for Analyzing Electrocardiograms to Detect Ventricular Fibrillation. WO 2013/003582 A1, 2013.
72. Kwok H, Coult J, Drton M, Rea TD, Sherman L. Adaptive rhythm sequencing: A method for dynamic rhythm classification during CPR. *Resuscitation* 2015;91:26–31. doi:10.1016/j.resuscitation.2015.02.031.
73. Kwok H, Coult J, Liu C, Blackwood J, Kudenchuk PJ, Rea TD, Sherman L. An accurate method for real-time chest compression detection from the impedance signal. *Resuscitation* 2016;105:22–28. doi:10.1016/j.resuscitation.2016.04.023.
74. C Liu, S Gehman, D Jorgenson, T Lyster, J Coult, M Eisenberg, P Kudenchuk, T Rea LS. A Shock Advisory Algorithm to Analyse through Chest Compressions for Reducing Interruptions during Cardiopulmonary Resuscitation. *Resuscitation* 2017;119:e6.
75. Graaf C de, Beesems SG, Stickney RE, Lank P, Chapman FW, Koster RW. Analyzing Heart Rhythm During Chest Compressions in Out-of-Hospital Cardiac Arrest Patients Using New Algorithm for Automated External Defibrillators. *Circulation* 2018;138:A18.
76. Lerner EB, Persse D, Souders CM, Sterz F, Malzer R, Lozano M, Westfall M, Brouwer M

a, van Grunsven PM, Whitehead A, Olsen J-A, Herken UR, Wik L. Design of the Circulation Improving Resuscitation Care (CIRC) Trial: a new state of the art design for out-of-hospital cardiac arrest research. *Resuscitation* 2011;82:294–299. doi:10.1016/j.resuscitation.2010.11.013.

77. Johnson B V., Coult J, Fahrenbruch C, Blackwood J, Sherman L, Kudenchuk P, Sayre M, Rea T. Cardiopulmonary resuscitation duty cycle in out-of-hospital cardiac arrest. *Resuscitation* 2015;87:86–90. doi:10.1016/j.resuscitation.2014.11.008.
78. Indik JH, Donnerstein RL, Berg R a, Hilwig RW, Berg MD, Kern KB. Ventricular fibrillation frequency characteristics are altered in acute myocardial infarction. *Crit Care Med* 2007;35:1133–1138. doi:10.1097/01.CCM.0000259540.52062.99.
79. Indik JH, Shanmugasundaram M, Allen D, Valles A, Kern KB, Hilwig RW, Zuercher M, Berg R a. Predictors of resuscitation outcome in a swine model of VF cardiac arrest: A comparison of VF duration, presence of acute myocardial infarction and VF waveform. *Resuscitation* 2009;80:1420–1423. doi:10.1016/j.resuscitation.2009.08.023.
80. Bonnes JL, Thannhauser J, Hermans MC, Westra SW, Oostendorp TF, Meinsma G, de Boer MJ, Brouwer MA, Smeets JLRM. Ventricular fibrillation waveform characteristics differ according to the presence of a previous myocardial infarction: A surface ECG study in ICD-patients. *Resuscitation* 2015;96:239–245. doi:10.1016/j.resuscitation.2015.08.014.
81. Hidano D, Coult J, Blackwood J, Fahrenbruch C, Kwok H, Kudenchuk P, Rea T. Ventricular fibrillation waveform measures and the etiology of cardiac arrest. *Resuscitation* 2016;109:71–75. doi:10.1016/j.resuscitation.2016.10.007.
82. Carew HT, Zhang W, Rea TD. Chronic health conditions and survival after out-of-hospital ventricular fibrillation cardiac arrest. *Heart* 2007;93:728–731. doi:10.1136/hrt.2006.103895.
83. Dumas F, Blackwood J, White L, Fahrenbruch C, Jouven X, Cariou A, Rea T. The relationship between chronic health conditions and outcome following out-of-hospital ventricular fibrillation cardiac arrest. *Resuscitation* 2017;120:71–76. doi:10.1016/j.resuscitation.2017.08.239.
84. Dumas F, Coult J, Blackwood J, Kudenchuk P, Cariou A, Rea TD. The association of chronic health status and survival following ventricular fibrillation cardiac arrest: Investigation of a primary myocardial mechanism. *Resuscitation* 2019;137:190–196.

doi:10.1016/j.resuscitation.2019.02.018.

85. Bhandari S, Doan J, Blackwood J, Coult J, Kudenchuk P, Sherman L, Rea T, Kwok H. Rhythm profiles and survival after out-of-hospital ventricular fibrillation cardiac arrest. *Resuscitation* 2018;125:22–27. doi:10.1016/j.resuscitation.2018.01.037.
86. Schoene P, Coult J, Murphy L, Fahrenbruch C, Blackwood J, Kudenchuk P, Sherman L, Rea T. Course of quantitative ventricular fibrillation waveform measure and outcome following out-of-hospital cardiac arrest. *Hear Rhythm* 2014;11:230–236. doi:10.1016/j.hrthm.2013.10.049.
87. Ruiz J, Ayala U, de Gauna SR, Irusta U, González-Otero D, Alonso E, Kramer-Johansen J, Eftestøl T. Feasibility of automated rhythm assessment in chest compression pauses during cardiopulmonary resuscitation. *Resuscitation* 2013;84:1223–1228. doi:10.1016/j.resuscitation.2013.01.034.
88. Endoh H, Hida S, Oohashi S, Hayashi Y, Kinoshita H, Honda T. Prompt prediction of successful defibrillation from 1-s ventricular fibrillation waveform in patients with out-of-hospital sudden cardiac arrest. *J Anesth* 2011;25:34–41. doi:10.1007/s00540-010-1043-x.
89. He M, Gong Y, Li Y, Mauri T, Fumagalli F, Bozzola M, Cesana G, Latini R, Pesenti A, Ristagno G. Combining multiple ECG features does not improve prediction of defibrillation outcome compared to single features in a large population of out-of-hospital cardiac arrests. *Crit Care* 2015;19:425. doi:10.1186/s13054-015-1142-z.
90. Chicote B, Irusta U, Alcaraz R, Rieta J, Aramendi E, Isasi I, Alonso D, Ibarguren K. Application of Entropy-Based Features to Predict Defibrillation Outcome in Cardiac Arrest. *Entropy* 2016;18:313. doi:10.3390/e18090313.
91. Coult J, Blackwood J, Sherman L, Rea TD, Kudenchuk PJ, Kwok H. Ventricular Fibrillation Waveform Analysis During Chest Compressions to Predict Survival From Cardiac Arrest. *Circ Arrhythm Electrophysiol* 2019;12:1–10. doi:10.1161/CIRCEP.118.006924.
92. Stecher FS, Olsen J-A, Stickney RE, Wik L. Transthoracic impedance used to evaluate performance of cardiopulmonary resuscitation during out of hospital cardiac arrest. *Resuscitation* 2008;79:432–437. doi:10.1016/j.resuscitation.2008.08.007.
93. Gonzalez-Otero D, de Gauna SR, Ruiz J, Ayala U, Alonso E. Automatic Detection of Chest Compression Pauses Using the Transthoracic Impedance Signal. *Comput Cardiol*

(2010) 2012;39:21–24.

94. Ayala U, Eftestøl T, Alonso E, Irusta U, Aramendi E, Wali S, Kramer-Johansen J. Automatic detection of chest compressions for the assessment of CPR-quality parameters. *Resuscitation* 2014;85:957–963. doi:10.1016/j.resuscitation.2014.04.007.
95. Alonso E, Ruiz J, Aramendi E, González-Otero D, Ruiz de Gauna S, Ayala U, Russell JK, Daya M. Reliability and accuracy of the thoracic impedance signal for measuring cardiopulmonary resuscitation quality metrics. *Resuscitation* 2015;88:28–34. doi:10.1016/j.resuscitation.2014.11.027.
96. González-Otero DM, Ruiz de Gauna S, Ruiz J, Daya MR, Wik L, Russell JK, Kramer-Johansen J, Eftestøl T, Alonso E, Ayala U. Chest compression rate feedback based on transthoracic impedance. *Resuscitation* 2015;93:82–88. doi:10.1016/j.resuscitation.2015.05.027.
97. Povoas HP, Bisera J. Electrocardiographic waveform analysis for predicting the success of defibrillation. *Crit Care Med* 2000;28:N210-1.
98. Marn-Pernat A, Weil MH, Tang W, Pernat A, Bisera J. Optimizing timing of ventricular defibrillation. *Crit Care Med* 2001;29:2360–2365.
99. Foomany FH, Umapathy K, Sugavaneswaran L, Krishnan S, Masse S, Farid T, Nair K, Dorian P, Nanthakumar K. Wavelet-based markers of ventricular fibrillation in optimizing human cardiac resuscitation. 2010 Annu Int Conf IEEE Eng Med Biol, IEEE; 2010, p. 2001–2004. doi:10.1109/IEMBS.2010.5627841.
100. Sherman LD. The frequency ratio: An improved method to estimate ventricular fibrillation duration based on Fourier analysis of the waveform. *Resuscitation* 2006;69:479–486. doi:10.1016/j.resuscitation.2005.09.024.
101. Shandilya S, Ward K, Kurz M, Najarian K. Non-linear dynamical signal characterization for prediction of defibrillation success through machine learning. *BMC Med Inform Decis Mak* 2012;12:116. doi:10.1186/1472-6947-12-116.
102. Rea TD, Cook AJ, Stiell IG, Powell J, Bigham B, Callaway CW, Chugh S, Aufderheide TP, Morrison L, Terndrup TE, Beaudoin T, Wittwer L, Davis D, Idris A, Nichol G. Predicting Survival After Out-of-Hospital Cardiac Arrest: Role of the Utstein Data Elements. *Ann Emerg Med* 2010;55:249–257. doi:10.1016/j.annemergmed.2009.09.018.
103. Gundersen K, Kvaløy JT, Eftestøl T, Kramer-Johansen J. Modelling ventricular

fibrillation coarseness during cardiopulmonary resuscitation by mixed effects stochastic differential equations. *Stat Med* 2015;34:3159–3169. doi:10.1002/sim.6539.

104. Lin L-Y, Lo M-T, Ko PC-I, Lin C, Chiang W-C, Liu Y-B, Hu K, Lin J-L, Chen W-J, Ma MH-M. Detrended fluctuation analysis predicts successful defibrillation for out-of-hospital ventricular fibrillation cardiac arrest. *Resuscitation* 2010;81:297–301. doi:10.1016/j.resuscitation.2009.12.003.
105. Shanmugasundaram M, Valles A, Kellum MJ, Ewy G a., Indik JH. Analysis of amplitude spectral area and slope to predict defibrillation in out of hospital cardiac arrest due to ventricular fibrillation (VF) according to VF type: Recurrent versus shock-resistant. *Resuscitation* 2012;83:1242–1247. doi:10.1016/j.resuscitation.2012.02.008.
106. Eilevstjønn J, Kramer-Johansen J, Sunde K. Shock outcome is related to prior rhythm and duration of ventricular fibrillation. *Resuscitation* 2007;75:60–67. doi:10.1016/j.resuscitation.2007.02.014.
107. Ajam K, Gold LS, Beck SS, Damon S, Phelps R, Rea TD. Reliability of the Cerebral Performance Category to classify neurological status among survivors of ventricular fibrillation arrest: a cohort study. *Scand J Trauma Resusc Emerg Med* 2011;19:38. doi:10.1186/1757-7241-19-38.
108. The Brain Resuscitation Clinical Trial II Study Group. A randomized clinical trial of calcium entry blocker administration to comatose survivors of cardiac arrest. *Control Clin Trials* 1991;12:525–545. doi:10.1016/0197-2456(91)90011-A.
109. Robin X, Turck N, Hainard A, Tiberti N, Lisacek F, Sanchez J-C, Müller M. pROC: an open-source package for R and S+ to analyze and compare ROC curves. *BMC Bioinformatics* 2011;12:77. doi:10.1186/1471-2105-12-77.
110. Martin DR, Brown CG, Dzwonczyk R. Frequency analysis of the human and swine electrocardiogram during ventricular fibrillation. *Resuscitation* 1991;22:85–91. doi:10.1016/0300-9572(91)90067-9.
111. Wu X, Bisera J, Tang W. Signal integral for optimizing the timing of defibrillation. *Resuscitation* 2013;84:1704–1707. doi:10.1016/j.resuscitation.2013.08.005.
112. He M, Lu Y, Zhang L, Zhang H, Gong Y, Li Y. Combining Amplitude Spectrum Area with Previous Shock Information Using Neural Networks Improves Prediction Performance of Defibrillation Outcome for Subsequent Shocks in Out-Of-Hospital

Cardiac Arrest Patients. *PLoS One* 2016;11:e0149115. doi:10.1371/journal.pone.0149115.

113. Jacobs I, Nadkarni V, Bahr J, Berg RA, Billi JE, Bossaert L, Cassan P, Coovadia A, D'Este K, Finn J, Halperin H, Handley A, Herlitz J, Hickey R, Idris A, et al. Cardiac arrest and cardiopulmonary resuscitation outcome reports: Update and simplification of the Utstein templates for resuscitation registries. A statement for healthcare professionals from a task force of the International Liaison Committee on Resusci. *Circulation* 2004;110:3385–3397. doi:10.1161/01.CIR.0000147236.85306.15.
114. Coult J, Sherman L, Kwok H, Blackwood J, Kudenchuk PJ, Rea TD. Short ECG segments predict defibrillation outcome using quantitative waveform measures. *Resuscitation* 2016;109:16–20. doi:10.1016/j.resuscitation.2016.09.020.
115. DeLong ER, DeLong DM, Clarke-Pearson DL. Comparing the Areas under Two or More Correlated Receiver Operating Characteristic Curves: A Nonparametric Approach. *Biometrics* 1988;44:837. doi:10.2307/2531595.
116. Eftestøl T, Sunde K, Ole Aase S, Husøy JH, Steen PA. Predicting Outcome of Defibrillation by Spectral Characterization and Nonparametric Classification of Ventricular Fibrillation in Patients With Out-of-Hospital Cardiac Arrest. *Circulation* 2000;102:1523–1529. doi:10.1161/01.CIR.102.13.1523.
117. Watson JN, Addison PS, Clegg GR, Steen PA, Robertson CE. Practical issues in the evaluation of methods for the prediction of shock outcome success in out-of-hospital cardiac arrest patients. *Resuscitation* 2006;68:51–59. doi:10.1016/j.resuscitation.2005.06.013.
118. Figuera C, Irusta U, Morgado E, Aramendi E, Ayala U, Wik L, Kramer-Johansen J, Eftestøl T, Alonso-Atienza F. Machine learning techniques for the detection of shockable rhythms in automated external defibrillators. *PLoS One* 2016;11:1–17. doi:10.1371/journal.pone.0159654.
119. Rea T, Prince D, Morrison L, Callaway C, Aufderheide T, Daya M, Stiell I, Christenson J, Powell J, Warden C, Van Ottingham L, Kudenchuk P, Weisfeldt M. Association between survival and early versus later rhythm analysis in out-of-hospital cardiac arrest: Do agency-level factors influence outcomes? *Ann Emerg Med* 2014;64:1–8. doi:10.1016/j.annemergmed.2014.01.014.
120. Berg RA, Hilwig RW, Kern KB, Ewy GA. Precountershock cardiopulmonary

resuscitation improves ventricular fibrillation median frequency and myocardial readiness for successful defibrillation from prolonged ventricular fibrillation: A randomized, controlled swine study. *Ann Emerg Med* 2002;40:563–570. doi:10.1067/mem.2002.129866.

121. Hayes MM, Berg RA, Otto CW. Monitoring during cardiac arrest: are we there yet? *Curr Opin Crit Care* 2003;9:211–217.
122. Strohmenger HU, Lindner KH, Brown CG. Analysis of the ventricular fibrillation ECG signal amplitude and frequency parameters as predictors of countershock success in humans. *Chest* 1997;111:584–589.
123. Gong Y, Chen B, Li Y. A Review of the Performance of Artifact Filtering Algorithms for Cardiopulmonary Resuscitation. *J Healthc Eng* 2013;4:185–202. doi:10.1260/2040-2295.4.2.185.
124. Weisfeldt ML, Becker LB. Resuscitation After Cardiac Arrest: A 3-Phase Time-sensitive Model. *JAMA* 2002;288:3035–3038. doi:10.1001/jama.288.23.3035.
125. Meier P, Baker P, Jost D, Jacobs I, Henzi B, Knapp G, Sasson C. Chest compressions before defibrillation for out-of-hospital cardiac arrest: A meta-analysis of randomized controlled clinical trials. *BMC Med* 2010;8:52. doi:10.1186/1741-7015-8-52.
126. Fitzgibbon E, Berger R, Tsitlik J, Halperin HR. Determination of the noise source in the electrocardiogram during cardiopulmonary resuscitation. *Crit Care Med* 2002;30:S148–S153.
127. Coult J, Kwok H, Sherman L, Blackwood J, Kudenchuk PJ, Rea TD. Ventricular fibrillation waveform measures combined with prior shock outcome predict defibrillation success during cardiopulmonary resuscitation. *J Electrocardiol* 2018;51:99–106. doi:10.1016/j.jelectrocard.2017.07.016.
128. Cummins RO, Chamberlain D a, Abramson NS, Allen M, Baskett PJ, Becker L, Bossaert L, Delooz HH, Dick WF, Eisenberg MS. Recommended guidelines for uniform reporting of data from out-of-hospital cardiac arrest: the Utstein Style. A statement for health professionals from a task force of the American Heart Association, the European Resuscitation Council, the Heart and Stroke. *Circulation* 1991;84:960–975. doi:10.1161/01.CIR.84.2.960.
129. Alonso E, Aramendi E, Daya M, Irusta U, Chicote B, Russell JK, Tereshchenko LG.

Circulation detection using the electrocardiogram and the thoracic impedance acquired by defibrillation pads. *Resuscitation* 2016;99:56–62. doi:10.1016/j.resuscitation.2015.11.014.

130. Ochoa FJ, Ramalle-Gómara E, Carpintero J., García A, Saralegui I. Competence of health professionals to check the carotid pulse. *Resuscitation* 1998;37:173–175. doi:10.1016/S0300-9572(98)00055-0.
131. Kuelz KW, Peng-Wie Hsia, Wise RM, Mahmud R, Damiano RJ. Integration of absolute ventricular fibrillation voltage correlates with successful defibrillation. *IEEE Trans Biomed Eng* 1994;41:782–791. doi:10.1109/10.310093.
132. Watson JN, Addison PS, Clegg GR, Holzer M, Sterz F, Robertson CE. A novel wavelet transform based analysis reveals hidden structure in ventricular fibrillation. *Resuscitation* 2000;43:121–127.
133. Sherman LD, Flagg A, Callaway CW, Menegazzi JJ, Hsieh M. Angular velocity: a new method to improve prediction of ventricular fibrillation duration. *Resuscitation* 2004;60:79–90. doi:10.1016/j.resuscitation.2003.07.001.
134. Gong Y, Lu Y, Zhang L, Zhang H, Li Y. Predict Defibrillation Outcome Using Stepping Increment of Poincare Plot for Out-of-Hospital Ventricular Fibrillation Cardiac Arrest. *Biomed Res Int* 2015;2015:1–7. doi:10.1155/2015/493472.
135. Takata T, Page R, Joglar J. Automated external defibrillators: technical considerations and clinical promise. *Ann Intern Med* 2001;135:990–998.
136. Brown CG, Dzwonczyk R. Signal analysis of the human electrocardiogram during ventricular fibrillation: frequency and amplitude parameters as predictors of successful countershock. *Ann Emerg Med* 1996;27:184–188.
137. Russell JK, White RD, Crone WE. Analysis of the ventricular fibrillation waveform in refibrillation. *Crit Care Med* 2006;34:S432–S437. doi:10.1097/01.CCM.0000246009.40599.F1.
138. Goldberger AL, Amaral LAN, Glass L, Hausdorff JM, Ivanov PC, Mark RG, Mietus JE, Moody GB, Peng C-K, Stanley HE. PhysioBank, PhysioToolkit, and PhysioNet. *Circulation* 2000;101:e215–e220. doi:10.1161/01.CIR.101.23.e215.
139. Jekova I, Mougeolle F, Valance A. Defibrillation shock success estimation by a set of six parameters derived from the electrocardiogram. *Physiol Meas* 2004;25:1179–1188. doi:10.1088/0967-3334/25/5/008.

140. Weaver WD, Cobb LA, Dennis D, Ray R, Hallstrom AP, Copass MK. Amplitude of ventricular fibrillation waveform and outcome after cardiac arrest. *Ann Intern Med* 1985;102:53–55.

141. Sherman LD, Rea TD, Waters JD, Menegazzi JJ, Callaway CW. Logarithm of the absolute correlations of the ECG waveform estimates duration of ventricular fibrillation and predicts successful defibrillation. *Resuscitation* 2008;78:346–354. doi:10.1016/j.resuscitation.2008.04.009.

142. Lever NA, Newall EG, Larsen PD. Differences in the characteristics of induced and spontaneous episodes of ventricular fibrillation. *EP Eur* 2007;9:1054–1058. doi:10.1093/europace/eum194.

143. Chicote B, Irusta U, Aramendi E, Alcaraz R, Rieta J, Isasi I, Alonso D, Baqueriza M, Ibarguren K. Fuzzy and Sample Entropies as Predictors of Patient Survival Using Short Ventricular Fibrillation Recordings during out of Hospital Cardiac Arrest. *Entropy* 2018;20:591. doi:10.3390/e20080591.

144. Howe A, Escalona OJ, Di Maio R, Massot B, Cromie N a, Darragh KM, Adgey J, McEneaney DJ. A support vector machine for predicting defibrillation outcomes from waveform metrics. *Resuscitation* 2014;85:343–349. doi:10.1016/j.resuscitation.2013.11.021.

145. Jin D, Dai C, Gong Y, Lu Y, Zhang L, Quan W, Li Y. Does the choice of definition for defibrillation and CPR success impact the predictability of ventricular fibrillation waveform analysis? *Resuscitation* 2017;111:48–54. doi:10.1016/j.resuscitation.2016.11.022.

146. Obuchowski NA. Nonparametric analysis of clustered ROC curve data. *Biometrics* 1997;53:567–578.

147. Barton C, Manning J, Batson N. Effect of selective aortic arch perfusion on median frequency and peak amplitude of ventricular fibrlilation in a canine model. *Ann Emerg Med* 1996;27:610–616.

148. Neumar RW, Browns CG, Robitaille PML, Altschul RA. Myocardial high energy phosphate metabolism during ventricular fibrillation with total circulatory arrest. *Resuscitation* 1990;19:199–226. doi:10.1016/0300-9572(90)90103-L.

149. Young C, Bisera J, Gehman S, Snyder D, Tang W, Weil MH. Amplitude spectrum area:

Measuring the probability of successful defibrillation as applied to human data. *Crit Care Med* 2004;32:S356–S358. doi:10.1097/01.CCM.0000134353.55378.88.

150. Zhang G, Wu T, Wan Z, Song Z, Yu M, Wang D, Li L, Chen F, Xu X. A method to differentiate between ventricular fibrillation and asystole during chest compressions using artifact-corrupted ECG alone. *Comput Methods Programs Biomed* 2017;141:111–117. doi:10.1016/j.cmpb.2017.01.015.
151. Tan L, Jiang J. Digital Signal Processing. 2nd ed. Elsevier; 2013.
152. Nowak CN, Neurauter a, Wieser L, Wenzel V, Abella B, Myklebust H, Steen P a, Strohmenger H-U. Prediction of countershock success in patients using the autoregressive spectral estimation. *Methods Inf Med* 2012;51:13–20. doi:10.3414/ME10-01-0033.
153. Jayant NS, Noll P. Digital Coding of Waveforms. Prentice-Hall; 1984.
154. Addison PS. The Illustrated Wavelet Transform Handbook. Taylor & Francis; 2002.
155. Peng C-KK, Havlin S, Stanley HE, Goldberger AL. Quantification of scaling exponents and crossover phenomena in nonstationary heartbeat time series. *Chaos* 1995;5:82–87. doi:10.1017/CBO9781107415324.004.
156. Sherman LD, Callaway CW, Menegazzi JJ. Ventricular fibrillation exhibits dynamical properties and self-similarity. *Resuscitation* 2000;47:163–173. doi:10.1016/S0300-9572(00)00229-X.
157. Callaway C, Sherman L, Jr VM. Scaling exponent predicts defibrillation success for out-of-hospital ventricular fibrillation cardiac arrest. *Circulation* 2001:1656–1661. doi:10.1161/01.CIR.103.12.1656.
158. Pincus SM. Approximate entropy as a measure of system complexity. *Proc Natl Acad Sci U S A* 1991;88:2297–2301. doi:10.1073/pnas.88.6.2297.
159. Boyd S, Vandenberghe L. Convex Optimization. 1st ed. Cambridge University Press; 2004.
160. Altman DG. Practical Statistics for Medical Research. 1st ed. Chapman & Hall; 1991.
161. Hastie T, Tibshirani R, Friedman J. The Elements of Statistical Learning. 1st ed. Springer; 2009.
162. Shalizi CR. Advanced Data Analysis from an Elementary Point of View. Cambridge University Press; 2019.
163. Devore J, Farnum N. Applied Statistics for Engineers and Scientists. 2nd ed. Brooks/Cole

Thomson Learning; 2005.

164. James G, Witten D, Hastie T, Tibshirani R. An Introduction to Statistical Learning. vol. 103. New York, NY: Springer New York; 2013. doi:10.1007/978-1-4614-7138-7.
165. Stathakis D. How many hidden layers and nodes? *Int J Remote Sens* 2009;30:2133–2147. doi:10.1080/01431160802549278.
166. Huang G Bin. Learning capability and storage capacity of two-hidden-layer feedforward networks. *IEEE Trans Neural Networks* 2003;14:274–281. doi:10.1109/TNN.2003.809401.
167. Raschka S, Mirjalili V. Python Machine Learning. 2nd ed. Packt Publishing; 2017.
168. Burges CJ. A Tutorial on Support Vector Machines for Pattern Recognition. *Data Min Knowl Discov* 1998;2:121–167. doi:10.1023/A:1009715923555.
169. Cortes C, Vapnik V. Support-Vector Networks. *Mach Learn* 1995;20:273–297.
170. Dutta S, Chatterjee A, Munshi S. Correlation technique and least square support vector machine combine for frequency domain based ECG beat classification. *Med Eng Phys* 2010;32:1161–1169. doi:10.1016/j.medengphy.2010.08.007.
171. Alpaydin E. Introduction to Machine Learning. 3rd ed. MIT Press; 2014.
172. Lerner Research Institute Department of Quantitative Health Sciences. ROC Analysis of Clustered Data with R 2018. https://www.lerner.ccf.org/qhs/software/lib/clusteredROC_help.pdf (accessed October 10, 2018).
173. Strohmenger HU, Lindner KH, Keller A, Lindner IM, Pfenninger EG. Spectral analysis of ventricular fibrillation and closed-chest cardiopulmonary resuscitation. *Resuscitation* 1996;33:155–161. doi:10.1016/S0300-9572(96)01003-9.
174. Gong Y, Gao P, Wei L, Dai C, Zhang L, Li Y. An Enhanced Adaptive Filtering Method for Suppressing Cardiopulmonary Resuscitation Artifact. *IEEE Trans Biomed Eng* 2017;64:471–478. doi:10.1109/TBME.2016.2564642.
175. Vaillancourt C, Everson-Stewart S, Christenson J, Andrusiek D, Powell J, Nichol G, Cheskes S, Aufderheide TP, Berg R, Stiell IG. The impact of increased chest compression fraction on return of spontaneous circulation for out-of-hospital cardiac arrest patients not in ventricular fibrillation. *Resuscitation* 2011;82:1501–1507. doi:10.1016/j.resuscitation.2011.07.011.

176. Christenson J, Andrusiek D, Everson-Stewart S, Kudenchuk P, Hostler D, Powell J, Callaway CW, Bishop D, Vaillancourt C, Davis D, Aufderheide TP, Idris A, Stouffer J a, Stiell I, Berg R. Chest Compression Fraction Determines Survival in Patients With Out-of-Hospital Ventricular Fibrillation. *Circulation* 2009;120:1241–1247. doi:10.1161/CIRCULATIONAHA.109.852202.

177. Valenzuela TD, Kern KB, Clark LL, Berg RA, Berg MD, Berg DD, Hilwig RW, Otto CW, Newburn D, Ewy GA. Interruptions of Chest Compressions During Emergency Medical Systems Resuscitation. *Circulation* 2005;112:1259–1265. doi:10.1161/CIRCULATIONAHA.105.537282.

178. Babbs CF, Kemeny AE, Quan W, Freeman G. A new paradigm for human resuscitation research using intelligent devices. *Resuscitation* 2008;77:306–315. doi:10.1016/j.resuscitation.2007.12.018.

179. Aase SO, Myklebust H. Compression depth estimation for CPR quality assessment using DSP on accelerometer signals. *IEEE Trans Biomed Eng* 2002;49:263–268. doi:10.1109/10.983461.

180. Kerber RE, Martins JB, Kienzle MG, Constantin L, Olshansky B, Hopson R, Charbonnier F. Energy, current, and success in defibrillation and cardioversion: clinical studies using an automated impedance-based method of energy adjustment. *Circulation* 1988;77:1038–1046.

181. Anantharaman V, Wan P, Tay S, Manning P, Lim S, Chua S, Mohan T, Rabind A, Vidya S, Hao Y. Role of peak current in conversion of patients with ventricular fibrillation. *Singapore Med J* 2017;58:432–437. doi:10.11622/smedj.2017070.

182. Ruiz J, Alonso E, Aramendi E, Kramer-Johansen J, Eftestøl T, Ayala U, González-Otero D. Reliable extraction of the circulation component in the thoracic impedance measured by defibrillation pads. *Resuscitation* 2013;84:1345–1352. doi:10.1016/j.resuscitation.2013.05.020.

183. Losert H, Risdal M, Sterz F, Nysæther J, Köhler K, Eftestøl T, Wandaller C, Myklebust H, Uray T, Sodeck G, Laggner AN. Thoracic impedance changes measured via defibrillator pads can monitor ventilation in critically ill patients and during cardiopulmonary resuscitation. *Crit Care Med* 2006;34:2399–2405. doi:10.1097/01.CCM.0000235666.40378.60.

184. Losert H, Risdal M, Sterz F, Nysæther J, Köhler K, Eftestøl T, Wandaller C, Myklebust H, Uray T, Aase SO, Laggner AN. Thoracic-impedance changes measured via defibrillator pads can monitor signs of circulation. *Resuscitation* 2007;73:221–228. doi:10.1016/j.resuscitation.2006.10.001.

185. Risdal M, Aase SO, Kramer-Johansen J, Eftesol T. Automatic Identification of Return of Spontaneous Circulation During Cardiopulmonary Resuscitation. *IEEE Trans Biomed Eng* 2008;55:60–68. doi:10.1109/TBME.2007.910644.

186. Greiner M, Pfeiffer D, Smith RD. Principles and practical application of the receiver-operating characteristic analysis for diagnostic tests. *Prev Vet Med* 2000;45:23–41. doi:https://doi.org/10.1016/S0167-5877(00)00115-X.

187. Aramendi E, Ayala U, Irusta U, Alonso E, Eftestøl T, Kramer-Johansen J. Suppression of the cardiopulmonary resuscitation artefacts using the instantaneous chest compression rate extracted from the thoracic impedance. *Resuscitation* 2012;83:692–698. doi:10.1016/j.resuscitation.2011.11.029.

188. Ewy GA, Taren D, Bangert J, McClung S, Hellman DA. Comparison of myocardial damage from defibrillator discharges at various dosages. *Med Instrum* 1980;14:9–12.

189. Xie J, Weil MH, Sun S, Tang W, Sato Y, Jin X, Bisera J. High-Energy Defibrillation Increases the Severity of Postresuscitation Myocardial Dysfunction. *Circulation* 1997;96:683–688. doi:10.1161/01.CIR.96.2.683.

190. Paradis N, Martin G. Coronary perfusion pressure and the return of spontaneous circulation in human cardiopulmonary resuscitation. *JAMA* 1990;263:1106–1113.

191. Menegazzi JJ, Wang HE, Lightfoot CB, Fertig KC, Chengelis NL, Sherman LD, Callaway CW. Immediate defibrillation versus interventions first in a swine model of prolonged ventricular fibrillation. *Resuscitation* 2003;59:261–270. doi:10.1016/S0300-9572(03)00212-0.

192. Box MS, Watson JN, Addison PS, Clegg GR, Robertson CE. Shock outcome prediction before and after CPR: a comparative study of manual and automated active compression-decompression CPR. *Resuscitation* 2008;78:265–274. doi:10.1016/j.resuscitation.2008.03.225.

193. Eftestol T. Effects of Interrupting Precordial Compressions on the Calculated Probability of Defibrillation Success During Out-of-Hospital Cardiac Arrest. *Circulation*

2002;105:2270–2273. doi:10.1161/01.CIR.0000016362.42586.FE.

194. Zabel M, Koller BS, Sachs F, Franz MR. Stretch-induced voltage changes in the isolated beating heart: Importance of the timing of stretch and implications for stretch-activated ion channels. *Cardiovasc Res* 1996;32:120–130. doi:10.1016/0008-6363(96)00089-2.
195. Sato Y, Weil MH, Sun S, Tang W, Xie J, Noc M, Bisera J. Adverse effects of interrupting precordial compression during cardiopulmonary resuscitation. *Crit Care Med* 1997;25:733–736.
196. Aase SO, Eftestøl T, Husøy JH, Sunde K, Steen P a. CPR artifact removal from human ECG using optimal multichannel filtering. *IEEE Trans Biomed Eng* 2000;47:1440–1449. doi:10.1109/10.880095.
197. Physio-Control. LIFEPAK 12 Defibrillator/Monitor Operating Instructions 2010.
198. Physio-Control. LIFEPAK 15 Defibrillator/Monitor Operating Instructions 2009.
199. Philips. HeartStart MRx Instructions for Use 2012.
200. Nanthakumar K, Walcott GP, Melnick S, Rogers JM, Kay MW, Smith WM, Ideker RE, Holman W. Epicardial organization of human ventricular fibrillation. *Hear Rhythm* 2004;1:14–23. doi:10.1016/j.hrthm.2004.01.007.
201. Witkowski FX, Leon LJ, Penkoske PA, Giles WR, Spano ML, Ditto WL, Winfree AT. Spatiotemporal evolution of ventricular fibrillation. *Nature* 1998;392:78–82.
202. Shannon CE. A Mathematical Theory of Communication. *Bell Syst Tech J* 1948;27:379–423. doi:10.1002/j.1538-7305.1948.tb01338.x.
203. Rosso OA, Blanco S, Yordanova J, Kolev V, Figliola A, Schürmann M, Başar E. Wavelet entropy: a new tool for analysis of short duration brain electrical signals. *J Neurosci Methods* 2001;105:65–75. doi:10.1016/S0165-0270(00)00356-3.
204. Nunes RR, Almeida MP de, Sleigh JW. Spectral Entropy: A New Method for Anesthetic Adequacy. *Rev Bras Anestesiol* 2004;54:404–422. doi:10.1590/S0034-70942004000300013.
205. Watson JN, Addison PS, Clegg GR, Steen PA, Robertson CE. Wavelet transform-based prediction of the likelihood of successful defibrillation for patients exhibiting ventricular fibrillation. *Meas Sci Technol* 2005;16:L1–L6. doi:10.1088/0957-0233/16/10/L01.
206. Vilke GM, Chan TC, Dunford J V, Metz M, Ochs G, Smith A, Fisher R, Poste JC, McCallum-Brown L, Davis DP. The three-phase model of cardiac arrest as applied to

ventricular fibrillation in a large, urban emergency medical services system. *Resuscitation* 2005;64:341–346. doi:10.1016/j.resuscitation.2004.09.011.

207. Callaway CW, Sherman LD, Scheatzle MD, Menegazzi JJ. Scaling structure of electrocardiographic waveform during prolonged ventricular fibrillation in swine. *Pacing Clin Electrophysiol* 2000;23:180–191.
208. Eftestøl T, Sunde K, Aase SO, Husøy JH, Steen P a. "Probability of successful defibrillation" as a monitor during CPR in out-of-hospital cardiac arrested patients. *Resuscitation* 2001;48:245–254.
209. Ivanović MD, Ring M, Baronio F, Calza S, Vukčević V, Hadžievski L, Maluckov A, Eskofier B. ECG derived feature combination versus single feature in predicting defibrillation success in out-of-hospital cardiac arrested patients. *Biomed Phys Eng Express* 2018;5:015012. doi:10.1088/2057-1976/aaebec.
210. Theiler J, Eubank S, Longtin A, Galdrikian B, Doyne Farmer J. Testing for nonlinearity in time series: the method of surrogate data. *Phys D Nonlinear Phenom* 1992;58:77–94. doi:10.1016/0167-2789(92)90102-S.
211. Schreiber T, Schmitz A. Improved surrogate data for nonlinearity tests. *Phys Rev Lett* 1996;77:635–638. doi:10.1103/PhysRevLett.77.635.
212. Anwar SM, Majid M, Qayyum A, Awais M, Alnowami M, Khan MK. Medical Image Analysis using Convolutional Neural Networks: A Review. *J Med Syst* 2018;42:226. doi:10.1007/s10916-018-1088-1.
213. Kiranyaz S, Ince T, Gabbouj M. Real-Time Patient-Specific ECG Classification by 1-D Convolutional Neural Networks. *IEEE Trans Biomed Eng* 2016;63:664–675. doi:10.1109/TBME.2015.2468589.
214. Xiong Z, Nash MP, Cheng E, Fedorov V V., Stiles MK, Zhao J. ECG signal classification for the detection of cardiac arrhythmias using a convolutional recurrent neural network. *Physiol Meas* 2018;39:094006. doi:10.1088/1361-6579/aad9ed.